

Appendix E

Structural Analyses and Quaternary Investigations in Support of the Hanford PSHA

Structural Analyses and Quaternary Investigations in Support of the Hanford PSHA

Mr. Ryan Coppersmith
Ms. Kathryn Hanson
Dr. Jeff Unruh
Mr. Christopher Slack

Coppersmith Consulting, Inc.
AMEC Environment & Infrastructure, Inc.
Lettis Consultants International, Inc.
AMEC Environment & Infrastructure, Inc.

September 2014

Summary

New data collection and analysis tasks were conducted as part of the Hanford Senior Seismic Hazard Advisory Committee (SSHAC) Level 3 project to address specific seismic source characterization (SSC) issues, in particular the probability that individual structures are seismogenic, the geometry (length, dip, and down-dip dimensions) of fault sources, the timing of most recent activity, and the rate of Quaternary deformation for individual folds and related fault sources. The activities were prioritized to meet the overall Hanford SSHAC Level 3 probabilistic seismic hazard analysis (PSHA) project schedule and needs. The key observations and results of these studies are outlined below:

Structural geologic analysis of topographic and subsurface data – Topographic data in conjunction with a three-dimensional (3-D) hydrogeologic model of the Columbia Plateau (Burns et al. 2011) and structure contour maps on the top of basalt (Myers et al. 1979) were used to evaluate the geometry of the Yakima Fold Belt (YFB) anticlines and derive models for the location, dip, and long-term slip rate of underlying thrust faults. Key observations from this analysis are as follows:

- Structural relief on the Saddle Mountains Basalt across the Yakima folds is comparable to the modern topographic relief, indicating that erosion rates in the YFB are extremely low and less than the tectonic uplift rates.
- The present structure and topography of the YFB largely post-dates the Saddle Mountains Basalt.
- Topographic relief and structural relief are similar, thus establishing a basis for using topographic relief as a proxy for assessing long-wavelength variations in structural relief.

The fold geometry and estimates of structural relief from these analyses were used to derive thrust fault geometry beneath the folds and estimate long-term average reverse slip rate.

Kinematic analysis of focal mechanisms – Focal mechanisms from small earthquakes were analyzed to characterize seismogenic deformation in the YFB and parts of the adjacent Cascade Range. The spatial domains were selected to evaluate deformation associated with specific structures or subdomains in the YFB. The data were further subdivided into discrete depth domains to compare and contrast seismogenic deformation in the upper 3 km, which generally encompasses the depth of the Columbia River Basalt (CRB), from seismicity below 8 km in the sub-basalt sedimentary and crystalline basement rocks.

The inversion results generally show approximately north-south ($\pm 15^\circ$) shortening throughout the YFB, with perhaps a slight bias toward a north-northeast–south-southwest orientation of maximum shortening strain (d_3). These results are consistent with those of a similar analysis performed by McCaffrey et al. (2013), who inverted focal mechanisms in the YFB for components of a reduced stress tensor and found approximately north-northeast–south-southwest directed maximum compressive stress σ_1 (here assumed to be parallel to d_3).

The approximately north-northeast–south-southwest orientations of σ_1 and d_3 derived from the focal mechanism inversions differ significantly from the N56°E ($\pm 4^\circ$) direction of maximum shortening in the YFB obtained by McCaffrey et al. (2013) from analysis of Global Positioning System (GPS) data. It is beyond the scope of this investigation to determine whether this represents a true kinematic difference between surface displacements measured by GPS and patterns of coseismic deformation at depth, or if it

is a function of the assumptions in the analytical approaches. Treated as epistemic uncertainty, however, the different analytical results imply different kinematic models for behavior of structures with a given orientation. For example, McCaffrey et al. (2013) concluded that the Rattlesnake-Wallula (RAW) structure (along the Olympic-Wallowa lineament, OWL) is likely to behave as a reverse/thrust fault because it is nearly normal to the direction of maximum shortening derived from the GPS analysis, whereas the north-northeast–south-southwest orientation of d_3 from the focal mechanism inversions would suggest components of both right-lateral shear and crustal thickening (i.e., transpression) resolved across the RAW structure.

There is a significant component of shearing in the majority of inversion results that indicates the regional deformation is transpressional in nature rather than the result of strictly uniaxial north-northeast–south-southwest shortening and vertical thickening. The transpressional results imply that faults oblique to the direction of maximum shortening are more likely to have a lateral component of slip. The inversion results further suggest that transpressional analogues are more appropriate for assessing the behavior and linkage of structures in the YFB than classic foreland fold-thrust belts.

Although seismicity in the upper 3 km is generally transpressional in character, there is more variability in the orientation of d_3 and the value of V for the shallow domains relative to the deep (>8 km)

Geologic Mapping and Field Reconnaissance – Office-based interpretation of high-resolution light detection and ranging (LiDAR) data and field mapping and reconnaissance along selected faults were conducted to provide information on the style of faulting, slip rate, and timing of most recent deformation. Faults closest to the U.S. Department of Energy (DOE) facilities and Columbia Generating Station (CGS), for which there was greater uncertainty in the source characterization parameters, were prioritized. These included structures along the RAW lineament or trend (Rattlesnake Mountain, the Rattles, and Wallula faults). The Rattles refer to a series of 10 elongated (northwest-southeast) hills that appear as distinct, subparallel, doubly plunging anticlines generally aligned along a N50–60°W trend between the Yakima River and Wallula Gap (CGS Final Safety Analysis Report, Energy Northwest 1982). Reconnaissance along more distant faults such as the Saddle Mountains and Frenchman Hills faults was conducted to evaluate the inception time of folding and the relationship of Ringold Formation sediment deposition and fold deformation. In conjunction with the cosmogenic dating studies conducted as part of the project’s Quaternary geologic studies program, limited reconnaissance was conducted in Kittitas Valley and along the reach of the Yakima River where it crosses the Manastash and Umtanum ridges and the intervening synclinal region.

Key conclusions and observations from these studies for individual structures are as follows:

- **Saddle Mountains.** The Ringold Formation is fully involved in the deformation and growth of the Saddle Mountains anticline; thus, growth of the fold has occurred since deposition ceased in Plio-Pleistocene time (post 3.7 Ma). The presence of a possible angular unconformity between the Elephant Mountain basalt and Ringold Formation suggests that growth of the structure may have begun sometime after 10.5 Ma but prior to about 4.5 Ma (age of fauna recovered from the middle Ringold Formation; Smith et al. 2000).
- **Rattlesnake Mountain.** Quaternary tectonic activity in the Rattlesnake Mountain study area is observed along at least two structures: the range-front fault and the gas field anticline. The range-front fault has produced clear vertical separation of an alluvial fan surface (Qaf4) estimated to be middle Pleistocene (>380–800 ka) in age based on soil profile development calibrated based on

Th/U-series dates for similar soils in nearby cataclysmic flood deposits. Younger inset alluvial fan surfaces (e.g., Qaf2 and Qaf1), however, are deposited across the fault in a few places, and field observations indicate that they are not deformed. Examination of topographic profiles along the younger fan surfaces and their continuation as terraces in the canyon upstream of the range front reveals that the surfaces are continuous and undeformed across the fault. Based on the estimated age of the Qaf2 fan the most recent surface rupture occurred prior to ~13 ka to as much as 70 ka ago. The Qaf4 surface is also clearly tectonically tilted down to the north and south on the forelimb and backlimb, respectively, of the gas field anticline. Cumulative vertical stratigraphic separation of the Qaf4 fan surface across both the range-front fault and gas field anticline ranges from 22–33 m with a preferred average of 25–30 m. The evidence of no measurable lateral offset of geomorphic features, combined with the evidence for vertical separation across a surface scarp at the range front and fold deformation on the gas field that is consistent with the presence of a blind thrust or reverse fault, demonstrates that the uplift of Rattlesnake Mountain in the Quaternary has been primarily been accommodated by reverse slip on a fault that includes both emergent and blind splays that likely merge at depth.

- RAW-Rattles and Horn Rapids Anticline. A major issue related to seismic source characterization of these structures has been the style of faulting. Various proponents both at the time of licensing of the CGS (WNP-2) and more recently have suggested that that the ~120 km-long RAW alignment or trend (which included Rattlesnake Mountain, the Rattles, and the Wallula fault) is a capable, strike-slip fault with reverse or reverse oblique motion from Rattlesnake Hill to the Hite fault. Alternatively, others argue that these structures are primarily anticlinal trends underlain by a blind reverse faults. Based on review of previous published and unpublished geologic mapping along the Rattles and in the vicinity of the Yakima River between Rattlesnake Mountain and Red Mountain and examination of a structure contour map on the top of basalt (Myers et al. 1979), there is evidence to suggest that there are relatively continuous faults having vertical displacement along both the Rattles and Horn Rapids anticlinal trends. Both structures appear to die out to the west near the Yakima River where undeformed Ice Harbor Basalt (~10.5 Ma) provides evidence for little to no deformation. Although small amounts of strike-slip cannot be precluded, no evidence of significant strike-slip has been identified based on surface geologic or geomorphic observations.
- Wallula fault. The Wallula fault zone (also referred to as the Wallula Gap fault), which is located along the northeast flank of the Horse Heaven Hills anticline in southeastern Washington and northeastern Oregon, forms the eastern end of the RAW alignment. The sense and amount of displacement on this fault was controversial in the late 1970s and early 1980s and continues to be so to this day. The fault variously has been interpreted as a normal fault, a strike-slip fault, and a monoclinial fold (with an associated blind reverse or reverse oblique fault at depth). Previous paleoseismic studies (Farooqui 1979; Gardner et al. 1981; Woodward-Clyde Consultants [WCC] 1982) provide documentation of high-angle reverse or oblique reverse Quaternary movement on this fault with evidence for the most recent event pre-dating late Pleistocene Missoula floods (pre-15 ka). Only limited reconnaissance was conducted along the Wallula fault as part of this study. A key locality, which had been reported to show evidence of Holocene normal faulting along a strand of the Wallula fault, referred to as the Umapine fault (Mann and Meyer 1993) was examined. Faulting of Holocene sediments appears to be due to slumping subparallel to the range front rather than tectonic faulting. The bedrock fault exposed at this location, which shows subhorizontal moulins, has a northwest trend as opposed to being parallel to the east-west trending range-front Wallula fault. Based on these observations, it is concluded that there is no evidence of Holocene faulting related to

the Wallula fault zone at this locality. Previous workers have measured kinematic indicators of strike-slip faulting along the Wallula fault zone. An analysis of 49 striae by WCC (1982), 47 of which were within 300 m of the surface trace of the Wallula Gap fault showed movement was more consistent with a reverse fault/fold model than with a strike-slip model. WCC (1982) concluded that strike-slip faults within the Wallula Gap structure have an orientation that is more consistent with a conjugate shear system associated with reverse faulting than with a right-lateral shear system or strike-slip faulting parallel to the Wallula Gap fault.

Geochronologic Investigations – To assist in developing a chronostratigraphic framework for alluvial fan and other Quaternary deposits and surfaces in the Hanford Site study region, two geochronology approaches were used: U-series dating of pedogenic carbonate and cosmogenic nuclide burial dating of fluvial deposits within the Yakima River Canyon.

Dr. James Paces, U.S. Geological Survey (USGS, Denver), was responsible for processing and analysis of pedogenic carbonate using uranium-series ($^{230}\text{Th}/\text{U}$) dating methods. Analysis of the innermost rings of pedogenic carbonate accumulations on clasts provides a method for estimating the minimum depositional age of the deposit sampled. Older flood gravels preserved in terraces above the Yakima River in the southern part of the Pasco Basin had been evaluated by Dr. TL Ku, University of Southern California, using this dating approach as part of previous licensing investigations (e.g., WCC 1981b; Baker et al. 1991). Key localities were re-sampled and re-analyzed as part of this SSHAC Level 3 study. Techniques have evolved since the approach was first implemented, and the objectives of the dating were to confirm previous dating results and to calibrate the Quaternary Studies Team efforts with regard to carbonate soil profile development that could be used to assess ages for similar soils observed elsewhere in the study region.

This study's results for three sites—South Bombing Range Road, Yakima Bluffs and Steptoe quarry—are similar to the previous results reported by Baker et al. (1991) in that these cataclysmic Ice Age flood deposits all appear to be of similar middle Pleistocene age. They are all capped by platy to massive, carbonate-plugged K horizons, characteristic of Stage III to Stage IV/V pedogenic carbonate development. The normal polarity of the sampled flood sediments at both the Yakima Bluffs and South Bombing Range Road sites indicates the deposits are probably younger than the ~780 ka Brunhes (normal)/Matuyama (reversed) boundary. The elevations of these three sites range from as low as ~140 m at Steptoe quarry to as high as 180+ m at South Bombing Range Road. This variation in elevation seems plausible for the same age deposit given the cataclysmic nature of the fluvial system.

The results of this study find the ages of the deposits are at least as old as ~350–400 ka, somewhat older than the preferred age of ~200 ka by Baker et al. (1991). A number of the samples at all three sites were approaching the limits of the $^{230}\text{Th}/\text{U}$ method, which suggests a likely antiquity of 380 ka or greater. This minimum age is consistent with deposition during glacial conditions in marine oxygen isotope stage (MIS) 12 (478–424 ka) or earlier glacial periods. A Monte Carlo approach, where multiple trials are calculated using values for isotope compositions that vary randomly within range of the given uncertainty, was used to extend the maximum ages that could be assessed using the $^{230}\text{Th}/\text{U}$ -series dating technique. Samples from all three sites yielded best estimate values between 500–700 ka (consistent with a flood during MIS 14 [563–533 ka], MIS 16 [676–621 ka], or possibly MIS 18 [761–712 ka]). Although the possibility that the deposits record more than one period of flooding cannot be precluded, the ages cannot be differentiated within the resolution of the dating method. Erosion of the upper portions of the

soils formed in these deposits during the latter Missoula floods further complicates the assessment and comparison of maximum soil profile development among the dated localities.

Dates from two other localities, the Mid-Columbia Basin Old Natural Education Sciences (MCBONES) and Finley quarry sites, provide informative minimum ages for carbonate soil development in younger deposits. The U-series results from the MCBONES site show that Stage III to III+ carbonate can form in gravel deposits in 268–200 kyr. At Finley quarry, thin (0.5-mm) carbonate rinds on clast bottoms formed in less than 17 kyr, possibly within only a few thousand years based on stratigraphic relationships.

The second dating approach, cosmogenic nuclide analysis of buried clasts from fluvial terrace deposits was used to assess the ages of Yakima River terraces that show evidence of Quaternary deformation by two YFB structures—the Manastash and Umtanum ridges. Dr. Paul Bierman, University of Vermont, collected and analyzed cosmogenic nuclide (^{10}Be and ^{26}Al) ratios in quartz derived from fluvial terrace deposits to estimate isochron burial ages for selected terraces along the Yakima River.

$^{26}\text{Al}/^{10}\text{Be}$ cosmogenic isochron ages were obtained for alluvium directly overlying three strath terraces within the canyon. One locality (YK05) sampled a terrace (Qg4) remnant on the hanging wall of the Manastash fault. Two other samples were collected further downstream—YK04 from deposits overlying a strath at an elevation of ~16 m in the synclinal region between the Manastash and Umtanum anticlines and YK03 from a deposits overlying a low terrace strath (<1.4 m above the modern river) on the hanging wall of the Umtanum fault.

$^{26}\text{Al}/^{10}\text{Be}$ cosmogenic isochron dating of quartz-rich, Cascade-sourced terrace cover gravels suggests a young age, indistinguishable from modern, for the lowest surface. Early- to mid-Quaternary ages (1.08 ± 0.29 Ma and 1.59 ± 0.25 Ma, 1 sigma) are suggested for the Qg4 terrace (YK05) that is ~50 m above the river within the Manastash Ridge anticline and downstream for a lower surface (~16 m) (YK04) within a syncline north of Umtanum Ridge. While the uncertainty in these ages reflects both low content and the narrow range of ^{10}Be concentrations for analyzed samples, the presence of similar-age clasts at notably different elevations is consistent with the Quaternary uplift of the Manastash and Umtanum anticlines relative to channel reaches between these folds. These results combined with the preliminary fluvial terrace mapping and geomorphic analysis discussed below support the hypothesis that anticlinal growth locally controls incision of the Yakima River, and that at least some portion of the total canyon relief represents the product of Quaternary uplift and continued structural development of the YFB.

The cosmogenic $^{26}\text{Al}/^{10}\text{Be}$ ages combined with previous (Ladinsky 2012; Ladinsky and Kelsey 2012) and preliminary fluvial terrace mapping of Yakima River fluvial terraces by Amos and Sorsby (Appendix E.2) were used to compare Quaternary rates of incision to long-term vertical rates of deformation for the Manastash and Umtanum structures. In general the results suggest Quaternary rates comparable to the long-term (post-CRB) rates assessed based on the structural analyses.

Yakima River Fluvial Geomorphology Analyses – A fluvial geomorphic analysis to identify and characterize tectonic deformation was completed by Dr. Colin Amos and Mr. Skyler Sorsby, University of Western Washington. The study used a combination of lab and field-based techniques to identify and isolate tectonically induced channel adjustments across major anticlinal ridges intersected by the Yakima and Columbia rivers. This work is based on the assumption that river channel geometry (specifically width and slope) adjusts in concert with incision driven by active surface deformation, and that such

adjustments can be used to identify and assess relative rates of tectonic activity. Preliminary LiDAR-based 1:5000-scale terrace mapping of the Yakima River fluvial terraces also was conducted to identify additional evidence for potential Quaternary deformation in the YFB. Preliminary observations and conclusions from the fluvial geomorphic analyses and preliminary mapping of fluvial terraces in Yakima Canyon conducted by Amos and Sorsby (Appendix E.2) are as follows:

- Differential uplift and tilting of older terraces is centered near Umtanum Ridge.
- Localized channel narrowing across Manastash, Umtanum, and Yakima ridges, as well as Selah Butte is coincident with increasing channel sinuosity suggesting modest late Quaternary deformation.

Paleoseismic Investigations-Finley quarry – A key locality for assessing the style of faulting and timing of most recent faulting along the RAW structure is a quarry exposure near Finley, Washington. Previous studies conducted during site characterization studies for both CGS (originally referred to as WNP2) and the Basalt Waste Isolation Project, which involved logging the quarry wall and a trench excavation in the quarry, recognized evidence of Quaternary faulting (Farooqui and Thoms 1980; WCC 1981a,b). The USGS, under the direction of Drs. Brian Sherrod and Richard Blakely, completed a paleoseismic log of the present quarry wall exposure and conducted additional mapping, geomorphic interpretation of high-resolution LiDAR data, and ground-based magnetic surveys in the vicinity of the Finley quarry.

Sherrod and co-workers interpret particular aspects of the stratigraphic sequence observed in the quarry exposure as evidence of up to four paleoearthquakes along the Wallula fault during the late Pleistocene and Holocene (Sherrod et al. [In Review]). This contrasts with previous interpretations and conclusions in licensing documents (CGS Final Safety Analysis Report [Energy Northwest 1982]; NRC 1982; Rockwell Hanford Operations 1982) that the most recent surface rupture pre-dates deposition of sediments having a minimum age of greater than 69–160 ka (WCC 1981b).

Alternative hypotheses related to Ice Age (glacial-outburst) flooding erosion and deposition can explain some of the features inferred as evidence of post-flooding (late Pleistocene and Holocene) surface faulting. Based on evaluation of the available data, the Quaternary Studies Team favors the previous interpretation that there have been no events post deposition of deposits that likely pre-date MIS 4 (71–58 ka). Low weight is given to the hypothesis that there has been one event post-dating $\sim 17 \pm 1.8$ ka (the minimum age of unfaulted deposits based on Th/U-series dating conducted as part of this study). Very low weight is given to two or three faulting event scenarios post- 17 ± 1.8 ka.

Compilation of Paleoseismic Data for the Yakima Fold Belt – Available paleoseismic data for YFB structures was compiled by the USGS and will be published as a USGS Scientific Investigations Map (Barnett and Sherrod [In Review]). A preliminary draft of this information is provided in Appendix E.4.

Acknowledgments

This report, which describes both office-based structural and seismological analyses and field studies conducted in support of the Hanford Senior Seismic Hazard Advisory Committee Level 3 Probabilistic Seismic Hazard Analysis project, was authored by the four members of the Quaternary Studies Team listed below:

- Mr. Ryan Coppersmith (SSC TI Team) Coppersmith Consulting, Inc.
- Ms. Kathryn Hanson (SSC TI Team) AMEC Environment and Infrastructure (AMEC E&I)
- Dr. Jeff Unruh (SSC TI Team) Lettis Consultants International
- Mr. Christopher Slack AMEC E&I

The Quaternary Studies Team collaborated with several researchers, listed below, who were funded to complete related special studies, including fluvial geomorphic analyses, geochronology and paleoseismic studies. Results of their work are summarized in reports appended to this report or in manuscripts submitted for publication.

- Dr. Colin Amos Western Washington University Fluvial Geomorphic Studies
- Mr. Skyler Sorsby Western Washington University Fluvial Geomorphic Studies
- Dr. Brian Sherrod U.S. Geological Survey Paleoseismological Investigations—Finley quarry
- Dr. Richard Blakely U.S. Geological Survey Analysis of Magnetic and Gravity Data
- Dr. James Paces U.S. Geological Survey Geochronology-²³⁰Th/U-series Dating of Pedogenic Carbonate
- Dr. Paul Bierman University of Vermont Geochronology- Cosmogenic Nuclide (²⁶Al/¹⁰Be) Analysis

Other individuals, who provided support to the various field activities, included the following:

- Dr. Steve Reidel Washington State University-Tri-Cities
- Dr. George Last Pacific Northwest National Laboratory
- Dr. Bruce Bjornstad Pacific Northwest National Laboratory
- Dr. Harvey Kelsey Humboldt State University

Robert Bryce (Project Manager, PNNL) and Susan Ennor (PNNL) provided logistical and technical editing support, respectively. Dr. Steve Reidel also provided technical review of the report.

Acronyms and Abbreviations

2-D	2-dimensional
3-D	3-dimensional
AMEC E&I	AMEC Environment and Infrastructure, Inc.
BWIP	Basalt Waste Isolation Project
cal. yr BP	calendar years before present
CCU	Cold Creek Unit
CGS	Columbia Generating Station (formerly WPN-2)
CLEW	Cle Elum-Wallula deformed zone
cm	centimeter(s)
CRB	Columbia River Basalt
CRBG	Columbia River Basalt Group
DEM	digital elevation model
DOE	U.S. Department of Energy
DOE-RL	U.S. Department of Energy-Richland Operations Office
FSAR	Final Safety analysis Report
GIS	geographic information system
GPS	Global Positioning System
IRSL	infrared Stimulated Luminescence
ka	kiloannus (thousand years [ago])
km	kilometer(s)
kyr	thousand years
kyr BP	thousand years Before Present
LCI	Lettis Consultants International, Inc.
LiDAR	light detection and ranging
m	meter(s)
Ma	megaannus (million years [ago])

Myr	million years
MCBONES	Mid-Columbia Basin Old Natural Education Sciences
MIS	marine oxygen isotope stage (also referred to as oxygen marine isotope stage [OIS])
mm	millimeter(s)
MSL	mean sea level
NED	National Elevation Dataset
NRC	U.S. Nuclear Regulatory Commission
OSL	optically stimulated luminescence
OWL	Olympic-Wallowa lineament
PPRP	Participatory Peer Review Panel
PSHA	probabilistic seismic hazard analysis
PNNL	Pacific Northwest National Laboratory
QGS	Quaternary geologic studies
RAW	Rattlesnake-Wallula
SSC	seismic source characterization
SSC TI	seismic source characterization technical integration
SSHAC	Senior Seismic Hazard Advisory Committee
Th	thorium
U	uranium
USBR	United States Bureau of Reclamation
USGS	United States Geological Survey
WCC	Woodward-Clyde Consultants
YFB	Yakima Fold Belt
yr BP	years before present

Contents

Summary	v
Acknowledgments.....	xi
Acronyms and Abbreviations	xiii
1.0 Introduction	1.1
2.0 Data Sets Used to Support the QGS	2.1
3.0 Scope of Work.....	3.1
3.1 Structural Analyses Using Topographic and Subsurface Well Data and Hydrogeologic Models.....	3.1
3.2 Kinematic Analyses of Earthquake Focal Mechanisms	3.2
3.3 Geochronology Studies	3.2
3.4 Quaternary Studies Team Paleoseismic Field Investigations.....	3.3
3.5 Yakima River Fluvial Geomorphic Analyses	3.4
3.6 Quarry Wall Mapping at Finley, Washington.....	3.4
3.7 Compilation of Paleoseismic Data for the Yakima Fold Belt	3.4
4.0 Stratigraphic Framework	4.1
4.1 Columbia River Basalt Group and Ellensburg Formation	4.1
4.2 Suprabasalt Sediments.....	4.1
4.2.1 Ringold Formation	4.4
4.2.2 Thorp Gravel	4.7
4.2.3 Cold Creek Unit	4.7
4.2.4 Cataclysmic Flood Deposits.....	4.7
4.2.5 Pleistocene Alluvial Fans	4.14
4.2.6 Holocene Deposits.....	4.15
4.2.7 Tephrochronology	4.15
4.2.8 Late Pleistocene Loess and Soil Stratigraphy	4.16
4.3 Geochronology Studies	4.17
4.3.1 ²³⁰ Th/U-Series Dating.....	4.17
4.3.2 Cosmogenic Nuclide Dating	4.30
5.0 Evaluation of Long-Term Structural Relief.....	5.1
5.1 Constraints on Structural Relief Provided by the Burns et al. 3-D Model.....	5.1
5.2 Evaluation of Structural Relief Using Top of Bedrock Analysis	5.6
5.2.1 Gable Mountain and Southeast Anticline Fault.....	5.6
5.2.2 Yakima Ridge Southeast Fault.....	5.6
5.2.3 RAW-Rattles Structure and the Horn Rapids Fault	5.8
5.3 Results of Structural Relief Analysis	5.10
6.0 Kinematic Analyses Using Earthquake Focal Mechanisms	6.1
6.1 Analytical Approach	6.3

6.2	Results	6.3
6.2.1	Spatial Domains Associated with Major Structures of the Yakima Fold and Thrust Belt.....	6.5
6.2.2	Evaluation of Seismicity Below the 8-km Depth for YFB Domains	6.5
6.2.3	Evaluation of Seismicity Above the 3-km Depth for YFB Domains	6.7
6.2.4	Seismicity in the Cascades	6.9
6.3	Discussion	6.12
7.0	Fault-Specific Observations and Evaluations Based on Field Mapping and Reconnaissance	7.1
7.1	Saddle Mountains.....	7.1
7.2	Frenchman Hills	7.2
7.3	Rattlesnake Mountain Study Area.....	7.3
7.3.1	Bedrock Structure.....	7.7
7.3.2	Description of Alluvial Fan Units	7.7
7.3.3	Quaternary Deformation	7.23
7.4	RAW-Rattles and Horn Rapids Anticline	7.29
7.4.1	Bedrock Structure.....	7.31
7.4.2	Finley Quarry Recurrence Data.....	7.34
7.5	Wallula Fault Zone (Wallula Gap Fault).....	7.43
7.5.1	Yellepit Station Canyon Trench Locality.....	7.47
7.5.2	Northwest-Striking Faults, U.S. Highway 730 Roadcut	7.47
7.5.3	Northwest-Striking Faults, Vansycle Canyon	7.48
7.5.4	Bingham Lineament	7.48
7.5.5	Warm Springs Canyon Locality	7.52
7.5.6	Umapine Fault	7.53
8.0	Fluvial Geomorphic Analyses	8.1
9.0	Preliminary Constraints on Quaternary Uplift Rates – Manastash and Umtanum Structures.....	9.1
9.1	Kittitas Valley	9.1
9.2	Manastash Ridge	9.6
9.3	Umtanum Ridge	9.6
10.0	References	10.1
	Appendix E-1 – Geochronology – Th/U Dating of Carbonate Rinds.....	E1.1
	Appendix E-2 – Fluvial Analysis of Active Deformation in the Yakima Fold and Thrust Belt, WA.....	E2.1
	Appendix E-3 – Geochronology–Cosmogenic Nuclide (10Be/26Al) Dating of Fluvial Gravels- Yakima River Canyon.....	E3.1
	Appendix E-4 – Inventory of Paleoseismic Studies from the Yakima Fold and Thrust Belt to the Puget Lowland	E4.1

Figures

4.1	Stratigraphic nomenclature for the Columbia River Basalt Group	4.2
4.2	Hanford Site stratigraphy	4.3
4.3	Topographic and stratigraphic relationships of Ringold faunas.....	4.5
4.4	Generalized interpretation of the paleogeography of the Pasco Basin during each of three phases of the Ringold Formation deposition.....	4.6
4.5	Yakima Bluff locality.....	4.8
4.6	Map showing principal features related to Ice Age cataclysmic floods.....	4.9
4.7	Digital elevation model map of part of the Pasco Basin	4.13
4.8	Magnetostratigraphy at eastern Cold Creek bar.....	4.14
4.9	Summary of regional stratigraphy including chronostratigraphic markers pedostratigraphy, and lithostratigraphy in relation to Oxygen Isotope Stages	4.17
4.10	²³⁰ Th/U-series sample sites relative to other locations where carbonate soils were observed during Quaternary Studies Team reconnaissance	4.19
4.11	Photograph showing the soil developed in Ice Age cataclysmic flood deposits exposed in the north wall of the inactive South Bombing Road quarry.....	4.20
4.12	Photographs of the Yakima Bluff locality.....	4.22
4.13	GoogleEarth image showing the location of the sample locality relative to the MCBONES mammoth excavation site.....	4.23
4.14	Annotated stratigraphy at the mammoth bone bed locality.....	4.24
4.15	Photograph showing location of carbonate rind sampling for ²³⁰ Th/U-series analysis, at exposure near the MCBONES site.....	4.25
4.16	Photomosaic showing the relationship between older gravels, late Pleistocene Touchet Beds, younger gravels, and loess deposits	4.26
4.17	Photographs showing flood deposits at the northern end of the exposure sampled for ²³⁰ Th/U-series analysis, and Finley quarry exposure, view southeast.....	4.28
4.18	Photograph of the Finley quarry south fault showing the sampled carbonate-cemented fault breccia.	4.29
4.19	Map showing the location of cosmogenic nuclide (²⁶ Al/ ¹⁰ Be) samples	4.31
4.20	Photographs illustrating the stratigraphy and soils exposed in the Potato Hill quarry cuts, Kittitas Valley, Washington	4.32
5.1	Western profile comparing results of the Burns et al. (2011) model with horizon picks from borehole well logs at nine locations along the transect.....	5.3
5.2	Central profile comparing results of the Burns et al. (2011) model with horizon picks from borehole well logs at nine locations along the transect.....	5.4
5.3	Eastern profile comparing results of the Burns et al. (2011) model with horizon picks from borehole well logs at seven locations along the transect.....	5.5
5.4	Map showing the extent of CRB structure contour maps from various sources.....	5.7
5.5	Map showing the Umtanum-Gable Mountain -Southeast Anticline and Yakima Ridge Southeast structures.....	5.8

5.6	Map showing the Horn Rapids fault and RAW-Rattles structure over a top-of-CRB structure contour map by Myers et al. (1979).....	5.9
5.7	Cross sections from the Thorne et al. (2014) top-of-basalt DEM. Profile 1 shows offset basalt across the doubly plunging anticlines associated with the two faults.....	5.10
5.8	Map showing average and maximum vertical structural relief for fault segments.	5.11
6.1	Earthquakes recorded during 1970–2011 for which focal mechanisms are available. Epicenters are color-coded to distinguish events occurring above and below the 8-km depth...	6.2
6.2	Inversion results from areas in the YFB using focal mechanisms from all depth ranges	6.6
6.3	Inversion results for selected YFB domains using only earthquakes from depths greater than 8 km.....	6.7
6.4	Inversion results for selected domains using only earthquakes from depths less than 3 km. Blue arrows show the azimuth of maximum shortening from inversion of focal mechanisms within the associated polygon.	6.8
6.5	Inversion results for domains in the Cascades	6.10
6.6	Inversion results for domains near Mount St. Helens	6.11
7.1	Photograph of south-dipping surface bearing the strong petrocalcic horizon on the backlimb of Saddle Mountains	7.2
7.2	1:100,000-scale geologic map of the Rattlesnake Mountain-Snively Basin area	7.4
7.3	Panoramic photograph view to the southeast along the eastern Rattlesnake Mountain range front, and hillshade map derived from 1-m LiDAR DEM showing the location of the Rattlesnake Mountain study area.	7.5
7.4	Hillshade map of study area with profile location and annotated topographic profile.	7.6
7.5	Photograph showing the Qaf4 fan surface in the hanging wall and footwall of the main range-front fault at the eastern end of the study area where the fault becomes blind	7.10
7.6	Photograph of typical carbonate soil development in the Qaf4 fan in a natural exposure along a drainage incising into the Qaf4 at field locality 13256sh01 and Quaternary geologic map showing location and view direction.....	7.19
7.7	Detailed surficial geologic map and topographic profiles showing undeformed Qaf2 fans crossing the projected trace of the main range-front fault.....	7.21
7.8	Photograph of the exposure (location 13257sh07) along a natural gully incised into Qaf2, showing in-place rocks with carbonate rinds covering the base of clasts; close-up view of clasts removed from the horizon to photograph the maximum carbonate rind thickness; and quaternary geologic map showing location of 13257sh07.....	7.22
7.9	Location 13257sh05 showing Stage IV carbonate horizon developed in Qaf4, and back-tilting of the Qaf4 soil on the southwest flank of the gas field anticline.....	7.25
7.10	Map and topographic profiles showing the position of the study area relative to the Rattlesnake Mountain anticlinal ridge.....	7.29
7.11	1:100,000-scale geologic map showing the Rattles and Horn Rapid anticline	7.30
7.12	1:100,000-scale geologic map showing the topographic profiles used to evaluate vertical separation across the projection of the RAW structure.....	7.33
7.13	Topographic profiles showing uncertainty in vertical separation across projection of the RAW structure.	7.34
7.14	Panoramic photograph of the west end of The Butte showing Finley quarry in the right center and the Columbia River in the left center of the photograph	7.35

7.15	Combined quarry and trench logs from the WPPSS studies conducted in 1980.....	7.36
7.16	Photomosaic and log of the Finley quarry exposure	7.36
7.17	Summary of Quaternary stratigraphy and geologic events in south-central Washington and Finley quarry	7.37
7.18	Location map showing key localities and structures associated with the Wallula fault zone	7.44
7.19	Comparison of a right-lateral strike-slip extensional duplex to the Wallula fault zone	7.45
7.20	Map showing locations of paleoseismic investigations along the Wallula fault.....	7.46
7.21	Photographs of the fault plane exposed along Highway 730	7.49
7.22	LiDAR-generated DEM base map near the mouth of Vansycle Canyon.....	7.50
7.23	Location map showing trenching and magnetometer studies from WCC (1982).....	7.51
7.24	Geologic sketch of faulted colluvium of probable Quaternary age at the Warm Springs locality.....	7.52
7.25	Detailed log of North Fault west wall of Trench WS-3, Warm Springs Locality	7.54
7.26	Diagram of the east wall of the gully exposure of the Umapine fault.....	7.55
7.27	Photographs from locality 13282sh01 showing the present outcrop, bedrock shear zone with N46°W subvertical fault exhibiting subhorizontal moulins, and fractures within loess/colluvium.	7.56
9.1	Map showing the location of Potato Hill and the cross section extending from Manastash range front northward to Potato Hill within the southern Kittitas Valley	9.5

Plates

1	Surficial geologic map of the Rattlesnake Mountain study area.....	7.8
2	Rattlesnake Mountain study area geomorphic map and topographic profiles.	7.28

Tables

4.1	Selected pre-Wisconsin cataclysmic flood localities in southeastern Washington	4.11
4.2	Late Pleistocene and Holocene tephra sequence and chronology in the Study Region	4.15
4.3	Radiometric ages from pre-Wisconsin cataclysmic flood deposits in southeastern Washington	4.18
5.1	Mean structural relief measurements for fault sources in the YFB.....	5.12
6.1	Results of the inversion analyses for individual domains	6.4
7.1	Calibration and sampling sites used to constrain the ages of carbonate soil profile development and weathering characteristics of alluvial fan and fluvial terraces in the study area.	7.12
7.2	Alternative interpretations of the number and timing of late Pleistocene surface ruptures on RAW-Rattles structure based on stratigraphic and structural relationships exposed at Finley quarry	7.38
9.1	Summary of estimated incision rates –Southern Kittitas and Yakima Canyon that constrain rates of uplift for the Manastash and Umtanum fault sources.....	9.2

1.0 Introduction

This report describes the results of the Quaternary geologic studies (QGS) that were conducted as part of the Hanford Senior Seismic Hazard Advisory Committee (SSHAC) Level 3 Probabilistic Seismic Hazard Analysis (PSHA) report. The overall objectives of these field and office-based studies were to 1) develop data to characterize the geometry of the Yakima folds and underlying thrust faults; 2) provide additional data and information that can be used to evaluate the presence or absence of Quaternary activity of structures within the Yakima Fold Belt (YFB); and 3) to constrain the rates and style of deformation for individual structures. These studies included the following activities:

- structural geologic analysis of topographic and subsurface data
- kinematic analysis of focal mechanisms from small earthquakes in the YFB
- interpretation of high-resolution light detection and ranging (LiDAR) data (Rattlesnake Mountain and Wallula Gap study areas)
- geologic mapping and field reconnaissance
- geochronologic investigations
- Yakima River fluvial geomorphology analyses
- paleoseismic investigations-Finley quarry
- compilation of paleoseismic data for YFB structures.

The results of field investigations completed as part of this study are considered in light of observations and conclusions outlined in various licensing and site characterization reports completed during the late 1970s–early 1980s, peer-reviewed publications, results of new analysis of focal mechanism data completed as part of the Hanford SSHAC PSHA, and ongoing research by other researchers and the U.S. Geological Survey (USGS) funded in part by this project.

The ensuing sections of this report, in particular, describe the data sets used to support the QGS, scope of work, stratigraphic framework, evaluation of long-term structural reliefs, kinematic analyses using earthquake focal mechanisms, fault-specific observations and evaluations based on field mapping and reconnaissance, fluvial geomorphic analysis, preliminary constraints on Quaternary uplift rates in the Manastash and Umtanum structures, and USGS paleoseismic studies of the Wallula fault. Appendices contain supplemental information describing $^{230}\text{Th}/\text{U}$ -series dating of carbonate rinds, fluvial analysis of active deformation in the YFB, a cosmogenic nuclide dating of fluvial gravels in Yakima River Canyon, and a compilation map and associated table documenting paleoseismic studies in the study region.

2.0 Data Sets Used to Support the QGS

A geographic information system (GIS) database was compiled to analyze new and existing spatial data relevant to the QGS and the Hanford SSHAC Level 3 PSHA. The GIS database was managed by Duane Ward (Pacific Northwest National Laboratory [PNNL]) and Ryan Coppersmith (Coppersmith Consulting, Inc.). The primary mapping objectives used spatial data such as digital elevation models (DEMs) derived from LiDAR data along with digital geologic maps to aid in field- and office-related mapping. In preparation for field mapping activities, many of these data sets were uploaded to the Garafa GIS application (<http://garafa.com/wordpress/all-apps/gis-pro>) on an iPad tablet for use in the field.

The data sets below were compiled for analyses related to the QGS mapping activities:

- 10-m resolution DEM and corresponding hillshade for the YFB region (Gesch et al. 2002; Gesch 2007)
- 1-m resolution LiDAR DEM for multiple locations within the YFB region
 - Yakima River U.S. Bureau of Reclamation (personal communications Edward Young USBR 2012)
 - Manastash Ridge (Open Topography <http://www.opentopography.org/>)
 - Yakima Ridge, Wenatchee, Wenas, Kittitas, Douglas, Rattlesnake Mountain (Puget Sound LiDAR Consortium <http://pugetsoundlidar.ess.washington.edu/index.htm>)
- Washington State 1:100,000 geologic map (Schuster 2000; ngnbd.usgs.gov/info/dmt/docs/schuster07b.pdf)
- Regional well database (Burns et al. 2011; <http://or.water.usgs.gov/proj/cpras/index.html>)
- Global Positioning System (GPS) field locations collected on iPad tablet

New data from QGS field mapping, such as data points and mapped polylines, were digitized into a GIS format and uploaded to the PNNL SharePoint site for documentation.

3.0 Scope of Work

New data collection and analysis tasks were conducted to address specific seismic source characterization (SSC) issues, in particular the probability that individual structures are seismogenic, the geometry (length, dip, and downdip dimensions) of fault sources, the timing of most recent activity, and rate of Quaternary deformation for individual folds and related fault sources. The activities were prioritized to meet the overall Hanford SSHAC Level 3 PSHA project schedule and needs. The general scope and objectives of the various activities are outlined in the following subsections.

3.1 Structural Analyses Using Topographic and Subsurface Well Data and Hydrogeologic Models

We analyzed topographic data in conjunction with a three-dimensional (3-D) hydrogeologic model of the Columbia Plateau (Burns et al. 2011) and structure contour maps on the top of basalt (Myers et al. 1979) to evaluate the geometry of the YFB anticlines and derive models for the location and dip of underlying thrust faults. This analysis, which is presented and discussed in more detail in Section 5.0, consisted of three primary activities:

1. Topographic Analysis: Using GIS software (ArcGIS) to visualize data from a 10-m DEM, we characterized the geometry of individual YFB structures by measuring the length of the anticlines and their widths (i.e., wavelengths), and by evaluating topographic relief normal to the crests of the folds (i.e., fold amplitude). The measurements were performed by extracting and analyzing numerous two-dimensional (2-D) topographic profiles across the folds using a standard ArcGIS tool. Profiles acquired normal to the trend of the folds allowed us to determine the locations of synformal hinges at the base of the forelimb and backlimb of each fold, and to accurately measure the full width or wavelength of the structure, as well as topographic relief across the fold crest. Profiles acquired along the fold axis allowed us to assess lateral variations in topographic relief and identify discrete structural or geometric reaches of the fold that potentially indicate variations in underlying thrust fault geometry and/or activity.
2. Comparison of Topographic Relief to Structural Relief: The Burns et al. (2011) hydrogeologic model is a 3-D representation of the first-order stratigraphic and structural framework of the Columbia Plateau. The model is derived from surface geology and data from more than 13,000 wells, and depicts uplift, folding, and faulting of Miocene Columbia River Basalt (CRB) units across the major YFB structures. The Burns et al. model is available as an interactive web-based tool (<http://or.water.usgs.gov/proj/cpras/index.html>) that allows users to define and extract arbitrary 2-D cross sections from the model and directly measure the relief of key stratigraphic contacts (e.g., the tops of the Saddle Mountains Basalt and Wanapum Basalt) across individual Yakima folds. We used this tool to compare structural relief on the CRB units across the folds to topographic relief and test the hypothesis that the two are similar, thus establishing a basis for using topographic relief as a proxy for assessing long-wavelength variations in structural relief. Locally, where erosion and deposition related to cataclysmic floods have significantly modified the surface expression of the folds, additional information from subsurface data used to develop a top-of-basalt structure contour map (Myers et al. 1979) also was used to assess structural relief.
3. Derivation of Source Geometry and Long-Term Slip Rate: We used the fold geometry and estimates of structural relief from the previous two activities to derive thrust fault geometry beneath the folds

and estimate the long-term average reverse slip rate. The analytical approach and assumptions involved in this analysis, as well as the derived fault geometry and long-term average slip rate, are presented in Section 5.3.

3.2 Kinematic Analyses of Earthquake Focal Mechanisms

Focal mechanisms from small earthquakes were analyzed to characterize seismogenic deformation in the YFB and parts of the adjacent Cascade Range. Earthquakes were sorted into groups based on patterns of spatial clustering and/or associations with geologic structure, and their focal mechanisms were used to invert for components of a reduced incremental strain tensor using the approach of Twiss and Unruh (1998). The inversion involves two key assumptions: 1) slip on faults during earthquakes occurs in the direction of maximum resolved shear strain; and 2) the local deformation accommodated by small earthquakes reflects the regional strain (Twiss et al. 1993; Twiss and Unruh 1998). The orientations and relative magnitudes of the principal strains derived from the inversions can be used to interpret how the crustal volume in which the earthquakes occurred changes shape as a consequence of distributed brittle faulting. In particular, the analysis can be used to quantitatively evaluate the relative contributions of horizontal shear and vertical thickening or thinning of the crust during deformation (i.e., a horizontal plane strain vs. transpression or transtension). Section 6.0 provides a summary of the data used and analytical approach; tabulated results of the data inversions; and a brief discussion of the implied deformation kinematics.

3.3 Geochronology Studies

To assist in developing a chronostratigraphic framework for alluvial fan and other Quaternary deposits and surfaces in the Hanford study region, two geochronology approaches were used—U-series dating of pedogenic carbonate and cosmogenic nuclide burial dating. Reports summarizing these two dating studies are provided in Appendices E.1 and E.3, respectively.

Dr. James Paces, USGS Denver, was responsible for processing and analyzing the pedogenic carbonate using uranium-series ($^{230}\text{Th}/\text{U}$, $^{234}\text{U}/^{238}\text{U}$) dating methods (Appendix E.1). Analysis of the innermost rinds of pedogenic carbonate accumulations on clasts provides a method for estimating the minimum depositional age of the deposit sampled. Older flood gravels preserved in terraces above the Yakima River in the southern part of the Pasco Basin had been evaluated by Dr. Ku (University of Southern California) using this dating approach as part of previous licensing investigations (e.g., Woodward-Clyde Consultants (WCC) 1981b; Baker et al. 1991). Key localities were re-sampled and re-analyzed as part of this SSHAC Level 3 study. Techniques have evolved since the approach was first implemented, and the objectives of the dating were to confirm previous dating results and to calibrate the Quaternary Studies Team (Quaternary Studies Team) mapping efforts with regard to carbonate soil profile development that could be used to assess ages for similar soils observed elsewhere in the study region. Members of the Quaternary Studies Team (Kathryn Hanson and Christopher Slack) assisted Dr. Paces in the sampling and description of sampling localities.

In conjunction with the fluvial terrace mapping investigations along the Yakima River (see Appendix E.2 and Section 8.0), Dr. Paul Bierman, University of Vermont, collected and analyzed ^{10}Be and ^{26}Al ratios in quartz derived from alluvial fan deposits to estimate burial ages for the selected terraces along the Yakima River (Appendix C). Tyler Ladinsky provided recommendations for sampling sites in

the vicinity of Manastash Ridge. Drs. Harvey Kelsey, Brian Sherrod, and Colin Amos, along with Skyler Sorsby and members of the Quaternary Studies Team (Ryan Coppersmith, Jeff Unruh, Kathryn Hanson, and Christopher Slack) participated in the sampling and prioritization of samples for dating.

3.4 Quaternary Studies Team Paleoseismic Field Investigations

Office-based LiDAR interpretation and field mapping and reconnaissance along selected faults were conducted to provide information about the style of faulting, slip rate, and timing of most recent deformation. Faults closest to the U.S. Department of Energy (DOE) facilities and Columbia Generating Station (CGS), for which there was greater uncertainty in the source characterization parameters, were prioritized. These included structures along the Rattlesnake-Wallula (RAW) lineament or trend (Rattlesnake Mountain, the Rattles, and Wallula faults). The Rattles refer to a series of 10 elongated (northwest-southeast) hills that appear as distinct, subparallel, doubly plunging anticlines generally aligned along a N50–60°W trend between the Yakima River and Wallula Gap (CGS Final Safety Analysis Report [FSAR], Energy Northwest 1998). Reconnaissance along more distant faults such as Saddle Mountains and Frenchman Hills faults was conducted to evaluate the inception time of folding and relationship of Ringold Formation sediment deposition and fold deformation. In conjunction with the cosmogenic dating studies, limited reconnaissance was conducted in Kittitas Valley and along the reach of the Yakima River where it crosses Manastash and Umtanum ridges and the intervening synclinal region.

As described above in Section 2.0, three LiDAR data sets were available for detailed study; each data set has a roughly 1-m resolution. The newly acquired LiDAR data sets are a significant improvement over the National Elevation Dataset (NED) 1/3 arc-second DEM provided by the USGS. The 1-m resolution LiDAR data allow for production of terrain models with roughly 100 times the resolution of the publicly available 1/3 arc-second DEM. The three data sets cover 1) a ~6-km strip along the Yakima River, extending from the southern end of Kittitas Valley to near the confluence of the Yakima River and the Columbia River, 2) a ~700-km² area including Rattlesnake Mountain, and 3) a ~31 by 8 km northwest-trending strip that extends from Badger Mountain to Vansycle Canyon.

Detailed mapping of terraces along the Yakima River using the LiDAR data was conducted by Amos and Sorsby as part of the fluvial geomorphic analyses task as described in Section 3.5 (see also Section 8.0 and Appendix E.2). The Quaternary Studies Team also used the DEM from these data to provide information about elevation of terraces and sampling sites for cosmogenic dating (Section 4.3.2). The Rattlesnake Mountain LiDAR data were used primarily to evaluate the distribution and deformation of Quaternary deposits and surfaces along the east-central part of the range (Section 7.3). Office-based analyses, including generation of multiple topographic profiles using the 3-D analyst extension for ArcMap by ESRI or the profile/line-of-sight tool in Global Mapper, were conducted both prior and subsequent to the field mapping. The third LiDAR data set, which was acquired specifically for this study, was used to evaluate evidence for Quaternary deformation along the southeastern part of the RAW structure in the vicinity of Wallula Gap (Section 7.4).

Three-dimensional viewing using Google Earth, ArcScene, and/or Global Mapper was used to map geomorphic surfaces and identify possible lineaments. Derivative maps from the LiDAR data, including hillshade maps using varying sun-angles and inclinations, and slope maps also aided in the evaluation of geomorphic features and lineaments related to possible surface tectonic deformation and late Pleistocene

cataclysmic flooding and subsequent erosion and deposition. Observations were digitized in ArcGIS and/or using the Global Mapper software.

3.5 Yakima River Fluvial Geomorphic Analyses

A fluvial geomorphic analysis to identify and characterize tectonic deformation was completed by Dr. Colin Amos and Mr. Skyler Sorsby, University of Western Washington. The study used a combination of lab and field-based techniques to identify and isolate tectonically induced channel adjustments across major anticlinal ridges intersected by the Yakima and Columbia rivers. As outlined in Appendix E.2, this work is based on the assumption that river channel geometry (specifically width and slope) adjusts in concert with incision driven by active surface deformation, and that such adjustments can be used to identify and assess relative rates of tectonic activity. Preliminary LiDAR-based terrace mapping of the Yakima River fluvial terraces also was conducted to identify additional evidence for potential Quaternary deformation in the YFB. The results of the study are discussed in a report included in Appendix E.2; a brief summary of observations and results is provided in Section 8.0.

3.6 Quarry Wall Mapping at Finley, Washington

A key locality for assessing the style of faulting and the timing of most recent faulting along the RAW lineament is a quarry exposure near Finley, Washington. Previous studies conducted during site characterization studies for both CGS (originally referred to as WNP2) and the Basalt Waste Isolation Project involved logging quarry wall and a trench excavation in the quarry (Farooqui and Thoms 1980; WCC 1981a, b). The USGS under the direction of Drs. Brian Sherrod and Richard Blakely completed a paleoseismic log of the existing quarry wall exposure, conducted additional mapping, geomorphic interpretation of high-resolution LiDAR data, and ground-based magnetic surveys in the vicinity of the Finley quarry. The results of the USGS studies are discussed by Sherrod et al. (In Review). An evaluation of the new data by the Quaternary Studies Team is provided in Section 7.4.2.

3.7 Compilation of Paleoseismic Data for the Yakima Fold Belt

Available paleoseismic data for YFB structures was compiled by the USGS and will be published as a USGS Scientific Investigations Map (Barrett and Sherrod [In Review]). The current draft of the map and database are provided in Appendix E.4.

4.0 Stratigraphic Framework

4.1 Columbia River Basalt Group and Ellensburg Formation

The Columbia River Basalt Group (CRBG) consists of ~210,000 km³ of tholeiitic flood basalt flows that were erupted between approximately 16.8 Ma and 5.5 Ma with the main phase of eruptions between about 16.8 million years ago (Ma) and 15 Ma (Reidel et al. 2013a). The CRBG in eastern Washington in the Hanford region is divided into four formations: 1) Grand Ronde Basalt, 2) Wanapum Basalt, 3) Saddle Mountains Basalt, and 4) Imaha Basalt (Figure 4.1). About 300 separate flows have been identified; the basalt reaches its maximum thickness, ~4570 m, in the southern Pasco Basin. The youngest flow to reach the Pasco Basin is the Goose Island flow of the 8.5 Ice Harbor Member (Reidel et al. 2013a). Individual eruptions have volumes as great as 10,000 km³, and the largest occurred during Grande Ronde time (Reidel and Tolan 2013). The extrusion of volcanic basalt flows occurred very rapidly at first and then slowed over time. More time between basalt eruptions allowed for more accumulation of sediments between the younger basalt flows (i.e., Saddle Mountains Basalt). Sedimentary interbeds of the Ellensburg Formation are intercalated with and in some places overlie the CRBG. These interbeds, along with the porous basalt flow tops and bottoms, form confined aquifers that may extend across the Pasco Basin (DOE 1988; Bjornstad et al. 2010).

4.2 Suprabasalt Sediments

The Pasco Basin has been the site of deposition of clastic sediments since the cessation of basaltic volcanism approximately 8.5 million years ago (Figure 4.2) (DOE-RL 2002; Fecht et al. 2004). Post-CRBG stratigraphic units provide datums (deposits and geomorphic surfaces) that can be used to evaluate patterns and rates of deformation. Reidel et al. (1994) state that alluvial-lacustrine sediments deposited primarily by the Columbia River system show that the YFB structures were growing and displacing river channels and that lateral distribution of facies, changes in depositional style, and structural deformation of these sediments can be used to evaluate the structural evolution of the YFB.

The oldest deposits include fluvial sands and gravels and lacustrine sands, silts, and clays of the late Miocene to Pliocene Ringold Formation (Newcomb 1958; Lindsey 1995; Gustafson 1978; DOE-RL 2002). The Thorp Gravel in Kittitas Valley is believed to be a time-equivalent to the upper Ringold Formation in the Pasco Basin (Waite 1979). According to Fecht et al. (2004), the region experienced a base-level change near the end of or immediately following Ringold deposition that resulted in rapid rejuvenation of rivers, which incised into and cut laterally across the sedimentary fill (Newcomb et al. 1972). A younger sequence of mainstream fluvial sands and gravels and associated overbank sands and silts were then deposited in the newly modified river valley. Tributary sidestreams also aggraded sediments and in a few locations discharged sediments into the main trunk streams of the Columbia Basin. The mainstream and sidestream fluvial sediments form the Cold Creek Unit and are Plio-Pleistocene in age. A standardized stratigraphic nomenclature for post-Ringold deposits was established by the DOE-Richland Operations Office (DOE-RL 2002) based on regional stratigraphic and sedimentary facies observations. In addition to the Cold Creek Unit (CCU, formerly referred to as the Plio-Pleistocene unit), these include the Hanford formation and Holocene deposits. Around the margins of the basin on the flanks of the basalt ridges, Pleistocene alluvial fan deposits also are present (Baker et al. 1991).

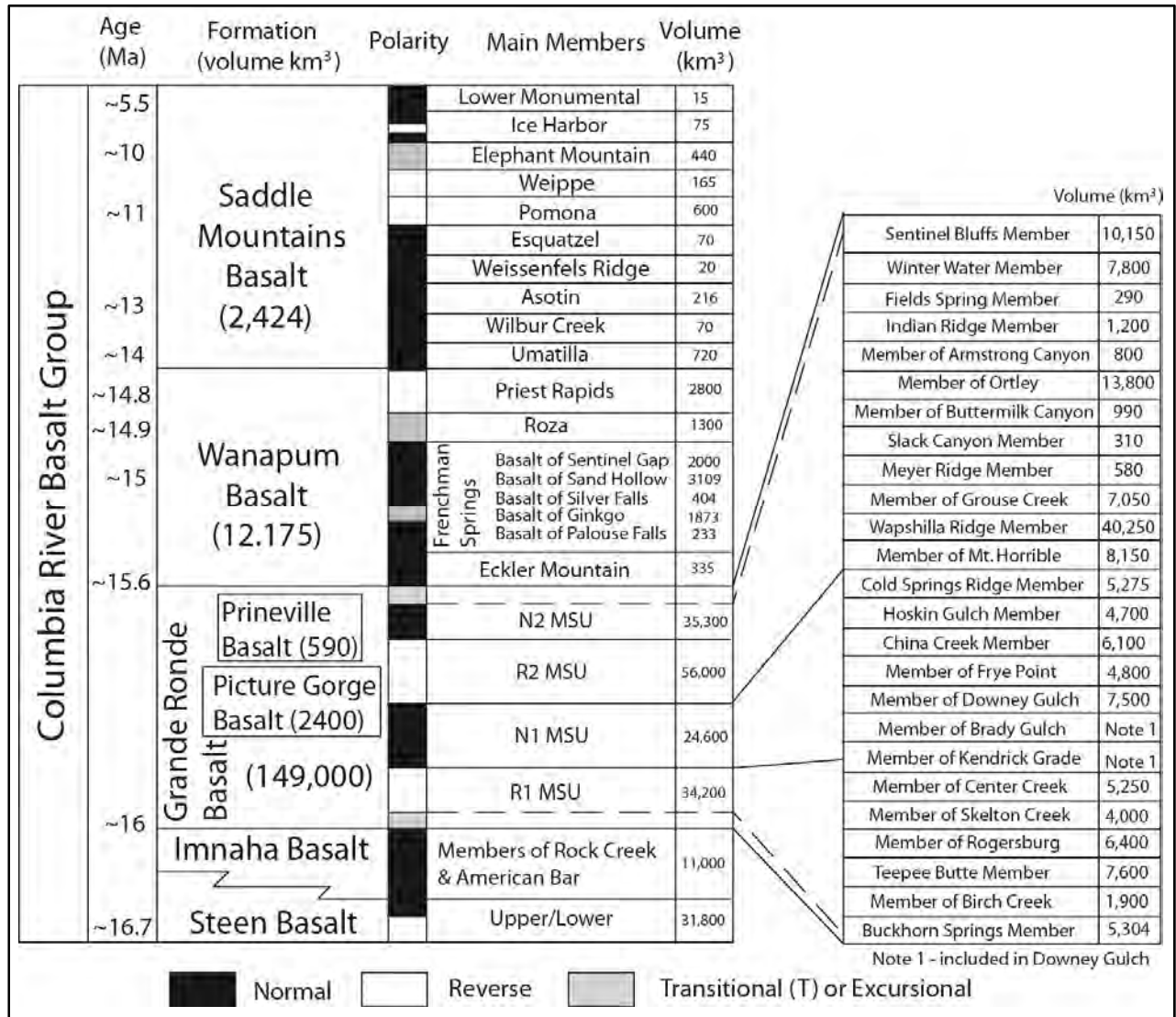


Figure 4.1. Stratigraphic nomenclature for the Columbia River Basalt Group (modified from Reidel et al. 2013b).

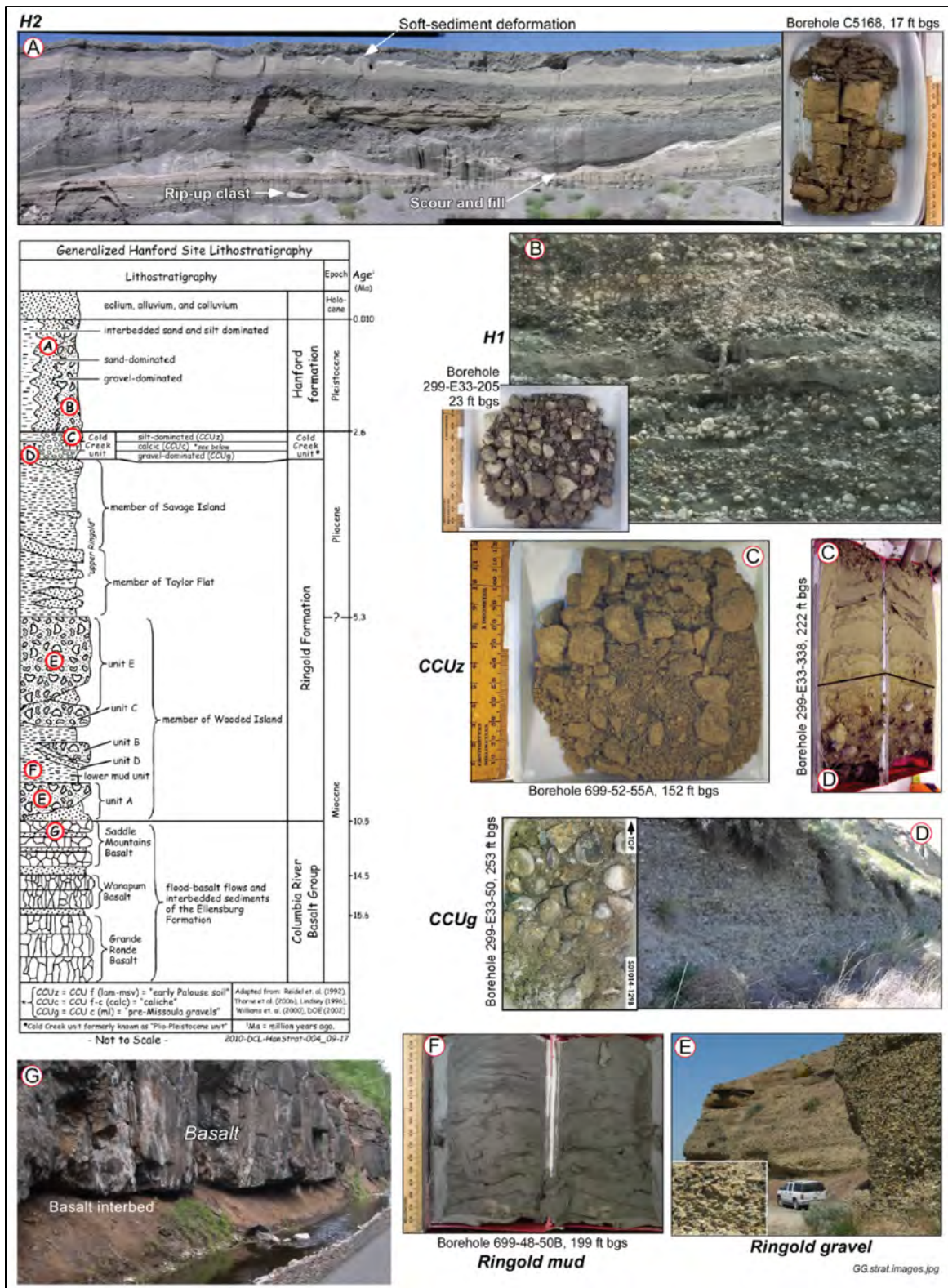


Figure 4.2. Hanford Site stratigraphy. Photos show examples of strata, both in drill core and outcrop, which are representative of the Gable Gap study area. Borehole number and depth of sample below ground surface (bgs) are shown where appropriate (from Bjornstad et al. 2010).

Brief descriptions of the key suprabasalt units used to provide constraints on the timing and rates of late Cenozoic deformation in the study area are provided below.

4.2.1 Ringold Formation

Sediments of the Ringold Formation, which were transported into the Pasco Basin by the ancestral Columbia, Clearwater/Salmon, and Yakima rivers, were derived from surrounding mountain ranges and upper margins of the Columbia Basin (Fecht et al. 1987; Lindsey et al. 1994).

The Ringold Formation, which overlies CRB in the Pasco Basin, is interpreted from fossil and paleomagnetic data to range from 10.5–3.32 Ma (i.e., late Miocene to late Pliocene age; Packer and Johnston 1979; McKee et al. 1977). Fecht et al. (1987) established a maximum age of 8.5 Ma for the Ringold Formation from K-Ar, whole rock dating of the underlying Miocene basalt (McKee et al. 1977) and a minimum age of 3.4 Ma on the basis of paleomagnetic data and vertebrate fossil evidence. More recent paleontology studies have provided additional information about the evolution of drainage systems within the Pasco Basin based on fish fossils and ages of the upper Ringold sediments (Smith et al. 2000). Smith et al. note that the fish fossils accompany three mammalian local faunas of Blancan land mammal age. White Bluffs local fauna is the oldest of three Pliocene faunas known from many localities at about 182-m (600-ft) elevation in fluvial sediments in the bluffs east of the Columbia River from 9 to 29 km north of Richland (Figure 4.3). The age of the White Bluffs fauna is estimated to be 4.5 Ma. The Blufftop locality and local fauna, which are lacustrine, are stratigraphically higher in the Ringold Formation, at 242 m (800 ft) in elevation. Its age is middle Pliocene, about 3.7 Ma. The Taunton locality is between the Pasco and Quincy basins, 27 km north of the Blufftop locality. It is stratigraphically the highest of the three faunas, at 285 m (933 ft) in elevation. Its age is 2.8–3.0 Ma. The analysis of fish species indicates that the eastern Pasco Basin was connected to the Pacific Ocean in the late Miocene, but isolated from the Pacific Ocean in the Pliocene by falls and by temperature.

Reidel et al. (1994) present a generalized interpretation of the paleogeography of the Pasco Basin during each of three phases of the Ringold Formation deposition (Figure 4.4), each of which was marked by rapid, apparently basin-wide transitions. The first change occurred at approximately 6 Ma and represents a shift from the gravelly braid plain and basin-wide paleosol systems of the lower Ringold Formation (Figure 4.4a) to the sandy alluvial systems of the middle part (Figure 4.4b). A second shift occurred by approximately 5 Ma, and is marked by the replacement of sandy alluvial systems by widespread lacustrine conditions (Figure 4.4c).

The Ringold Formation, which is up to 185 m thick in the center of the basin and pinches out against the basin-bounding ridges, is classified into five sediment facies associations as described by Lindsey (1995, 1996) (Bjornstad et al. 2010). The associations include the following:

- fluvial gravel
- fluvial sand
- overbank deposits
- lacustrine deposits
- alluvial fan deposits.

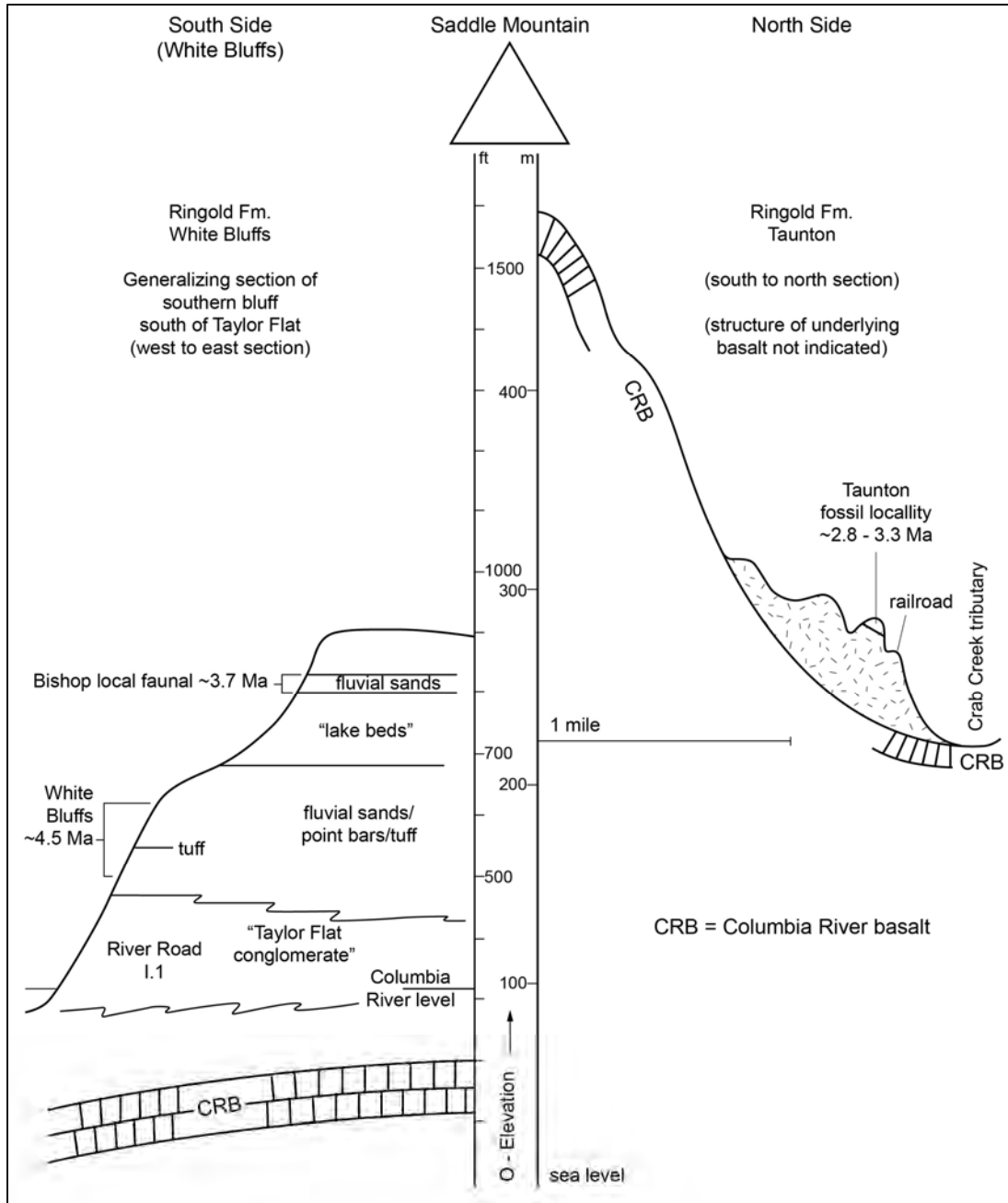


Figure 4.3. Topographic and stratigraphic relationships of Ringold faunas. Vertical scale is exaggerated. (Modified from Smith et al. 2000)

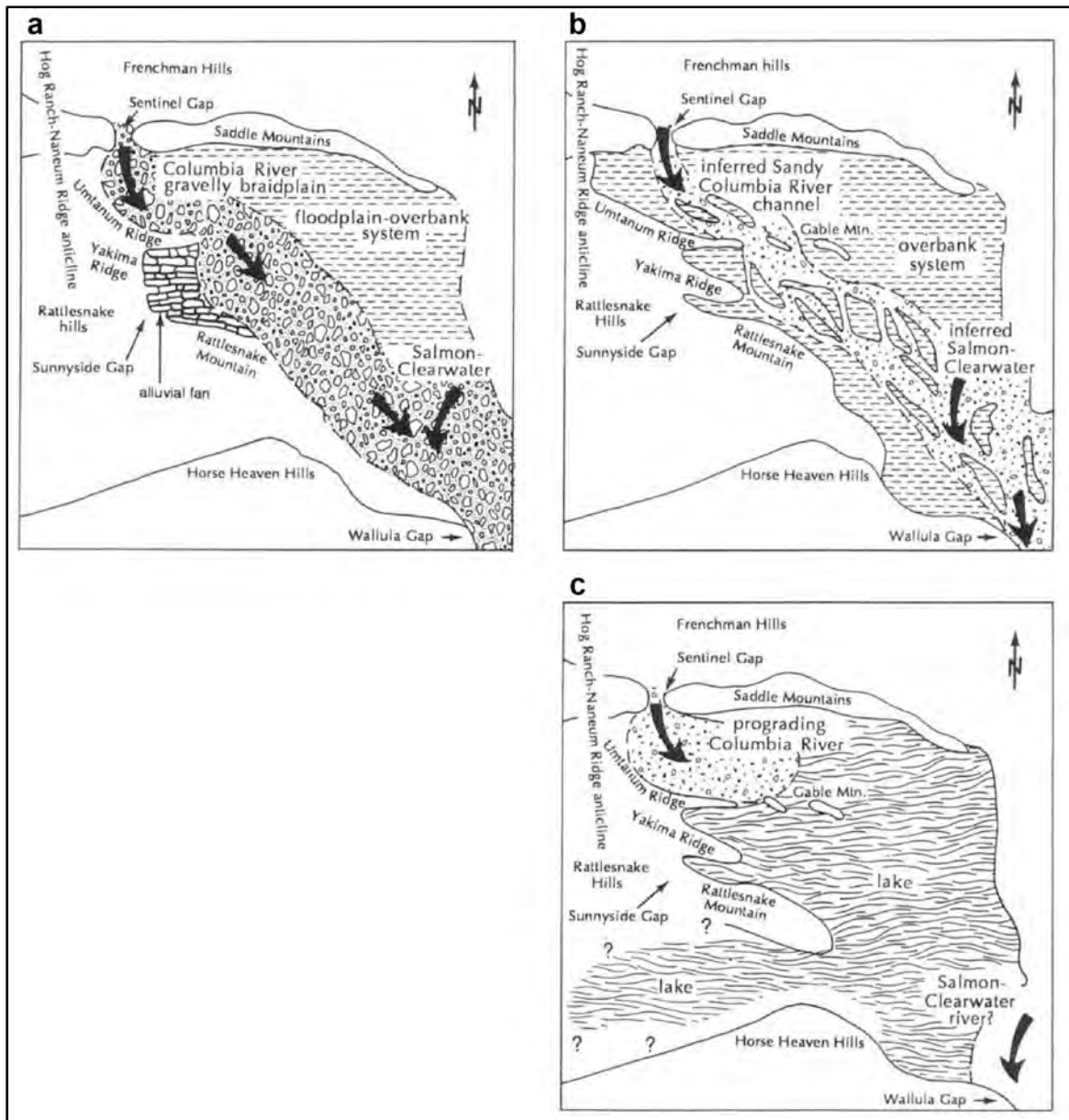


Figure 4.4. Generalized interpretation of the paleogeography of the Pasco Basin during each of three phases of the Ringold Formation deposition. The first phase (a) ended approximately 6.0 Ma, the second phase (b) approximately 5.0 Ma, and the third phase (c) approximately 3.4 Ma (from Reidel et al.1994).

Localized occurrences of talus, alluvial fans, colluviums, and slope wash on the flanks of anticlinal ridges are included in the Ringold Formation as a fanglomerate facies (Grolier and Bingham 1978; WCC 1981b). A thick sequence (~120 m) of these deposits is exposed along the north flank of Saddle Mountains in the vicinity of Smyrna Bench. There is some disagreement regarding the age of the youngest sediments in this sequence, but West (1997) suggests that the upper deposits mapped as Ringold fanglomerate may be Pleistocene (as young as 100 to 400 thousand years ago [ka]).

4.2.2 Thorp Gravel

The Thorp Gravel, located in the Kittitas Valley along the western Columbia Plateau, is believed to be the lateral equivalent to the Pliocene age upper Ringold unit (Waitt 1979). Fission track dates on tephra from the upper part of this deposit are Pliocene (approximately 3.7 Ma). Deposits of the Thorp Gravel are deeply weathered, weakly cemented and well-rounded gravel, and coarse sand that occur in high terraces along the Yakima River and its tributaries. Thorp Gravel unconformably overlies the CRBG and Ellensburg Formation and consists mainly of sidestream gravels of locally derived CRB and mainstream gravels of silicic to intermediate volcanic and plutonic rocks (Rigby and Othberg 1979; Waitt 1979).

4.2.3 Cold Creek Unit

Regional incision triggered by rapid downcutting of the ancestral Columbia-Clearwater-Salmon River system began about 3.4 Ma (Fecht et al. 1987; DOE 1988; Reidel et al. 1994) and resulted in the removal of up to 200 m of Ringold Formation sediments in the central part of Pasco Basin. Tolan and Beeson (1994) suggest that the present Columbia Gorge was formed by entrenchment during post-Troutdale time due to rapid uplift of the Cascade Range in northwest Oregon in the past 1–2 Myr. The CCU comprises deposits that accumulated within the central Pasco Basin during the period 3–2 Ma, after regional incision of the Ringold Formation and prior to the initiation of Ice Age cataclysmic flooding about 1.5 to 2.5 Ma (Bjornstad et al. 2001). After incision a new base level was established at approximately the 90-m elevation at Wallula Gap, after which aggradation and backfilling occurred locally on the post-Ringold Formation landscape.

The CCU deposits are known primarily from subsurface borings in the central Pasco Basin, but some exposures are reported around the basin perimeters. DOE-RL (2002) reports that a surface deposit of the CCU is present at the base of Yakima Bluffs (Baker et al. 1991; Lindsey et al. 1994) (Figure 4.5).

4.2.4 Cataclysmic Flood Deposits

Multiple episodes of cataclysmic Ice Age floods are recorded in the Pacific Northwest. Based on evaluation of surface exposures and borehole studies in southeastern Washington, Bjornstad et al. (2001) suggested the oldest floods occurred as early as 1.5–2.5 Ma. However, more detailed magnetostratigraphy of sediments composing the Cold Creek cataclysmic flood bar in the Pasco Basin, Washington (Pluhar et al. 2006), suggests the onset of Missoula floods or similar events prior to 1.1 Ma, later than previously suggested by Bjornstad et al. (2001).

During the most recent ice age, starting ~30 kyr BP, the Purcell Trench lobe of the continental ice sheet spread down the Pend Oreille River near the Idaho-Montana border. This lobe dammed the Clark Fork River, impounding glacial Lake Missoula (Figure 4.6). This dam then broke out episodically throughout marine oxygen isotope stage (MIS)-2 (29–14 ka) with the most recent floods occurring during the late Wisconsin. Limiting ages on the Cordilleran ice sheet range from ^{14}C dates as young as ~17,200 years before present (yr BP), and postglacial dates as old as 11,000 yr BP in southernmost British Columbia (Clague 1981).

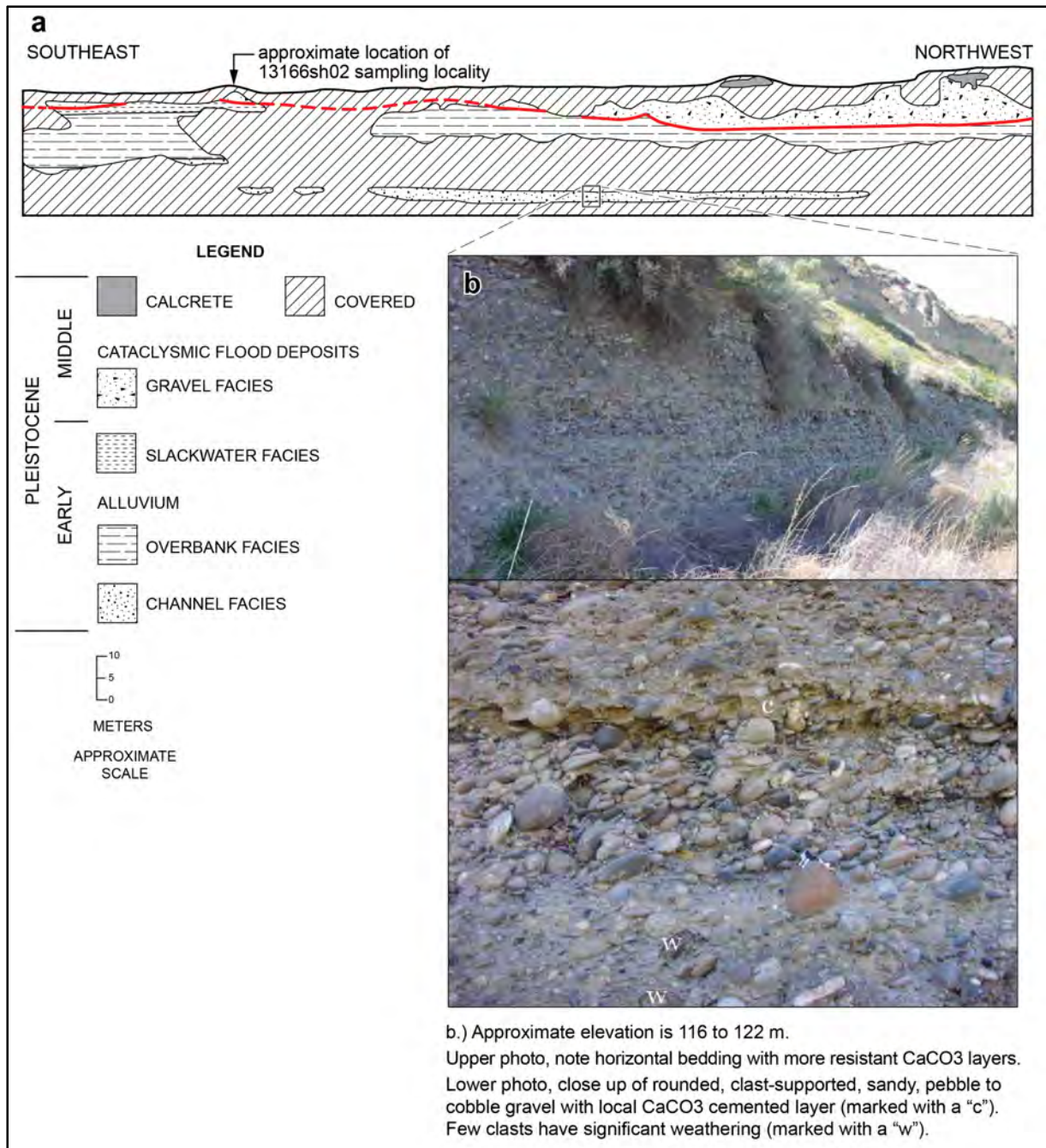


Figure 4.5. Yakima Bluff locality. a) Trace of a photomosaic of the Yakima Bluffs exposure. Deposits above red line have normal polarity, below red line they are reversed (modified from Baker et al. 1991). b) Coarse-grained multilithic lithofacies of the Cold Creek Unit at Yakima Bluffs (from DOE-RL 2002).

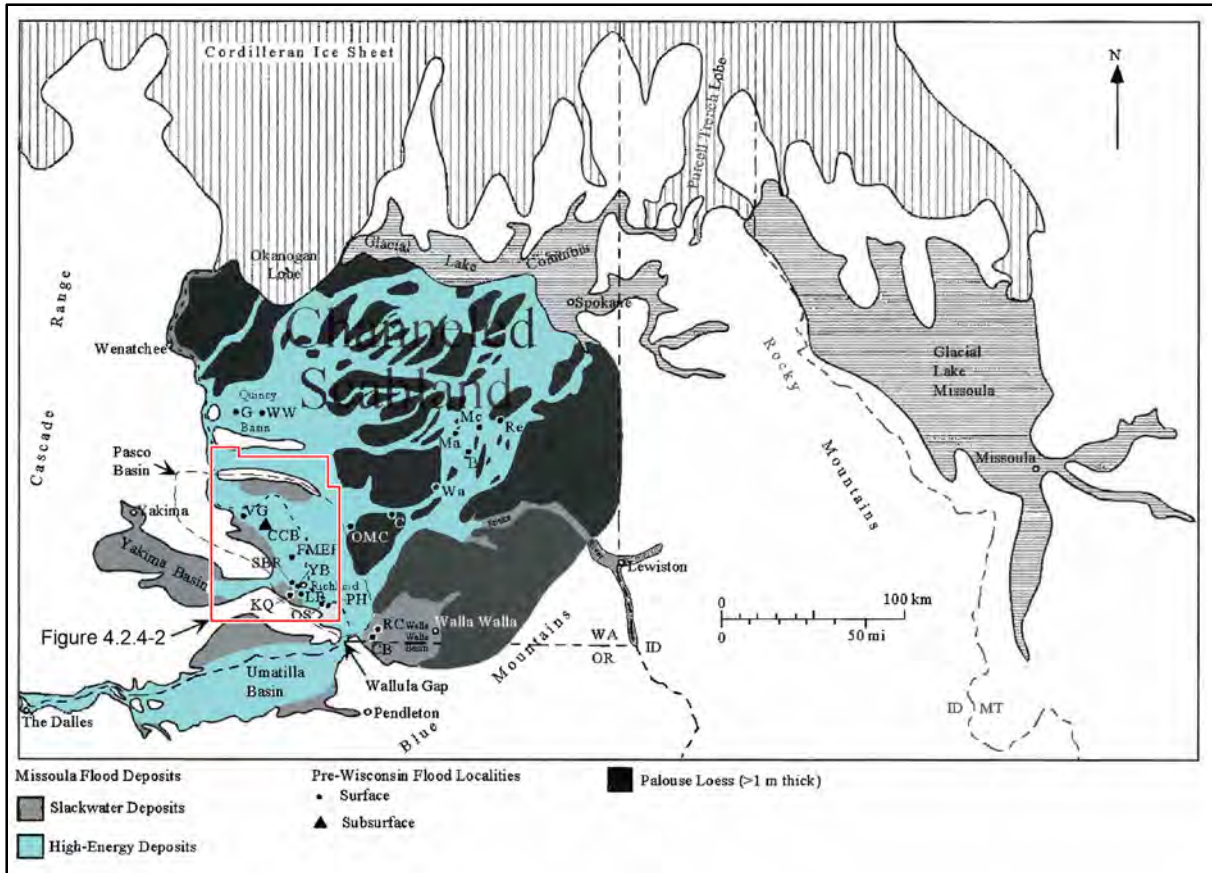


Figure 4.6. Map showing principal features related to Ice Age cataclysmic floods (modified from Bjornstad et al. 2001). (See Section 4.2.4, Table 4.1 for explanation of locality abbreviations.)

Hydraulic damming of flood waters at Wallula Gap periodically generated a temporary lake, Lake Lewis, that resulted in deposition of bedded, fine-grained sediment (commonly referred to as slackwater deposits or Touchet Beds) in the Pasco, Walla Walla, and Yakima basins. There is some disagreement among researchers regarding the number of glacial-outburst floods recorded in the Touchet bed stratigraphy. Waitt (1985) concludes that there were more than 40 successive, flood-laid, sand-to-silt graded rhythmites and that each represents a separate flooding event. Waitt presents evidence that glacial Lake Missoula discharged episodically and repeatedly with an average period between floods of a few decades. Other researchers (WCC 1981b; Bjornstad 1980, 1982; Bunker 1982) argue that the sequence of rhythmites exposed in Walla Walla Basin was deposited by one or two floods, each depositing numerous graded beds.

MIS 2 slackwater sediment, ice-rafted debris, and other flood features are observed at elevations as high as 365 m, the estimated maximum height of flood waters in south-central Washington (Baker et al. 1991; O'Connor and Baker 1992). The maximum height of Lake Lewis at Wallula Gap was approximately 380 m (Last et al. 2012). Prior to the mega floods in the latest Pleistocene there is evidence of other episodes of cataclysmic flooding during MIS-4 (65-80 ka) (McDonald and Busacca 1992). McDonald et al. (2012) identify a regional flood-cut unconformity in the Channeled Scabland and Palouse region of Washington to about 77–46 ka. This unconformity is overlain by loess deposits that

began to accumulate in MIS4 and continued through MIS3 in response to increased sediment supply and availability following this penultimate episode of glacial-outburst flooding.

At least two pre-Wisconsinan (>130 ka) periods of glacial-outburst flooding are indicated by field evidence (Figure 4.7). One or more middle Pleistocene flooding events is evidenced by normal magnetic polarity, calcrete-capped deposits that yield Th/U-series age dates from 200 to >400 ka (Baker et al. 1991; Table 4.1). Surface exposures of these gravels have been identified at several locations in the southern part of Pasco Basin (Figure 4.7). At these locations prominent >1-m-thick petrocalcic horizons (Stage III-IV carbonate development) are present. Baker et al. (1991) report that these deposits lie along a prominent terrace at an elevation of ~140 m. Further inspection of elevation and new dating analyses completed as part of this study show that the deposits range in elevation from as high as ~180 m on the Bombing Range Road surface (location 13168sh01) to as low ~130 m along Leslie Road (location 13129sh01) (see Section 4.3.1 for more detailed discussion of the deposits at these locations). The variation in elevation could be due to a variety of factors attributed to the unique “mega” depositional character of the deposits; alternatively the varying elevations could be due to separate flooding events. Differential tectonic uplift also could be a factor.

Early Pleistocene flooding is recorded by surface exposures of fine-grained slackwater deposits and by subsurface evidence of buried giant flood bar deposits with reversed polarity (>780 ka) (Baker et al. 1991; Bjornstad et al. 2001; Pluhar et al. 2006). Magnetostratigraphic data from borings in the Cold Creek bar in the western Pasco Basin indicate cataclysmic flood deposits with normal magnetic polarity occur between reversed magnetic polarity flood deposits. Pluhar et al. (2006) favor an interpretation that the normal zone correlates with the Jaramillo subchron (1.07–0.99 Ma), but acknowledge that the previous Bjornstad et al. (2001) correlation to the Olduvai normal subchron (1.95–1.75 Ma) cannot be precluded (Figure 4.8). It appears that at least three glacial maxima during the early Pleistocene are recorded at the eastern Cold Creek bar (Pluhar et al. 2006).

Yakima Bluffs is a key locality where reversed fine-grained flood deposits are exposed beneath normally magnetized flood gravels of middle Pleistocene age (locality 13166sh02) (Figure 4.5). At the base of the flood sequence at this site are at least eight reversed-polarity rhythmite beds that are evenly bedded, exhibit upward grading in grain size, and are characterized by planar- to climbing-ripple laminations similar to late Pleistocene slackwater flood deposits (Bjornstad et al. 2001). Other less definitive locations where early Pleistocene floods may be indicated by weathered horizons underlying middle Pleistocene flood deposits are exposures within and around Badger Coulee (i.e., the A&B quarry near Kiona and Leslie Road).

In the Pasco Basin, cataclysmic flood deposits informally referred to as the Hanford formation are ubiquitous below an elevation of about 250 m and are subdivided into three main facies (interbedded sand and silt dominated, sand dominated, and gravel dominated) (DOE-RL 2002). Coarse-grained flood gravels from the last (late Wisconsin) episode of Missoula flooding locally overlie the older flood gravels. Soil development in these younger gravels is characterized as weak, and is limited to filaments and thin coatings of carbonate on the undersides of gravel clasts (Stage I carbonate development) (Baker et al. 1991). Fine-grained flood deposits are divided into two facies: 1) a plane-laminated sand facies and 2) a rhythmite facies, also referred to as Touchet Beds. Plane-laminated beds, which are most common in the central part of the basin, grade laterally into slackwater rhythmite deposits toward basin margins and are considered to be a facies transitional between the coarse-grained and rhythmite-flood facies (Baker et al. 1991).

Table 4.1. Selected pre-Wisconsin cataclysmic flood localities in southeastern Washington. See Figure 4.6 for map showing locations. (Table modified from Bjornstad et al. 2001)

Locality ^(a)	Pre-Wisconsin Flood Period	Description	Reference ^(b)
Surface			
Benge (B) SE27/17N/37E	One middle and one early Pleistocene	Flood-scoured unconformities in Palouse loess; reversed below lower unconformity	McDonald and Busacca 1988 (BEH-1)
Connell (C) ^(c) SWI0/13N/33E	One middle Pleistocene?	Flood-scoured erosional unconformity in Palouse loess	McDonald and Busacca 1988, 1992 (CON-2)
Cummings Bridge (CB) ^(c) SE35/7N/32E	One middle Pleistocene?	Two slack water flood sequences separated by a high relief flood-scoured unconformity that truncates a clastic dike; perhaps only early Wisconsin?	Bjornstad 1980; Moody 1987
Fuels and Materials Examination Facility (FMEF) S18/11N/28E	One middle and maybe one early Pleistocene?	Three flood sequences with truncated elastic dikes; lowermost dike truncated along calcic soil; lower sequences early and/or middle Pleistocene?	Baker et al. 1991
George (G) NW31/19N/24E	One early Pleistocene	Basaltic flood gravels capped with a 1.5-m-thick Stage III-VI calcrete cap; thick (8 cm) weathering rinds on basalt cobbles; floods from a surmised unknown western(?) source	Baker 1973, 1978; Nummedal 1978; Patton and Baker 1978
Kiona Quarry (KQ) (A&B Asphalt Borrow Pit) ^(d) NE29/9N/27E	One middle and possibly one early Pleistocene?	Normally magnetized flood gravel with calcrete cap (calcrete dated at >210 and >400 ka); oxidized flood gravels at depth	Baker et al. 1991; Fecht et al. 1999
Leslie Road (LR) NW25/9N/28E	One middle and possibly one early Pleistocene?	Flood gravels capped by calcrete with maximum age of >400 ka; another zone of calcrete-capped flood gravels at depth	Baker et al 1991
Macall (Mc) NW17/18N/38E	One early Pleistocene	Reversed-polarity soil over flood gravels capped by calcrete dated at >350 ka	Baker 1978; Patton and Baker 1978; Baker et al. 1991
Marengo (Ma) NW31/18N/37E	One early Pleistocene	Flood gravel overlain by reversely magnetized loess and calcrete cap dated at 800 ka	Baker 1978; Nummedal 1978; Patton and Baker 1978; Baker et al. 1991
Oak Street (OS) SE19/8N/30E	One middle Pleistocene	Normally magnetized flood gravel with calcrete cap	Baker et al. 1991
Old Maid Coulee (OMC) NE24/13N/31E	One early Pleistocene	Reversed-polarity soil over flood gravels with calcrete cap dated at >350 ka; 20% of basalt clasts in calcrete zone completely weathered	Bryan 1927; Flint 1938; Bretz et al. 1956; Baker 1973, 1978; Patton and Baker 1978
Poplar Heights (PH) N29/8N/30E	One early Pleistocene	Reversed-polarity sand lens within flood gravels	Baker et al. 1991

Table 4.1. (contd)

Locality ^(a)	Pre-Wisconsin Flood Period	Description	Reference ^(b)
Surface			
Reese Coulees (RC) N25/7N/32E	One early Pleistocene	Hanging flood coulee partially filled with reversed-polarity, pedogenically altered, colluvium/slope wash containing ice-rafted erratics near base	Bjornstad and Fecht 1989; Jaffee and Spencer 2000
Revere (Re) SE31/19N/39E	One early Pleistocene	Reversed-polarity, pedogenically altered loess sequence over flood gravels	Baker 1978; Patton and Baker 1978; Baker et al. 1991
South Bombing Range Road (SBR) SW8/9N/28E	One middle Pleistocene	Normally magnetized soil over flood gravel with calcrete cap	Baker et al. 1991
Vernita Grade (VG) SE18/13N/25E	One early Pleistocene	Reversed-polarity sand lenses within flood gravels	Baker et al. 1991
Washtucna (WA) SW14/15N/35E	One middle Pleistocene	Flood-scoured erosional unconformity in Palouse; loess filled with normal-polarity loess	McDonald and Busacca 1988 (WA-9); Baker et al. 1991 (WA-9)
Winchester Wasteway (WW) NW6/19N/2S E	One early Pleistocene and possibly one middle Pleistocene	Platy calcrete over flood gravels believed to correlate with early Pleistocene flood at George, 10 km to the west; overlying flood sand may be middle Pleistocene	Bahr 1973, 1978; Nummedal 1978
Yakima Bluffs (YB) NE16/9N/28E	One middle and several or more early Pleistocene	Reversed slack water sequence (up to eight rhythmites) overlain by normally magnetized flood gravel and calcrete cap dated at 205 ka	Baker et al. 1991; Fecht et al. 1999
Subsurface			
Cold Creek bar (CCB) boreholes W22-48 and -50) NE 12/12N/25E	At least one earliest Pleistocene	Base of sand-dominated flood sequence in pair of adjacent boreholes is normally magnetized; probably represents Olduvai subchron of the Maruyama	
Cold Creek bar (CCB) (borehole E 1 7-21) NW11/12N/26E	At least one early Pleistocene and probable earliest Pleistocene	Thick (13-m) sand-dominated flood sequence with reversed polarity toward middle of CCB	Reidel et al. 1998
Cold Creek bar (CCB) (borehole E33-33SI SE34/13N/26E	At least one early Pleistocene and one earliest Pleistocene	Reversed polarity over normal polarity in sand-dominated flood facies from lower half of CCB	
Note: The middle Pleistocene includes period from 130 to 783 ka, early Pleistocene includes period from 783 ka to 2.58 Ma, and earliest Pleistocene includes period from 1.77 to 2.58 Ma.			
(a) Coordinates indicate section/township/range.			
(b) Site identification abbreviation in parentheses. (See Bjornstad et al. [2001] for references cited in the table.)			
(c) Questionably pre-Wisconsin			
(d) The exposure cited is not in the Kiona Quarry, which is a basalt quarry. The exposure is in the A & B Asphalt Borrow Pit.			



Figure 4.7. Digital elevation model map of part of the Pasco Basin. Arrows show principal flood routes. Significant accumulations of flood deposits, including several giant flood bars, signify areas of deposition as floodwaters entered hydraulically dammed Lake Lewis (from Bjornstad et al. 2001).

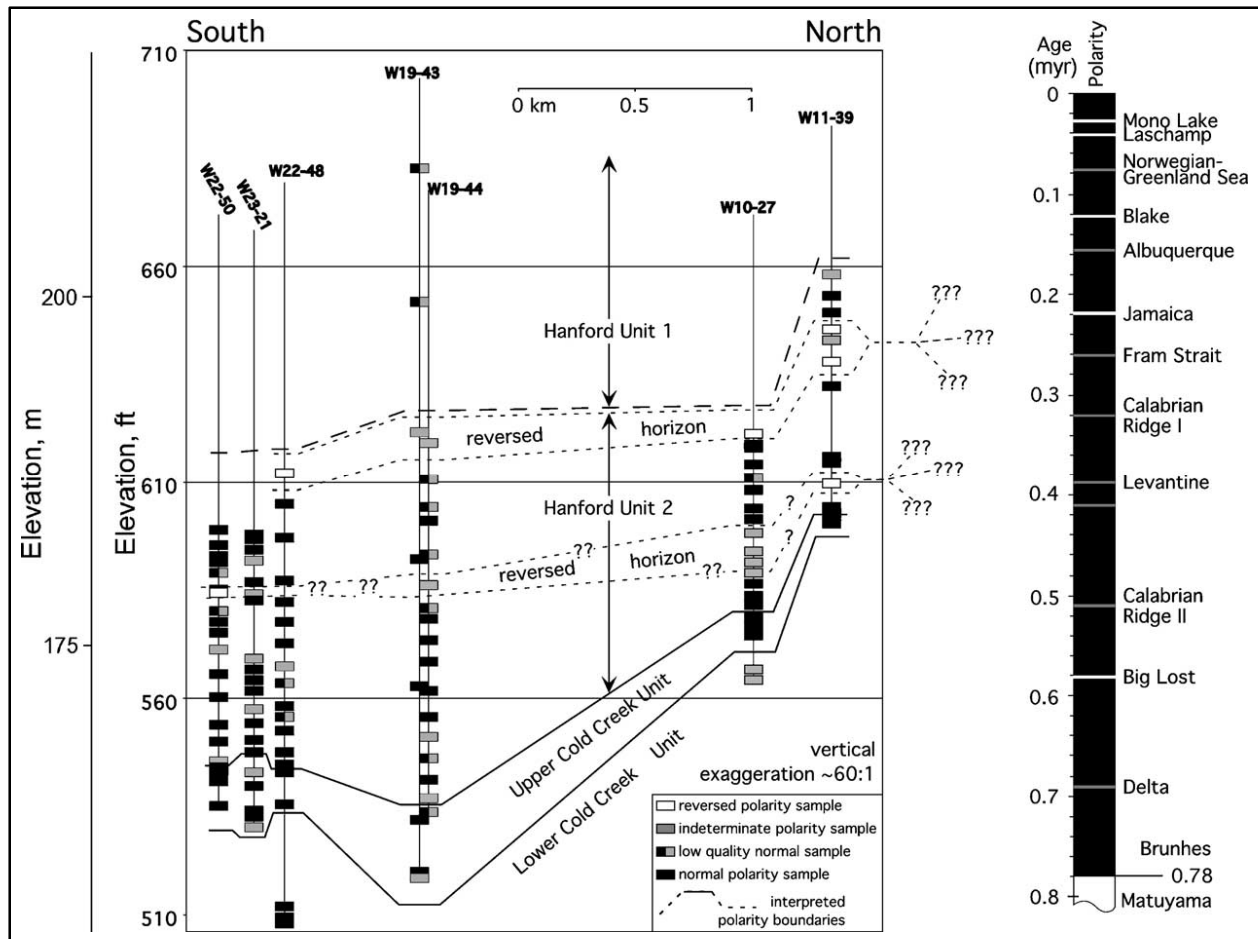


Figure 4.8. Magnetostratigraphy at eastern Cold Creek bar. Paleosols are related to interglacial episodes. (From Pluhar et al. 2006)

4.2.5 Pleistocene Alluvial Fans

Baker et al. (1991) summarize previous studies that mapped and estimated ages of Quaternary deposits and soils in the Pasco Basin. At least three ages of sidestream alluvium are identified by Baker et al. (1991) based on paleosol development, tephra dating, and stratigraphic relationship with other units. The oldest sidestream alluvium, rarely exposed, is weathered, subangular to subrounded, basaltic alluvium capped by silcrete. This alluvium is estimated to have formed in late Pliocene and/or early Pleistocene time, perhaps under more humid conditions. No exposures of the silcrete-capped deposits were observed during field reconnaissance for this study.

The second, younger coarse-grained alluvial unit, which is locally present along exposed basin margins, consists of angular, unweathered basalt clasts, cemented with one or more carbonate horizons ranging from Stage II to IV in development. This unit is estimated to be early to late Pleistocene in age, based on correlation with intertonguing loess units having both reversed and normal polarities. The oldest alluvial fan unit mapped on Rattlesnake Mountain as part of geologic studies conducted for this study exhibited Stage IV carbonate development and is inferred to be of middle Pleistocene age based on correlation to $^{230}\text{Th}/\text{U}$ -series dated pedogenic carbonate rinds in nearby deposits exhibiting similar Stage IV development (see Section 7.3.2.1).

Younger alluvial fans of late Pleistocene to Holocene age are observed on the flanks of the basalt ridges. On the northern flank of Rattlesnake Mountain, three such fan units have been differentiated (see Section 7.3.2).

4.2.6 Holocene Deposits

Holocene fluvial deposition started soon after the final cataclysmic floods from Glacial Lake Columbia upstream of the Pasco Basin, which have been radiocarbon dated at $12,800 \pm 50$ years before present (Lenz et al. 2010). Fecht et al. (2004) provide detailed description of late Pleistocene and Holocene fluvial deposits and bedforms in the Hanford Reach of the Columbia River. Nonfluvial surficial processes active on the lower slopes of the river valley have resulted in eolian, colluvial, sidestream-alluvial, and landslide deposition (WCC 1981b; NRC 1982).

4.2.7 Tephrochronology

Widespread tephra units in the Pacific Northwest, which have been dated and correlated using the composition of various oxides in the volcanic glasses, provide useful temporal datums within the study area (WCC 1981b; Fecht et al. 2004). Table 4.2, which is modified from WCC (1981b) summarizes the estimated ages of the tephra units commonly cited in the licensing documents (Energy Northwest 1982; NRC 1982). Revised ages for some of the key tephra used in this study to evaluate timing of possible latest Pleistocene to Holocene events based on more recent publications and research are provided in the last two columns of Table 4.2.

Table 4.2. Late Pleistocene and Holocene tephra sequence and chronology in the Study Region. (Modified from WCC 1981b)

Volcano/Tephra	Age (ka)	Source	Revised Age (cal. kyr BP)	Source
St. Helens "W"	0.45 to 1.1	Mullineaux and others (1975)		
St. Helens "B"	1.5 to 2.5	Mullineaux and others (1975)		
St. Helens "P"	2.5 to 3	Mullineaux and others (1975)		
St. Helens "Y"	3 to 4	Mullineaux and others (1975)		
Mazama	7	Davis (1978)		
St. Helens "J"	8 to 12	Mullineaux and others (1975)		
Glacier Peak "C"	11.07 to 11.3	Westgate and Evans (1978)		
Glacier Peak "G"			13.7 to 13.4	Kuehn et al 2009
Glacier Peak "M"	12 to 12.57	Westgate and Evans (1978)		
St. Helens "J"	12	Moody (1978)		
St. Helens "S"	13	Mullineaux and others (1977)	15.5	Mullineaux 1986
St. Helens "S"	--	--	16	Clynne et al. 2008
St. Helens "K"	13.6 \pm 0.04 to 18.6	Moody (1978)		
St. Helens "M"	18 to 20	Smith (1980)		
Mazama (Wono bed)	24.48 \pm 0.43 to 33.65 \pm 1.72	Davis (1978)		
St. Helens "C"	36 to 37.6	Smith (1980)	46.3 \pm 4.8	Berger and Busacca 1995

Some of the key volcanic tephra in the study area are briefly described below:

- Mount St. Helens Set “S” (commonly observed as a couplet or triplet), was initially dated at 13 ka (Mullineaux et al. 1977) and is observed within flood sediments and loess deposits (WCC 1981b). At Burlingame Ditch near Walla Walla, this tephra is observed at an elevation of ~185 m and is overlain by 11 rhythmites. McDonald et al. (2012) summarize more recent age estimates for this tephra unit that has been identified at the base of the youngest post-flooding LI loess unit. These include a commonly reported calibrated radiocarbon age of 15.5 ka (Mullineaux 1986) that was recently refined to about 15.8 ka based on secular variation (13,350 to 14,400 ¹⁴C yr BP; Clague et al. 2003). These ages combined with other luminescence and radiocarbon ages (e.g., Richardson et al. 1997; Spencer and Knapp 2010) suggest the eruptions occurred about 16 ka (Clyne et al. 2008).
- Glacier Peak tephra (typically found as a couplet, per WCC 1981b), was initially dated at 12 ka (Porter 1978). This tephra, which is commonly observed within loess on ridges above an elevation of 150m in the Columbia River valley, post-dates the larger cataclysmic floods (Fecht et al. 2004). Foit et al. (1993) report a ¹⁴C age of 11,200 yr BP for a distal Glacier Peak couplet(s) that occurs stratigraphically, both above and below Mount St. Helens J tephra in east-central Washington. Based on a more complete analysis of the highest quality ages in a Bayesian framework, Kuehn et al. (2009) obtained an age of 13,710–13,410 cal. yr BP (2 sigma or 95% confidence) or ca. 11,600 ± 50 ¹⁴C yr BP.
- Mazama tephra, dated at 7 ka (Bacon 1983). All samples assigned to the 7-ka Mount Mazama tephra collected and analyzed by WCC (1981b) were from eolian loess units.

4.2.8 Late Pleistocene Loess and Soil Stratigraphy

McDonald et al. (2012) presents a regional stratigraphic framework that integrates late Pleistocene loess stratigraphy, pedostratigraphy, and tephrochronology (Figure 4.9). The timing and nature of loess accumulation, which is constrained by detailed luminescence dating and tephrochronology, is related to glacial advances and associated glacial-outburst floods in the study region. Buried soils, which are correlated to the major loess units, are briefly described below.

- Sand Hills Coulee Soil. This buried soil, which underlies the Modern soil, is developed in the top of the L1 loess unit, and likely formed during the latest Pleistocene to early Holocene (McDonald and Busacca 1992; Sweeney et al. 2005). The base of the L1 loess unit contains the Mount St. Helens set “S” tephra at its base.
- Washtucna Soil. This soil, formed in the L2 loess (~77 to 16 ka) is a well-developed buried soil, characterized by Stage III to IV carbonate morphology (Gile et al. 1966) with vertical and horizontal seams of soil carbonate in most exposures (McDonald and Busacca 1990, 1992). The soil is estimated to have formed between approximately 40 and 20 ka under cold and dry conditions during the last glacial maximum.
- Old Maid Coulee Soil. This moderately developed soil underlies the Washtucna soil. The Mount St. Helens “C” tephra (46.3 ± 4.8 ka) provides a constraint on the age of this soil.
- Devils Canyon Soil. This soil, which lies at the top of the L3 loess unit, exhibits soil structure (carbonates and cylindrical nodules) similar to the Washtucna soil; based on luminescence dates, this soil likely formed during the cold conditions of MIS 4 (Berger and Busacca 1995; Richardson et al. 1997).

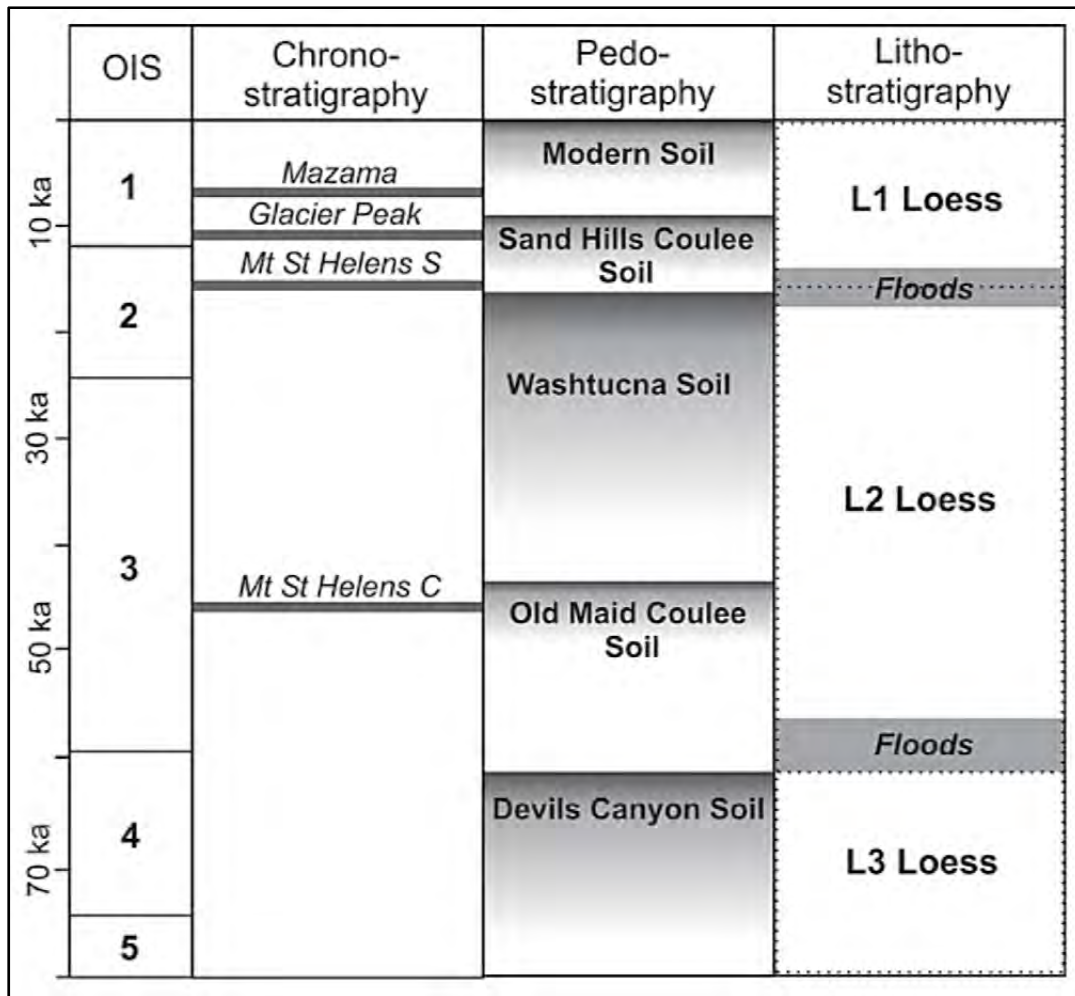


Figure 4.9. Summary of regional stratigraphy including chronostratigraphic markers (tephras) pedostratigraphy (buried soils), and lithostratigraphy in relation to Oxygen Isotope Stages (from McDonald et al. 2012)

4.3 Geochronology Studies

This section describes geochronology studies that were conducted as part of the Quaternary geologic studies (QGS) for the Hanford Level 3 PSHA.

4.3.1 ²³⁰Th/U-Series Dating

A number of well-developed carbonate soils in the Pasco Basin were identified in previous studies (e.g., WCC 1981b; Baker et al. 1991; Bjornstad et al. 2001). We visited a number of these sites to identify well-suited localities for geochronology studies using the ²³⁰Th/U-series dating method. The purpose of dating these deposits is to calibrate the relative carbonate soil development with a numerical age date. The numerical ages obtained using this approach provide a minimum age for the pedogenic carbonate (calcrete and caliche) and hence the deposit in which the carbonate was deposited. This calibration could then be used elsewhere in the study area where carbonate soils were identified to estimate the approximate age of the deposits. This approach was very helpful in the Rattlesnake

Mountain area, where sensitive cultural issues prohibited the collection of carbonate rinds for dating purposes. Members of the Quaternary mapping team and Dr. Jim Paces (USGS) visited a number of localities in June 2013. Five sites were selected at which to attempt $^{230}\text{Th}/\text{U}$ -series dating of pedogenic rinds of gravel clasts. A number of these sites had been dated using a similar approach as part of earlier investigations as reported by Baker et al. (1991) (Table 4.3); however, improvements in the $^{230}\text{Th}/\text{U}$ -series technique allows for more precise results, reducing the uncertainty of possible ages. Sites dated in this study, referenced using geographic names, include South Bombing Range Road, Yakima Bluffs, MCBONES (Mid-Columbia Basin Old Natural Education Sciences), Steptoe quarry, and Finley quarry (Figure 4.10). The following sections provide descriptions of each site and the findings of the dating.

Table 4.3. Radiometric ($^{230}\text{Th}/\text{U}$ -series) ages from pre-Wisconsin cataclysmic flood deposits in southeastern Washington. See Figure 4.6 for map showing locations. (Table modified from Bjornstad et al. 2001)

Sample Locality	Sample Number	Description	Reported Age (ka) ^(a)	Remarks
Kiona Quarry (KQ) (A & B Asphalt Borrow Pit) ^(b)	C9052	Flood gravel	>210	Carbonate-coated gravel, resample of C9260
Kiona Quarry((KQ) (A & B Asphalt Borrow Pit) ^(b)	C9260	Flood gravel	>400	Carbonate-coated gravel, resample of C9052
Sample Locality	Sample Number	Description	Reported Age (ka) ^(a)	Remarks
Leslie Road (LR)	C9264	Flood gravel	>400	Same as RHT-10 and RHT-11
Leslie Road (LR)	RHT-10	Flood gravel	250 +250/-70	Same as C9264 and RHT-11
Leslie Road (LR)	RHT-11	Flood gravel	220 +380/-70	Same as C9264 and RHT-10
Macall (Mc)	C3005	Flood gravel	50 ± 9 (>350)	
Marengo (Ma)	C3014	Calcrete over lower flood gravel sequence	120 ± 15 (>260)	
Old Maid Coulee (OMC)	C4002	Calcified loess over flood gravel	>350	
Yakima Bluffs (YB)	C9116	Flood gravel	92 ± 8 (205 ± 20)	From normal-polarity zone

Source: Baker et al. 1991.

(a) Probable age in thousands of years. Maximum age in parentheses.

(b) The exposure cited is not in the Kiona Quarry, which is a basalt quarry. The exposure is in the A & B Asphalt Borrow Pit.

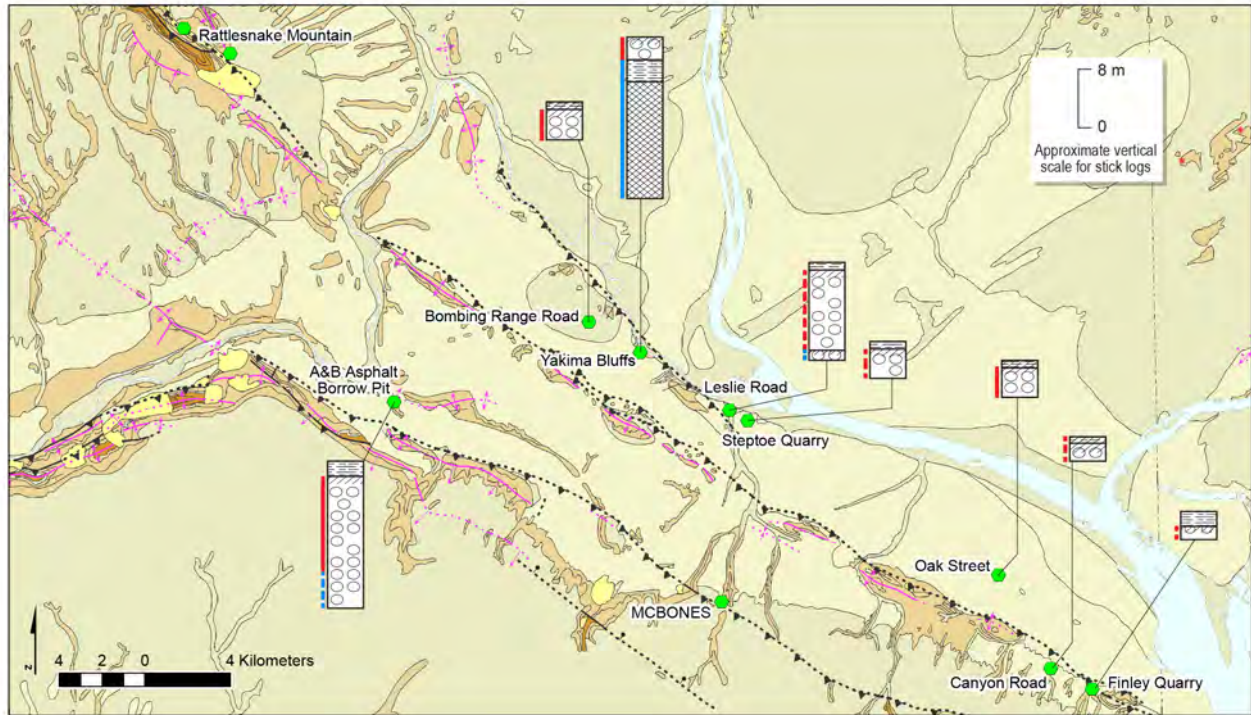


Figure 4.10. $^{230}\text{Th}/\text{U}$ -series sample sites (this study) relative to other locations where carbonate soils were observed during Quaternary Studies Team reconnaissance. Stick logs and paleomagnetic data are modified from Baker et al. (1991). Red and blue lines indicate normal and reverse polarity, respectively. Solid line indicates polarity was measured; dashed line indicates the polarity is inferred.

4.3.1.1 South Bombing Range Road

The South Bombing Range Road site (13168sh01) is on a broad flat plain located between the aligned RAW-Rattles anticlines and the northwest-trending Horns Rapids anticline. As shown on the State 100k scale geologic map, the surface is underlain by Quaternary flood gravels. The approximate elevation of the site is 180 m. Based on a structure contour map on the top of basalt (Myers et al. 1979), a relatively flat bedrock surface at an elevation of approximately 140 m underlies the sediments that are approximately 30–40 m thick.

The site is a former small gravel quarry, and as a result the upper ~80 cm, which may have been a loess cap, has been disturbed by machinery. Below the disturbed loess cap is a well-sorted, rounded to well-rounded, sandy gravel parent material, with clasts typically 2–5 cm in diameter and rare clasts up to 25 cm in diameter. Within the upper portion of the sandy gravel is a prominent K horizon exhibiting Stage V-IV carbonate development. Laminae k-fabric is present throughout this horizon, with strongly cemented plates 1–2 cm thick; concentric rinds on individual clasts are up to 10 mm thick. This most prominent horizon is 27 cm thick, and grades into a Stage III+ carbonate horizon below it. Pedogenic carbonate extends to the base of the exposure 2 m below the surface. Clasts sampled from this site were taken from near the base of the most developed carbonate horizon ~1 m bgs (Figure 4.11).



Figure 4.11. Photograph showing the soil developed in Ice Age cataclysmic flood deposits exposed in the north wall of the inactive South Bombing Road quarry.

Four inner rinds from clasts from this site yield ages ranging from 308 ± 12 ka to $564 +310/-180$ ka (Appendix E.1). The younger ages (308 ± 12 ka and 346 ± 14 ka) have low age uncertainties. The two older ages have substantially larger uncertainties, allowing the possibility of ages in the range of ~ 400 ka or less. Baker et al. (1991) report that the sediments at the South Bombing Range Road site exhibited normal polarity and thus are younger than 780 ka.

4.3.1.2 Yakima Bluffs

The Yakima Bluffs site (13166sh02) is located along a naturally eroded bluff flanked by the Yakima River at an approximate elevation of 160 m. The geomorphic surface at this site is the same as or slightly lower surface than the South Bombing Range Road site (Section 4.3.1.1). In some locations along the bluff the surface has been excavated into for mining purposes. Previous studies by Baker et al. (1991) described the stratigraphy here as normally polarized middle Pleistocene gravels overlying fine-grained reversed deposits (Figure 4.5). We sampled and described the upper gravels, which are overlain by a disturbed approximately 0.5-m-thick loess cap. The parent material is dominantly gravel with some sand. The ~ 2 -m-high soil exposure has a generally whitish appearance but lacks a horizon with prominent k-fabric having laminar plates. The pedogenic carbonate development present is up to Stage III, with generally greater development in parent material that has increased fines in the matrix. Concentric rinds on clasts were up to 5 mm thick.

We sampled two depth intervals, from a depth of 0–70 cm and from 70–170 cm (Figure 4.12). Samples from this site showed the greatest amount of evidence for open-system behavior. Of the seven samples analyzed by Dr. Paces (Appendix E.1) from 0–70 cm, only three samples yielded results. One sample yielded a robust age of 408 ± 34 ka, which is within the error overlap of the 370 ± 34 ka result for a sample collected from the 70- to 170-cm-depth range. Two other samples from the 0 - to 70-cm-depth range yielded Monte Carlo age estimates of $630 +300/-180$ ka and $775 +300/-210$ ka. Three samples were analyzed from the sampling depth of 70–170 cm and yielded considerably more scatter in the results. Relatively young ages of 27.5 ± 0.2 ka and 52.5 ± 0.4 ka suggest that carbonate was added or mobilized in the late Pleistocene. Variations in ages at this site are suggestive of a partially open system, with the introduction of more recent carbonate into the soil profile. It is possible that these inconsistencies are the result of the outcrop being a natural bluff that has been exposed to more recent input of eolian dust.

4.3.1.3 MCBONES (Coyote Canyon Mammoth Site)

The MCBONES (Mid-Columbia Basin Old Natural Education Sciences) sample site (13167sh03) is located off of Clodfelter Road in Coyote Canyon south of Kennewick. The site lies on the northern slope of the Horse Heaven Hills on a broad plain southeast and topographically higher than Badger Coulee. The approximate elevation of the sampling site in a quarry cut is 320 m, close to the high-water level of the temporary late Pleistocene Lake Lewis. A nearly complete mammoth bone skeleton is located within fine-grained Pleistocene Ice Age flood deposits at an elevation of 293 m MSL approximately 165 m southeast of the Th/U sampling site (Figure 4.13). This is one of the highest known mammoth finds in flood deposits in south-central Washington (Barton and Last 2010), and it has been associated with one of the largest floods (Last and Bjornstad 2009). Two samples for radiocarbon analysis taken from an in situ humerus yielded a pooled mean value of $17,449 \pm 168$ cal. yr. BP (with a 95.4% probability) (Barton et al. 2012).



Figure 4.12. Photographs of the Yakima Bluff locality. a) View northwest of bluff exposure. b) Close-up of magnetically reversed slackwater sediments. c) Sample 13166sh02 included samples from depths of 0–70 cm and 70–170 cm.



Figure 4.13. GoogleEarth image showing the location of the sample locality (13167sh03) relative to the MCBONES mammoth excavation site.

The stratigraphy at the Canyon Creek mammoth site as described by Guettinger et al. (2010) and by Last et al. (2012) consists of north-dipping Saddle Mountains Basalt overlain by a coarse angular basaltic conglomerate interpreted to be of alluvial fan origin (fanglomerate) that in turn is overlain by a thin tephra deposit of unknown age and a fairly thick (meters) sequence of rhythmically bedded fine-grained sediment. Guettinger et al. (2010) identify four different graded bed sequences over the mammoth bone bed that are believed to represent distinct Ice Age flood events. Barton et al. (2012) note that an overprint of pedogenic calcium carbonate in the lowermost flood deposits containing the bone bed suggests a

period of weathering and subaerial erosion prior to deposition of the younger flood deposits. Approximately 1 m of loess, which is subdivided into two different units, overlies the flood deposits (Guettinger et al. 2010; Barton et al. 2012) (Figure 4.14).

The exposure at the sampling site consisted of approximately 3 m of loess and Touchet Beds overlying approximately 1.5 m of gravel colluvium (fanglomerate). The pedogenic carbonate development developed in the gravel unit is Stage III+, with a zone near the top of the deposit containing discontinuous k-fabric.

The team sampled near the most strongly developed K horizon at the top of the sandy gravel colluvium (Figure 4.15). Six samples analyzed by Dr. Paces (Appendix E.1) yielded best-estimated ages ranging from 145 ± 20 ka to 268 ± 7 ka. Although a small sample size, the samples generated relatively low error. The results suggest that the closest minimum age to the depositional event may be 268 ± 7 ka.

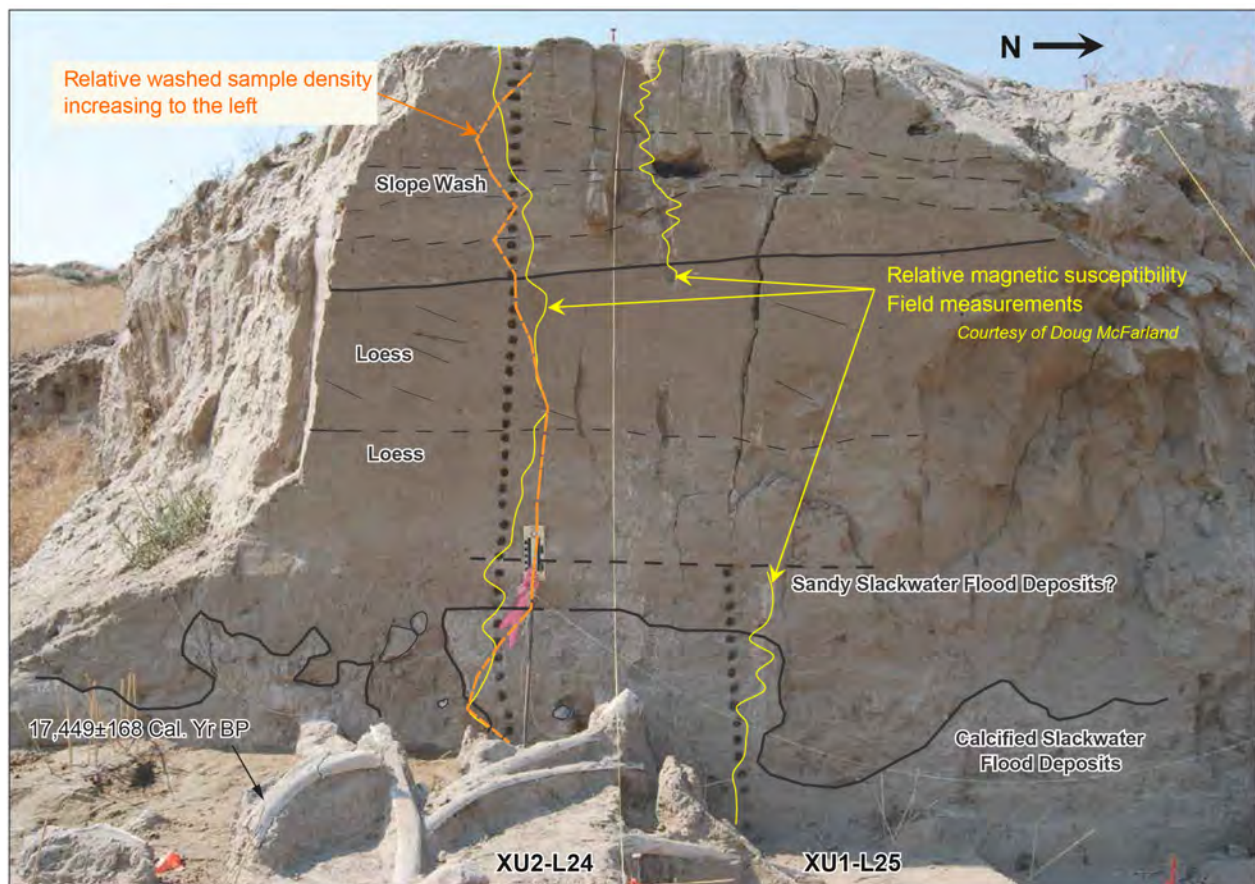


Figure 4.14. Annotated stratigraphy at the mammoth bone bed locality (from Last et al. 2012). The approximate elevation of the site is 293 m.



Figure 4.15. Photograph showing location of carbonate rind sampling for $^{230}\text{Th}/\text{U}$ -series analysis, at exposure near the MCBONES site (see Figure 4.10 for location relative to the mammoth excavation site).

4.3.1.4 Steptoe Quarry

The Steptoe quarry site (13166sh01) is located south of the confluence of the present-day Yakima and Columbia rivers (Figure 4.11). The quarry is surrounded by a fairly continuous surface with an approximate elevation of 140 m. The surface extending beyond the quarry includes the exposure along Leslie Road to the west of Steptoe quarry. According to a home owner whose home is adjacent to Steptoe

quarry, the quarry was operational until the mid-1990s. The present-day walls of the quarry are laid back into a ~2:1 slope, and are covered with grasses. Hand excavation of the upper portions of the slopes exposed fine-grained loess overlying sandy gravel with a pedogenic K horizon. Within the upper portion of the sandy gravel was the area with the most developed carbonate, which was at least Stage III+. Given the laidback nature of the exposure with vegetation cover it was difficult to examine the nature of the carbonate horizons along the cut. However, k-fabric was observed as well as some laminar plates, and concentric rinds on clasts were up to 1 cm thick. We sampled in the upper half meter of the gravel.

WCC (1981b) described exposures in a gravel pit near Kennewick (NE ¼, SE ¼, Section 25, T9N, R28E) that appear to have been exposed in what is herein referred to as the Steptoe quarry. Samples collected by Tallman et al. (1978) from this gravel pit were dated using the U-series method at 200 (+250, -70) ka and 225 (+380, -70) ka (WCC 1981b). As illustrated Figure 4.16, the poorly sorted older flood gravels exposed in the wall of the quarry exhibited a well-developed petrocalic horizon (Stage IV-V) in the upper 1.5 m of the deposit. The older gravel is overlain by younger flood gravels and was disrupted by a younger clastic dike. The upper surface of the older gravel was truncated and channeled prior to deposition of the younger gravel.

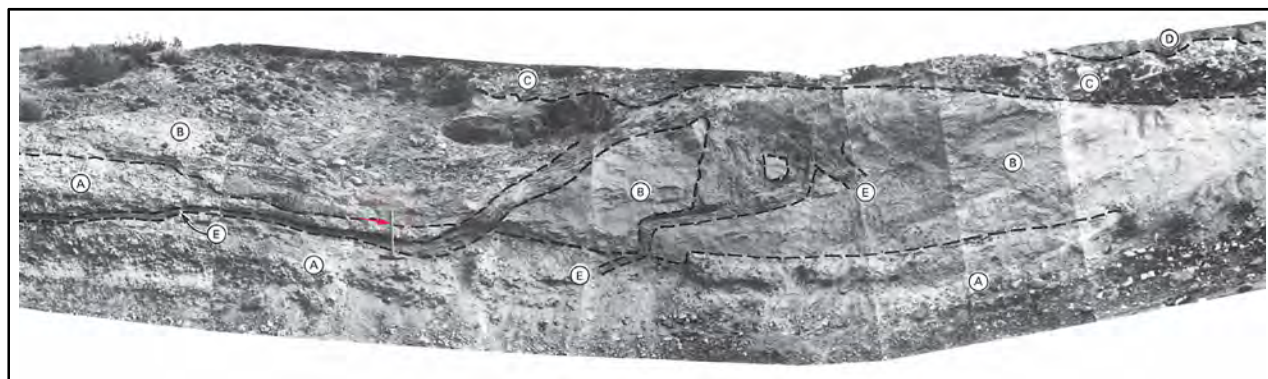


Figure 4.16. Photomosaic showing the relationship between older gravels (A), late Pleistocene Touchet Beds (B), younger gravels, (C) and loess deposits (D). Note the clastic dikes (E) penetrating horizontally into the calcrete cap of the older gravels (pick is 56 cm long). (modified from WCC 1981b).

Four of five samples analyzed by Dr. Paces (Appendix E.1) yielded compositions near secular equilibrium implying substantial antiquity. The estimated ages ranged from 509 ± 86 ka to 736 ± 831 ka. Although the large uncertainties suggest the samples are approaching secular equilibrium (maximum limiting age of ~380–400 ka), several of the samples yielded reasonably consistent finite ages suggesting the cataclysmic flood sediments at this site were deposited shortly before ~500 ka, and most likely after 700 ka. The apparent outlier sample dated to 17.3 ± 1 ka is of a very thin rind, likely reflecting continued addition or mobilization of cements long after original deposition of the deposit.

4.3.1.5 Finley Quarry

The Finley quarry site (13167sh02) is located primarily in basalt. The north end of the quarry exposes a fault juxtaposing gravel units against Umatilla Basalt. The exposure was originally logged by Farooqui and Thoms (1980) and then by WCC (1981a). These original logging efforts varied in detail and the available documentation of the efforts is partially incomplete. As part of the QGS conducted for

this study the fault exposure was re-logged by a separate team of geologists led by Brian Sherrod (USGS) (Appendix E.4). The logging effort cleaned the exposure, exposing the upper units identified in the WCC (1981a) study. At the base of the north end of the recently cleaned exposure was a pedogenic carbonate horizon developed in a sandy gravel to gravelly sand deposit. Scattered exotic lithologies (e.g., quartzite, coarse-grained felsic igneous clasts) suggest the gravel was likely deposited in or derived from cataclysmic flood deposits. Only the upper ~40 cm of the carbonate horizon was exposed (Figure 4.17). The horizon matrix was generally loose, and calcareous enough to give a whitened appearance, a few clasts were weakly cemented together, and no k-fabric was observed. Concentric rinds were generally confined to the base of the clasts with thicknesses of up to 3 mm but generally 1–2 mm thick, consistent with Stage IIB-IIA development of Forman and Miller (1984). We sampled near the base of the exposure that had been cleaned by the USGS team at that time. Because of the limited exposed extent of the unit it was difficult to ascertain whether we were sampling in the horizon of greatest carbonate accumulation. The thickest rinds were observed during subsequent site visits when the exposure was slightly deepened. Carbonate rinds also were collected from the carbonate-cemented fault breccia zone associated with the southernmost fault zone (between F1 and F2 as mapped by the USGS team (see Appendix E.4) (Figure 4.18).

Dr. Paces (Appendix E.1) ran eight rind samples for the carbonate horizon developed in gravels containing exotic clasts at the base of the exposure. The rinds sampled were thin (~0.5 mm). The results yielded a fairly tight age range with an average age of 17.0 ± 1.8 ka. The uncertainty in the interpretation of this age stems from the limited extent of the exposure. It is unclear whether we were sampling in a zone of maximum accumulation of pedogenic carbonate in latest Pleistocene flood deposits (possibly equivalent to the ~17.5 ka bone bed flood deposits at the MCBONES site described above in Section 4.3.1.3), or whether we were sampling from a section of a pedon developed in much older flood deposits that has been overprinted by younger carbonate accumulation. Previous dating of pedogenic carbonate from the northern end of the Finley quarry wall cut reported by WCC (1981b) suggested that the pre-Wisconsin gravel was probably older than 69–160 ka. Two samples (JB-7 and JB-8) were collected from the northern end of the then existing quarry wall. Sample JB-7 (clast rind) yielded ages of 19 ± 1 ka (probable) to 51 ± 3 ka (maximum). Sample JB-8 (massive caliche collected from unit 1 as noted in the response to Q. 360.015 (Amendment No. 23, WNP-2 FSAR, Energy Northwest 1982)) yielded ages of 75 ± 6 ka to 147 ± 13 ka. The ages obtained for sample JB-8 were judged to be more representative of the antiquity of the pre-Wisconsinan deposit (WCC 1981b). Sherrod et al. (In Review) note that felsic igneous clasts within this unit (unit 11) are deeply weathered. Assuming these clasts were not reworked, the weathering would be more consistent with the older minimum age of 69–160 ka. This minimum age constraint suggests the flood sediments may have been deposited during glacial floods as young as MIS 4 (71–58 ka), but more likely during an older glacial period such as MIS 6 (190–131 ka).

Four samples from the fault gouge all yielded relatively old ages of greater than or equal to middle Pleistocene in age, with best estimates ranging from $700 +270/-160$ ka to 224 ± 36 ka.



Figure 4.17. Photographs showing a) flood deposits at the northern end of the exposure sampled for $^{230}\text{Th}/\text{U}$ -series analysis (Sample 13167sh02), and b) Finley quarry exposure, view southeast. Approximate locations and names of faults exposed in the quarry wall and trench excavations logged by WCC (1981a) are indicated by the red arrows. The northern and central faults are not currently exposed in the quarry wall.



Figure 4.18. Photograph of the Finley quarry south fault showing the sampled carbonate-cemented fault breccia.

4.3.1.6 Conclusions

This study's results for the three sites—South Bombing Range Road, Yakima Bluffs and Steptoe quarry—are similar to the previous results reported by Baker et al. (1991) in that these cataclysmic Ice Age flood deposits, all of which are capped by platy to massive, carbonate-plugged K horizons, characteristic of Stage III to Stage IV/V pedogenic carbonate development (Gile et al. 1966; Machete 1985), appear to be of similar middle Pleistocene age. The normal polarity of the flood sediments at both the Yakima Bluffs and South Bombing Range Road sites indicates the deposits are probably younger than the ~780 ka Brunhes (normal)/Matuyama (reversed) boundary. The elevation of these three sites range

from as low as ~140 m at Steptoe quarry to as high as 180+ m at South Bombing Range Road. This variation in elevation seems plausible for the same age deposit given the cataclysmic nature of the fluvial system.

The study finds the ages of the deposits to be at least as old as ~350–400 ka, somewhat older than the preferred age of ~200 ka by Baker et al. (1991). A number of the samples at all three sites were approaching the limit of the $^{230}\text{Th}/\text{U}$ dating method, suggesting a likely antiquity of 380 ka or greater. This minimum age is consistent with deposition during glacial conditions in MIS 12 (478–424 ka) or earlier glacial periods. A Monte Carlo approach, where multiple trials are calculated using values for isotope compositions that vary randomly within range of the given uncertainty, was used to gain additional information from samples that may have experienced slight open-system behavior. In this approach, only trials that result in positive, finite ages are considered reliable. The best-estimated ages of the samples from all three generally range between 500–700 ka (consistent with a flood during MIS 14 [563–534 ka], MIS 16 [659–622 ka], or possibly MIS 18 [712–677 ka]). Although the possibility that the deposits record more than one period of flooding cannot be precluded, the ages cannot be differentiated within the resolution of the dating method. Erosion of the upper portions of the soils formed in these deposits during the latter Missoula floods further complicates the assessment and comparison of maximum soil profile development among the dated localities.

Other dates from the MCBONES and Finley quarry site provide informative minimum ages for carbonate soil development. The U-series results from the MCBONES site show that Stage III to III+ carbonate can form in gravel deposits in 268–200 kyr. At Finley quarry, thin (0.5-mm) carbonate rinds on clast bottoms formed in less than 17 kyr, possibly within only a few thousand years based on stratigraphic relationships.

4.3.2 Cosmogenic Nuclide Dating

Recent studies near the northern end of the Yakima River Canyon by Ladinsky (2012) focused on age dating of uplifted fluvial terraces. Ladinsky (2012) intended to use optically stimulated luminescence (OSL); however, due to the slow decay signal from the quartz this method was inadequate. Infrared Stimulated Luminescence (IRSL) was adopted as an alternative approach. IRSL is particularly well-suited for younger deposits (<100 ka) but has an increased uncertainty in older deposits. The additional limitation of this method is that it is generally restricted to finer-grained deposits in the fluvial packages, or to dating loess packages that overlie the deposits of interest, providing a minimum age. Ladinsky (2012) also used tephrochronology to date deposits. Ages reported by Ladinsky (2012) using these various approaches ranged from as young as ~88 ka to as old as ~250 ka.

As part of this study we reexamined many of the terraces identified by Ladinsky (2012) that could provide information about rates of uplift for the Manastash anticline/fault as well as other terraces downstream that could provide information about uplift in both the hanging and footwalls of the Umtanum Ridge anticline/fault (Figure 4.19). Evaluation of potential dating sites took place in May 2013. In addition to the cosmogenic specialist Paul Bierman (University of Vermont) and the Quaternary Studies Team, Harvey Kelsey (Humboldt State University), Brian Sherrod (USGS) and, Colin Amos and Skyler Sorsby (Western Washington University), took part in the field sampling. In total, six different fluvial deposits were sampled for cosmogenic nuclide ($^{26}\text{Al}/^{10}\text{Be}$) dating, from four locations: Potato Hill in Kittitas Valley (YK01 and YK02), and from preserved fluvial terraces perched above the active

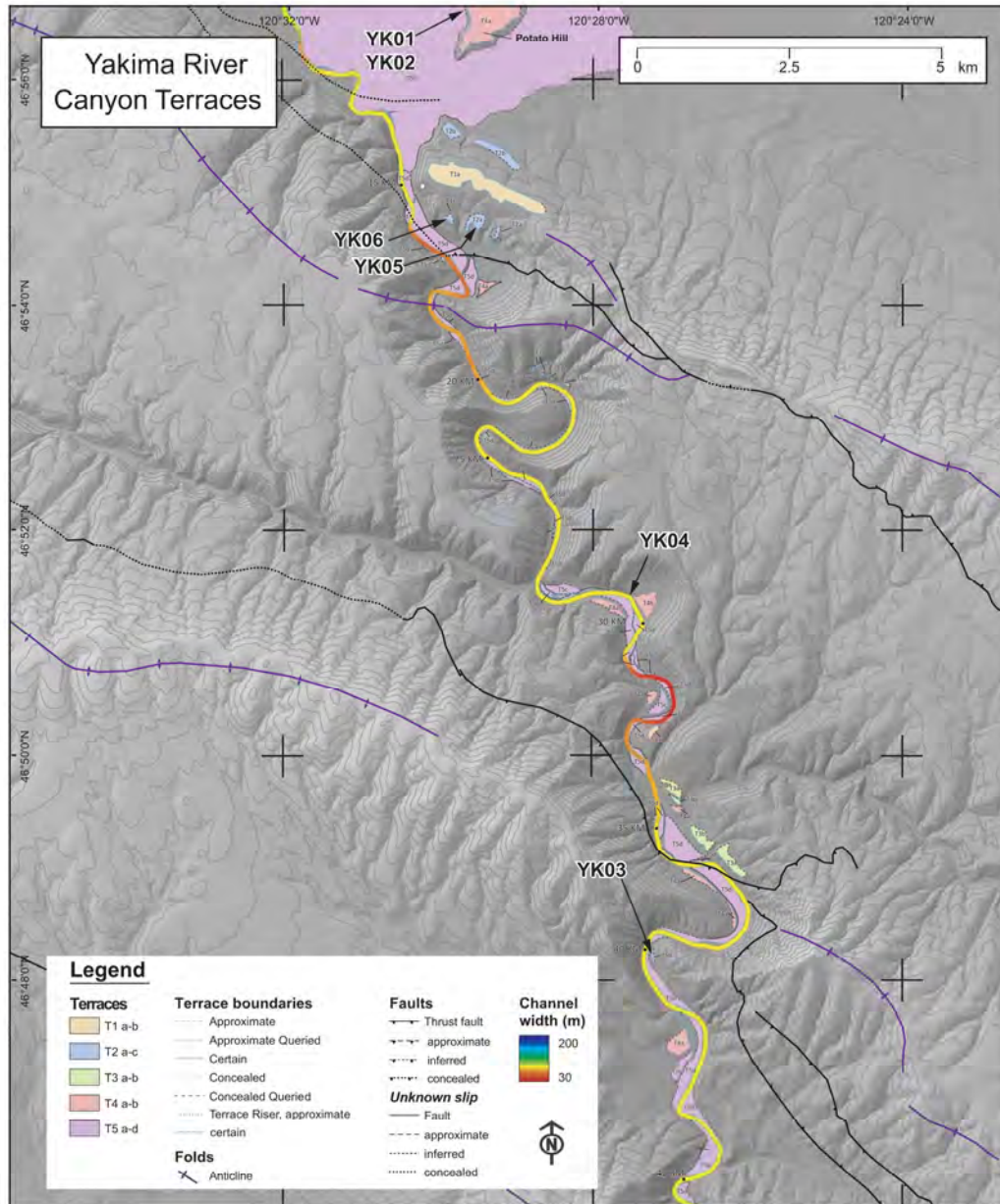


Figure 4.19. Map showing the location of cosmogenic nuclide ($^{26}\text{Al}/^{10}\text{Be}$) samples. Base map from Amos and Sorsby (Plate 1, Appendix E.2).

Yakima River located approximately 3 km (location 13133sh02[YK06] and 13133sh01[YK05]), 14 km (the “Meander” location 13128sh02[YK04]), and 24km (“Big Pine terrace” location 13132sh07[YK03]) downstream from the Kittitas Valley range front. The available budget for the project did not allow for analysis of all of the samples collected; so the Quaternary Studies Team and sampling team prioritized the samples and selected samples collected from three terraces for analysis. A report by Dr. Bierman summarizing the sample collection and analysis is provided in Appendix E.3. The following sections provide descriptions of each sampling locality and the findings of the dating results for the three localities that were analyzed. Additional discussion of the dating results with regard to evaluating Quaternary uplift rates of the Manastash and Umtanum Ridges is given in Section 9.0.

4.3.2.1 Potato Hill

Potato Hill (location 13132sh02) is located 1.5 km north of the Kittitas Valley geomorphic range front. Potato Hill is a roughly planar surface that is up to 2 km long, and is approximately 20 m higher than the valley floor (Figure 4.19). An old quarry cut on the west side of hill near the intersection of Number 6 road and Fern Road provides a good exposure of the sediments composing the hill (Figure 4.20).



Figure 4.20. Photographs illustrating the stratigraphy and soils exposed in the Potato Hill quarry cuts, Kittitas Valley, Washington. a) View to the east toward Potato Hill quarry excavations. Note the northward-dipping bedding in the lower gravels (Ellensburg Formation) (yellow arrows) relative to the nearly horizontal pediment surface and carbonate soil horizon (blue arrows). b) Samples YK01 and YK02 were collected from gravels interpreted as Thorp Gravel (~3.7 Ma; Waitt 1979) and Ellensburg Formation, respectively. The massive white unit in the upper left corner of the image, identified as a zeolitized tuff (this study), is indicative of ponding in Kittitas Valley during deposition of the tuff. c) Close-up view of Stage IV carbonate soil development on the Thrall pediment surface eroded into Thorp Gravels (note laminar plates and k-fabric).

The deposits consist of cobble- to boulder-sized clasts as well as some fine-grained packages. Clasts are commonly completely weathered, and iron staining is common. In places, imbricated clasts suggest an originally southerly-flowing depositional environment. A few discrete beds dominated by boulders > 0.5 m in diameter suggest high water flow. Previous mapping of Potato Hill by Bentley (1977) mapped Thorp Gravel (~3.7 Ma) overlying Miocene Ellensburg sediment (Figure 4.20). Two sampling depths were targeted, one above the interpreted Thorp Ellensburg unconformity (YK01, ~ 2.5-3.1 m bgs) and a second location below the unconformity (YK02; ~ 6.9-7.6 m bgs).

Given the previous constraints on the age of the Thorp sediments based on the fission track age of ~3.7 Ma (see Section 4.2.2), the samples collected from Potato Hill were assigned the lowest priority for dating. The samples were processed, but due to budget limitations they were not analyzed.

4.3.2.2 Locations 13133sh02 and 13133sh01

Locations 13133sh02 (YK06) and 13133sh01 (YK05) are in a meander approximately 3 km south (downstream) of the geomorphic range front (Figure 4.19). Previous mapping of Quaternary deposits by Ladinsky (2012) identified a flight of six fluvial terraces in the meander. The terrace surfaces range from ~10 to 100+ m above the active channel. We targeted two of the upper terraces for sampling: Qg4 (location 13133sh01 [YK05]) and Qg5 (location 13133sh02 [YK06]) of Ladinsky (2012). A minimum age for the Qg4 terrace had been reported by Ladinsky (2012) based on an IRSL age of 237-271 ka for terrace sediment. The Qg5 terrace had not been previously dated.

Location 13133sh01 (sample YK05) is located on a rounded eroded shoulder of the Qg4 terrace, which had recently been cut into for a residential driveway. We hand excavated into the cut exposing in situ subrounded to rounded gravel- to boulder-sized clasts. The sampling depth was located 2.1–3.1 m below the top of the cut. This was approximately 10 m below the terrace surface, which was approximately 60 m above the present river level. Clasts within the exposure were generally severely weathered. Ladinsky and Kelsey (2012) estimated the basalt bedrock strath for this terrace is ~48 m above the present river level. Sample YK05 yielded a $^{26}\text{Al}/^{10}\text{Be}$ cosmogenic nuclide burial age of 1.08 ± 0.29 Ma (see Appendix E.3).

Location 13133sh02 (sample YK06) is located near the Qg5 terrace surface at an elevation of approximately 85 m above present river level. The exposure is in a recent cut generated for a cut-and-fill pad for a garage. The exposure extends from near the ground surface to 2.5 m bgs. The deposits in the cut are composed of rounded gravels generally less than 15 cm in diameter, in a silty sand matrix. Clasts were sampled from a gravelly pedogenic Stage III-IV carbonate horizon, located between 1.4-1.6 m bgs. We attempted to sample from a greater depth, but there was generally a paucity of quartz-rich clasts deeper in the cut. Given the quality of the processed sample, YK06 was not analyzed (see Appendix E.3).

4.3.2.3 Meander Terrace (Location 13128sh02)

Location 13128sh02 (Sample YK04) is located in a meander bend 14 kilometers downstream of the geomorphic range front. A roadcut along State Highway 821 exposes rounded, stratified, fluvial gravel with cobble- to boulder-sized clasts, overlain by shallow (<5 m thick) landslide deposits. The clasts were typically weathered, with 1-2 cm thick weathering rinds on the fine-grained basalt boulders. Approximately 1 m below the road surface the basalt bedrock strath crops out along the river channel, the

strath is approximately 16 m above the active channel. We sampled and analyzed the fluvial gravels exposed near the base of the roadcut, which yielded a $^{26}\text{Al}/^{10}\text{Be}$ cosmogenic nuclide burial age of 1.6 ± 0.25 Ma (Appendix E.3).

4.3.2.4 Big Pine Terrace (location 13132sh07)

The Big Pine terrace (location 13132sh07 [YK03]) is named after a campground near a roadcut exposure along State Highway 821. The terrace is approximately 24 km downstream from the mouth of the Yakima Canyon and approximately 2.5 km downstream from the geomorphic range front of Umtanum Ridge (Figure 4.19). The terrace surface is approximately 7 m above the active river channel; the bedrock strath of the terrace is not exposed in the road outcrop. The cut exposes stratified cobble- to boulder-sized gravel with sandy interbeds. We sampled from a depth range of 5.2–5.6 m below the surface of the terrace. A weak carbonate soil characterized by weak carbonate cementation of clasts and sand, 50–90% coatings of clast bottoms and rinds up to 1 mm thick (Stage IC of Forman and Miller 1984; and 1+ of Birkeland 1999) is formed in the deposit. This terrace was targeted as a sampling location due to its position on the backlimb of the Umtanum Ridge anticline. The samples collected from this terrace yielded a $^{26}\text{Al}/^{10}\text{Be}$ cosmogenic nuclide burial age indistinguishable from modern (see Appendix E.3).

5.0 Evaluation of Long-Term Structural Relief

The topographic expression of the YFB is directly related to the folding of the CRB across major faults that have created distinct anticlinal ridges and thrust sheets. Because only modest amounts of erosion have occurred along the peaks and flanks of the ridges since the time of uplift, the topography provides a good first-order estimate of structural relief in most areas of the YFB. However, due to differing amounts of erosion and burial occurring within the synclinal valleys between the ridges, there is some uncertainty associated with directly measuring structural relief from the topography in these areas. To obtain the most accurate measurement of structural relief across all faults while also quantifying the uncertainty in the structural relief for purposes of estimating long-term slip rates associated with each structure, two approaches were used. The Burns et al. (2011) 3-D model (hereafter referred to as the Burns et al. model) is based on a regional borehole compilation and provides structural information for evaluating vertical separation of CRBG flows across major faults. Cross sections were extracted from the model and compared with topographic relief measurements taken from the regional 10-m DEM. In cases where topographic expression was lacking due to erosion by Pleistocene flooding events, the surface topography imaged in the regional DEM is not a good measure of the structural relief in these areas. In these circumstances, such as within the Hanford Site boundary and along the RAW structure, structural contour maps of the top of basalt from Myers et al. (1979) and Thorne et al. (2014) were used to measure fold amplitude.

Further discussion of the approaches used to measure and evaluate structural relief relative to the Burns et al. model and uncertainties associated with the approach are described below.

5.1 Constraints on Structural Relief Provided by the Burns et al. 3-D Model

The Burns et al. model can be used to analyze the long-wavelength geometry of Yakima folds, as well as variations in the thickness of the CRBG units, which provide a means to assess systematic variations indicative of growth of the folds during eruption of the basalts. We used the model to measure the apparent vertical stratigraphic separation of distinct units of the CRBG and through comparison with topography to test the hypothesis that topographic relief in the YFB is approximately equivalent to post-CRB structural relief measured using the 10-m DEM. The goal of this comparison is to test the hypothesis that topographic relief in YFB is approximately equivalent to post-CRB structural relief, and therefore topographic relief can be used as a proxy for evaluating the dimensions and geometric segmentation of individual structures.

The Burns et al. model was constructed using a large database of elevations of key stratigraphic horizons compiled from oil, gas, and water well data (see Burns et al. 2011 for a detailed discussion). The model uses a simplified stratigraphy for the CRB consisting of the top Saddle Mountains Basalt, top Wanapum Basalt, and top Grande Ronde Basalt. Late Neogene and Quaternary stratigraphic units overlying the CRB are generalized in the model as “Overburden.” The model is available to the public for analysis through an interactive web-based tool (<http://or.water.usgs.gov/proj/cpras/index.html>). The tool allows users to extract arbitrary cross sections from the model, from which structural relief across individual YFB structures can be directly evaluated from the vertical separation of stratigraphic units.

Once a cross section is generated using the tool, a vertical cursor appears that can be moved through the cross section, showing the elevations of the tops of stratigraphic units at any selected point.

In the model documentation, Burns et al. (2011) discuss a statistical evaluation of the fit of the modeled surfaces to the data. We performed an independent check of the 3-D model against well data to assess whether the first-order stratigraphic and structural relationships were rendered accurately enough to perform a comparison of structural relief to the topographic relief. We extracted three north-south cross sections from the model where the well data intersecting the cross sections could be readily compared to the model (Figure 5.1, Figure 5.2, and Figure 5.3). By checking the cross sections against the well data at several locations along each of the three transects, we were able to quantify the accuracy of the model for key horizons at those locations.

Listed below are the major horizons with respective uncertainties based on our analysis:

- overburden: ± 0.15 m
- Saddle Mountains Basalt: ± 1.8 m
- Wanapum Basalt: ± 3.5 m
- Grande Ronde Basalt: ± 6.8 m.

Based on this analysis and comparison, we find that the accuracy of the Burns et al. model decreases with depth, but generally is sufficient for making regional, long-wavelength, comparisons of the structural relief on the Saddle Mountains Basalt and Wanapum Basalt of the CRB with topography.

Where the Saddle Mountains Basalt is preserved over the crests of folds and captured in the 3-D model, the long-wavelength structural relief on the basalt is similar to or the same as the topographic relief associated with individual YFB structures. These relationships are illustrated in Figure 5.1, Figure 5.2, and Figure 5.3. These relationships are well expressed south and east of the Columbia River where the Saddle Mountains Basalt is about 250 m thick and well preserved. Inspection of cross sections extracted from the Burns et al. model demonstrates that the Saddle Mountains Basalt progressively thins north of Rattlesnake Mountain and the Columbia River, and disappears north of Frenchman Hills. This pattern of regional northward thinning is not localized over individual YFB structures, and is most likely related to the geometry of the Miocene Basin in which the basalt accumulated.

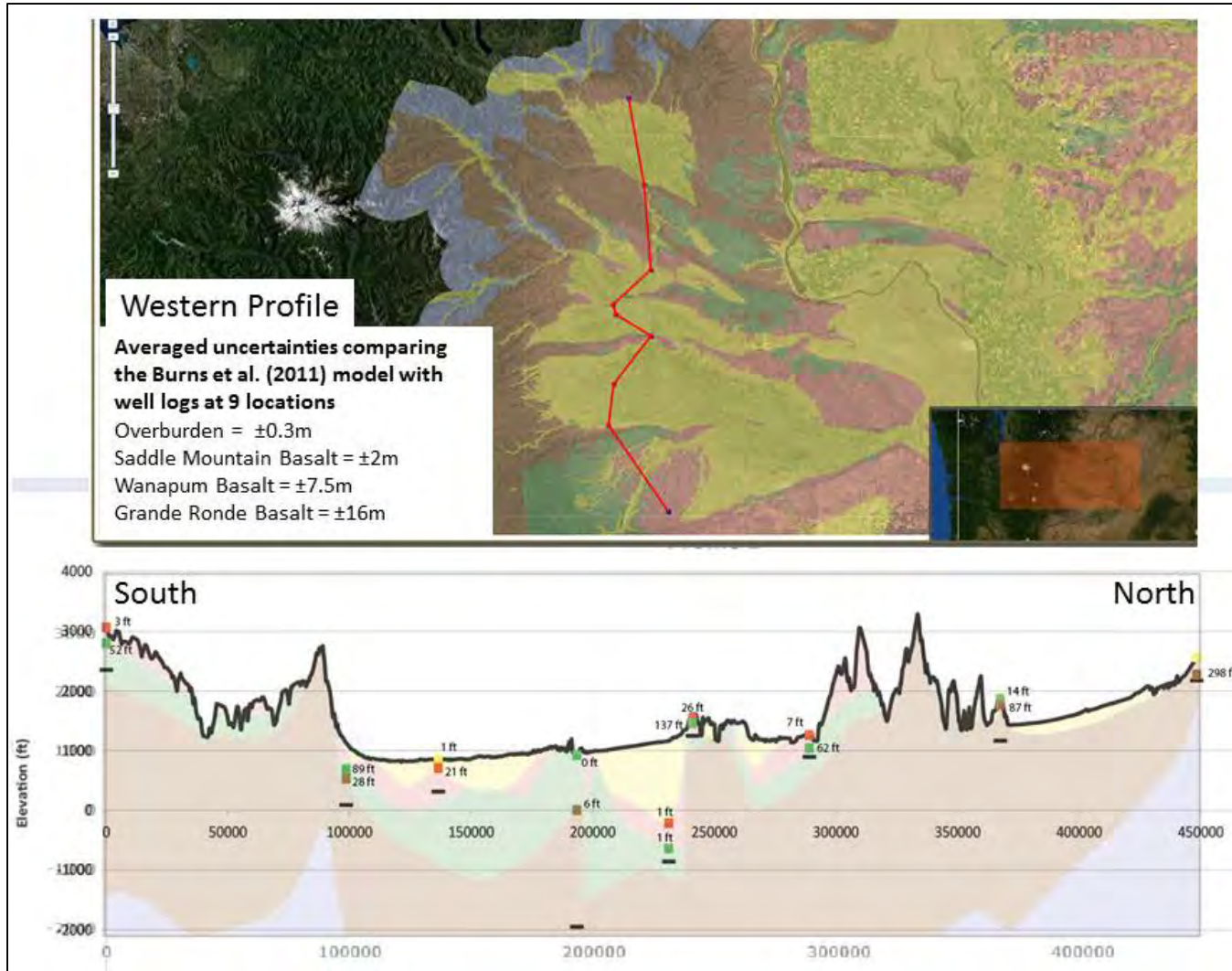


Figure 5.1. Western profile comparing results of the Burns et al. (2011) model with horizon picks from borehole well logs at nine locations along the transect (colored squares). Numbers next to colored squares in the cross section indicate the difference between the model horizon and the elevation derived from well logs. The results of the analysis, displayed in the white box, provide uncertainty estimates for various major horizons.

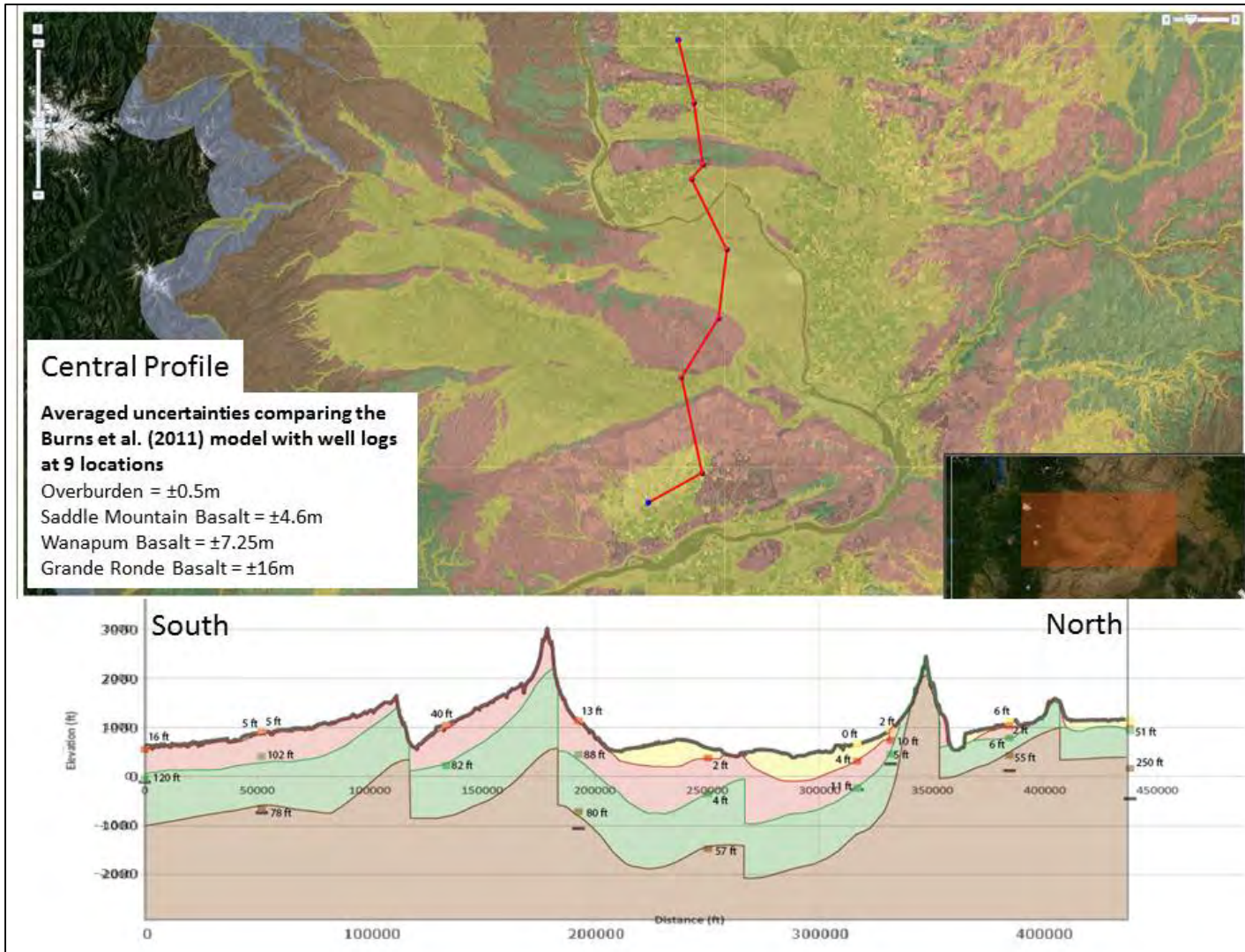
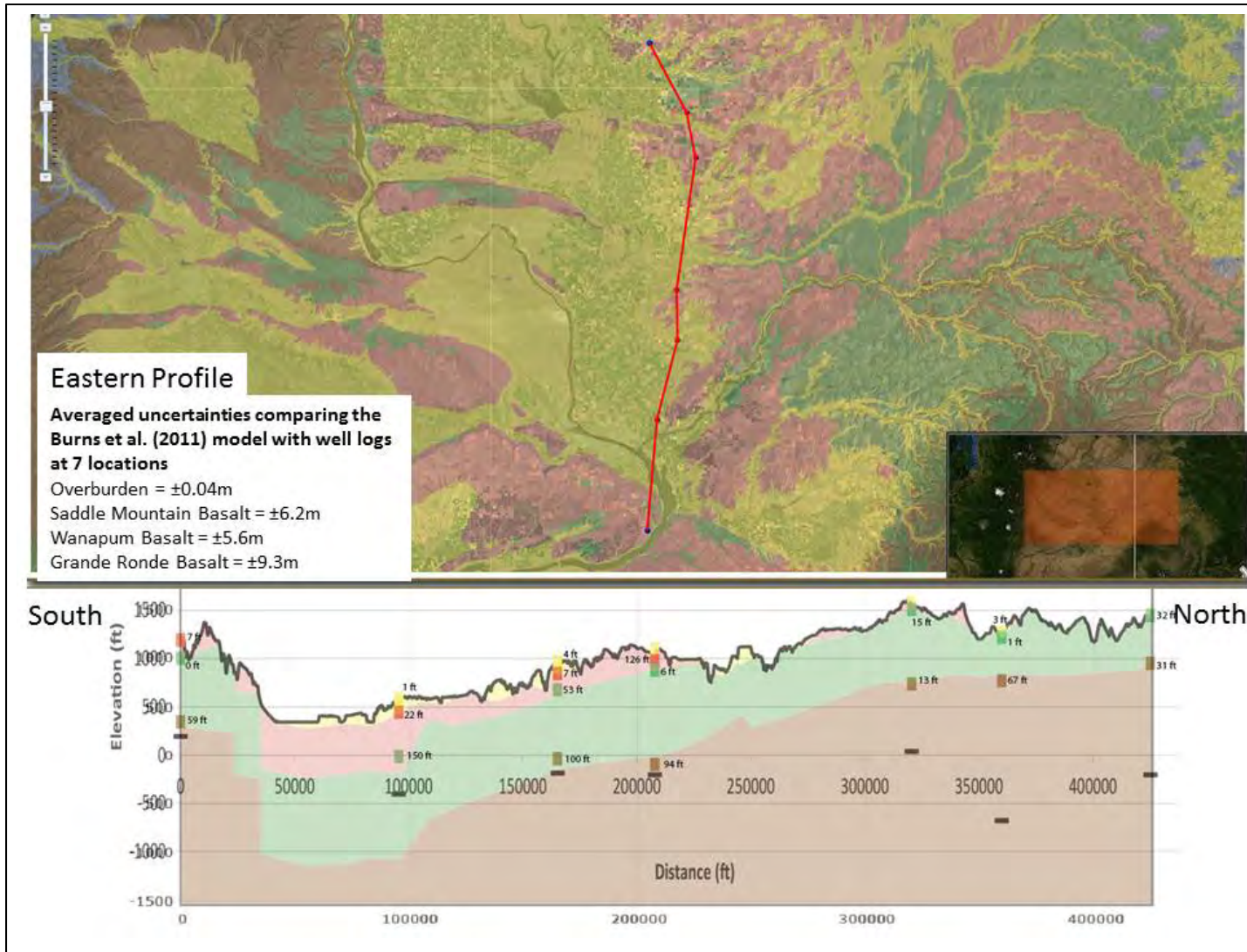


Figure 5.2. Central profile comparing results of the Burns et al. (2011) model with horizon picks from borehole well logs at nine locations along the transect (colored squares). Numbers next to colored squares in the cross section indicate the difference between the model horizon and the elevation derived from well logs. The results of the analysis, displayed in the white box, provide uncertainty estimates for various major horizons.



5.2 Evaluation of Structural Relief Using Top of Bedrock Analysis

In locations where Pleistocene flood erosion has made it difficult to directly measure structural relief, structure contour maps of the top of CRBG were used. The structure contour maps were developed from regional borehole data as part of the BWIP and other Hanford Site studies (Myers et al. 1979; Fecht et al. 1992; and Thorne et al. 2014). The maps are constrained by regional borehole logs and vary in resolution, ranging from 10- to 30-m-contour intervals. Figure 5.4 is a map showing the extent of the various structure contour maps. The map coverage extends from just north of Saddle Mountains in the north to just north of Wallula Gap in the south.

The five structures evaluated using the top-of-basalt maps include the Umtanum-Gable Mountain fault, the Southeast Anticline fault, the Yakima Ridge Southeast fault, the Horn Rapids fault, and the RAW-Rattles structure. In order to measure structural relief, contour elevations were measured from the frontal thrust to where the backlimb of the structure intersects the synformal hinge. These steps mimic the approach that was used along other structures within the YFB where topography was more closely related to structural relief. Structural relief measurements were taken at several locations along the strike of each structure in order to average any minor variations. Further discussion of how these faults were located and evaluated using the top-of-basalt maps is provided below.

5.2.1 Gable Mountain and Southeast Anticline Fault

These faults are located within the Hanford Site boundary and are the eastern extension of the easterly plunging Umtanum Ridge structure. The Umtanum-Gable Mountain fault system loses significant amounts of structural relief as the fold dissipates toward the Hanford Site. Due to both the low-amplitude folding and the intense erosion from Pleistocene flooding, it is difficult to evaluate the structural relief from topography alone, especially the Southeast Anticline that has little to no topographic expression (Figure 5.5).

Using the top-of-basalt map from Myers et al. (1979), Fecht et al. (1992), and Thorne et al. (2014), the structural relief was measured along Gable Mountain and the Southeast Anticline faults. The average structural relief across the Gable Mountain fault and the Southeast Anticline fault are 160 m and 90 m, respectively. The decrease in relief from west to east is consistent with the structure tapering off toward the east to where the Southeast Anticline no longer has structural relief.

5.2.2 Yakima Ridge Southeast Fault

The Yakima Ridge SE fault is the eastern extension of the Yakima Ridge structure. Similar to Umtanum Ridge, Yakima Ridge plunges to the east, losing structural relief from west to east before terminating within the Hanford Site boundary (Figure 5.5). Intense erosion during Pleistocene flooding together with low-amplitude folding resulted in little to no topographic expression of this structure. The top-of-basalt maps indicate an average structural relief of 65 m along this fault segment. Furthermore, the right pane in Figure 5.5 shows the location of the frontal thrust and the tapering of the structure to the east to where the relief becomes zero.

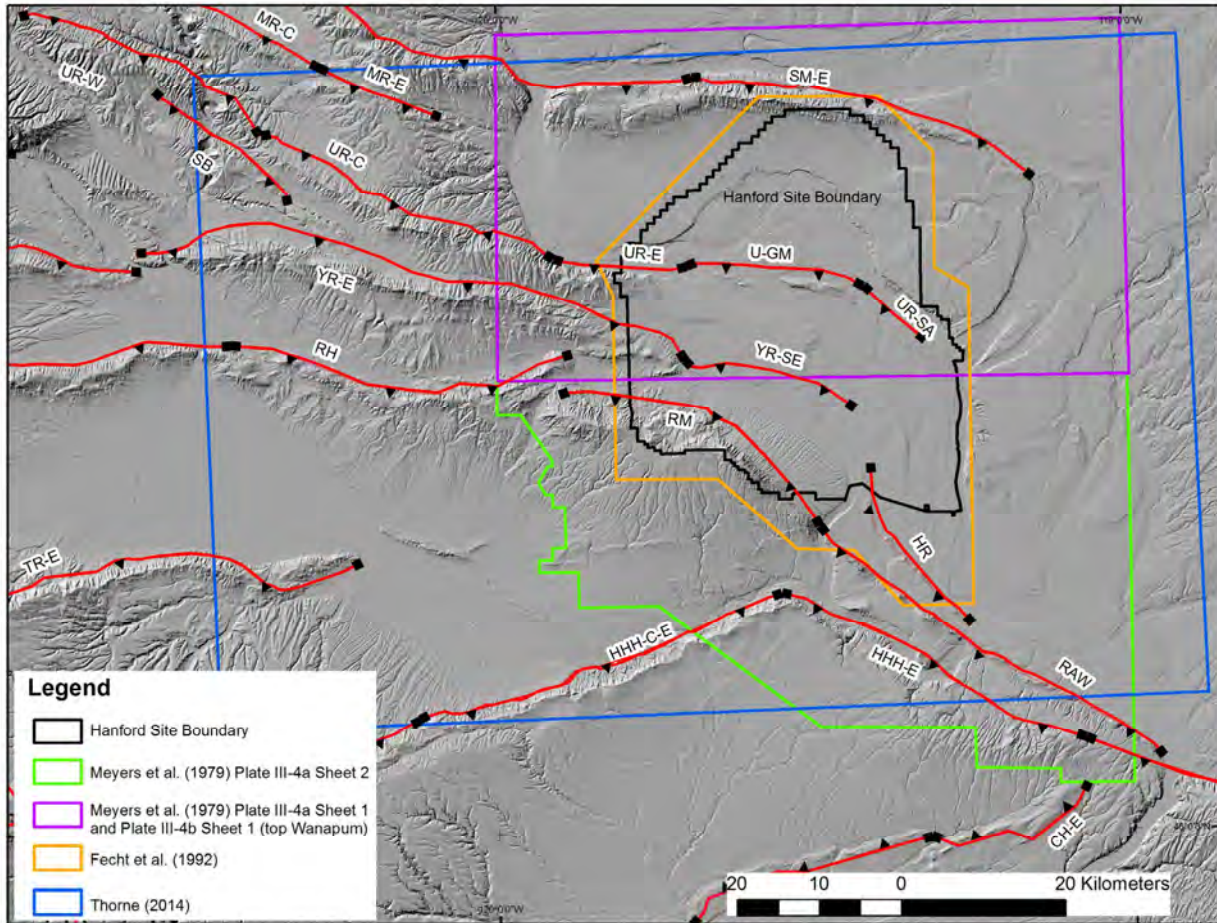


Figure 5.4. Map showing the extent of CRB structure contour maps from various sources.

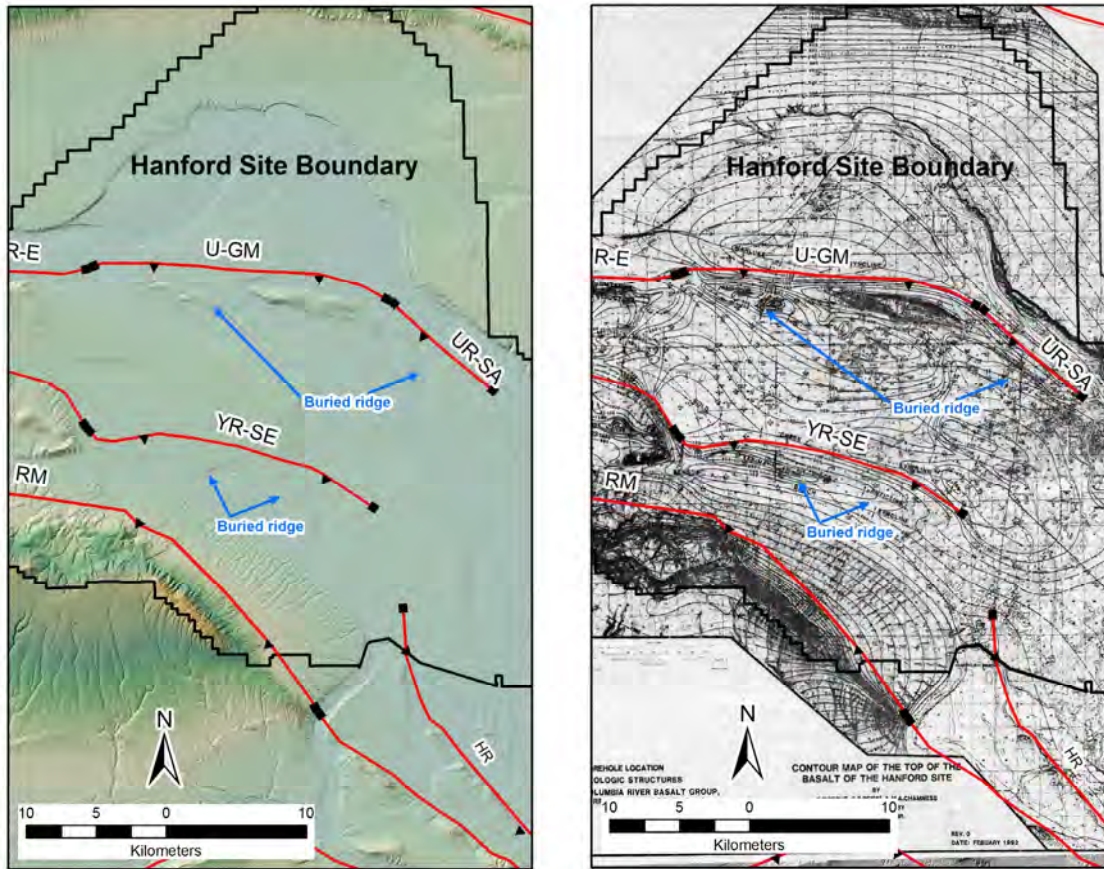


Figure 5.5. Map showing the Umtanum-Gable Mountain (U-GM) -Southeast Anticline (UR-SA) and Yakima Ridge Southeast (YR-SE) structures. The left pane shows the lack of topographic expression from Pleistocene flood erosion and burial. The right pane shows the CRB structure contour map by Fecht et al. (1992) that highlights the subsurface extent of the anticlinal ridges.

5.2.3 RAW-Rattles Structure and the Horn Rapids Fault

These faults are located south-southwest of the Hanford Site and run subparallel to one another with a northwest strike orientation. Both faults are reverse faults that dip steeply to the southwest. Past studies mostly have focused on the fault associated with the RAW alignment of doubly plunging anticlines (see Section 7.4.1 for details of past studies) extending from southeast of Rattlesnake Mountain to Wallula Gap. Outboard to the northeast of this structure is the Horn Rapids fault that has a shorter trace than the RAW alignment and lower amplitude folds associated with it (Figure 5.6). The double plunge of the anticlines along with the highly fractured basalt exposures, make it difficult to evaluate the structural relief in the field. Furthermore, the master faults that are responsible for uplifting the anticlines are buried by flood deposits, precluding identification of marker horizons in the field. The structure contour maps show a vertical offset of the CRB across both structures. Further, the structural relief can be measured across the locations between the anticlines suggesting that the ridges are being uplifted by a single reverse fault as opposed to some type of en echelon oblique fault zone (Figure 5.7). The top-of-basalt map from Myers et al. (1979) indicates an average structural relief across the RAW fault and Horn Rapids fault of 130 m and 90 m, respectively.

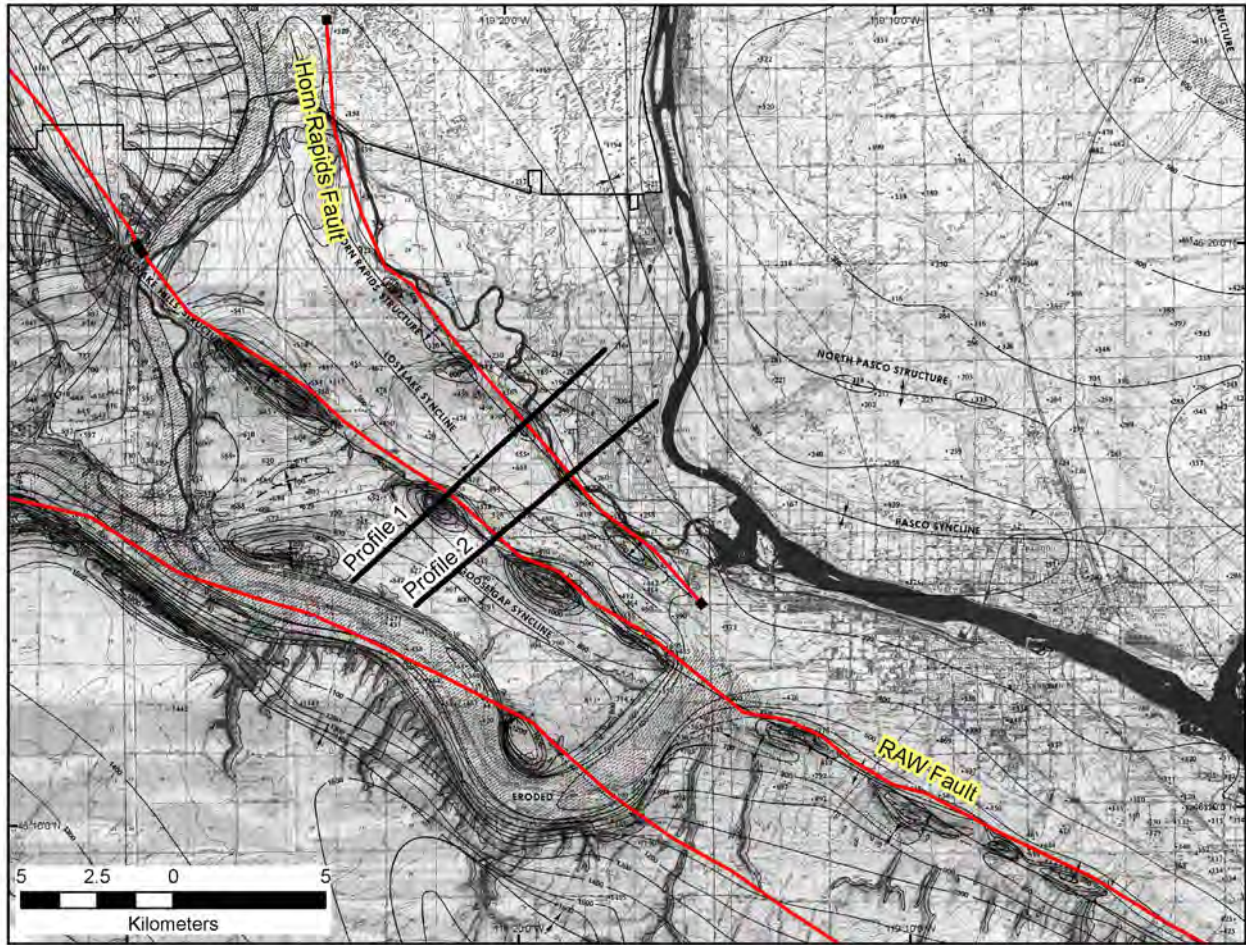


Figure 5.6. Map showing the Horn Rapids fault and RAW-Rattles structure over a top-of-CRB structure contour map by Myers et al. (1979). Cross sections of Profile 1 and 2 are shown in Figure 5.7.

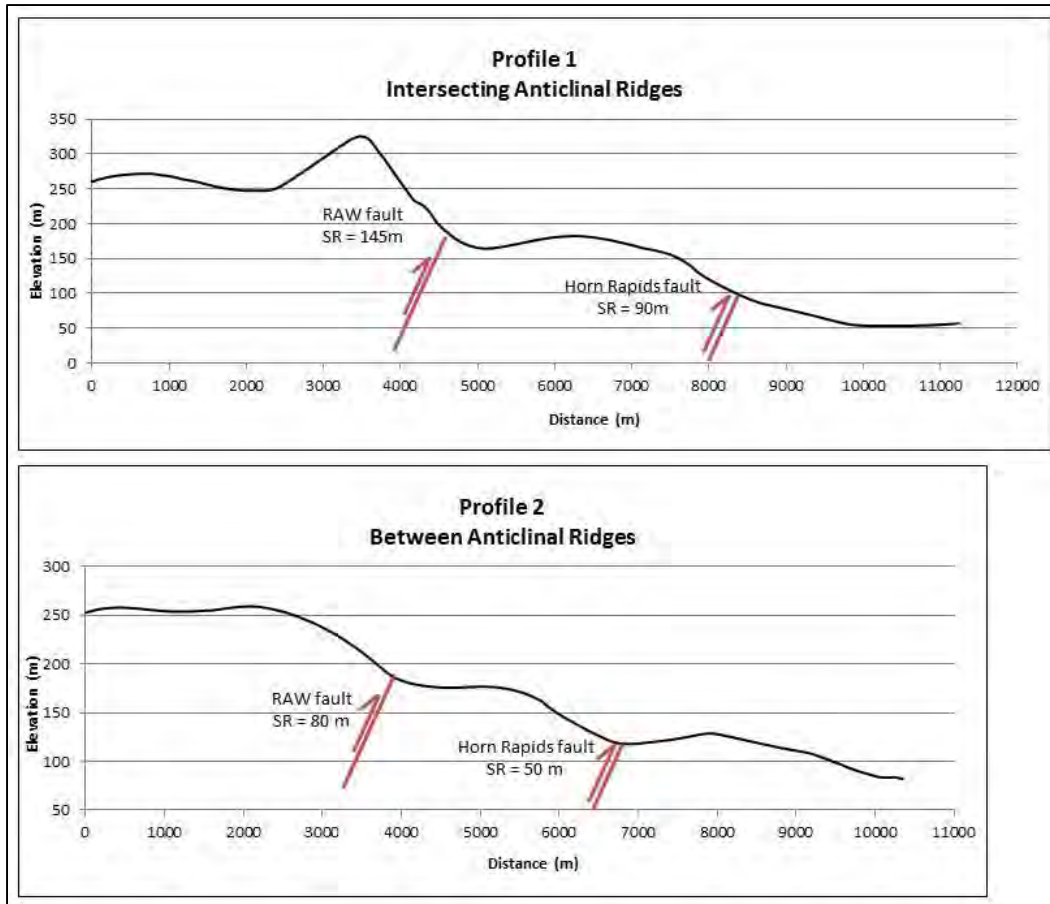


Figure 5.7. Cross sections from the Thorne et al. (2014) top-of-basalt DEM. Profile 1 shows offset basalt across the doubly plunging anticlines associated with the two faults (locations and dip of faults is schematic). Profile 2 shows offset basalt between the anticlines. (SR = structural relief.)

5.3 Results of Structural Relief Analysis

Using the methods described above, structural relief information was tabulated for each major structure within the YFB study area. In all of these cases, multiple relief measurements were collected along the folds in order to capture the range of uncertainty and best estimates for average (mean) and maximum values (Figure 5.8). The average (mean) value for each fault segment was used in the evaluation of the fault sources. Results of the structural relief analysis are provided in Table 5.1.

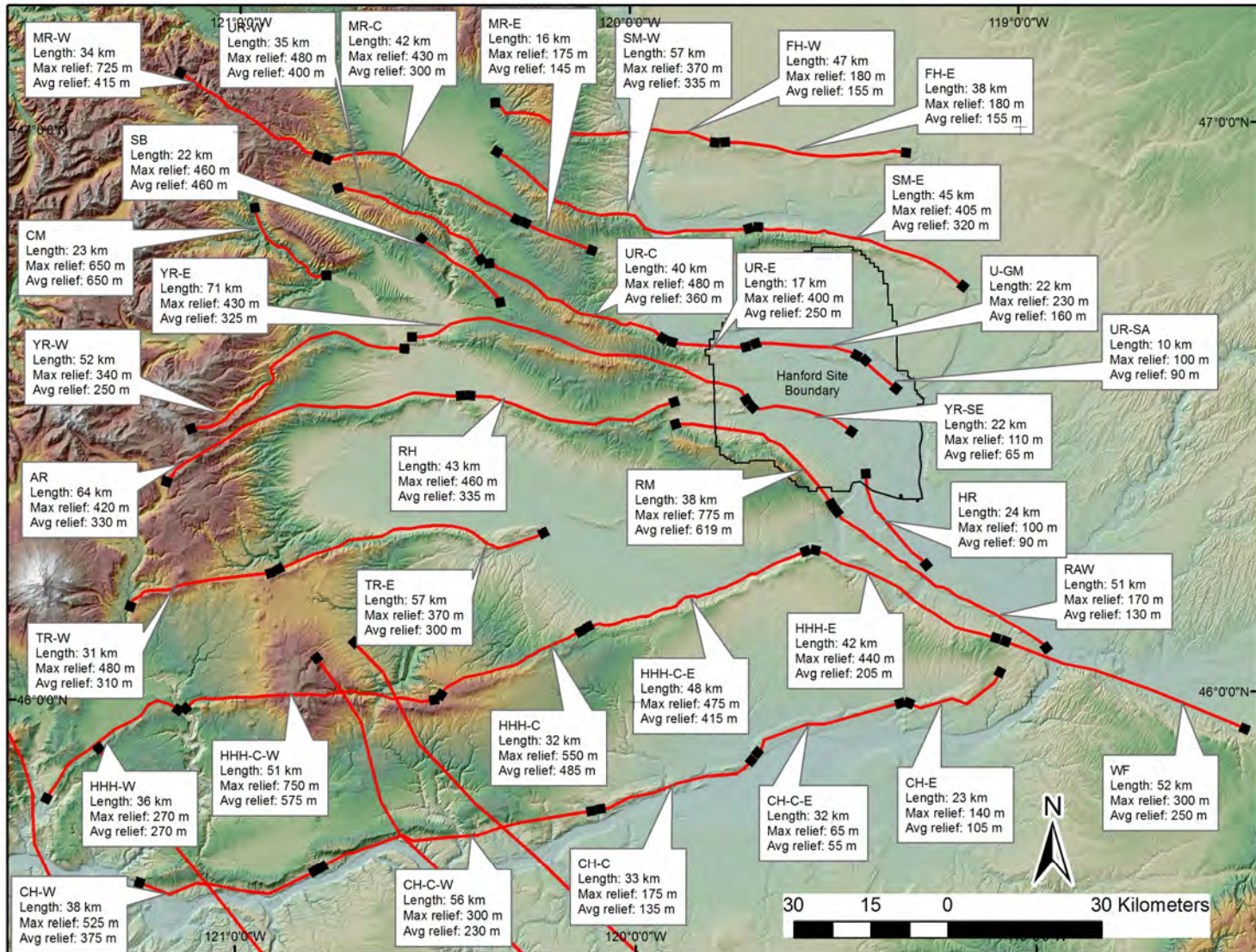


Figure 5.8. Map showing average and maximum vertical structural relief for fault segments.

Table 5.1. Mean structural relief measurements for fault sources in the YFB.

Fault Source	Fault Source Acronym	Structural Relief (m)
Ahtanum Ridge	AR	330
Cleman Mountain	CM	650
Columbia Hills Central-East	CH-C-E	55
Columbia Hills-East	CH-E	105
Columbia Hills-West	CH-W	375
Columbia Hills-Central	CH-C	135
Columbia Hills-Central-West	CH-C-W	230
Frenchman Hills-East	FH-E	155
Frenchman Hills-West	FH-W	155
Horn Rapids Fault	HR	90
Horse Heaven Hills-Central	HHH-C	485
Horse Heaven Hills Central-East	HHH-C-E	415
Horse Heaven Hills Central-West	HHH-C-W	575
Horse Heaven Hills-East	HHH-E	205
Horse Heaven Hills-West	HHH-W	270
Manastash Ridge-Central	MR-C	300
Manastash Ridge-East	MR-E	145
Manastash Ridge-West	MR-W	415
Rattles	RAW	130
Rattlesnake Hills	RH	335
Rattlesnake Mountain	RM	619
Saddle Mountains-East	SM-E	320
Saddle Mountains-West	SM-W	335
Selah Butte	SB	460
Toppenish Ridge-East	TR-E	300
Toppenish Ridge-West	TR-W	310
Umtanum Ridge-Central	UR-C	360
Umtanum Ridge-East	UR-E	250
Umtanum Ridge-Southeast Anticline	UR-SA	90
Umtanum Ridge-West	UR-W	Q
Umtanum-Gable Mountain	U-GM	160
Wallula Fault	WF	250
Yakima Ridge-East	YR-E	325
Yakima Ridge-West	YR-W	250
Yakima Ridge-Southeast	YR-SE	65

6.0 Kinematic Analyses Using Earthquake Focal Mechanisms

The seismicity data analyzed for this study are focal mechanisms of earthquakes recorded between 1970 and 2012 by the Pacific Northwest Seismographic Network (Figure 6.1). The focal mechanisms were transmitted via email from Alan Rohay to J. Unruh on 27 February 2013. The vast majority of earthquakes in the focal mechanism catalog are small magnitude events (M1-M4). The focal mechanisms were calculated and evaluated for quality by the University of Washington. A readme file with metadata on the compilation, review and archival of the focal mechanisms is available from:

ftp://ftp.ess.washington.edu/pub/seis_net/focal.readme.

The earthquakes and their associated focal mechanisms were grouped into distinct spatial domains containing a minimum of about 25 events. As discussed in greater detail below, the spatial domains were selected to evaluate deformation associated with specific structures or subdomains in the YFB. The data were further subdivided into discrete depth domains to compare and contrast seismogenic deformation in the upper 3 km, which generally encompasses the depth of the CRB, from seismicity below 8 km in the sub-basalt sedimentary and crystalline basement rocks. Each domain is identified by a four-letter tag that is used to label and track the associated data input and output files throughout the various steps in the analytical process.

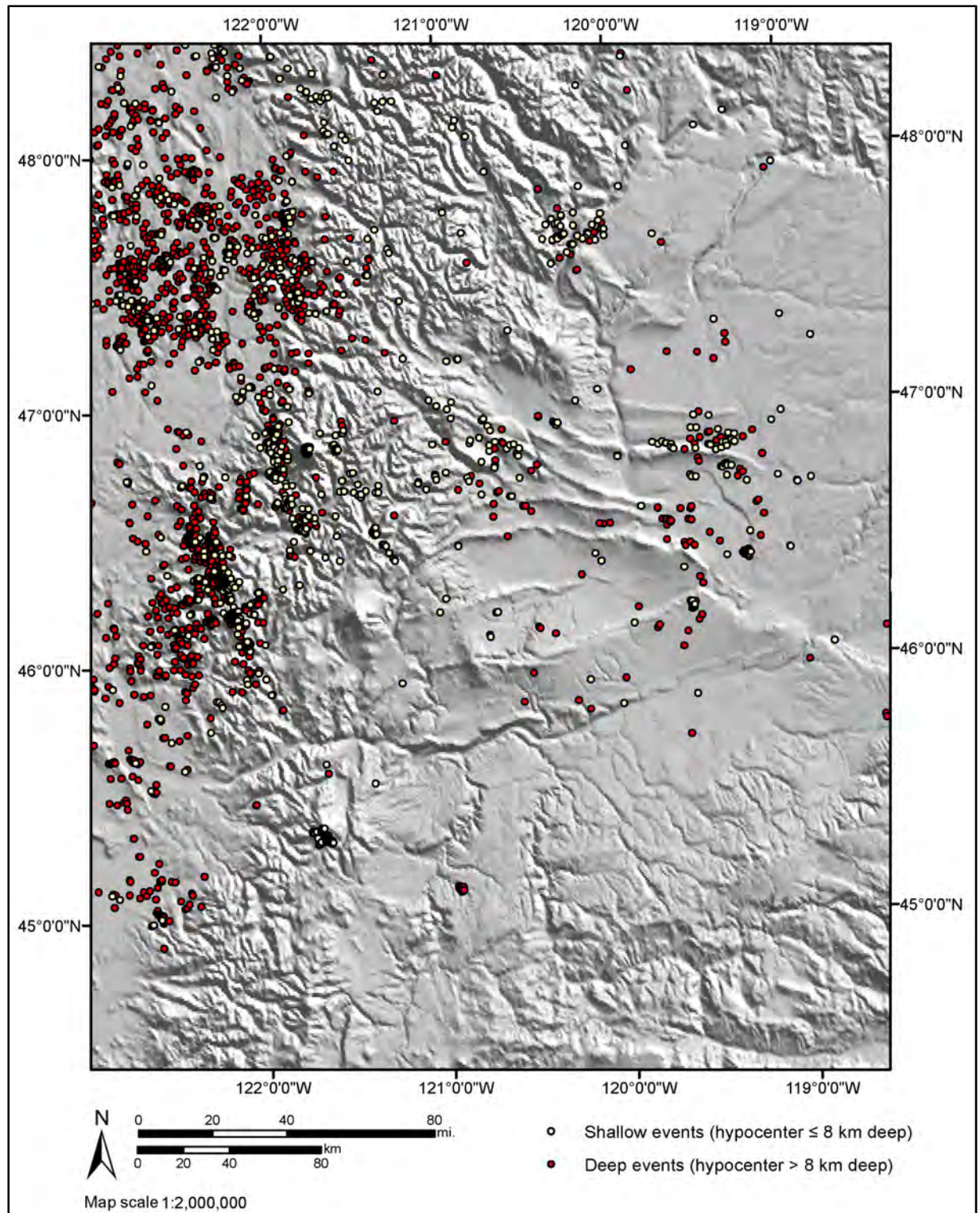


Figure 6.1. Earthquakes recorded during 1970–2011 for which focal mechanisms are available. Epicenters are color-coded to distinguish events occurring above (yellow) and below (red) the 8-km depth. Earthquake locations and focal mechanisms from the University of Washington (for source and metadata, see readme file available from ftp://ftp.ess.washington.edu/pub/seis_net/focal/readme).

6.1 Analytical Approach

We used a micropolar continuum model for distributed brittle deformation (Twiss et al. 1993; Twiss and Unruh 1998) as the basis for inverting groups of focal mechanisms from individual domains for components of a reduced deformation rate tensor. Unruh and Hauksson (2009; and references cited therein) provide a detailed description of the analytical approach. Data inversions were performed using an automated gridsearch algorithm called FLTSLP_2K6 (L. Guenther and R. Twiss, University of California, Davis; see Appendix D in Guenther 2004, for user's manual). The inversion algorithm incorporates standard bootstrap methods to estimate uncertainties in the best-fit model parameters. The micropolar deformation model is parameterized by the following:

- the orientations of the three principal strain rates ($d_1 > d_2 > d_3$; lengthening positive)
- a scalar parameter (D) formed by a ratio of the differences in the principal strain rates, and which characterizes the shape of the strain rate ellipsoid
- a scalar parameter (W) that characterizes the relative vorticity of rigid, fault-bounded blocks about an axis parallel to the intermediate principal strain rate axis d_2
- the ratio V of the vertical deviatoric deformation rate to the maximum deformation rate (Unruh et al. 2002). Positive values of V indicate net crustal thickening, negative values indicate net crustal thinning, and a value of zero indicates horizontal plane strain (Lewis et al. 2003).

The micropolar continuum theory that forms the basis for the inversion relates patterns of distributed seismogenic slip to regional velocity boundary conditions (Twiss et al. 1993; Twiss and Unruh 1998). Because the period of time over which the earthquakes used in the analysis occurred is very short and essentially instantaneous relative to geologic time during which significant deformation accumulates, the incremental strains represented by the seismicity data are assumed to be equivalent to the strain rates that form the basis of micropolar theory. For ease of discussion, the principal strain rates will be referred to simply as “maximum extension” and “maximum shortening” (d_1 and d_3 of the inversion solution, respectively).

6.2 Results

In the following discussion, the location and extent of the spatial domains defined for the inversions are shown on a series of maps. The results of the inversion analyses for individual domains, identified by their four-letter tags, are presented in Table 6.1. For each domain, the table lists the best-fit values of the inversion parameters obtained from the bootstrap analysis, as well as the mean values of the parameters within their 95% confidence limits. The table provides the standard deviations for the orientations of the maximum extensional and shortening strains, and the 95% confidence limits for the scalar parameters D , W , and V .

The following sections describe the assumptions used to define the spatial domains and discuss details of the inversion results for those domains.

Table 6.1. Results of the inversion analyses for individual domains

Domain Number	Domain Tag	Best-Fit d1 Trend	Best-Fit d1 Plunge	Mean d1 Trend	Mean d1 Plunge	Std. Dev. (°)	Best-Fit d3 Trend	Best-Fit d3 Plunge	Mean d3 Trend	Mean d3 Plunge	Std. Dev. (°)	Best Fit D	Mean D	95% C.L.	Best Fit W	Mean W	95% C.L.	Best-Fit V	Mean V	95% C.L.	Num. Data	Domain Description*
1	CRVR	59	-64	60	-64	20.2	155	-3	156	-3	13.8	0.5	0.5	0.2/-0.2	-0.09	-0.04	0.9/-0.5	0.79	0.79	0.2/-0.4	47	Columbia River domain, all events
2	HHHC	288	-87	292	-81	20.8	204	0	199	0	13.4	0.5	0.5	0.2/-0.2	0.05	0.09	0.5/-0.4	1.00	0.83	0.2/-0.7	30	Horse Heaven Hills-Central domain, all events
3	NRVR	98	-47	98	-48	19.9	179	8	178	9	14.2	0.6	0.6	0.2/-0.2	-0.13	-0.12	0.8/-0.5	0.57	0.48	0.5/-0.9	62	Naches River domain, all events
4	RSHL	82	-18	85	-9	39.9	173	-3	175	0	21.9	0.4	0.5	0.2/-0.2	0.04	0.04	0.6/-0.8	0.02	0.20	0.7/-0.6	67	Rattlesnake Hills domain, all events
5	SDMT	121	-41	119	-42	27.2	180	31	181	27	27.2	0.6	0.6	0.2/-0.3	0.31	0.34	0.4/-0.4	0.18	0.34	0.7/-0.6	71	Saddle Mountains domain, all events
6	SDMD	111	-58	111	-56	21.3	174	16	173	18	12.9	0.5	0.5	0.3/-0.3	-0.02	-0.01	0.5/-0.6	0.63	0.54	0.5/-0.9	29	Saddle Mountains domain, deep events
7	HHHD	278	-73	278	-71	10.4	194	2	193	1	7.5	0.5	0.5	0.2/-0.2	0.08	0.1	0.4/-0.4	0.91	0.85	0.1/-0.7	24	Horse Heaven Hills domain, deep events
8	NRVD	98	-61	94	-60	6.1	187	0	189	-3	5.6	0.5	0.5	0.1/-0.2	0.24	0.31	0.3/-0.3	0.78	0.75	0.2/-0.2	23	Naches River domain, deep events
9	RSHD	84	32	84	30	6.4	173	-2	174	0	12	0.5	0.5	0.2/-0.2	-0.23	-0.22	0.3/-0.4	0.25	0.23	0.4/-0.5	30	Rattlesnake Hills domain, deep events
10	NRVS	103	45	104	37	23.3	188	-6	187	-10	25.9	0.5	0.5	0.4/-0.4	-0.09	-0.04	0.9/-0.7	0.50	0.22	0.8/-1.0	11	Naches River domain, shallow events (≤ 3km)
11	WSMS	64	-36	64	-36	25.4	135	24	135	24	25.3	0.3	0.3	0.5/-0.3	0.61	0.62	0.4/-1.2	0.09	0.15	0.8/-1.1	10	Western Saddle Mountains domain, shallow events (≤ 3km)
12	ESMS	114	49	114	49	9.3	210	5	209	4	8.4	0.6	0.6	0.2/-0.3	-0.17	-0.13	1.0/-0.9	0.63	0.61	0.4/-0.7	19	Eastern Saddle Mountains domain, shallow events (≤ 3km)
13	WISS	233	14	233	14	39.8	335	37	335	38	29.5	0.2	0.3	0.5/-0.2	0.37	0.41	0.6/-1.4	-0.37	-0.15	1.1/-0.7	26	Wooded Island Swarm domain, shallow events (≤ 3km)
14	MTRN	107	-26	106	-37	22.7	192	11	192	6	7.4	0.5	0.5	0.2/-0.2	0.38	0.35	0.3/-0.4	0.13	0.45	0.5/-0.6	224	Mount Rainier domain, all events
15	OWLW	261	-74	269	-74	9.7	148	-7	153	-7	13.7	0.4	0.5	0.2/-0.1	0.39	0.44	0.2/-0.2	0.90	0.88	0.1/-0.5	248	Western Olympic-Wallowa lineament domain, all events
16	MSH1	133	21	134	21	6	220	-9	220	-10	8.3	0.5	0.5	0.2/-0.3	0.05	0.05	0.4/-0.5	0.12	0.09	0.4/-0.5	31	Mount St. Helens, domain 1
17	MSH2	103	-41	103	-41	7.3	193	-1	194	-1	7.3	0.5	0.5	0.3/-0.2	-0.60	-0.57	1.0/-0.4	0.44	0.44	0.5/-0.5	22	Mount St. Helens, domain 2
18	MSH3	97	-27	98	-26	17.2	190	-6	191	-7	10.4	0.6	0.6	0.2/-0.2	0.21	0.24	0.6/-0.7	0.30	0.33	0.7/-0.7	51	Mount St. Helens, domain 3
19	MSH4	89	-34	91	-33	9.5	186	-11	188	-11	9.2	0.5	0.5	0.3/-0.2	0.13	0.16	0.4/-0.6	0.26	0.26	0.7/-0.4	29	Mount St. Helens, domain 4
20	MSH5	140	12	139	9	7.9	43	31	43	32	8.4	0.6	0.5	0.1/-0.2	-0.33	-0.31	0.5/-0.5	-0.18	-0.24	0.3/-0.3	44	Mount St. Helens, domain 5
21	MSH6	134	-14	134	-15	8.3	222	8	222	8	4.1	0.6	0.6	0.1/-0.2	0.04	0.05	0.5/-0.5	0.12	0.15	0.4/-0.2	55	Mount St. Helens, domain 6
22	MSH7	286	-54	286	-54	8.3	36	-14	36	-14	12.5	0.6	0.6	0.0/-0.2	0.49	0.51	0.2/-0.7	0.65	0.65	0.3/-0.6	918	Mount St. Helens, domain 7
23	MSH8	130	1	130	0	4.1	220	-13	220	-14	3.4	0.6	0.5	0.1/-0.1	0.31	0.29	0.2/-0.3	0.03	-0.01	0.1/-0.1	208	Mount St. Helens, domain 8

6.2.1 Spatial Domains Associated with Major Structures of the Yakima Fold and Thrust Belt

The first subdivision of data was based on identifying major clusters of earthquakes generally associated with structures of the YFB. All earthquakes from all depths in each domain were used in the inversion. The outlines of these domains are shown in Figure 6.2 and described as follows:

- HHC: earthquakes in the central part of the Horse Heaven Hills
- RSHL: earthquakes in the vicinity of Rattlesnake Mountain and Rattlesnake Hills (including the 2009 Wooded Island swarm events; Wicks et al. 2011)
- SDMT: earthquakes in the vicinity of Saddle Mountains and Frenchman Hills
- NRVR: earthquakes in the northwestern YFB near the Naches River
- CRVR: cluster of earthquakes straddling the Columbia River north of the YFB.

The results for the four domains in the YFB (i.e., HHC, RSHL, SDMT, and NRVR) generally show a similar north-south to north-northeast–south-southwest orientation of the maximum shortening strain (d_3), with shallow plunges ranging from about 0° to 30° (Figure 6.2; Table 6.1). The maximum extensional strain (d_1) plunges more steeply (about 20° to 65°), indicating that the deformation accommodates net crustal thickening. Values of the vertical parameter V for HHC, RSHL, and SDMT are about 0.4 (Table 6.1), which implies that the deformation is “transpressional”; i.e., intermediate between a horizontal plane strain ($V=0$) and pure horizontal shortening and vertical thickening ($V=1$). The value of V for NRVR is near zero (Table 6.1), indicating that strike-slip deformation and crustal shearing is dominant over crustal shortening in this domain.

In contrast to the north-northeast–south-southwest shortening in the YFB domains, the direction of maximum shortening in the CRVR domain to the north is northwest-southeast, and the value of $V = 0.8$ suggests that crustal shortening in this domain is dominant over strike-slip deformation (Figure 6.2).

6.2.2 Evaluation of Seismicity Below the 8-km Depth for YFB Domains

To assess deformation below the CRB in the YFB, the analysis for the domains described in the previous section was repeated using only data from earthquakes with hypocenters below the 8-km depth. The outlines of these domains are shown in Figure 6.3 and described as follows:

- HHHD: earthquakes below 8 km in the central part of the Horse Heaven Hills
- RSHD: events below 8 km in the vicinity of Rattlesnake Hills
- NRVD: events below 8 km in the northwestern YFB near the Naches River
- SDMD: events below 8 km in the vicinity of Saddle Mountains and Frenchman Hills; note that the boundary of SDMD (Figure 6.3) was redrawn from SDMT (Figure 6.2) to capture six events north of the Frenchman Hills.

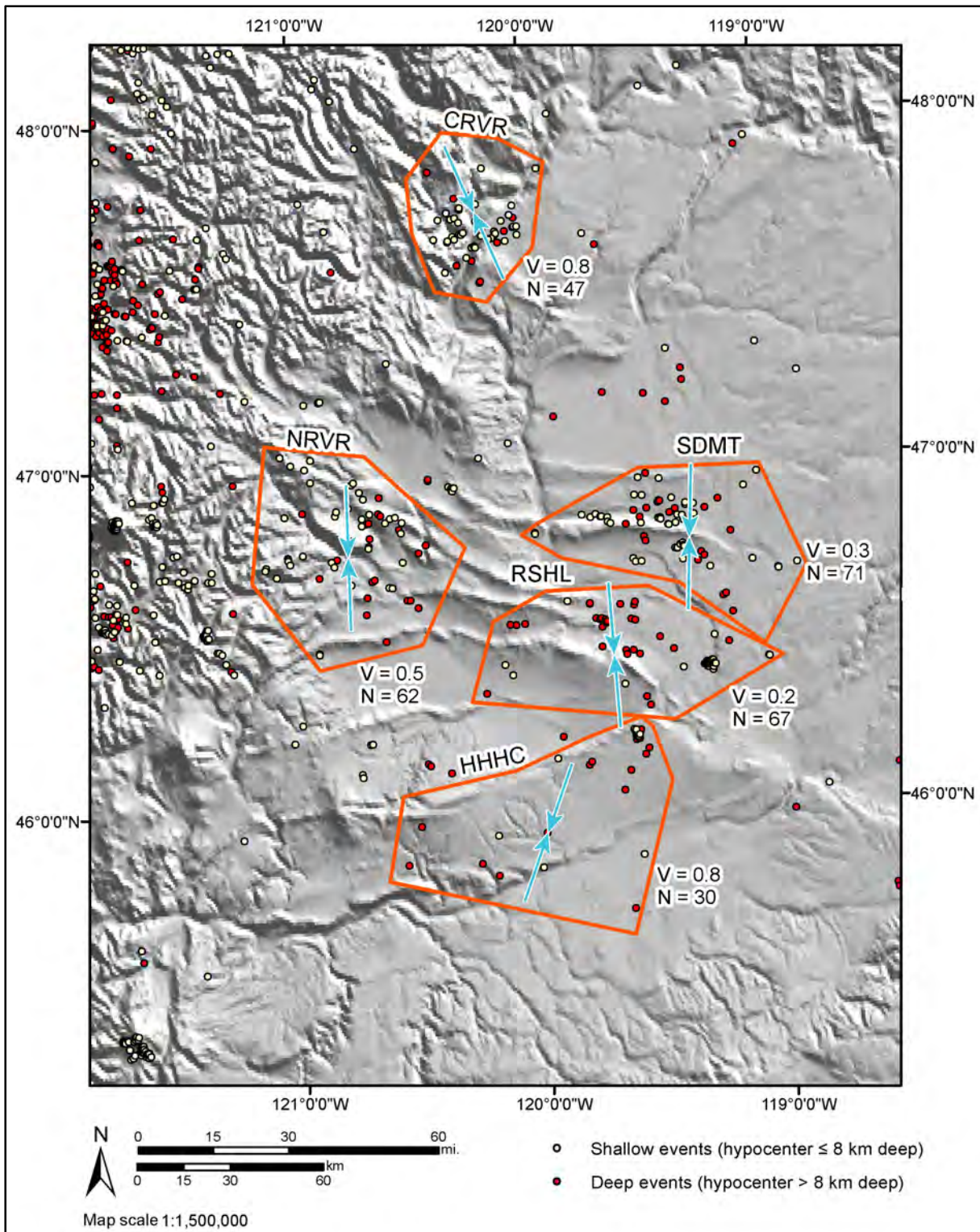


Figure 6.2. Inversion results from areas in the YFB using focal mechanisms from all depth ranges. Polygons show outlines of capture areas for data used in the inversions. Blue arrows show the azimuth of maximum shortening (d_3) derived from the inversion; numbers indicate the value of the vertical deformation parameter V . See text for additional explanation.

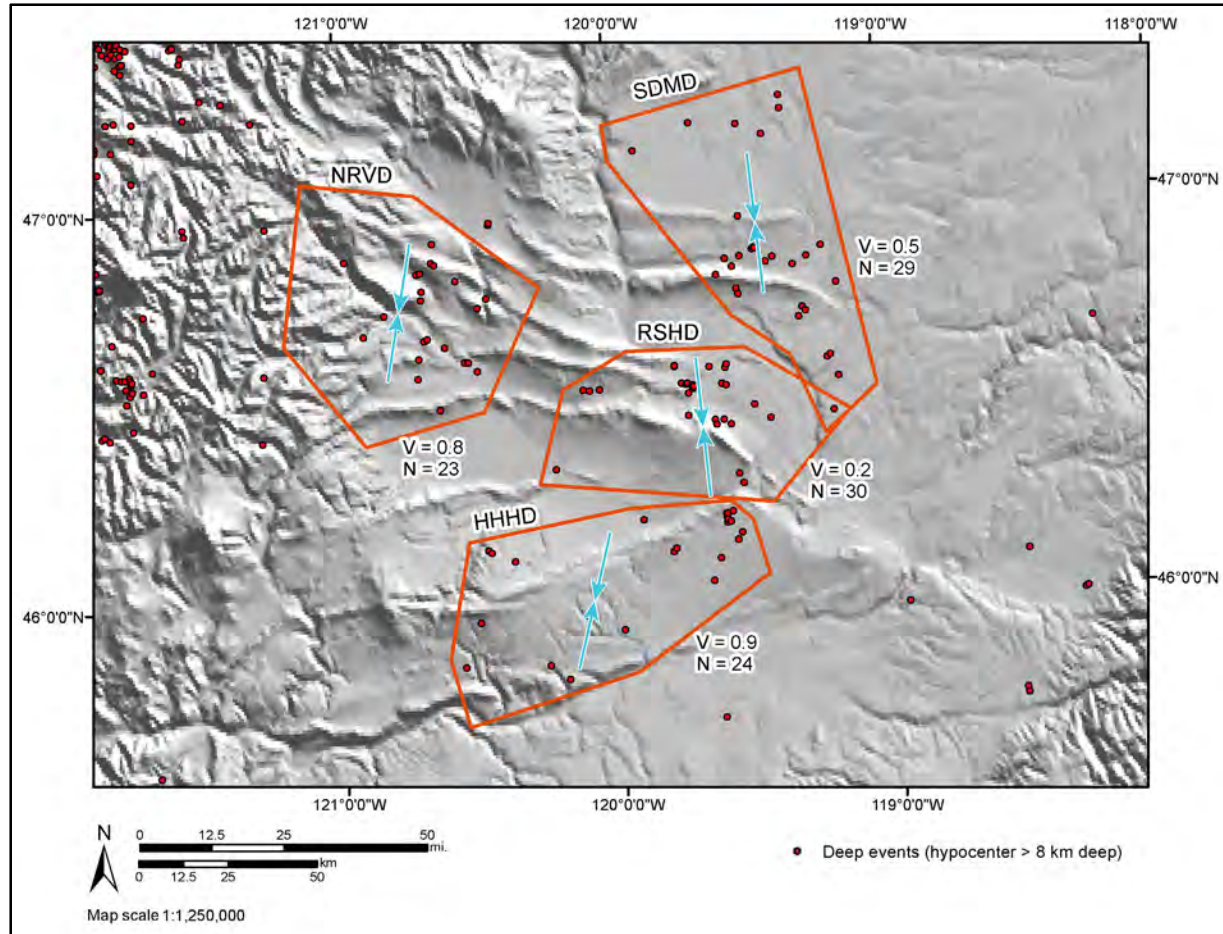


Figure 6.3. Inversion results for selected YFB domains using only earthquakes from depths greater than 8 km. Blue arrows show the azimuth of maximum shortening (d_3) from inversion of focal mechanisms within the associated polygon.

The results generally show north-south orientation of the maximum shortening strain (Figure 6.3; Table 6.1). Values of the vertical parameter V for RSHD and SDMD are about 0.2 and 0.5, respectively (Table 6.1), implying a generally transpressional deformation similar to the results obtained from inverting all data (shallow and deep) in these domains. Values of V for NRVD and HHHD are close to 1 (Table 6.1), indicating that crustal shortening is dominant over crustal shearing for earthquakes below 8 km in these domains. Notably, the crustal shortening accommodated by deep events in the Naches River domain is in contrast to the strike-slip solution obtained from inverting the deep and shallow events together (contrast NRVD vs NRVR in Table 6.1). These results imply significant vertical heterogeneity in deformation style.

6.2.3 Evaluation of Seismicity Above the 3-km Depth for YFB Domains

To assess seismogenic deformation within the CRB in the YFB, the analysis described in the previous sections was repeated using only earthquakes with hypocenters above the 3-km depth (Figure 6.4). In most cases, the boundaries of the domains shown in Figure 6.4 were modified to account for the different spatial distribution of earthquakes above 3 km relative to deeper events. No analysis of shallow seismicity was performed for the central Horse Heaven Hills (domain HHHC; Figure 6.2), because nearly

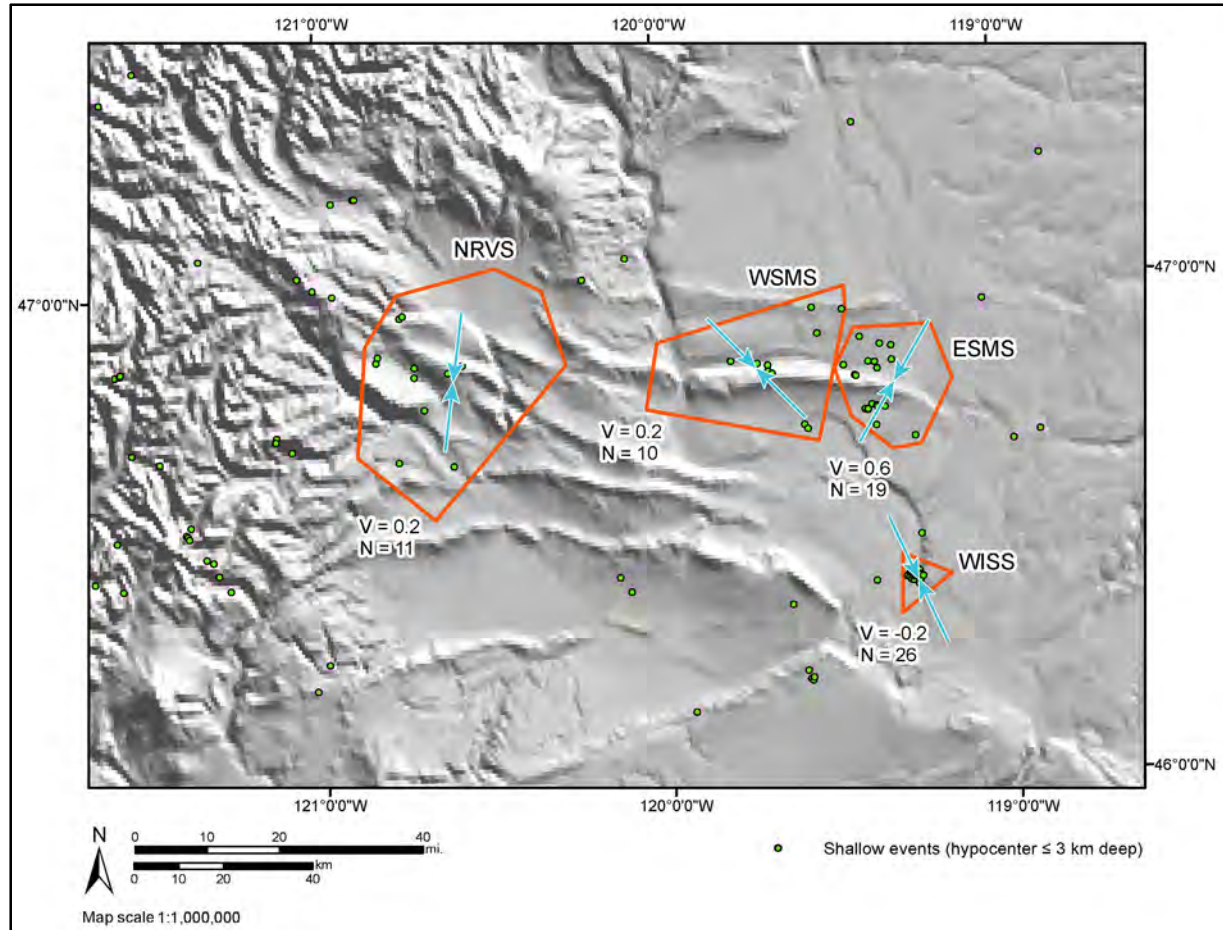


Figure 6.4. Inversion results for selected domains using only earthquakes from depths less than 3 km. Blue arrows show the azimuth of maximum shortening (d_3) from inversion of focal mechanisms within the associated polygon.

all of the seismicity in this domain is located below 8 km and an insufficient number of data were available to obtain a well-constrained solution for shallow events only. Also, no analysis of shallow seismicity was performed for the northwest corner of the YFB (i.e., the NRVR domain described in Section 6.2.1 above) because the basalt is thinner than 3 km and it is uncertain whether shallow events are occurring within basement rocks. The domains used for analysis of shallow seismicity in the CRB are described as follows (and listed in Table 6.1):

- SDMT_3: events above 3 km in the SDMT domain, which encompasses the Saddle Mountains
- ESMS: events above 3 km in the eastern part of the Saddle Mountains
- WSMS: events above 3 km in the western part of the Saddle Mountains
- WISS: shallow events in the epicentral region of the 2009 Wooded Island swarm (Wicks et al. 2011).

The orientations of d_3 from inversions of events in the upper 3 km range from northeast-southwest to northwest-southeast (Figure 6.4; Table 6.1), exhibiting greater variability than those obtained from inverting deeper data. The bulk deformation kinematics also vary considerably among the shallow domains. For example, inversion of shallow events from the western Saddle Mountains provides a strike-

slip solution, whereas shallow events in the eastern Saddle Mountains indicate a dominantly thrust/reverse style of deformation (Table 6.1). The orientation of d_3 for events composing the Wooded Island swarm is oriented northwest-southeast, subparallel to the trend of eastern Rattlesnake Mountain, which is oblique to the shortening in the Saddle Mountains, as well as the regional north-south shortening expressed by the map-scale pattern of folding in the YFB, and the generally north-south orientation of shortening derived from analysis of seismicity below 8 km (Section 6.2.2).

6.2.4 Seismicity in the Cascades

We evaluated seismicity within the Cascades Range for comparison with the YFB. The specific areas of interest focused on a cluster of earthquakes near Mt. Rainier (Figure 6.5), and a NW-trending alignment of seismicity known as the St. Helens seismic zone (Figure 6.5 and Figure 6.6). Inversion results for the Cascades domains are provided in Table 6.1. In general, the seismogenic deformation in the Cascades domains is similar to that in the YFB: transpressional deformation with NNE-SSW directed maximum shortening. In detail, the direction of shortening for individual clusters of events in the St. Helens seismic zone ranges from north-south to northeast-southwest, and the values of V are generally positive, including the events clustered directly beneath the volcano (domain MSH7; Figure 6.6 and Table 6.1).

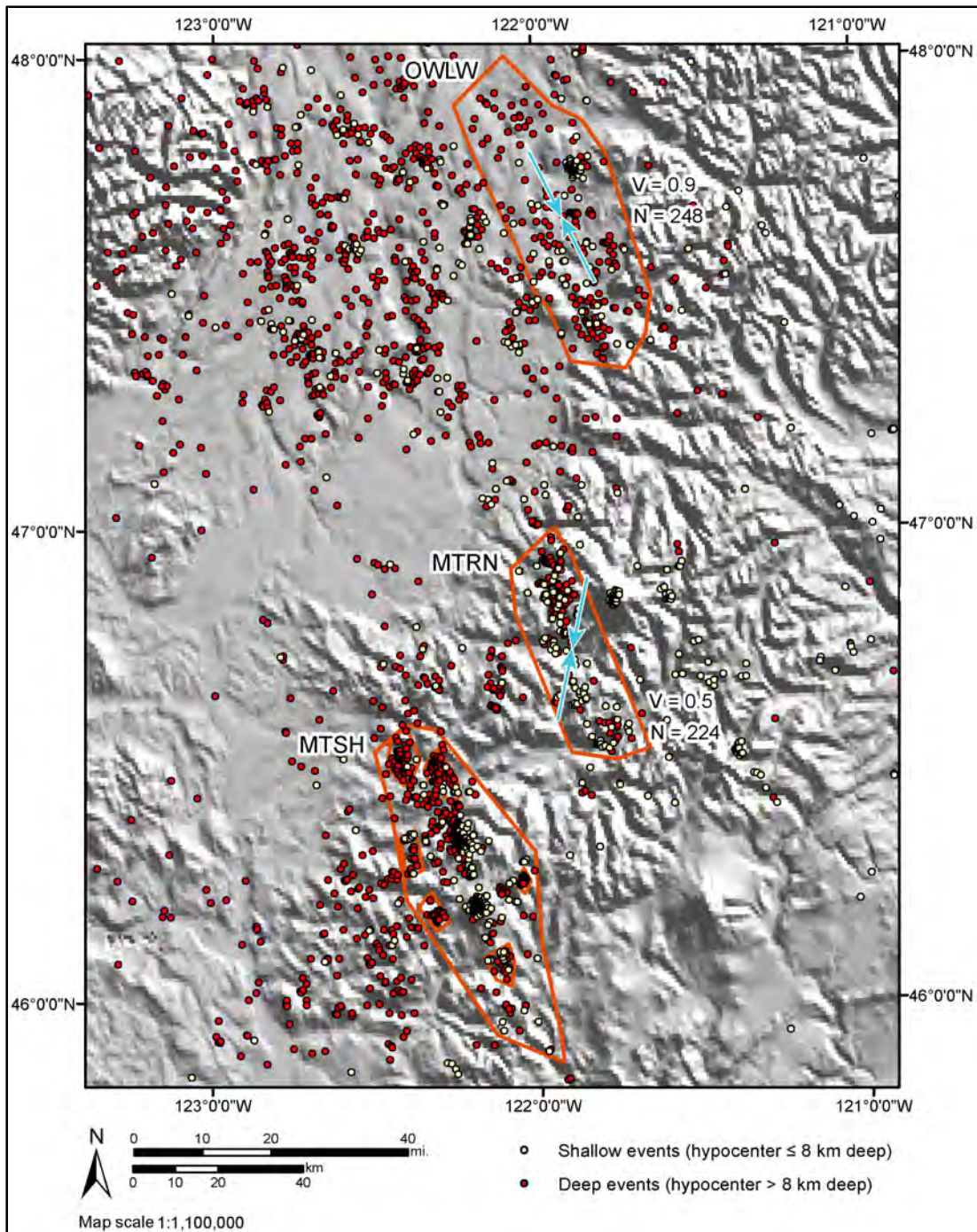


Figure 6.5. Inversion results for domains in the Cascades (all depths). Blue arrows show the azimuth of maximum shortening (d_3) from inversion of focal mechanisms within associated polygon. The domains around Mount St. Helens are shown in greater detail in Figure 4.6. Seismicity shown comes from the project crustal earthquake catalog including only those earthquakes having focal mechanisms.

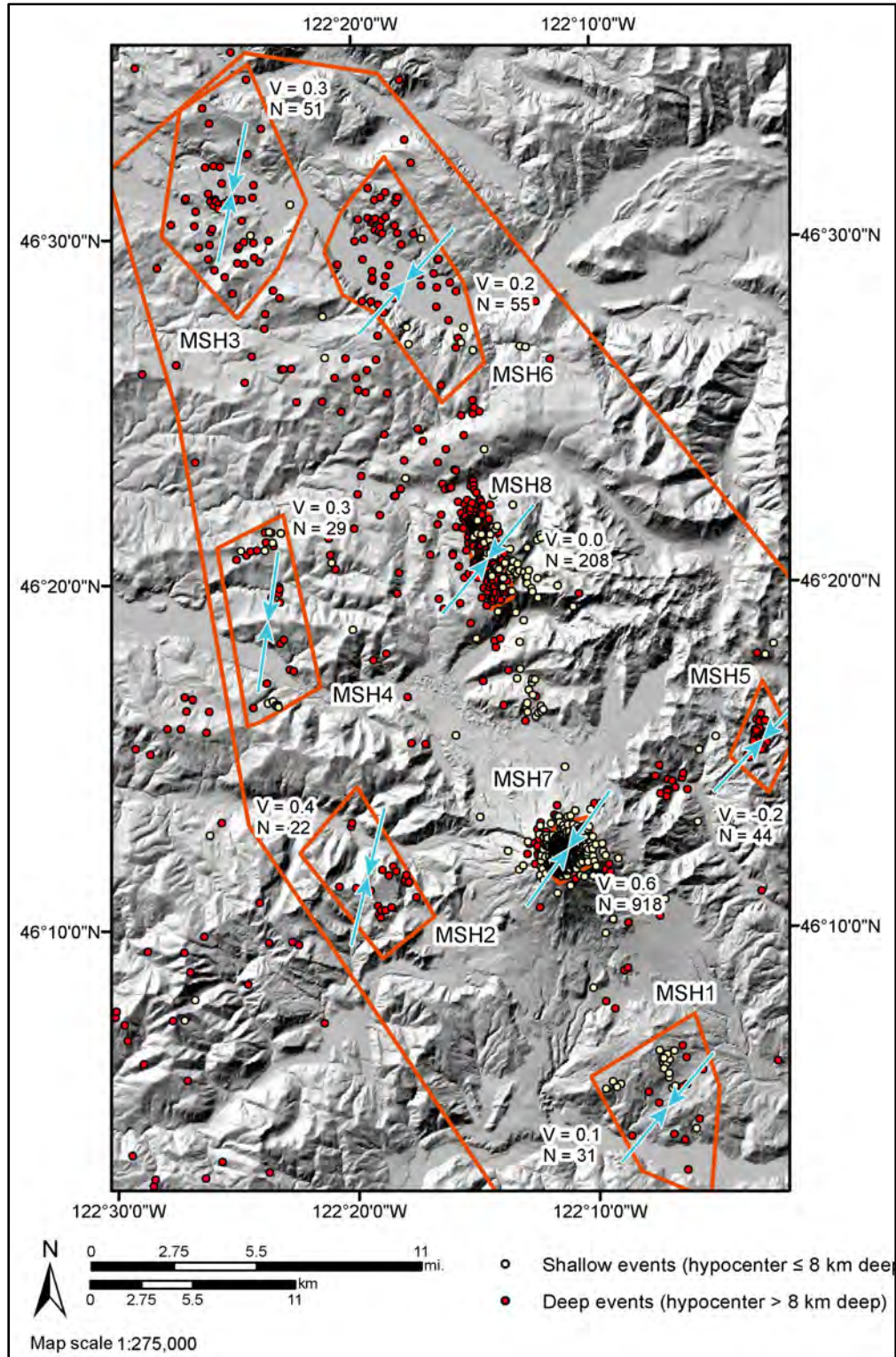


Figure 6.6. Inversion results for domains near Mount St. Helens (all depths). Blue arrows show the azimuth of maximum shortening (d_3) from inversion of focal mechanisms within the associated polygon.

6.3 Discussion

The inversion results generally show approximately north-south ($\pm 15^\circ$) shortening throughout the YFB, with perhaps a slight bias toward a north-northeast–south-southwest orientation of d_3 . These results are consistent with those of a similar analysis performed by McCaffrey et al. (2013), who inverted focal mechanisms in the YFB for components of a reduced stress tensor and found approximately NNE-SSW directed maximum compressive stress σ_1 (here assumed to be parallel to the maximum shortening strain d_3). McCaffrey et al. (2013) did not provide details of their analysis of the focal mechanisms; based on the discussion in their paper, we infer that they inverted all available focal mechanisms for a single stress tensor to characterize the entire YFB.

The approximately north-northeast–south-southwest orientations of σ_1 and d_3 derived from the focal mechanism inversions differ significantly from the $N56^\circ E$ ($\pm 4^\circ$) direction of maximum shortening in the YFB obtained by McCaffrey et al. (2013) from analysis of GPS data. It is beyond the scope of this investigation to determine whether this represents a true kinematic difference between surface displacements measured by GPS and patterns of coseismic deformation at depth, or a function of the assumptions in the analytical approaches. Treated as epistemic uncertainty, however, the different analytical results imply different kinematic models for behavior of structures with a given orientation. For example, McCaffrey et al. (2013) concluded that the RAW structure (along the OWL) is likely to behave as a reverse/thrust fault because it is nearly normal to the direction of maximum shortening derived from the GPS analysis, whereas the north-northeast–south-southwest orientation of d_3 from the focal mechanism inversions would suggest components of both right-lateral shear and crustal thickening (i.e., transpression) resolved across the RAW structure.

There is a significant component of shearing in the majority of inversion results that indicates the regional deformation is transpressional in nature rather than the result of strictly uniaxial north-northeast–south-southwest shortening and vertical thickening. The transpressional results imply that faults oblique to the direction of maximum shortening are more likely to have a lateral component of slip. The inversion results further suggest that transpressional analogues (e.g., McClay and Bonora 2001) are more appropriate for assessing behavior and linkage of structures in the YFB than in classic foreland fold-thrust belts.

Although seismicity in the upper 3 km is generally transpressional in character, there is more variability in the orientation of d_3 and the value of V for the shallow domains relative to the deep (>8 km) domains (Table 6.1). We assume that most of the seismicity above 3 km occurs in the CRB; thus, the variations in the shallow inversion results indicate that the basalts may be deforming under local stress concentrations, possibly exacerbated by the presence of fluvial interbeds in the basalt (e.g., Wicks et al. 2011), and/or are mechanically decoupled from deformation occurring below 8 km in the “basement.” If this is the case, then the seismogenic deformation in the basement (i.e., below 8 km) is a better indicator of how the crust is responding regionally to the large-scale forces driving active deformation in the YFB, and therefore it may be more representative of the style of deformation in the depth range that large earthquakes are likely to nucleate.

7.0 Fault-Specific Observations and Evaluations Based on Field Mapping and Reconnaissance

Field reconnaissance and mapping investigations were conducted at varying levels of effort. The following sections are organized to first discuss reconnaissance mapping along the Saddle Mountains and Frenchman Hills (Sections 7.1 and 7.2, respectively) that focused on evaluating unconformities and evidence for pre-Ringold growth of these anticlinal folds. The most extensive office-based and field mapping studies were conducted in a field study area along the southeastern part of Rattlesnake Mountain (Section 7.3). More limited field reconnaissance was conducted along the RAW-Rattles structure and much of the effort focused on office-based analysis of previous geologic mapping and interpretations of key structural and stratigraphic relationships at both the northwestern end of the RAW-Rattles structure (near Yakima River) as well as previous and new interpretations of the exposures at Finley quarry to evaluate the style of faulting and recurrence (Section 7.4). Likewise, much of our assessment of the style of faulting and timing of most recent faulting of the Wallula (Wallula Gap) fault relies on previous studies that we have summarized in Section 7.5 along with pertinent field observations made during two limited field reconnaissance trips.

7.1 Saddle Mountains

Members of the Quaternary Studies Team (Ryan Coppersmith and Jeff Unruh) accompanied by Steve Reidel conducted a 1-day reconnaissance of Saddle Mountains to assess exposures of deposits mapped as Ringold Formation on the flanks and crest of the anticline. We made the following key observations regarding the Ringold Formation and its involvement in the growth of the Saddle Mountains anticline:

1. The Ringold Formation and its distinctive petrocalcic horizon are present on the south limb of Saddle Mountains anticline and well exposed along a power line access road north of the town of Mattawa. Here, the Ringold Formation rests unconformably on the 10 Ma Elephant Mountain Member of the Saddle Mountains Basalt, and is associated with a gently south-dipping geomorphic surface that is directly underlain by the petrocalcic horizon (Figure 7.1). The Elephant Mountain basalt appears to dip more steeply toward the south than the upper surface of the Ringold Formation, suggesting that the Elephant Mountain-Ringold contact may be an angular unconformity. A crude estimate of the dip of the contact, using a pocket transit sighted along the contact from a distance, is about 3° to 4° toward the south. The Elephant Mountain basalt that underlies the crest of the mountain also is present and exposed in the footwall of the Saddle Mountains thrust to the north, demonstrating that the structural relief on the Elephant Mountain basalt is equivalent to the topographic relief of Saddle Mountains at this location. These relationships are consistent with our assessment of topography and structure using the Burns et al. model, as discussed in Section 5.1.
2. A thin remnant of fluvial deposits, mapped as Ringold Formation and bearing a strongly developed petrocalcic horizon, overlies the Elephant Mountain basalt at the crest of Saddle Mountains. The deposits are fine-grained, relatively massive, and about 2–3 m thick.
3. A thicker section of fluvial deposits mapped as Ringold Formation also is present along the crest of the anticline farther east. These deposits are gravelly and exhibit preserved bedding. The contact with the underlying Elephant Mountain basalt is exposed in the north-facing escarpment that composes the front of Saddle Mountains.



Figure 7.1. Photograph of south-dipping surface bearing the strong petrocalcic horizon on the backlimb of Saddle Mountains.

These observations indicate that the Ringold Formation is fully involved in the deformation and growth of the Saddle Mountains anticline; thus, growth of the fold has occurred since deposition ceased in Plio-Pleistocene time (post 3.7 Ma; Smith et al. 2000). The presence of a possible angular unconformity between the Elephant Mountain basalt and Ringold Formation suggests that growth of the structure may have begun sometime after 10.5 Ma but prior to about 4.5 Ma (age of fauna recovered from the middle Ringold Formation; Smith et al. 2000).

7.2 Frenchman Hills

We conducted a 1-day vehicle reconnaissance of the Frenchman Hills to assess potential involvement of the late Neogene Ringold Formation in the growth of the Frenchman Hills anticline. The reconnaissance was motivated by inspection of the Washington State geologic map compiled by Schuster (2005; also, see <https://fortress.wa.gov/dnr/geology/?Theme=wigm>), which shows large contiguous areas of the Ringold Formation mapped along the north and south limbs of the Frenchman Hills, suggesting that this unit may once have covered the entire structure. Topographic profiles across the Frenchman Hills extracted from the 10-m DEM further indicate that the Ringold Formation, as mapped, underlies dip slopes associated with the limbs of the fold. These relations suggest that deposition of the Ringold Formation may pre-date uplift of the modern Frenchman Hills, and thus provide post-10 Ma age constraints on the timing and rate of post-CRB uplift.

Based on examination of exposures accessible along public roads, we were not able to independently verify that the Ringold Formation is folded into an antiform across the Frenchman Hills. Much of the area shown on the state map as underlain Ringold Formation is covered by late Quaternary loess deposits. Ringold Formation may underlie the loess, but if so then the roadcuts were not deep enough to expose it.

We observed local exposures of a strongly developed petrocalcic horizon extending down into the CRB on the southern slope of the Frenchman Hills, similar to the petrocalcic horizon commonly reported in the upper parts of the Ringold Formation (Fecht and Marceau 2006). We did not observe clearly identifiable Ringold Formation deposits bearing the petrocalcic horizon in the Frenchman Hills, however.

Probable Ringold Formation deposits are locally present along the southern flank of the Frenchman Hills, and one exposure revealed basalt juxtaposed against the north-northeast-dipping Ringold Formation (strike 281/dip 58°NNE) along a fault approximately oriented N68°E/66°NW (orientation taken of most measurable plane in exposure; may not be most representative). If these measurements are correct, and if the Ringold Formation is in place, then the north dip of the Ringold on the south limb of the Frenchman Hills anticline suggests that unmapped secondary folds (and faults) are present.

Although we did not observe the Ringold Formation along or near the crest of the hills, we did observe an approximately 2- to 3-m exposure of fluvial deposits near the top of the hills (elevation 420 m). The deposits consist of poorly sorted, matrix-supported conglomerate. Clasts are subangular, range in size from about 1 to 10 cm, and consist primarily of basalt and fragments of pedogenic carbonate, which may be rip-ups of the upper Ringold petrocalcic horizon. The deposits exhibit crude, subhorizontal bedding. The deposits lack the intense weathering and induration observed in exposures of the Ringold Formation. We prefer the interpretation that the conglomerate was deposited during the Missoula floods.

7.3 Rattlesnake Mountain Study Area

Rattlesnake Mountain is a linear topographic ridge trending approximately N50°W (Figure 7.2 and Figure 7.3). This anticline is part of the RAW alignment, a fold-dominated structural trend west of Wallula Gap, which is part of a longer topographic and structural alignment that trends northwest from near Milton-Freewater, Oregon, to the northwest end of Rattlesnake Mountain (CGS FSAR; Energy Northwest 1998). As described by Myers et al. (1979), previous mapping identified only a steeply dipping, possibly reverse, fault along the steep northeastern slope of Rattlesnake Mountain. The fault was inferred to die out to the southeast into the Hodges Ranch extension anticline (Figure 7.2). There is little to no discussion of Quaternary deposits or deformation in previous characterization reports describing the Rattlesnake Mountain structure (e.g., Myers et al. 1979; Energy Northwest 1982; NRC 1982). The CGS FSAR (Energy Northwest 1998) states that the Rattlesnake Mountain fault does not appear to displace mapped Quaternary deposits. More recent mapping by Steve Reidel has been incorporated into the state of Washington 1:100,000 geologic map (Reidel and Fecht 1994) (Figure 7.2) and 1:24,000-scale maps (Reidel in press [Iowa Flats] and Reidel and Chamness in press [Snively Basin]) (Figure 7.4) and is discussed below.

The primary objective of the mapping program conducted in the Rattlesnake Mountain study area was to assess the location, style, timing, and rate of Quaternary deformation associated with the Rattlesnake Mountain anticline.

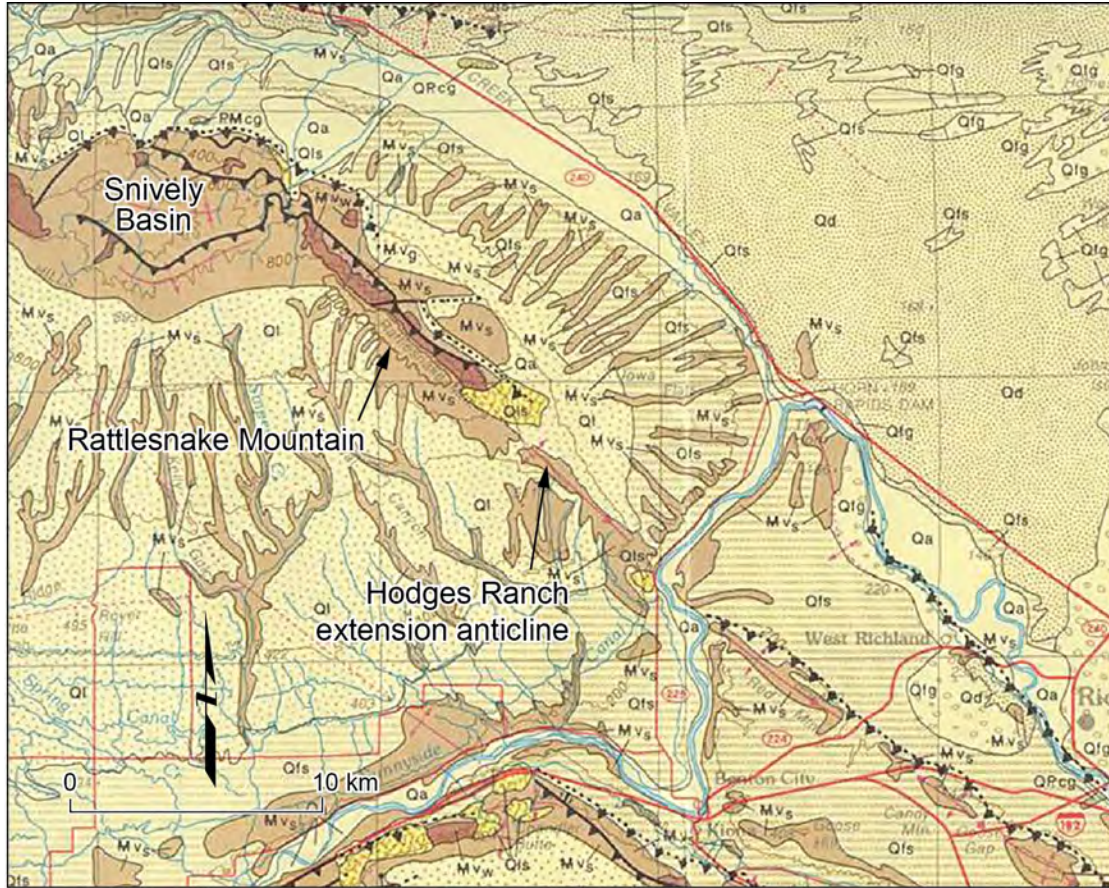


Figure 7.2. 1:100,000-scale geologic map of the Rattlesnake Mountain-Snively Basin area (from Reidel and Fecht 1994).

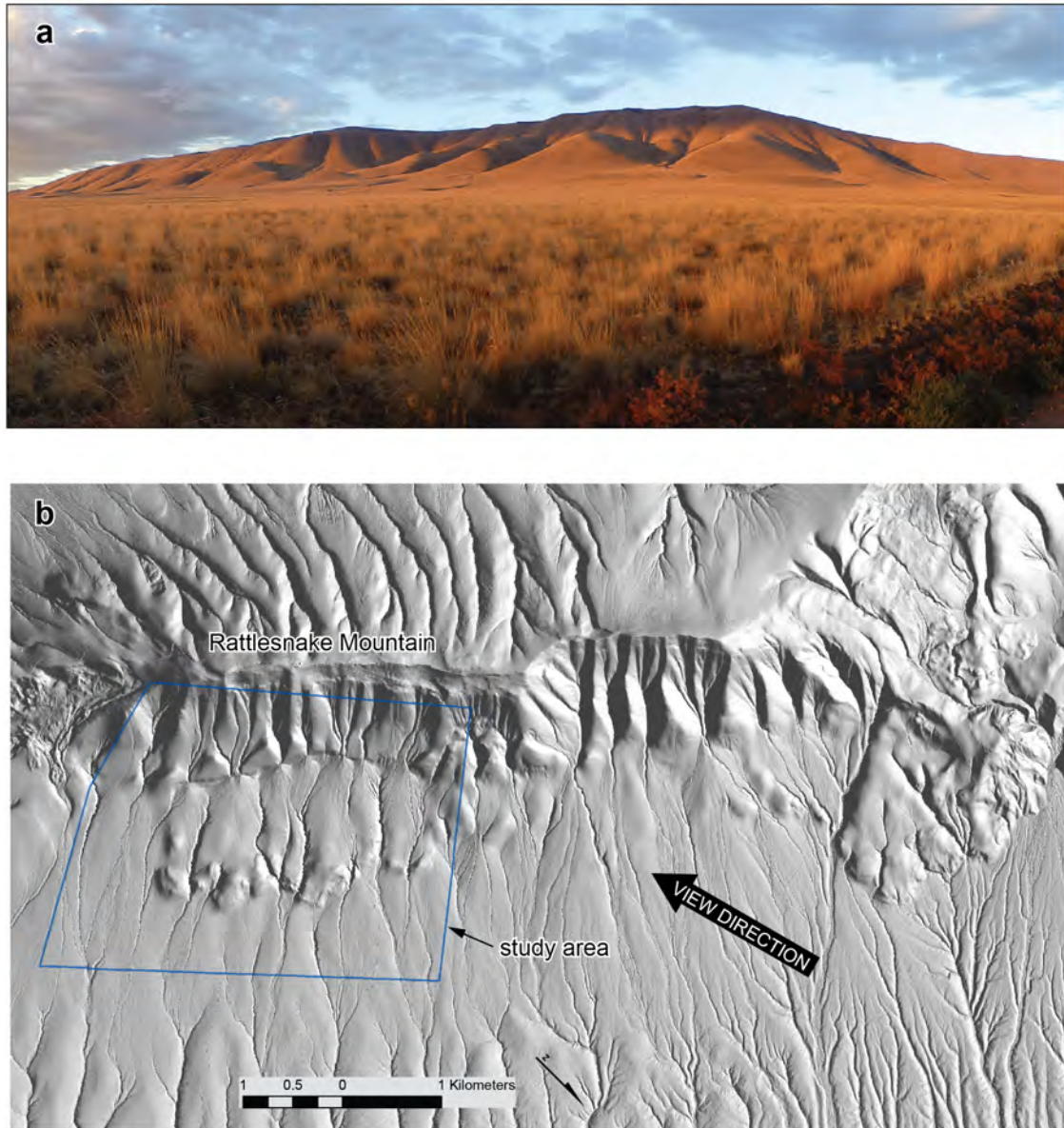


Figure 7.3. a) Panoramic photograph view to the southeast along the eastern Rattlesnake Mountain range front, and b) hillshade map derived from 1-m LiDAR DEM showing the location of the Rattlesnake Mountain study area.

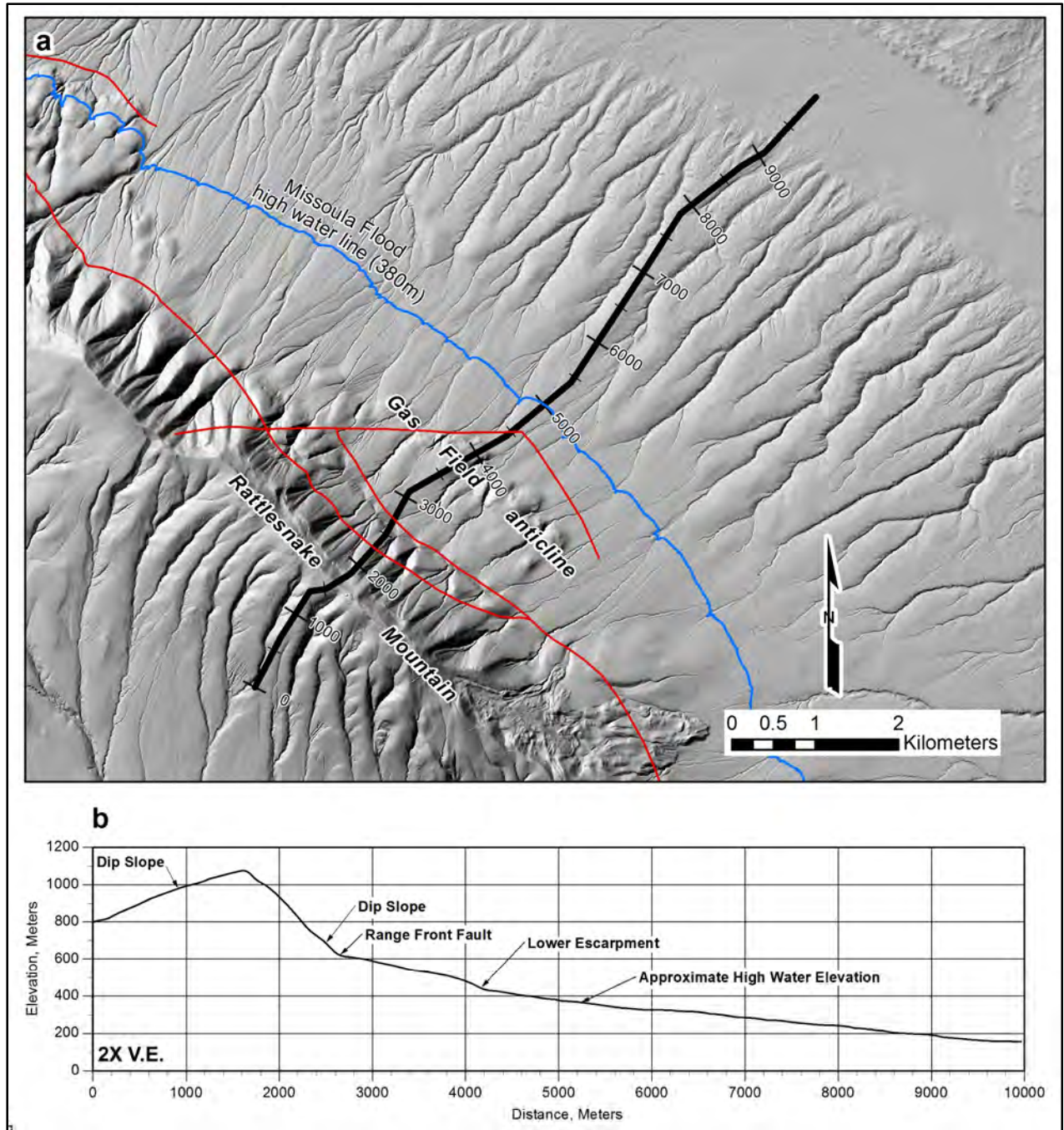


Figure 7.4. a) Hillshade map (1-m LiDAR DEM) of study area with profile location, and b) annotated topographic profile.

7.3.1 Bedrock Structure

Several faults are identified or inferred from mapping of CRBG units on the northern flank of Rattlesnake Mountain (Figure 7.2). Emergent thrust faults are mapped along the eastern end of Rattlesnake Mountain and as a series of three imbricate thrusts within Snively Basin. Reidel et al. (in press) describe Rattlesnake Mountain as an asymmetrical anticline with a faulted, steeply dipping north limb and gently south-dipping backlimb. Beds of basalt dip less than 5° to the south, whereas the north limb beds dip in excess of 50° and in some places are overturned. Reidel et al. (in press) map two faults along the north limb: a reverse fault along the prominent scarp at the geomorphic range front, and a secondary reverse fault segment that is higher in elevation and merges with the range-front fault to the southeast. Bedrock relationships mapped by Reidel et al. (in press) suggest that the structurally higher of the two faults has moved out of sequence. A third high-angle “tear fault” runs roughly east-west and is described as truncating the range-front fault but not the upper fault by Reidel et al. (in press). Based on these observations, Reidel et al. (in press) favor the upper fault segment to have the most recent movement on it. Reidel et al. (in press) do not show offset alluvium along the range-front fault, and maps no alluvium deposited over the upper fault segment in the vicinity of the study area.

Approximately 1 km outboard of the range-front fault lies the gas field anticline (Figure 7.4). The structure was drilled for natural gas production between 1913 and 1941 (Hammer 1934). Previous workers (GRC 1978 in Myers et al. 1979) mapped the structure as a landslide. The irregular topographic surface expression does resemble the toe of a slide, but no uphill source area or slide body is present. Reidel et al. (in press) map the field as an anticline that has been dissected by stream erosion. Reidel et al. (in press) speculate that there is an associated thrust fault north of the structure that is obscured.

7.3.2 Description of Alluvial Fan Units

Surficial deposits in the Rattlesnake Mountain study area include 1) alluvial fan and fluvial terrace deposits in active washes, 2) colluviums and debris-flow deposits that occur along the base and mantle the lower parts of the northern flank of the Rattlesnake Mountain, 3) areas of mixed bedrock and thin colluvial deposits, and 4) eolian deposits.

Based on interpretation of 1-m LiDAR data sets and 4 days of field reconnaissance, a sequence of up to four alluvial fan units have been identified on the northeastern flank of Rattlesnake Mountain. These are referred to as Qaf1 to Qaf4 (youngest to oldest) (Plate 1). Unit Qaf4 represents large alluvial fans that coalesce to form a broad alluvial apron or bajada. The size and lateral extent (distance from the range front) of the Qaf4 fans are considerably larger than the younger fans (units Qaf1 through Qaf3). In plan view the younger fans are cone shaped and appear to have truncated and buried parts of the older fans.

With the exception of the distal parts of the oldest Oaf4 fan, all of the mapped fan units lie well above the high-water elevations of the Pleistocene catastrophic floods and Lake Lewis, which are inferred from the presence of ice-rafted erratics stranded at elevations of 370–385 m (Baker 1973; Waitt 1980; Bjornstad et al. 2001). The ice-rafted erratics mapped on Rattlesnake Mountain lie on the distal margins of the Qaf4 fan. Weak strandlines interpreted from aerial photo lineaments between the elevations of 245 and 305 m are reported on the flanks of Rattlesnake Mountain in Snively Basin west of the study area; exposures in trenches excavated across these features confirmed the flood origin (Baker et al. 1991).

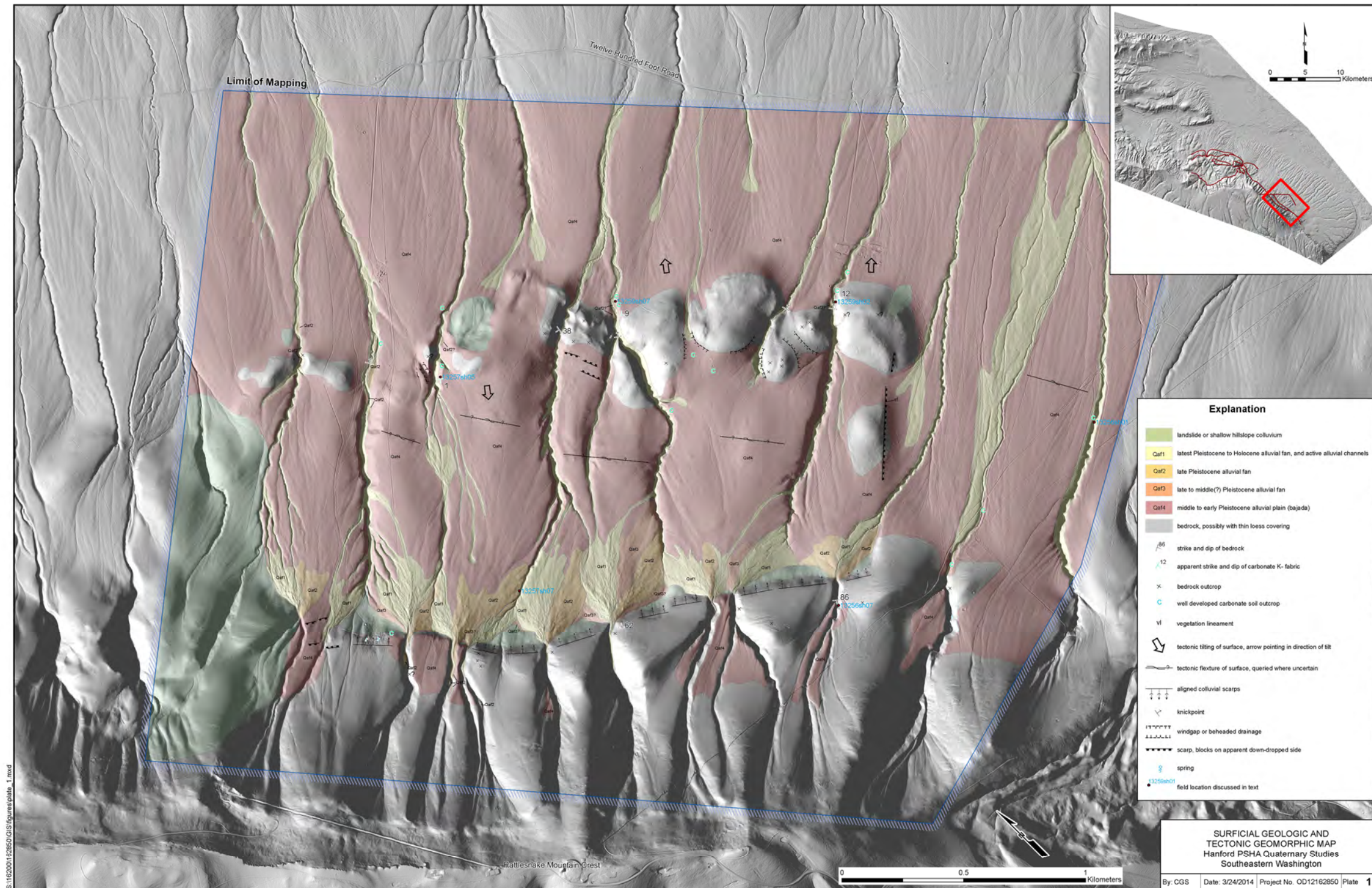


Plate 1. Surficial geologic map of the Rattlesnake Mountain study area.

There are no direct ages for the fan deposits and surfaces on Rattlesnake Mountain. Direct sampling and dating of material from the mountain were not allowed by the Cultural Permit issued for field activities for this project. Therefore, the ages of mapped fan units are estimates based on relative soil profile development and correlations to nearby localities where numerical ages from $^{230}\text{Th}/\text{U}$ -series dating of pedogenic carbonate from this study (Appendix E.1) and from previous studies (Table 4.3), along with magnetic polarity data, provide constraints on the ages of deposits (WCC 1981b; Baker et al. 1991; DOE-RL 2002). The general geomorphic and soil profile development characteristics of carbonate soils observed during this study at various localities in the study are discussed below.

7.3.2.1 Qaf4

The oldest, most extensive alluvial fan deposit identified on the northern flanks of Rattlesnake Mountain is Qaf4. Remnants of these deposits and the relict fan surface are preserved on the hanging and footwall blocks of the range-front fault, and are folded about the gas field anticline. This fan and associated soil thus provide a marker horizon that can be used to assess the vertical separation rate across the entire fault zone.

In the hanging wall of the range-front fault, the erosional surface at the base of the Qaf4 fan is cut across steeply dipping to overturned CRB and interbed units mapped as the Ellensburg Formation. This demonstrates that significant folding and growth of the Rattlesnake anticline had occurred prior to formation of the Qaf4 fans. The upper fan surface south of the range front is approximately 8–14 m above the modern channel (Figure 7.5).

Directly northeast of the range front, the Qaf4 fan surface is generally buried by younger fans (units Qaf3, Qaf2, and Qaf1). The overall morphology of the Qaf4 fans suggests the alluvial fan apices were pinned to the same drainages as the younger fans. Some of the rounding of the surface parallel to the range front into a convex form is at least in part due to post-depositional erosion of the Qaf4 surface. Relief on the Qaf4 fan surface is low relative to that of the younger fan surfaces. This is due to burial by thicker accumulations of loess. Postulated windgaps along the crest of the gas field structure suggest that channels emanating from the range during deposition of Qaf4 (Plate 1) have been abandoned following uplift along the gas field anticline. Stream-cut exposures through Qaf4 reveal typically rotten basalt clasts that are easily broken in one's fingers (e.g., locality 13256sh01, Plate 1).

The Qaf4 fan is associated with a strongly developed soil characterized by carbonate morphology Stage IV development. As noted in Table 7.1, the soil formed on the Qaf4 fan typically consisted of approximately 1 m of loess overlying a prominent, 0.5-m thick white K horizon. The K horizon was composed of an estimated 90% carbonate cementing clasts together. Throughout the K-horizon k-fabric is pervasive forming plates that are up to 5 cm thick, but typically approximately 2 cm thick. The plates sometimes are so well cemented that it takes heavy manual pressure to break them in one's hands. Where the upper portion of the K horizon was well exposed, a 5- to 10-mm-thick rind of crystalline carbonate was present at the top of the k-fabric.

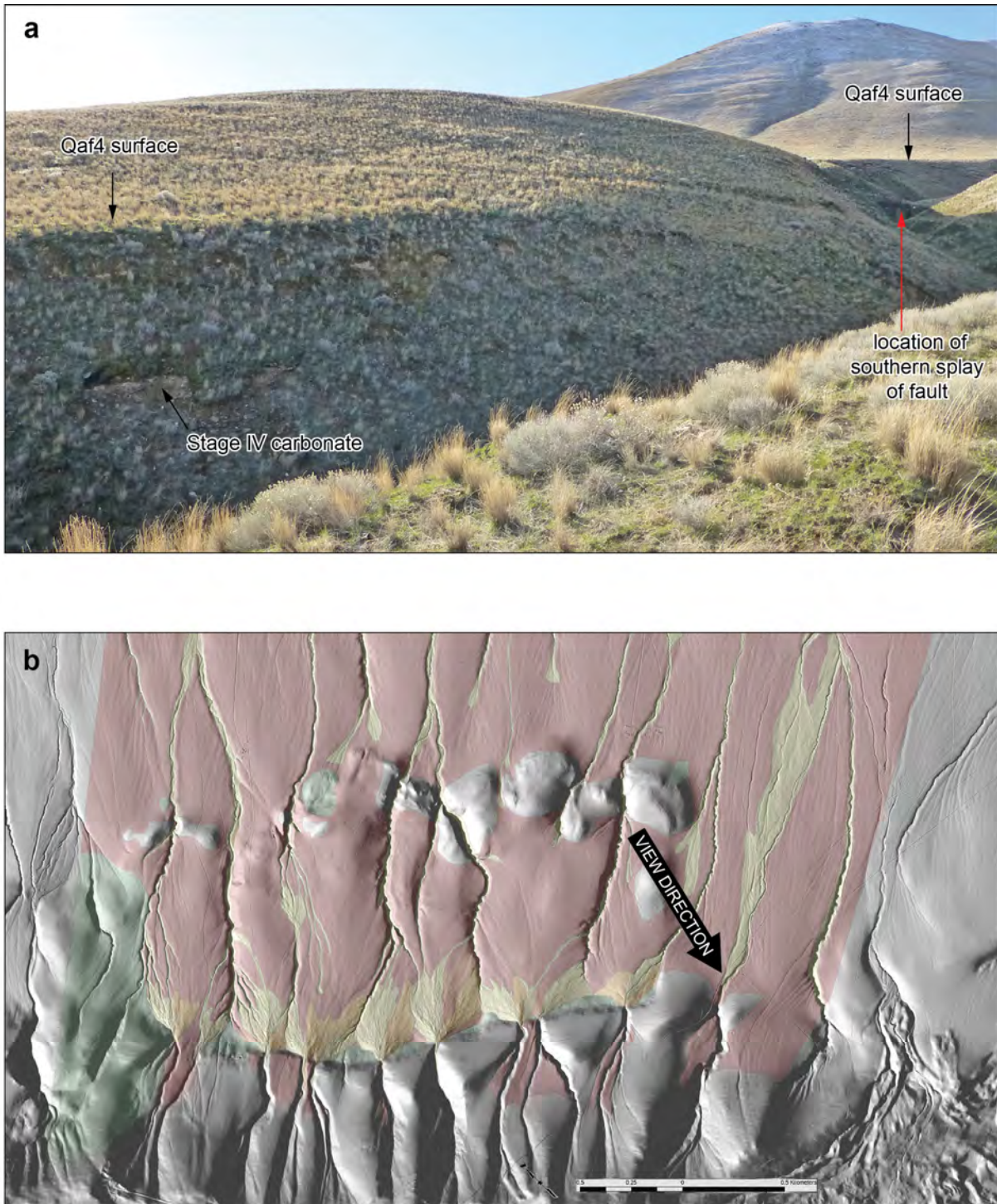


Figure 7.5. a) Photograph showing the Qaf4 fan surface in the hanging wall and footwall of the main range-front fault at the eastern end of the study area where the fault becomes blind. The pediment surface underlying the Qaf4 fan deposits north of the range front cuts across steeply dipping to overturned CRB and interbed units. Stage IV pedogenic carbonate is observed in limited exposures along the eastern margin of the drainage. b) Quaternary geologic map (see Plate 1 for explanation) showing location and view direction.

The age of the Qaf4 fan is estimated to be middle Pleistocene based on comparison of the degree of soil profile development and clast weathering of this unit relative to nearby flood gravel deposits in the Badger Coulee area that have been dated using both Th/U analysis of pedogenic carbonate rinds and magnetic polarity data (Baker et al. 1991; Table 4.3 and Table 7.1). The thickness and degree of carbonate soil development in the Qaf4 fan observed at several locations is illustrated in Figure 7.6. Although the quality of the available exposures was variable and it was not always possible to measure a complete soil profile, existing exposures did provide information about the degree of carbonate soil development.

This soil shares similar carbonate morphology to soils described and sampled at the Steptoe quarry, the Yakima Bluffs exposure, and the South Bombing Range Road quarry (Section 4.3.1; Table 7.1). $^{230}\text{Th}/\text{U}$ -series dating of the carbonate rinds in Stage IV horizons of these soils indicated minimum ages of 350 to 400 ka (Appendix E.1). These ages are close to the limit of the $^{230}\text{Th}/\text{U}$ -series dating system, which is usually estimated at about five times the half-life of ^{230}Th , or about 380 ka. Older ages, however, are calculated using a Monte Carlo approach where multiple trials are calculated using values for isotope compositions that vary randomly within the range of the given uncertainty. Trials that resulted in positive, finite ages are accepted. Using this approach much older estimated ages ranging from 500–700 ka are suggested by the results (Section 4.3.1.6, Appendix E.1).

At the Yakima Bluffs locality the older flood gravels and associated strongly developed calcic soil overlie slackwater deposits that are magnetically reversed, indicating a maximum age of 780 ka for the gravels/calcic soil at that location (Figure 4.5). Paleomagnetic data collected at the South Bombing Range Road locality also indicated the Ice Age cataclysmic flood deposits there are normally magnetized as well (Baker et al. 1991) (Figure 4.10).

Similar maximum constraining age data are not available for the Rattlesnake Mountain fan sequence. The inferred middle Pleistocene age of the Qaf4 fan based on relative soil profile development to these dated soils is consistent with the long period of cooler temperatures and conditions during that time that may have favored erosion and fan development. The period from ~ 380 to 800 ka spans four glacial periods (MIS 12 [478–424 ka], MIS 14 [563–533 ka], MIS 16 [676–621 ka], and MIS 18 [761–712 ka]) (Figure 4.8). As noted above, significant folding and growth of the Rattlesnake Mountain anticline had occurred prior to the development of the Qaf4 fan. We speculate that increased sedimentation and erosion related to periglacial conditions during the long period of relatively low sea level (glacial conditions) in the ~ 424 to 761 ka time frame provided significantly more sediment than was generated during subsequent warmer interglacial periods like the present.

Table 7.1. Calibration and sampling sites used to constrain the ages of carbonate soil profile development and weathering characteristics of alluvial fan and fluvial terraces in the study area.

	Locality Name	Unit/Landform	Exposure Thickness (m)	Maximum K-horizon thickness (m)	Soil Description	Age (ka) (dating method)	Estimated Age (ka)
13256sh01	Rattlesnake Mountain	Qaf4/alluvial fan	2.4	0.9	0–0.9 m: loess. 0.9–1.5 m: K-horizon grading into very well-developed K horizon near base. ~30–50% carbonate. Stage III. 1.5–2.4 m: K horizon with prominent k-fabric, crystalline carbonate rind on upper K–fabric that is 5-10 mm thick. Plates up to 2 cm thick common. Stage IV–IV+. Rotten basalt clasts and boulders common.	Not dated	>350–800
13256sh05	Rattlesnake Mountain	Qaf4/alluvial fan	0.7	≥0.7	Overlying natural exposure of carbonate soil is 1.5–2-m-thick loess cap that includes the ~ 7 ka Mazama ash. Carbonate plates up to 2 cm thick present, 2–5mm thick nearly pure crystalline carbonate rind near top of exposed K–horizon, horizon is composed of >90% carbonate engulfing clasts. Stage IV. Rotten basalt clasts and boulders common.	Not dated	>350–800

Table 7.1. (contd)

	Locality Name	Unit/Landform	Exposure Thickness (m)	Maximum K-horizon thickness (m)	Soil Description	Age (ka) (dating method)	Estimated Age (ka)
13357sh05	Rattlesnake Mountain	Qaf4/alluvial fan	1.5	≥0.5	0–1.5 m: loess. 1.5–2 m: K horizon with prominent k-fabric plates up to 3 cm thick. Plates can be broken in hands with heavy manual pressure. Plates in upper part of horizon are >95% carbonate. Stage IV. Rotten basalt clasts common, finer-grained basalt clasts have a prominent inner rind when broken open on a fresh face.	Not dated	>350–800
13257sh07	Rattlesnake Mountain	Qaf2/alluvial fan	0.3	0	0–0.9 m: loess. 0.9–1.2 m: Bk horizon largely matrix supported with grayish white fine-grained sand. Matrix violently effervesces with acid. Bottom of clasts are covered 85–100% with carbonate rind that is 0.5–1 mm thick. Stage Ic of Forman and Miller (1984), or Stage I+ of Birkeland (1999). Basalt clasts have iron staining on surface.	Not dated	15–75

Table 7.1. (contd)

	Locality Name	Unit/Landform	Exposure Thickness (m)	Maximum K-horizon thickness (m)	Soil Description	Age (ka) (dating method)	Estimated Age (ka)	
	13259sh07	Rattlesnake Mountain	Qaf4/alluvial fan	~2	~0.5	Rounded and laid back natural stream cutbank. 0–1 m: loess. 1–1.5 m: K horizon with prominent k-fabric, plates up to 5 cm thick coming out in float. Stage IV carbonate.	Not Dated	>350–800
	13129CU01	Saddle Mountains	Ringold Formation	~2.5	~1	K horizon with prominent k-fabric. Carbonate engulfing clasts.	Not Dated	<2,800–3000
7.14	13167sh01 (SBR, Table 4.1)	South Bombing Range Road Quarry	Middle Pleistocene cataclysmic flood deposit	1.7	1	0–0.7 m: Disturbed soil mixed with fill and loess. 0.7–1 m: Most developed K horizon, plates up to 3 cm thick, plates can be broken in hands with heavy manual pressure. Stage IV. 1–1.7 m: Less developed k-fabric, with weak plates, clasts still engulfed in carbonate matrix.	Minimum 350–400 ka (²³⁰ Th/U, Appendix E.1)	<780 ka (normally magnetized)

Table 7.1. (contd)

	Locality Name	Unit/Landform	Exposure Thickness (m)	Maximum K-Horizon Thickness (m)	Soil Description	Age (ka) (dating method)	Estimated Age (ka)
	13166sh02 (YB, Table 4.1)	Yakima Bluffs	Middle Pleistocene cataclysmic flood deposit	~2.5	1.7	0-0.2 m: Disturbed soil composed mostly of loess. 0.2-0.7 m: Carbonate accumulation on clast bases. 0.7-1.7 m: Most developed K horizon, weak k-fabric present in sandier lenses, some clasts engulfed in carbonate.	Minimum 370–400 ka (²³⁰ Th/U, Appendix E.1) <780 ka (normally magnetized)
	13166sh01	Steptoe Quarry	Middle Pleistocene cataclysmic flood deposit	~2.5	≥0.5	0-1.5 m: loess. 1.5-2 m: Most developed K horizon ≥Stage III+, clasts engulfed in carbonate with 1+ cm thick rinds common. Difficult to tell total thickness of horizon due to laidback nature of exposure.	Minimum ~400 ka Best estimate 500–700 ka (²³⁰ Th/U, Appendix E.1)
	13168sh02 (OS, Table 4.1)	Oak Street	Middle Pleistocene cataclysmic flood deposit	~4+	~0.75-1	White K horizon with weakly cemented incipient k-fabric in most developed carbonate horizon. Stage III+. ~2–5% granitic clasts present that are completely grussified.	-- <780 ka (normally magnetized)

Table 7.1. (contd)

	Locality Name	Unit/Landform	Exposure Thickness (m)	Maximum K-Horizon Thickness (m)	Soil Description	Age (ka) (dating method)	Estimated Age (ka)
13167sh02	Finley Quarry	Pre- to Late Wisconsinan flood deposit(s)	~3	0.0	0–2.7 m: loess and bioturbated flood deposits. 2.7–3 m: Bk horizon white to grayish white matrix, with carbonate coatings covering the base of all clasts and some clasts nearly 100% covered with a rind that is 1–1.5 mm thick. Stage IIA of Forman and Miller (1984) and Stage II of Birkeland (1999).	17 ± 1.8 (²³⁰ Th/U minimum age), (Appendix E.1). Previous Th/U dating (WCC 1981b) from probable same unit yielded a similar age (Sample JB-7, 19 ± 1 ka, probable; 51 ka maximum). Sample JB-8, which may have been collected from the same or possibly older unit suggested a minimum age of 69–160 ka (WCC 1981b).	
13281sh02	Canyon Road	Pre-late Wisconsin flood deposit or Ancestral Columbia River gravel	~3	~0.5-1	Laidback road outcrop lacking a vertical face. Broken up k-fabric in float, with clasts that commonly have a >5-mm rind. Stage III(?). Rotten basalt clasts common, finer-grained basalt clasts have a prominent inner rind when broken on a fresh surface.		>130 ka to Pliocene?

Table 7.1. (contd)

	Locality Name	Unit/Landform	Exposure Thickness (m)	Maximum K-Horizon Thickness (m)	Soil Description	Age (ka) (dating method)	Estimated Age (ka)
13133sh02 (Sample YK06, Appendix C)	Qg5 (~80 m above modern base level) (Ladinsky 2012)	Yakima River fluvial terrace	~2.5	~0.5	0-1.1 m: loess. 1.1-1.6 m: K horizon, white with prominent k-fabric. Clasts are cemented in horizon. Stage III-IV. Granitic and volcanic clasts typically grussified or rotten. Eroded and degraded exposure.	Older than Qg4 terrace (48 m above present river level) that is estimated based on IRSL analysis to be a minimum of 237–271 ka (Ladinsky and Kelsey 2012) or 1.08 ± 0.29 Ma based on a $^{26}\text{Al}/^{10}\text{Be}$ cosmogenic nuclide burial age (see Appendix C)	
13132sh05	Qg2 (Ladinsky 2012)	Yakima River fluvial terrace	~1.5	0.0	Roadcut exposure is laidback, approximately 1–1.2-m-thick loess overlying Bk horizon in fluvial gravels with a grayish white matrix. Bottom of clasts are covered 100% with a carbonate rind that is up to 1.5 mm thick. Stage IIA of Forman and Miller (1984) and Stage II of Birkeland (1999).	~88 ka (IRSL) (Ladinsky 2012)	

Table 7.1. (contd)

	Locality Name	Unit/Landform	Exposure Thickness (m)	Maximum K-Horizon Thickness (m)	Soil Description	Age (ka) (dating method)	Estimated Age (ka)
13128sh01 (Sample YK03, Appendix E.2)	Big Pine Campground terrace	Yakima River fluvial terrace (strath is estimated to be ~1.4 to <3m above modern river level)	~6	0.0	<p>0–2 m: Fluvial gravels with boulders up to 0.5 m in diameter.</p> <p>2–2.3 m: Bk horizon, white matrix that is relatively loose, with some weak carbonate cementation of clasts and sand. Bottom of clasts are covered 50–90% with a rind that is up to 1 mm thick. Stage IC of Forman and Miller (1984) and 1+ of Birkeland (1999).</p> <p>2.3–3.5 m: weak Bk horizons.</p> <p>3.5–6 m: C/Cox horizon.</p>	Indistinguishable from modern based on $^{26}\text{Al}/^{10}\text{Be}$ cosmogenic nuclide burial age (see Appendix C)	

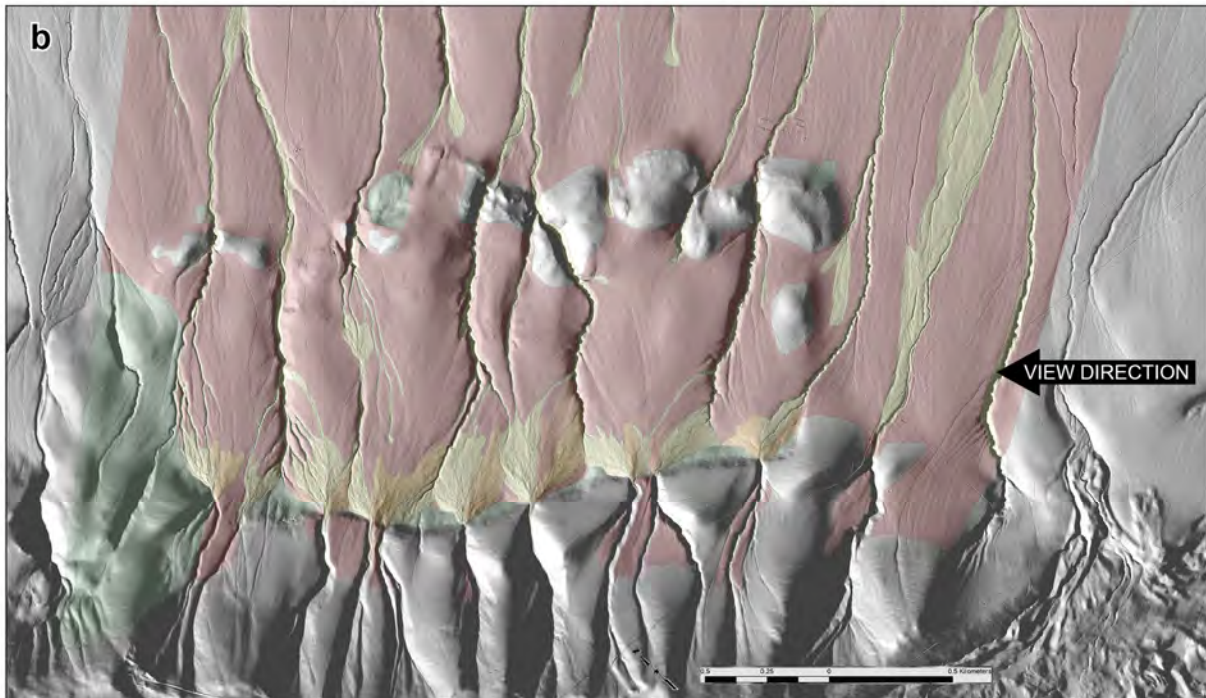


Figure 7.6. a) Photograph of typical carbonate soil development in the Qaf4 fan in a natural exposure along a drainage incising into the Qaf4 at field locality 13256sh01. b) Quaternary geologic map (see Plate 1 for explanation) showing location and view direction.

Modification of the distal parts of the Qaf4 fans during Missoula floods at elevations below approximately 366 m, as well as post-middle Quaternary incision, limits our abilities to evaluate the base level at the time of fan formation. Projection of the slope of the lower part of the fans to the Yakima River suggests that base level may have been approximately 50–60 m above present base level during the time of fan deposition.

7.3.2.2 Qaf3

The Qaf3 unit is an intermediate alluvial fan deposit that appears to be younger and less extensive than Qaf4. The deposits that have been mapped as Qaf3 generally appear to be debris-flow lobes that are only slightly inset into Qaf4 surfaces by a couple meters. The amount of incision is difficult to measure because there has been a considerable amount of loess that has filled in relict channels. This apparent lack of significant incision combined with subtleties in surface morphology characteristics, that can be used to differentiate the Qaf4 and Qaf3 units suggests that Qaf3 may not be significantly younger. It is possible that Qaf3 debris flows covered the preexisting topography of Qaf4 by overbank flow prior to significant incision into Qaf4 deposits.

7.3.2.3 Qaf2

The Qaf2 unit represents distinct intermediate age fan deposits that emanate from major canyon mouths along the north flank of Rattlesnake Mountain at the base of the range front (Figure 7.7, Plate 1). Generally the Qaf2 fan deposits bury the older Qaf3 surfaces and are 1–2 m higher in relative elevation. Along some of the larger of these drainages, the apices of the Qaf2 fan cones extend south into the canyons and grade smoothly to terrace surfaces.

In general the bulk of the Qaf2 fan deposits are within approximately 200–400 m north of the range front. The Qaf2 fan surfaces are approximately 2 m above the present, active channel thalwegs. The morphology of individual debris-flow lobes composing the Qaf2 fan surface is still visible, but is subdued due to infilling by loess. Subangular to angular boulder clasts exposed at the surface exhibit reddening and surface weathering.

Limited exposures of the Qaf2 deposit and soil made estimation of the age difficult. The relict soil formed in the Qaf2 is partially exposed at location 13257sh07 (Figure 7.8). The stream-cut exposure at this location is of a grass-vegetated, ~60–70° south-facing slope. Along the steeper portion of the slope, below the loess cap, cobble-sized clasts generally less than 25 cm in length crop out in place approximately 1 m below the fan surface. A small exposure in the stream bank revealed the clasts were set in a sandy gravel matrix. The sandy portion of the matrix that is relatively loose has a slight grayish white color, and effervesces violently with acid. The bottoms of the clasts were covered 85 to 100% with carbonate rinds that were typically 0.5 to 1.0 mm thick. This degree of development is consistent with Stage I+ of Birkeland (1999) and Stage IC of Forman and Miller (1984).

Based on comparison with other dated carbonate soils in arid environments, we infer that the soil on the Qaf2 fan is consistent with an age of approximately 13 to 70 ka. The variability in the rate of carbonate development depends on a number of factors. The primary influences are climate (principally precipitation amount and character) and source influx rate (typically dust) (Schaetzl and Anderson 2005). Machette (1985) tabulated carbonate stage development versus time in a number of locations primarily in

7.21

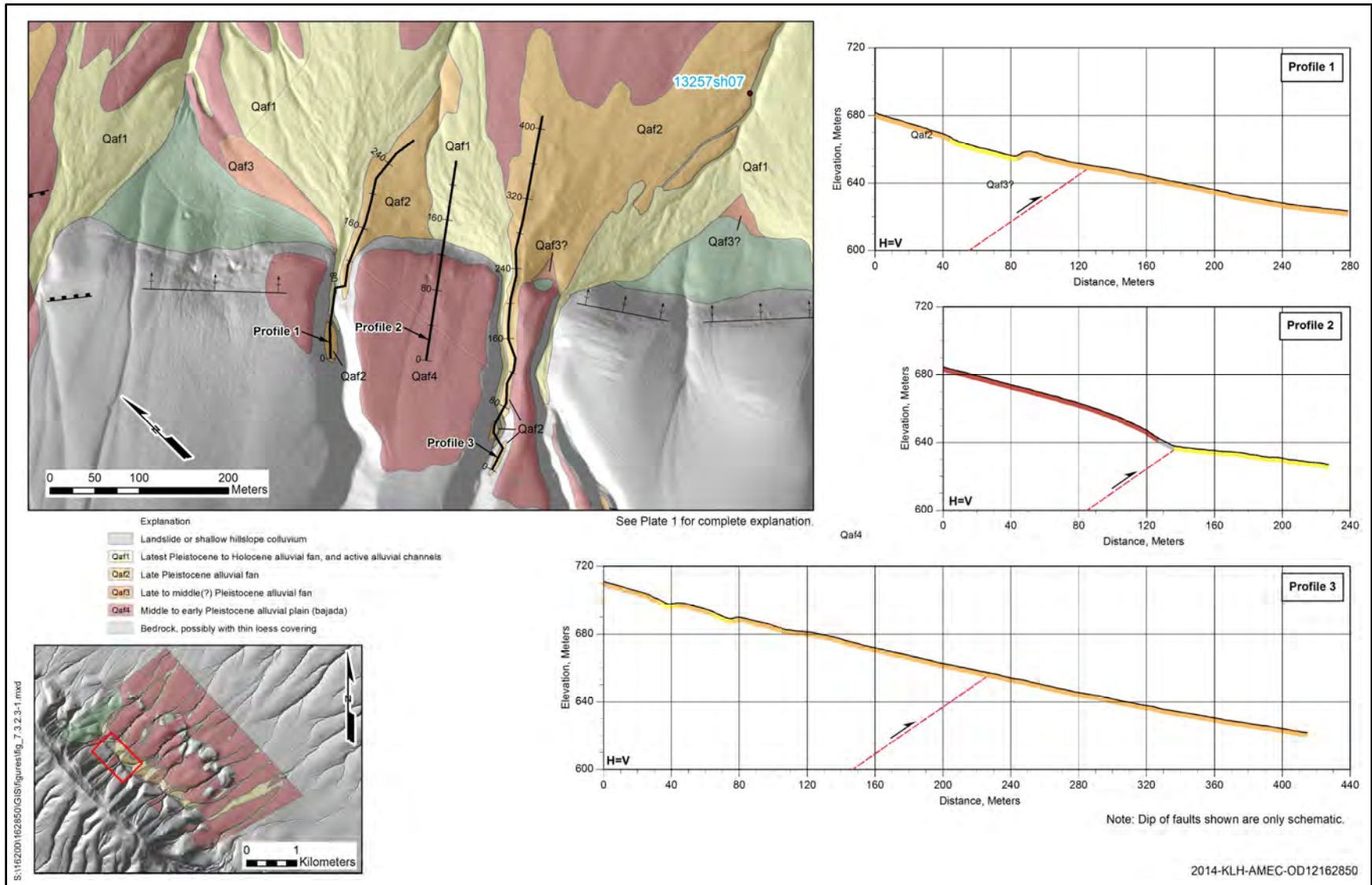


Figure 7.7. Detailed surficial geologic map and topographic profiles showing undeformed Qaf2 fans crossing the projected trace of the main range-front fault.

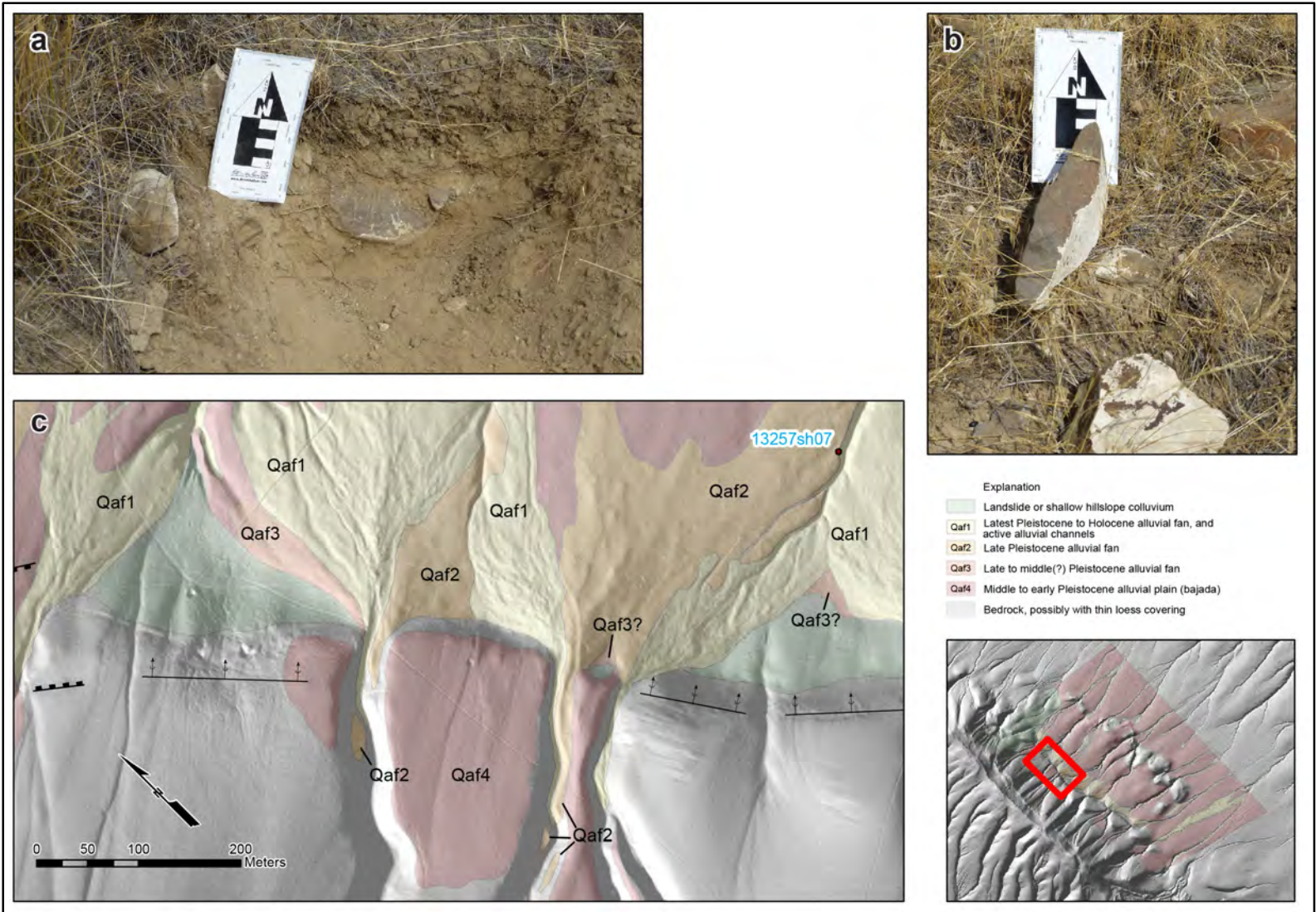


Figure 7.8. a) Photograph of the exposure (location 13257sh07) along a natural gully incised into Qaf2, showing in-place rocks with carbonate rinds covering the base of clasts. b) Close-up view of clasts removed from the horizon to photograph the maximum carbonate rind thickness. c) Quaternary geologic map showing location of 13257sh07.

the southwestern United States. Machette's findings were that in the fastest carbonate-forming environments in New Mexico, advanced Stage I development similar to what we observed at location 13257sh07 takes approximately 10 kyr. In slower carbonate-forming environments advanced Stage I can take up to approximately 90 kyr to form. Because the exposure was relatively small it is difficult to ascertain that we were describing the maximum development in the soil profile. We therefore consider this development to be a minimum description of the carbonate development. Based upon these observations and tentative correlation to regional studies by Machette (1985), we consider ~10 ka to be a minimum age. We find it reasonable to assume that the fans developed in concert with increased precipitation associated with global wet and cool time periods. We therefore prefer a minimum age of ~13 ka associated with MIS-2 (29–14 ka), and consider that the age of the fan could be as old as ~70 ka correlative with MIS-4 to possibly ~130 ka correlative to late MIS 6.

7.3.2.4 Qaf1

The youngest alluvial deposits in the study area, mapped as Qaf1, have a distinctly rougher surface texture than the older surfaces due to a thinner accumulation of loess. The Qaf1 terrace surface is generally inset into the Qaf3 and Qaf2 surface up to 1 and 3 m, respectively. Youthful flood levees and channels can easily be discerned from the LiDAR data as well in the field. The age of this youngest surface may vary from recent (mid to late Holocene) to possibly latest Pleistocene (~13 ka). If the penultimate Qaf2 fans are genetic to the MIS 4/3 transition, then we think it is reasonable that the latest deposition of Qaf1 could be in response to the MIS 2/1 transition. It is also worth noting that on Plate 1 the present-day active channels were not split out of the mapped limits of the Qaf1 surfaces. These active channels are acutely incised into the Qaf1 deposits.

7.3.3 Quaternary Deformation

Quaternary tectonic activity in the Rattlesnake Mountain study area is observed along at least two structures: the range-front fault and the gas field anticline. Along the upper bedrock fault as mapped by Reidel et al. (in press), we observed an alignment of bedrock saddles, but as noted by Reidel et al. (in press), there is a paucity of Quaternary deposits that high up on the range, providing little evidence for or against recent activity. At the southeastern margin of the study area, however, where Qaf4 terrace surfaces appear to cross the mapped trace of the southernmost fault trace, there is no geomorphic expression of surface faulting. We would expect to see a more prominent bedrock fault scarp if there was middle to late Pleistocene activity. We also did not observe Quaternary deformation along the high-angle tear fault mapped by Reidel et al. (in press) at the northwest end of the gas field. The Qaf4 fan surface extends across this feature with no obvious surface deformation.

The range-front fault is a prominent curvilinear scarp that is coincident or nearly coincident with steeply to vertically dipping bedrock strata, presumably in the hanging wall. Also coincident with the scarp are a series of aligned colluvial headscarps (Plate 1). The southeast end of the fault terminates abruptly against a northeast-striking tear fault, which is expressed as a southeast-facing monoclinical fold in the Qaf4 fan surface. The northwest end of the range-front fault is clearly detectable until it intersects a large landslide. Although there may be more subtle breaks in slope within the landslide on the projected trend of the range-front fault, a surface scarp comparable to the scarp to the east is not apparent in the hillshade maps crossing the landslide. The total length of the geomorphically well-expressed fault is approximately 2.5 km.

The range-front fault has produced clear vertical separation of the Qaf4 surface. Younger inset alluvial fan surfaces (e.g., Qaf2 and Qaf1), however, are deposited across the fault in a few places, and field observations indicate that they are not deformed. Examination of topographic profiles along the younger fan surfaces and their continuation as terraces in the canyon upstream of the range front reveals that the surfaces are continuous and undeformed across the fault (Figure 7.5).

The Qaf4 surface is also clearly tectonically warped to the north and south on the forelimb and backlimb, respectively, of the gas field anticline. Between the range-front fault and the gas field anticline we mapped a rough alignment of low rises in the surface topography of Qaf4 that may be tectonic flexures (Plate 1).

The gas field structure was previously mapped as an anticline by Reidel and Fecht (1994) and Reidel et al. (in press). Geomorphically the structure is characterized as a somewhat irregular ridge with local relief up to 100 m into which a number of drainages have incised. A few landslides emanate off this steeper northeast limb of the structure. CRB crops out along almost the entire length of the crest of the structure. Near the northwest end, however, it appears that the oldest Qaf4 unit was deposited across top of the anticline and buried the basalt. Other fluvial units, likely correlative with Qaf2- and Qaf1-aged fan deposits, cross the structure flanking the modern drainages. Preserved inset terraces of Qaf1 and Qaf2 that cross the gas field structure are best preserved in the two drainages at the northwest end of the structure.

Of the units Qaf4, Qaf2, and Qaf1, only Qaf4 appears to be tectonically deformed across the gas field structure. Evidence for deformation of Qaf4 is most clearly demonstrated through observations of over-steepened and back-tilted K horizons on the northeast and southwest sides of the gas field anticline, respectively. At location 13259sh02 (Plate 1) a natural stream-cut exposure shows laminar k-fabric with plates up to 5 cm thick dipping 12° to the northeast. By comparison terraces associated with Qaf1, Qaf2 and the modern stream channel slope $6\text{--}7^\circ$ to the northeast, suggesting $5\text{--}6^\circ$ of post-depositional/soil formation tilting. A similar relation exists at location 13259sh07 where $2\text{--}3^\circ$ of post-depositional/soil formation tilting is estimated. Northeasterly tilting of the Qaf4 surface can also be observed through the geomorphic inflection of the Qaf4 surface north of the structure. At location 13257sh05 a natural stream-cut exposure shows laminar k-fabric dipping 1° upslope (southwest) (Figure 7.9). Assumedly, the original slope was at least $3\text{--}6^\circ$ to the northeast, so a minimum of $4\text{--}7^\circ$ post-deposition/soil formation tilting is inferred. Postulated wind gaps and beheaded drainages along the crest of the structure are further suggestions of tectonic deformation of Qaf4. The topographic expression of the structure dies out rapidly near the toe of the large landslide. The total length of the structure could be as long as 4 km but it is at least as long as the 2.5-km range-front fault. The subtle topography outboard of the range front to the northwest of the Rattlesnake study area (Figure 7.3) could reflect uplift along a longer fault, but detailed office and field studies were not conducted to confirm the northwestward extent of the gas field structure.

7.3.3.1 Style of Faulting

Recent studies by Blakely et al. (2013) have suggested that the streams along the range front of Rattlesnake Mountain are right laterally offset by as much as 250 m. Blakely et al. (2013) base this upon the observation that the drainages outboard of the range-front fault do not line up with the mouths of the canyons incised into Rattlesnake Mountain. Contrary to Blakely et al. (2013), our field and desktop

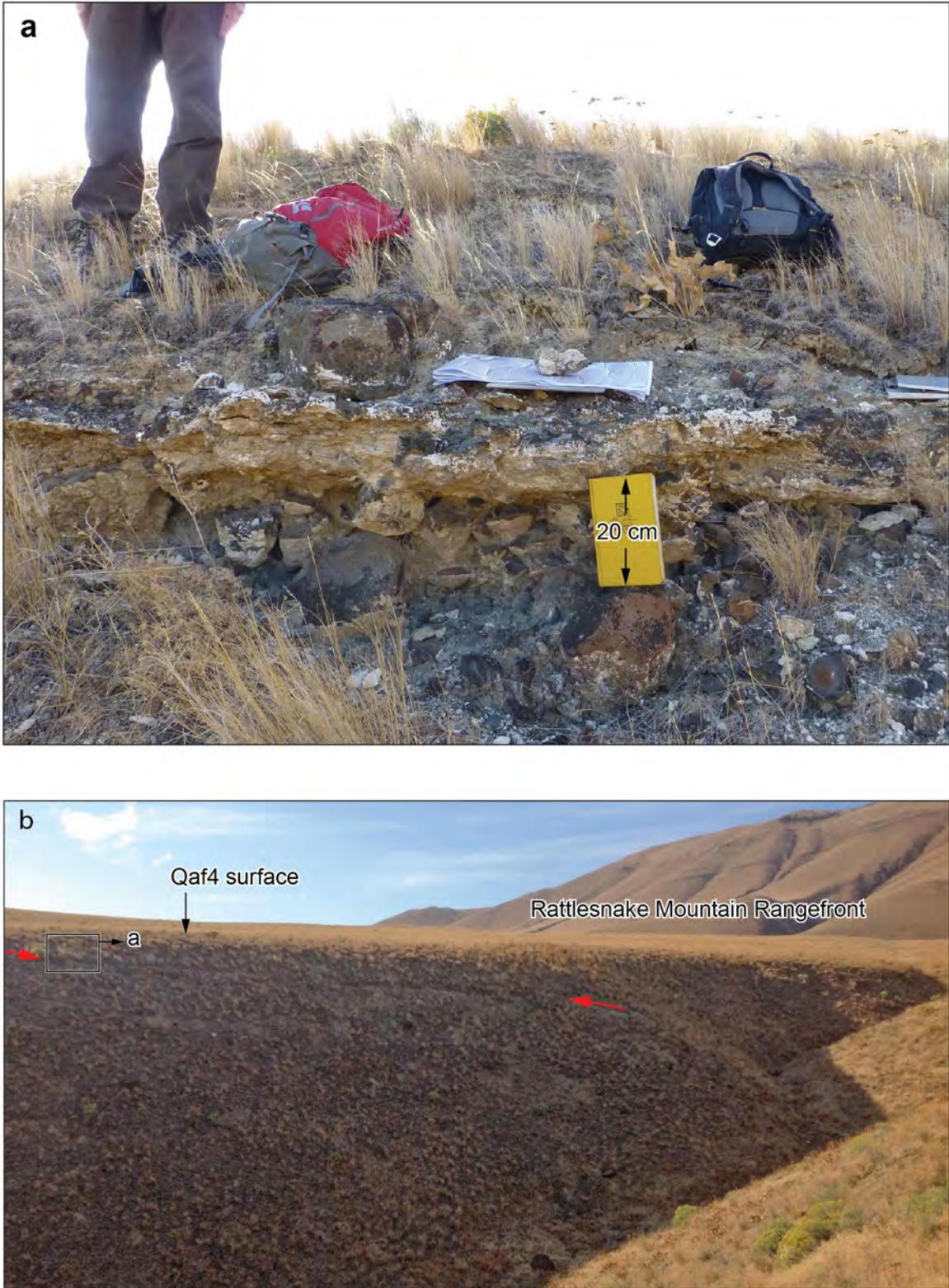


Figure 7.9. Location 13257sh05 showing a) Stage IV carbonate horizon developed in Qaf4, and b) back-tilting of the Qaf4 soil on the southwest flank (backlimb) of the gas field anticline.

mapping observations suggest that the style of faulting is primarily reverse along the range-front fault, and there is primarily northeast-southwest compression along the gas field structure.

The primary lines of reasoning supporting a lack of right-lateral offset are as follows:

- There are no remnants of displaced heads of fans along the range-front escarpment or strike-slip tectonic features, such as shutter ridges.
- Drainages are not consistently offset by the same distance along strike.
- Small gullies that are deeply incised into the steeply dipping basalt beds in the hanging wall of the range-front fault cross the fault with no apparent deflection (Figure 7.7).
- Along the gas field structure, drainages are clearly not offset right laterally and observed vertical deformation is consistent with NE-SW shortening.

An alternative interpretation for the misalignment of drainages with canyon mouths is that they are consequent streams eroding headward (upslope), subsequent to the last surface faulting event, and during deposition of the Qaf3/Qaf2/Qaf1 fan sequence. In this interpretation, the drainages emanating from the range front prior to offset of Qaf4 (or earlier) were similar to the drainages southeast of the tear fault near the southern edge of the mapping on Plate 1. This would include a broad gently inclined surface extending from the base of the mountain with subtle undulating convexities due to the component fans (i.e., bajada). Following the reverse faulting of the Qaf4 surface, the subsequent Qaf3/Qaf2/Qaf1 alluvial fans were deposited as steeper and more conical features than the Qaf4 fans.

The drainage system north of the range-front fault was likely formed by headward erosion of gullies that propagated southward from the margins of the Cold Creek syncline in response to general base-level lowering due to both climatic and tectonic forcing. Blair and McPherson (2009) describe similar processes of headward eroding gullies into the uplifted fan surface in the Owens Valley, California. The conical shapes of the fans near the range front deflect surface water to the sides causing incision to be focused between the younger Qaf3/Qaf2/Qaf1 alluvial fan complexes in these areas. Supporting the interpretation that the drainage pattern present today was formed antecedent to the onset of Quaternary faulting, is the observation that incision depths into Qaf4 are roughly equivalent to the topographic vertical separation of the Qaf4 surface (see profile 7 Plate2). For these reasons we interpret the drainage pattern to be consequent to the topography produced by deposition of Qaf3/Qaf2/Qaf1, and headward erosion of drainages rather than a result of lateral tectonic offset.

The evidence of no measurable lateral offset of geomorphic features, combined with the evidence for vertical separation across a surface scarp at the range front and fold deformation on the gas field that is consistent with the presence of a blind thrust or reverse fault demonstrates that the uplift of Rattlesnake Mountain in the Quaternary has been primarily been accommodated by reverse slip on a fault that includes both emergent and blind splays that likely merge at depth.

7.3.3.2 Vertical Separation Rates

Based on field and desktop observations from this study the most suitable deposit to use for evaluating total vertical stratigraphic separation across the entire Rattlesnake Mountain fault zone (including both the range-front fault and the gas field anticline) is Qaf4. Using ESRI ArcGIS and Global Mapper software packages, we generated a number of topographic profiles both orthogonal and parallel to

the range-front fault and gas field anticline (Plate 2). Profiles orthogonal to the two structures were located near the apex of the Qaf4 surface to mitigate the effect of headward erosion into the surfaces. Profiles located parallel to the traces were generated to estimate the relative amount of incision into the surface post uplift (Plate 2).

Profiles 1 through 5 on Plate 2 are most useful in estimating cumulative vertical stratigraphic separation across the range-front fault and the gas field anticline. Profiles 1–4 show there is a clear vertical displacement of the Qaf4 surface at the geomorphic range front. Because the original bajada surface likely had a slight concave shape to it (similar to the shape of the fan surface at the southeastern margin of the study area, Profile 5), rather than a planar morphology, reconstructing the surface requires estimating the original topography. Estimating this surface topography introduces some uncertainty into the profile projections, which we estimate to be on the order of 1.5 to 3 m. Given this uncertainty, there could be as much as 3 m of offset or warping along Profile 5. Total cumulative vertical stratigraphic separation across both the range-front and gas field structures estimated from the reconstructed projections range from 20 ± 3 m at Profile 4 to 30 ± 3 m at Profile 3, with an average value of approximately 25 m. Profiles 2 and 3, which span the central part of the emergent range-front fault, show similar cumulative offsets of 29–30 m.

Using the estimated age for the deposition of the Qaf4 fan (800 to 380 ka), and the range of estimated average cumulative vertical separation of the Qaf4 fan surface (30 m, -8 m, $+3$ m) across the range-front and gas field structures, yields an integrated middle to late Quaternary separation rate of 0.03 to 0.09 m/kyr. Rates at the middle to higher end of this range are preferred because the measured offset of the surface post-dates abandonment of the surface and inception of soil development. In addition, the large extent of the Qaf4 fans suggest a long period of deposition, possibly throughout much of the MIS 16, MIS 14, and MIS 12 glaciations and transitional periods to intervening interglacial periods. It is assumed that the final abandonment and initiation of soil profile development likely occurred toward the latter part of this time period. The ages for the initiation of the carbonate soil development on the middle Pleistocene cataclysmic flood deposits that appear to be roughly equivalent in age based on relative soil profile development are in the 380–700 ka range (see Section 4.3.1). A preferred rate of 0.04–0.06 m/kyr (25–30 m/424–600 kyr) honors the best-estimated average age of the cataclysmic flood deposits based on $^{230}\text{Th}/\text{U}$ -series ages used for correlation and the best constrained offset measurements in the central part of the study area. Although we cannot preclude that the fan surface was abandoned earlier and the average vertical separation is at the low end of the estimates ($22 \text{ m}/800 \text{ kyr} = 0.03 \text{ m/kyr}$), or that the highest vertical separation and youngest age ($33 \text{ m}/380 \text{ kyr} = 0.09 \text{ m/kyr}$) are representative of the average vertical slip rate on the entire Rattlesnake Mountain structure, these estimates are considered less likely.

The average Quaternary (post-Qaf4 fan) vertical separation rate can be compared to long-term average post-CRB vertical separation rates based on the structural analysis described in Section 5.0. Based on the general location of the study area relative to the crestal profile of the entire Rattlesnake Mountain fold (Figure 7.10), it is reasonable to assume that the cumulative vertical separation of the Qaf4 fan in the central part of the study area is representative of the average post-middle Pleistocene separation. Using an average post-Qaf4 vertical stratigraphic separation of 25–30 m and an estimated age range of 380–800 ka, yields vertical separation rates ranging from 0.03–0.09 m/kyr. This estimate is comparable to the long-term vertical separation rate based on post-CRB topography ($618 \text{ m}/6\text{--}10 \text{ Myr} = 0.06\text{--}0.1 \text{ m/kyr}$) and the estimated rate (0.06 m/kyr) from the beginning of Saddle Mountains Basalt time based on thinning of basalt flows across the structure (Reidel et al. 1983).

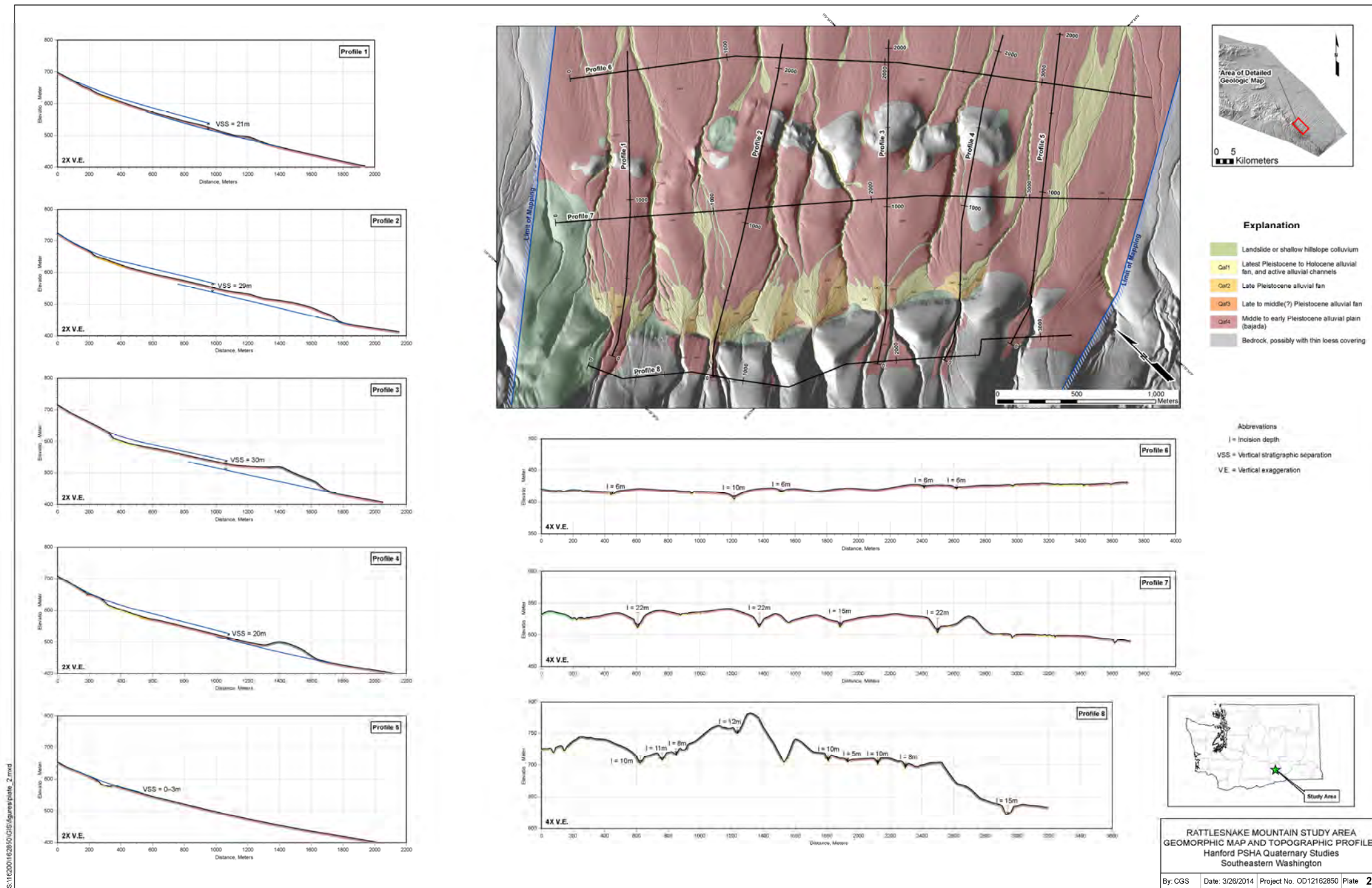


Plate 2. Rattlesnake Mountain study area geomorphic map and topographic profiles.

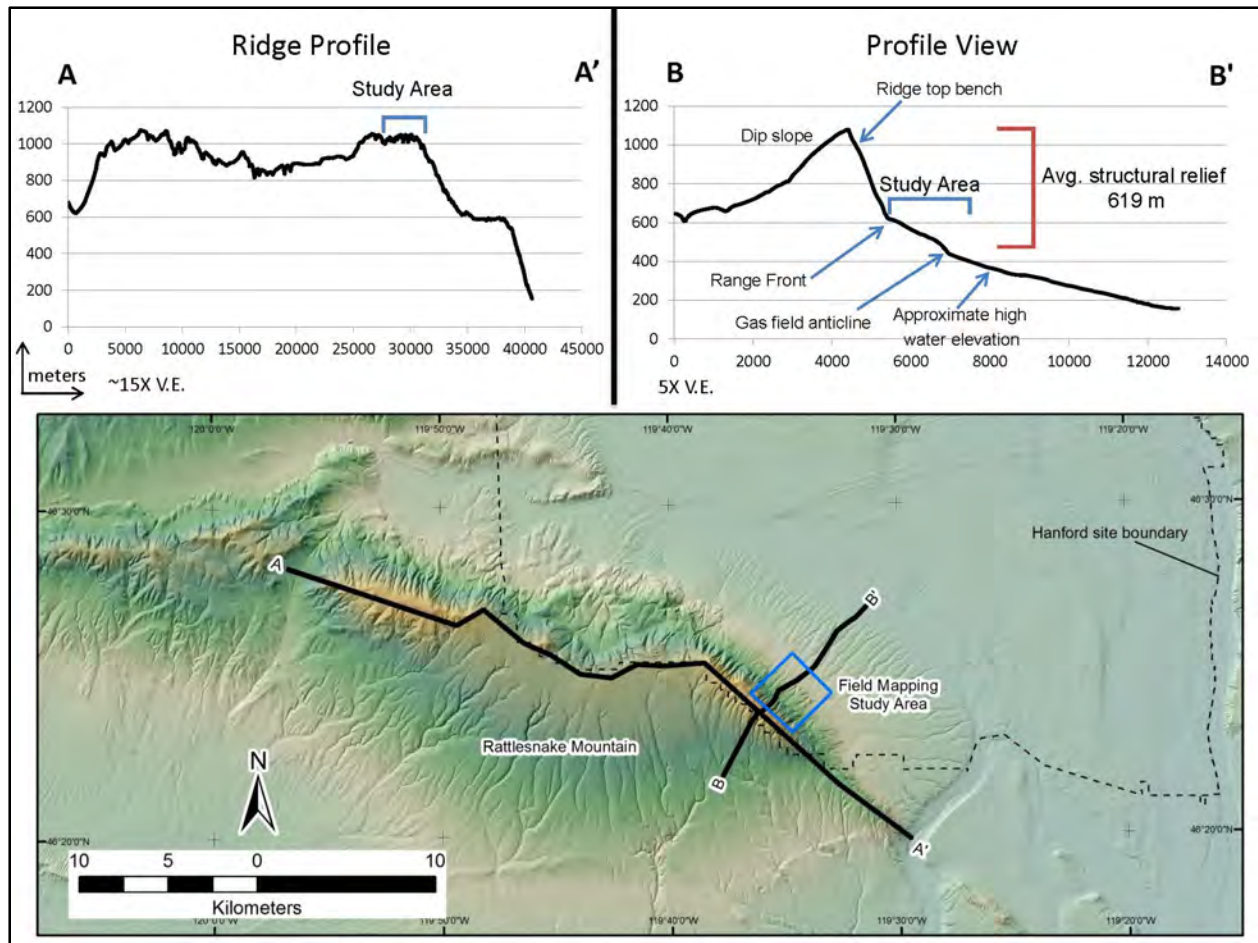


Figure 7.10. Map and topographic profiles showing the position of the study area relative to the Rattlesnake Mountain anticlinal ridge.

7.4 RAW-Rattles and Horn Rapids Anticline

The RAW alignment between the Yakima River and Wallula Gap is defined by a series of 10 elongated (northwest-southeast) hills that appear as distinct, subparallel, doubly plunging anticlines generally aligned along a N50–60°W trend (CGS FSAR, Energy Northwest 1998). These domes and doubly plunging anticlines (referred to as brachyanticlines) are commonly referred to as the Rattles. Formally and informally named folds within the Rattles are (from west to east): Red Mountain, Candy Mountain, Badger Mountain, Little Badger Mountain (“O-Hill”), ‘N-Hill’, ‘M-Hill’, ‘L-Hill’, K-Hill’, The Butte, and Molly Hill (Energy Northwest 1998; Figure 7.11). Northeast of the Rattles is another series of northwesterly aligned basalt knolls that were identified as the Horn Rapids lineament by Bingham et al. (1970). Bond et al. (1978) as reported by Myers et al. (1979) interpreted these to be open, plunging folds, possibly of the same origin as the Rattles. Reidel and Fecht (1994) (1:100,000-scale geologic map) show the structure as the Horn Rapids anticlinal trend underlain by a blind reverse fault.

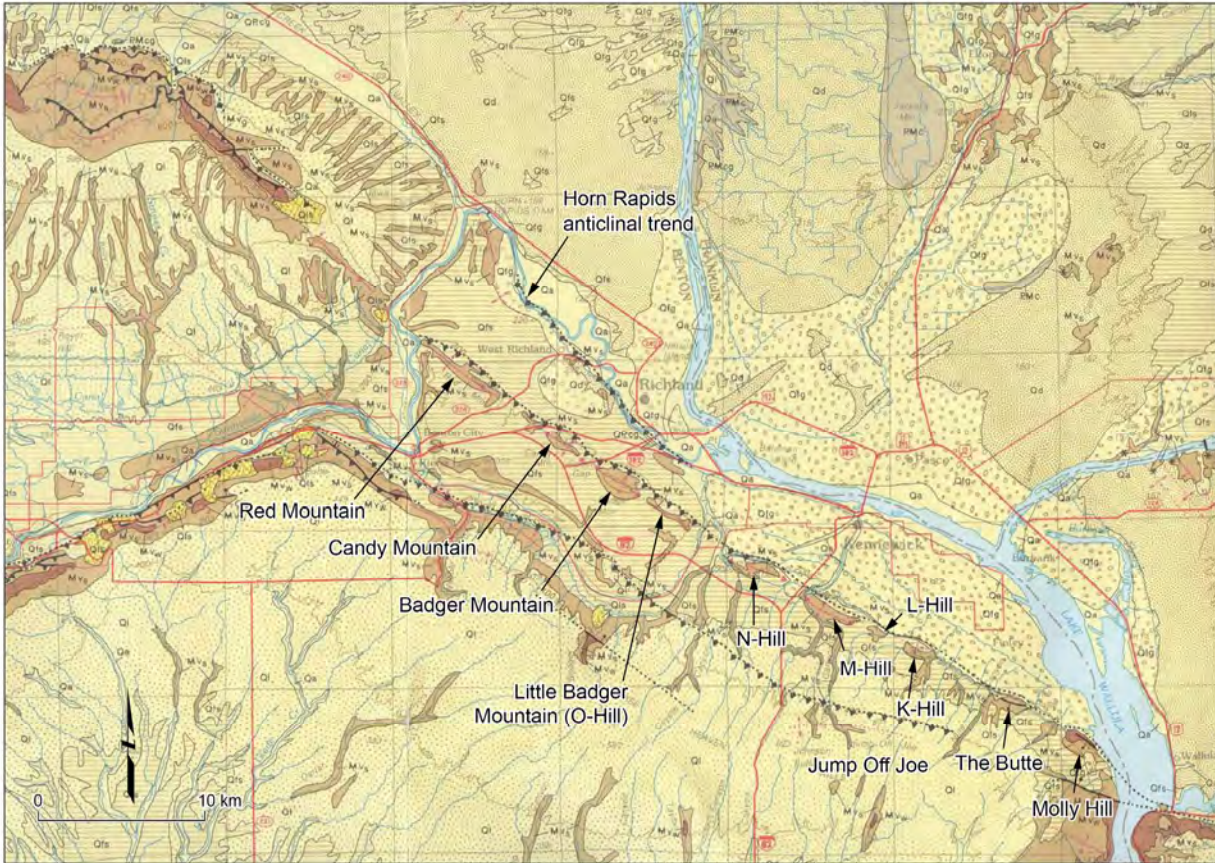


Figure 7.11. 1:100,000-scale geologic map showing the Rattles and Horn Rapid anticline (Reidel and Fecht 1994).

This belt of topographically expressed domes and doubly plunging anticlines (Red Mountain to Wallula Gap) was the middle domain of three domains identified along Cle Elum Wallula deformed zone (CLEW), all of which were interpreted to contain features characteristic of dextral transcurrent strain (Energy Northwest 1998, Appendix N). The two other domains included a broad zone of deflected or anomalous fold and fault trends (south from Cle Elum to Rattlesnake Mountain) and the Wallula fault zone (Wallula Gap to vicinity of Milton-Freewater, Oregon).

Based on interpretation of magnetic data, a continuous fault was inferred to extend between the brachyanticlines (CGS FSAR, Energy Northwest 1998). However, the FSAR also states that although Weston Geophysics modeled a steep fault, north side down along the RAW structure, the fault does not align with faults exposed within the hills (e.g., faults exposed within Finley quarry and the two hills to the west, which are not parallel and do not show similar kinematic indicators such as slickensides).

Personius and Lidke (2003) describe the Rattles structures as a series of anticlines underlain by south-to southwest-dipping thrust or reverse faults in rocks of Miocene age that are buried by Quaternary loess, landslide, and glacial-outburst flood deposits along much of their length. Because no unequivocal evidence of deposits of Quaternary age has been described, the structures were classified as Class B structures in the Quaternary fault and fold database.

The NRC (1982) concluded that the ~120-km-long RAW structure (which included Rattlesnake Mountain and the Wallula fault) was a capable, strike-slip fault with reverse or reverse oblique motion from Rattlesnake Hill to the Hite fault. The CGS FSAR concluded, however, that the isolated fold structures of the Wallula Gap to Red Mountain folds (i.e., the Rattles) attest to limited strike-slip movement (Energy Northwest 1998). In this section we focus on the smaller folds associated with the Rattles and Horn Rapid anticline. Sections 7.3 and 7.5 discuss new data and observations related to the Rattlesnake Mountain fault zone and the Wallula fault (also referred to as the Wallula Gap fault), respectively.

The Rattles have been linked with the Wallula fault and share a common history of controversy regarding the style of faulting and association with a basement shear zone. Proponents of strike-slip argue for an active basement shear (wrench) zone (e.g., Appendices N and O of the CGS FSAR; Energy Northwest 1998). The slight en echelon arrangement of the long axes of the isolated folds between Wallula Gap and Red Mountain are cited as evidence of limited strike-slip within this domain (Appendix N, Energy Northwest 1998; Mann and Meyer 1993). Alternatively, more recent geologic mapping shows southwest-dipping thrust or reverse faults underlying these folds (Reidel and Fecht 1994; Schuster et al. 1997). Reidel and Tolan (1994) present arguments for little or no strike-slip along the RAW structure.

Evidence for Quaternary deformation along the RAW-Rattles structure has been documented in only one location, a basalt-quarrying operation at the northwestern end of The Butte near Finley, Washington that is informally referred to as the Finley quarry (Farooqui and Thoms 1980; WCC 1981a, b; NRC 1982; Energy Northwest 1982). As part of the QGS for the Hanford SSHAC Level 3 PSHA, the USGS was funded to re-log the existing exposure at this quarry (Appendix E.4).

The Quaternary Studies Team conducted limited reconnaissance along the RAW-Rattles structure including short visits to the Finley quarry during the initial stages of the USGS work and subsequently during field reviews with the Hanford SSHAC Level 3 PSHA Participatory Peer Review Panel (PPRP) and NRC (September 2013) and with Quaternary research specialists from PNNL (George Last and Bruce Bjornson in October 2013).

The following subsections of this report discuss bedrock geologic relationships from previous mapping and limited field observations of the Quaternary Studies Team that bear on the assessment of the style of faulting (Section 7.4.1) and the implications of the new interpretations of the stratigraphic and structural relationships exposed in Finley quarry (Section 7.4.2).

7.4.1 Bedrock Structure

Bedrock mapping of the region between the Yakima River, where it crosses between Rattlesnake Mountain and Red Mountain, to Wallula Gap is summarized on 1:100,000-scale (Reidel and Fecht 1994) (Figure 7.11) and 1:250,000-scale (Schuster et al. 1997) maps. In addition, unpublished mapping completed by Dr. Ross Wagner during the late 1970s as part of the WCC CGS (WNP2) site characterization studies also was obtained for portions of Benton City SE, Benton City NE, Benton City SW, Benton City NW, Badger Mountain NE, and Badger Mountain NW 7.5-minute quadrangles. These maps showed detailed bedrock mapping near the Horn Rapids area across the Horn Rapids lineament, Red Mountain, and Badger Mountain.

Blind reverse or thrust faults are inferred continuously along the northern margins of both the Rattles and Horn Rapids anticline (Reidel and Fecht 1994) (Figure 7.11). Surface exposures of faults within the uplifted folds are very limited. Reidel and Fecht (1994) show an exposure of a southwest-dipping thrust fault at the far northwestern end of Red Mountain. The unpublished Wagner maps also show southwest-dipping (24° and 30°) thrust faults at the northwestern end of Red Mountain at slightly higher elevations. Reidel showed photos of faults exposed in CRBG at the eastern end of Badger Mountain (S. Reidel, Hanford SSHAC Level 3 Workshop 2). Fault exposures are also identified within the core of The Butte (Finley quarry) and Molly Hill (Reidel and Fecht 1994). Reidel and Tolan (1994) observe that both the fault observed to cut The Butte and bedding within the uplift subparallel the northwest trend of the RAW structure and are not en echelon to the trend as suggested by Mann and Meyer (1993). Additional discussion of the orientations and kinematic indicators of the faults in Finley quarry exposures is provided in Section 7.4.2 and Appendix E.4.

7.4.1.1 Top of Bedrock Structure Contour Map

The continuity and structural relief of both the RAW-Rattles and the Horn Rapids structures are illustrated by the structure contours on the top-of-basalt map (Myers et al. 1979) (Figure 5.6). In both cases, although the geomorphically well expressed folds show the highest relief, there is evidence of continuous down-to-the-northeast steps in the top of the bedrock across both structures that can be extended between the aligned doubly plunging folds (Figure 5.7).

7.4.1.2 Evidence for Lack of Significant Strike-Slip Deformation Between Rattlesnake Mountain and Red Mountain

Bedrock relationships exposed along the Yakima River between Rattlesnake Mountain and Red Mountain provide information to assess the continuity and style of faulting along the RAW structure. Reidel et al. (1989) note that both Rattlesnake Mountain and Red Mountain anticlines plunge toward the Yakima River where flows of the Ice Harbor (8.5 Ma), Elephant Mountain (10.5 Ma), and Pomona (12 Ma) Members are exposed and undeformed between these folds.

Further analysis of the constraints provided by mapped bedrock outcrops was completed as part of this study. On either side of the mapped projection of the RAW structure the basalt exposures are relatively flat lying and undeformed. Ice Harbor and Elephant Mountain Member flows are exposed to the southwest and northeast of the fault projection, allowing for direct correlation across the projected fault (Figure 7.12). The northeast section of mapped basalt shows a continuous stratigraphic column of CRB from the Horn Rapids structure in the northeast to the RAW structure in the southwest. The top of the basalt flow between these two structures is nearly flat lying, showing a slight (0.006) slope to the north-northwest. The stratigraphic continuity, flat lying nature, and lack of faulting as observed by Reidel et al. (1989) are strong indicators of no major nearby faulting since the deposition of the Ice Harbor flow (8.5 Ma).

The stratigraphic continuity of these flows can be traced up to the Yakima River, nearly but not completely across the trace of the RAW structure (Figure 7.12). To assess the potential for fault-related vertical separation across the projected fault, topographic profiles were extracted from the 10-m DEM to compare the flow elevations on the northeast side of the projected fault to the elevation of the flows on the southwest side. The profile shown in Figure 7.13 intersects multiple basalt contacts on both sides of the projected fault. Given the slope of the basalt, the contact between the Elephant Mountain and Ice

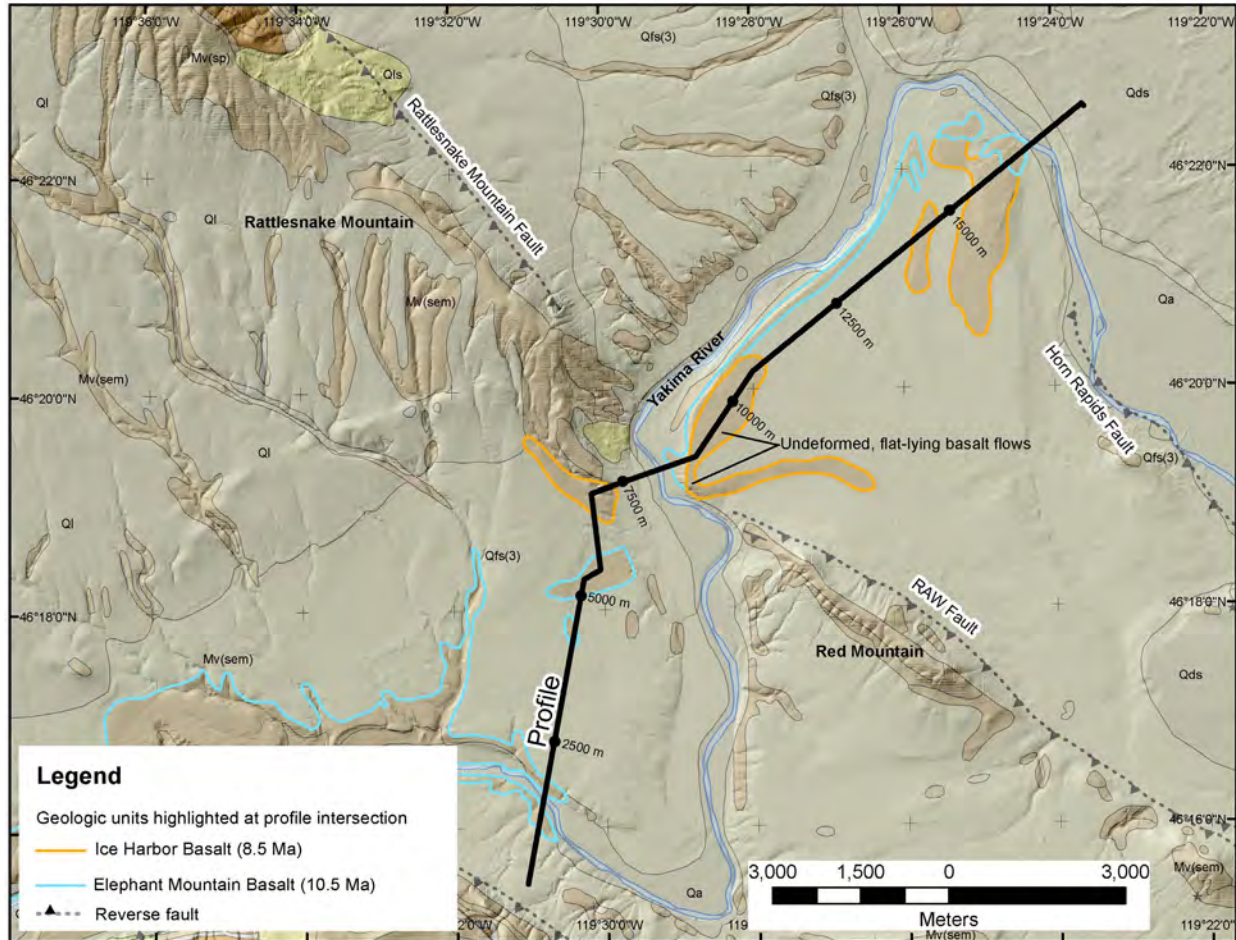


Figure 7.12. 1:100,000-scale geologic map showing the topographic profiles used to evaluate vertical separation across the projection of the RAW structure.

Harbor Members (8.5 Ma) has little to no vertical separation (≤ 20 m) across the projected trend of RAW alignment in the vicinity of the Yakima River. It should be noted that the exposure of the Ice Harbor Member on the southwest side of the river (~6500 m mark on Profile in Figure 7.13) is positioned on the southeast edge of the backlimb of Rattlesnake Mountain. Therefore, the maximum vertical separation of 20 m is more likely related to the uplift of the neighboring Rattlesnake Mountain structure. The top of the Elephant Mountain Member is therefore more appropriate to use to measure vertical separation across the RAW fault, rather than the top of the Ice Harbor Member. When this is done, there is little to no vertical separation observable across the RAW fault.

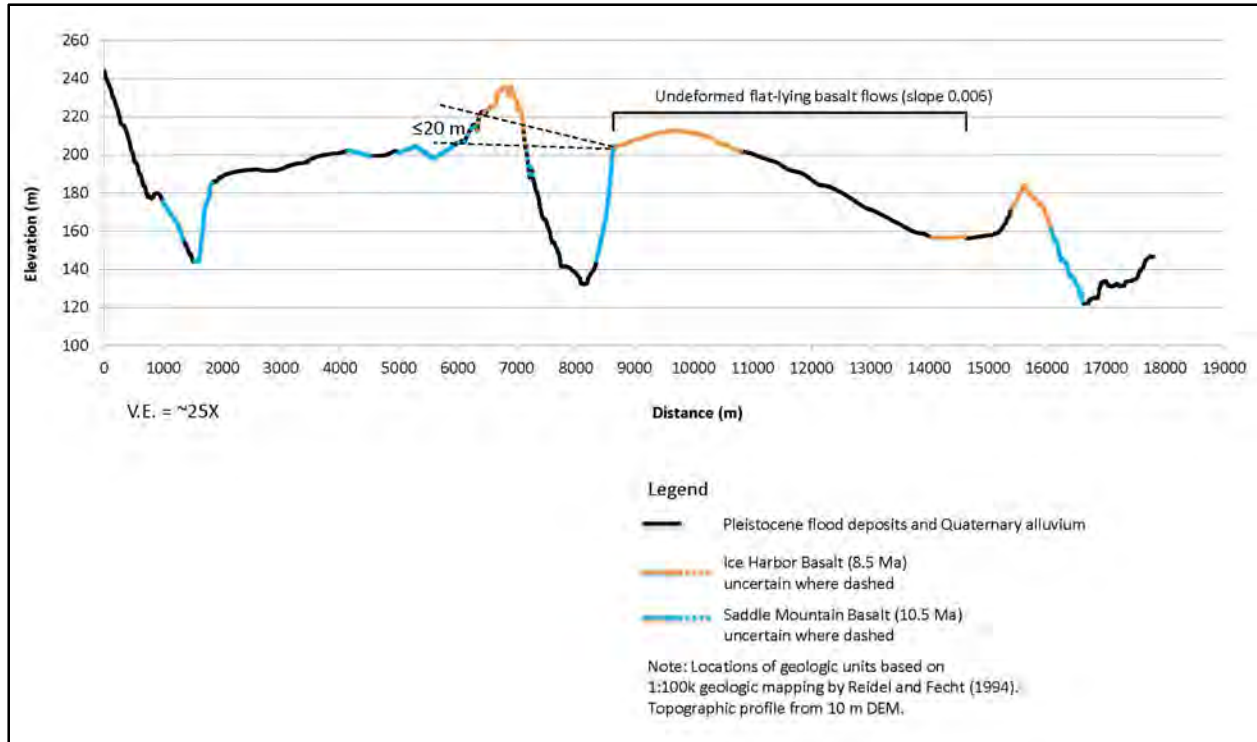


Figure 7.13. Topographic profiles showing uncertainty in vertical separation across projection of the RAW structure.

7.4.2 Finley Quarry Recurrence Data

Cataclysmic flooding events (both erosional and depositional in nature) and subsequent deposition of loess have modified and obscured the Quaternary record of faulting along the RAW structure. Excavations in a basalt quarry, informally referred to as the Finley quarry, provide the best and, to this date, the only exposures of faulted sediments of Quaternary age that are judged to be indicative of Quaternary tectonic deformation of the RAW structure. The quarry is located at the western end of The Butte approximately 4.5 km south of Finley and 11 km southeast of Kennewick (Figure 7.11). The fault zone exposed in the quarry wall was logged by both Farooqui and Thoms (1980) and WCC (1981a). WCC (1981a) also excavated a trench at the base of the quarry wall to provide additional exposure (see Figure 7.14 and Figure 7.15). A 13-m-wide zone containing three fault traces was exposed and logged by WCC (1981a). The northern and central fault traces displace colluvial deposits that post-date the CRBG (units l- 1–5 and m- 2–4). These faults were interpreted to be overlain by unfaulted colluvium (unit u-1). Samples of carbonate were collected by WCC (1981b) from the quarry wall. $^{230}\text{Th}/\text{U}$ -series analysis of the samples yielded ages of 19 ± 1 ka (probable age) and 51 ± 3 ka (maximum) (sample JB-7) and 75 ± 6 ka and 147 ± 13 ka (sample JB-8). The results for sample JB-8 were judged to be more representative of the antiquity of the deposit (WCC 1981b); the caliche was therefore regarded as having a minimum age of between 69 and 160 ka. Although it is not certain if the samples dated correspond to sample locations shown on the WCC (1981a) logs (sample numbers are 1–5 on the logs), a response to a NRC question (Q 360.15, Amendment 23 February 1982) states that unit u-1 is at least 75 ka based on these dates and that the north and center faults (faults F8 and F7, Figure 7.15) are capped by this unit.

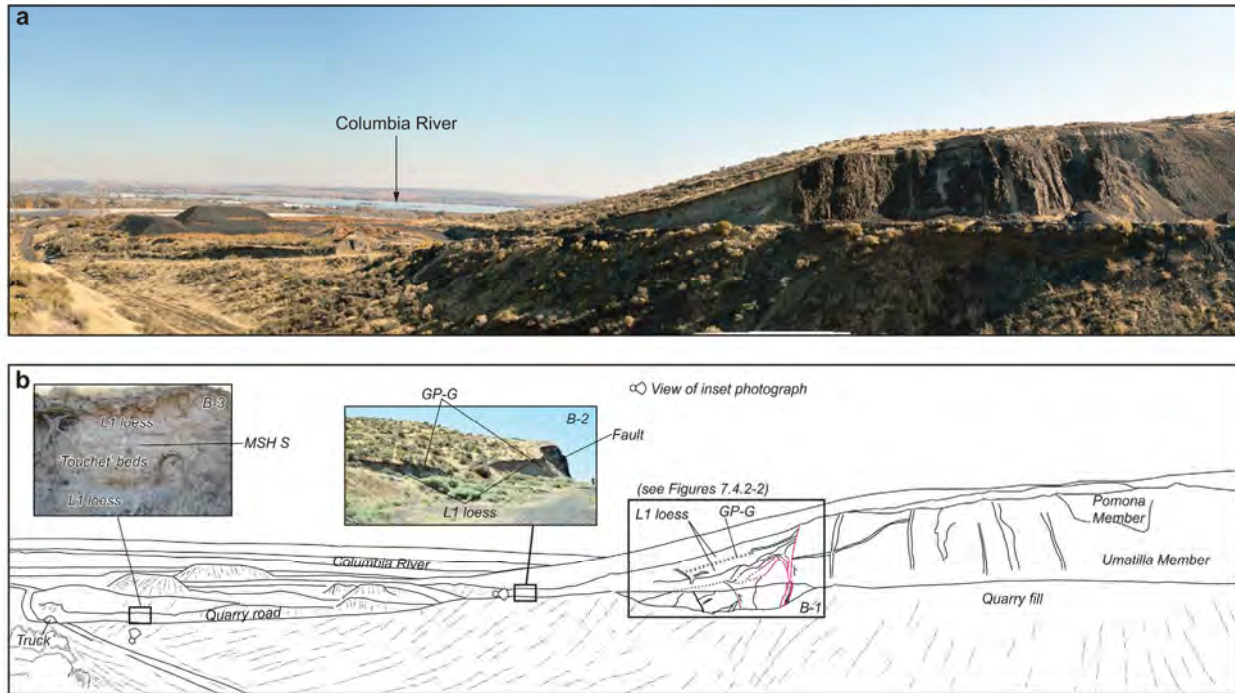


Figure 7.14. A) Panoramic photograph of the west end of The Butte showing Finley quarry in the right center and the Columbia River in the left center of the photograph. B) Line drawing of panorama. Left insert is a photograph of outcrop at the quarry inset containing MSH S tephra intercalated in Missoula flood backwater deposits. Middle inset shows a small outcrop of L1 loess at the toes of the quarry exposure containing tephra that can be traced into L1 loess in the main part of the outcrop in the background. The right inset is the location of the main quarry outcrop and the former Washington Public Power Supply System (WPPSS) quarry and trench exposures (WCC 1981a) shown in Figure 7.15 (modified from Sherrod et al. [In Review]).

Sherrod et al. (In Review) provides a discussion of the mapping of the present quarry wall (which is judged to be approximately 12–20 m east of the previously mapped quarry wall) and new age constraints based on OSL ages and tephra correlations (Figure 7.16 and Figure 7.17). Sherrod interprets as many as four earthquakes along the Wallula fault (which as defined by the Sherrod et al. includes Rattlesnake Mountain, the RAW structure, and the Wallula Gap fault) (Figure 7.16). The three youngest events at Finley quarry are estimated to post-date a late Pleistocene erosional unconformity (labeled unconformity 3). $^{230}\text{Th}/\text{U}$ -series dating of carbonate rinds in deposits truncated by this unconformity suggest these events would all post-date 17 ± 1.8 ka (see discussion in Section 4.3.1.5).

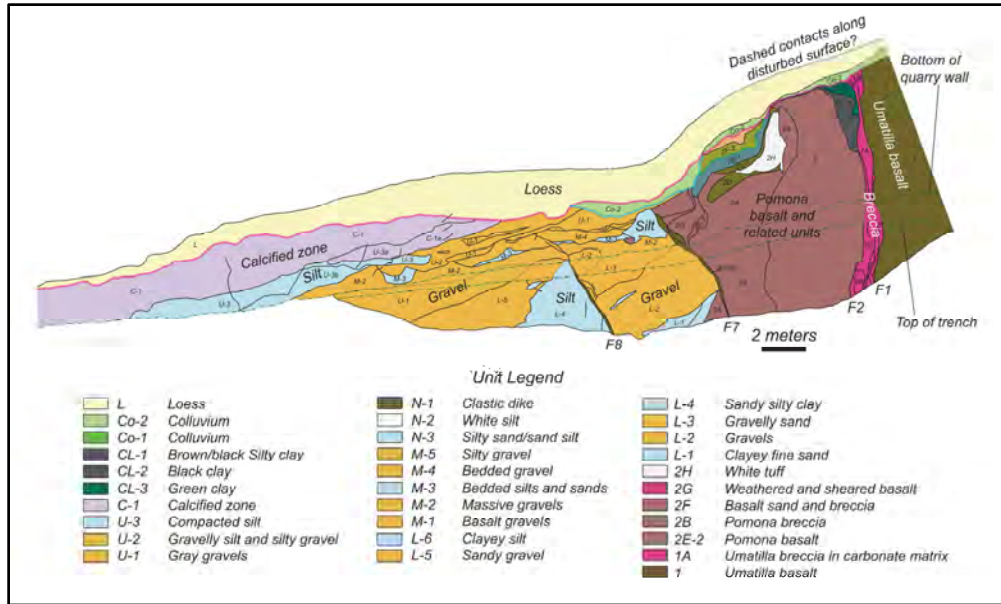


Figure 7.15. Combined quarry and trench logs from the WPPSS studies conducted in 1980 (WCC 1981a). The logs were stretched to the same scale and matched based on similar contacts and faults observed in both logs. Pre-MIS 2 glacial-outburst flood deposits (U, M, and L units of WCC 1981a) are colored light blue and orange to reflect silt and gravel content, respectively. Fault numbering follows recent quarry wall mapping as shown in Figure 7.16 (modified from Sherrod et al. [In Review]).

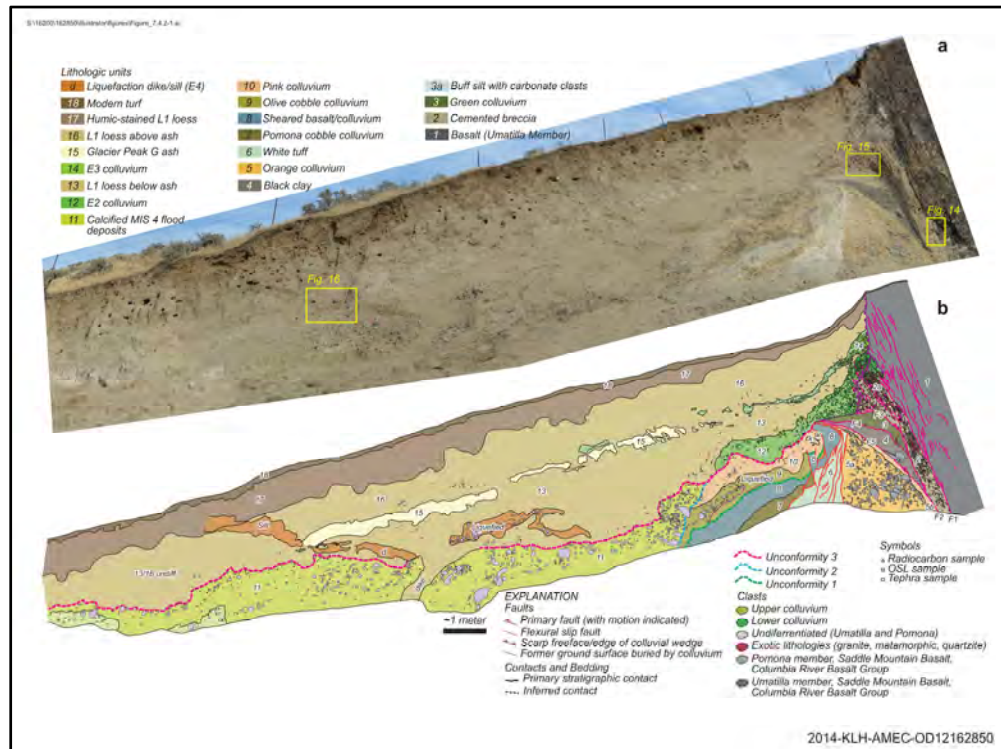


Figure 7.16. Photomosaic and log of the Finley quarry exposure (June 2013; modified from Sherrod et al. [In Review]).

Table 7.2. Alternative interpretations of the number and timing of late Pleistocene surface ruptures on RAW-Rattles structure based on stratigraphic and structural relationships exposed at Finley quarry (The Butte).

Earthquake Count/Interval	Relative Weight	Comments
<p>3 earthquakes post 17.5–15.5-ka flood unconformity (unconformity 3 as shown on Figure 7.16)</p>	<p>Very low weight is assigned to this option because one or both of the colluviums may not be directly related to surface faulting and the clastic dike, if related to strong ground motion, is not clearly related to movement on the RAW-Rattles, but could be related to an event on another nearby fault (e.g., Horse Heaven Hills fault)</p> <p>The lower part of colluvium 12 appears to be more fluvial in nature than would be expected if it was strictly a tectonic scarp-derived colluvium.</p>	<p>Three events:</p> <ul style="list-style-type: none"> • Assumes unit 12 colluvium was formed in response to a surface faulting earthquake post-17.5 to 15.5 ka flood unconformity (unconformity 3) and pre-MG G tephra (13,710-13,410 cal. yr BP); • Unit 14 colluvium formed in response to a surface faulting earthquake shortly following deposition of MG G (13,710-13,410 cal yr BP) • Clastic dike (liquefaction feature, dike and sill d) formed during earthquake on the RAW-Rattles that produced strong ground-shaking likely during late Holocene (post deposition of unit 16) and formation of modern soil. <p>Elevation at base of Finley quarry wall ~230 m</p> <p>The ~17.5-ka limiting age is based on the assumption that the erosional contact (unconformity 3 as shown on the USGS log) at the base of unit 12 is related to erosion during the MIS 2 Missoula floods. The 17 ± 1.8-ka age (see Appendix E.2) for carbonate rinds developed in unit 11 provide a maximum limiting age for this erosional event. WCC (1981b) also reported a similar age of 19 ± 1 ka (probable) to 51 ± 3 ka (maximum) for a carbonate rind on a clast collected from approximately the same location (note: the exact location of the WCC 1981a sample is not known). This age is also consistent with the age of the mammoth bone in flood deposits (elev. 293 m MSL) observed at the MCBONES mammoth site ($17,449 \pm 168$ cal. yr BP [2-sigma] [Barton et al. 2012]).</p>

Table 7.2. (contd)

Earthquake Count/Interval	Relative Weight	Comments
		<p>The unconformity could be slightly younger, i.e., related to the post-mammoth bone bed flood (slackwater deposits) at the MCBONES site, but is clearly older than 13,710–13,410 cal yr BP (the age of the GP G tephra). Slackwater deposits with ~15.5-ka MSH S tephra are exposed near the gate into the Finley quarry at an elevation of ~190 m MSL (Sherrod et al. [In Review]) to 198 m MSL (WCC 1981b).</p> <p>Sherrod et al. (In Review) suggest the unconformity underlying unit 12 could be as old as 47 ka based on the assumption that unit 3a is loess that may be correlative to loess L2 observed regionally. The Quaternary Studies Team SSC team members interpret this feature to be a clastic dike similar to the clastic dike (liquefaction feature) observed in unit 9. The contact between unit 3a and unit 2 (cemented tectonic breccia), therefore, is not sheared and is not indicative of a pre-unit 12 faulting event.</p> <p>Erosion during the Missoula flood(s) (the flood that deposited the MCBONES mammoth bed; ~17.5 ka or possibly older flood) and a later high flooding event that eroded the mammoth bone bed (MCBONES locality) could have formed fault-line scarps in the basalt and/or strongly carbonate-cemented tectonic breccia at Finley quarry from which colluvial units 12 and 14 were derived. Stringers of colluvium in loess beds overlying flood deposits that were observed at Gable Butte (see WCC 1981b, Figure D3-A7) are possible analogs for nontectonic colluviation post-MIS 2 floods. Stone lines and boulder clasts also are observed at the MCBONES site overlying the loess deposits.</p>

Table 7.2. (contd)

Earthquake Count/Interval	Relative Weight	Comments
		<p>Note: The unit 11 flood deposits may be significantly older than ~17.5 ka (i.e., deposited during MIS 4 or older glaciations). The deeply weathered coarse-grained clasts of felsic granite in unit 11 as noted by Sherrod et al. (In Review) suggest an older age. In this case the carbonate ages of 17 ± 1.8 ka would represent a late stage of carbonate formed in the deposits prior to the most recent MIS 2 floods. WCC (1981b) reported U-series ages of 75 ± 6 ka and 147 ± 13 ka for massive pedogenic carbonate in unit u-1 (WCC 1981b, CGS (WNP2) FSAR Response to Q 360.15, Amendment 23 February 1982). These ages represent minimum ages for unit u-1. If unit 11 (Sherrod et al. [In Review]) is equivalent to unit u-1 (WCC 1981a), this would suggest the unit 11 flooding event may have been deposited during MIS 4 (58–71 ka) or likely an older glaciation such as MIS 6 (130–191 ka) or possibly MIS 8 (243-300 ka).</p>
<p>2 earthquakes post 17.5–15.5-ka flood unconformity</p>	<p>As discussed above the evidence for the two to three youngest postulated faulting events at Finley quarry is not conclusive. The arguments for the postulated tectonic origin of the upper colluvium are judged by the Quaternary Studies Team SSC members to be weak and the liquefaction feature (dike and sill d) if due to earthquake-induced strong ground motion is not definitely associated with a rupture of the RAW-Rattles. Therefore, the two post-17.5–15.5-ka option is also given low weight.</p>	<p>Event 1</p> <ul style="list-style-type: none"> The two-earthquake scenario assumes that there was a surface faulting earthquake on fault F2 post deposition of the unit 12 colluvium (after 17.5–15.5 ka and pre-deposition of unit 13). Observations of possible aligned clasts and fractures within unit 12 and the apparent down-to-the-north step in the base of the unit 12 were noted by members of the Quaternary Studies Team as being possible evidence to support post-unit 12 faulting. Younger units (units 13 and 14) are not displaced by fault F2 or clearly displaced by fault F1, suggesting that this event pre-dates the deposition of MG G (13,710-13,410 cal yr BP). <p>Event 2 (two alternatives)</p> <ul style="list-style-type: none"> The interpretation of a clastic dike extending into loess deposits (up to the base of the modern soil) that overlie the GP G tephra layer is the strongest evidence for a latest Pleistocene (possibly late Holocene) earthquake on the RAW-Rattles or a nearby fault-causing strong ground motion.

Table 7.2. (contd)

Earthquake Count/Interval	Relative Weight	Comments
		<ul style="list-style-type: none"> Alternatively, if the clastic dike was not caused by an earthquake on the RAW-Rattles, the hypothesis that the upper unit 14 colluvium was derived from a surface fault scarp, may be evidence of an event shortly following deposition of MG G (13,710-13,410 cal yr BP).
1 earthquake post 17.5–15.5-ka flood unconformity	<p>This hypothesis is judged more likely than the 2- or 3-earthquake options. Two alternative times for the event are considered.</p> <p>Option 1</p> <p>Post 17.5–15.5 ka (post-unit 12, which overlies unconformity 3) and pre-13,710-13,410 cal yr BP (unit 15)</p> <p>Option 2</p> <p>Holocene (possibly late Holocene) post 13,710-13,410 cal yr BP (post units 15 and 16, possibly into modern soil)</p>	<p>Event 1 as described above. The lack of significant weathering of unit 12 (carbonate observed on clasts may be reworked from bedrock where carbonate coatings along fractures is common) is consistent with an age of postulated faulting of between 17.5– 15.5 ka and 13.5 ka. However, the evidence for post-unit 12 surface faulting is equivocal. Based on post-field review of photographs clear evidence of faulting of colluvium overlying or juxtaposed against the tectonic breccia is not demonstrated.</p> <p>Alternatively, the post-GP G tephra liquefaction event (extends up into modern soil). This option is considered less likely because it would be expected that there would be evidence of movement on faults exposed in the logged quarry exposure if there had been a moderate to large magnitude earthquake on a blind thrust fault associated with the RAW-Rattles at depth in the Holocene.</p>
No earthquakes post 17.5–15.5-ka flood unconformity	This hypothesis is judged by the Quaternary Studies Team to be most likely. As noted above, flood-related erosion and deposition can explain most if not all of the features observed in the Finley quarry exposure.	This hypothesis is consistent with conclusions cited in the CGS FSAR (Energy Northwest 1998) and the NRC FSER (NRC 1982) based on review of the quarry wall and trench exposures documented in WCC (1981a).

Table 7.2. (contd)

Earthquake Count/Interval	Relative Weight	Comments
		<p>The postulated liquefaction feature (dike and sill d) that appears to post-date the deposition of GP-G tephra is the strongest evidence for a strong shaking earthquake in the general vicinity of Finley quarry (which may or may not be on the RAW-Rattles fault source). The best expressed part of the mapped feature cross cuts unit 13. The USGS log interprets unit 13 as L1 loess. However, this unit shares characteristics similar to massive to poorly bedded slackwater deposits observed elsewhere (e.g., at the MCBONES locality) (i.e., it contains scattered clasts and irregular blocks of pre-flood ice-rafted or ripped up material). Although the mapped extent of the feature up into the modern soil suggests a post-flooding event, additional work or review is needed to preclude a flood-related liquefaction phenomenon.</p>

7.5 Wallula Fault Zone (Wallula Gap Fault)

The Wallula fault zone, which is located along the northeast flank of the Horse Heaven Hills anticline in the southeastern Washington and northeastern Oregon, forms the eastern end of the RAW alignment (Figure 7.18). Farooqui (1979) considered the fault to be capable based on a lineament and associated topographic scarp identified by Bingham et al. (1970) that was inferred to be tectonic and an exposure of faulted colluvium of probable Quaternary age near Warm Springs Canyon. WCC (1982) conducted additional field studies, including trenching and mapping studies to evaluate both of these features. Based on these studies, the FSAR (Energy Northwest 1982) identified the Wallula Gap fault as a capable fault. The NRC (1982) concurred with this assessment.

As discussed below, the sense and amount of movement on this fault was controversial in the late 1970s and early 1980s and continues to be uncertain to this day. The fault variously has been interpreted as a normal fault, a strike-slip fault, and a monoclinial fold (with an associated blind reverse or reverse oblique fault at depth).

Different names have been applied to the various strands within the fault zone. Newcomb (1965) initially traced the fault southeastward from Wallula Gap to a point just south of Touchet. As reported by WCC (1982), Brown (1968) questioned the existence of the fault and suggested that breccias associated with the fault were volcanic rather than tectonic, and that the structural alignment was the result of monoclinial flexure rather than faulting. Bingham et al. (1970) identified a down-to-the-north vertical stratigraphic displacement of more than 60 m west of the Wallula Gap along the Wallula Gap fault. Due east of the Gap, they described the apparent juxtaposition of stratigraphic units (north side down) with no evidence of sharp monoclinial folding, and suggested hundreds of feet of displacement. Based on the presence of fault-line scarps and sporadic outcrops of breccia, Bingham et al. (1970) traced the fault approximately 20 km. Gardner et al. (1981) identified the Wallula Gap fault as a complex zone of faulting that strikes N65°W and is traceable for approximately 11 km from Yellepit area west of Wallula Gap to near Vansycle Canyon approximately 8 km east of the Gap where it intersects the OWL. WCC (1982) define the Wallula Gap fault zone as a complex zone of folding and faulting that extends along a N70–80°W trend for at least 25 km from the vicinity of Wallula Gap southeastward to a point southeast of Touchet. The WCC (1982) report further discusses previous interpretations and terminology used to describe the fault zone, noting that previous workers were all in agreement that there is a fault west of Vansycle Canyon near the base of the hills and south of the Walla Walla River, but that only some workers (e.g., Farooqui 1979; Swanson et al. 1980; Gardner et al. 1981) suggest that the fault bifurcates west of a geomorphic feature referred to as the Nub and extends westward to the last bedrock exposure of the fault at Molly Hill (Figure 7.18). The southern trace is considered to be the Wallula Gap fault (Swanson et al. 1980; Gardner et al. 1981). WCC (1982) follows Kienle (1980) in referring to the northern branch as the RAW fault, and consider the Wallula Gap fault zone to refer to the Wallula Gap fault and the RAW fault together. WCC (1982) concludes that part of the Wallula Gap fault zone is spatially related to a monoclinial fold and that the fold and faults together are referred to as the Wallula Gap structure.

Several previous workers suggested that the group of north- to northwest-trending en echelon faults that are present south of the Wallula Gap fault had experienced normal displacement (Newcomb 1965; Gardner et al. 1981). Horizontal slickensides common within cataclastic breccia zones along these faults, however, suggest that the most recent movements have been strike-slip (Gardner et al. 1981). Mann and Meyer (1993) suggested that the Wallula fault zone was an extensional strike-slip duplex in which the northern range-front trace was referred to as the lower main fault zone and the southern trace (including the fault they refer to as the Umapine fault) as the upper normal fault zone (Figure 7.19).

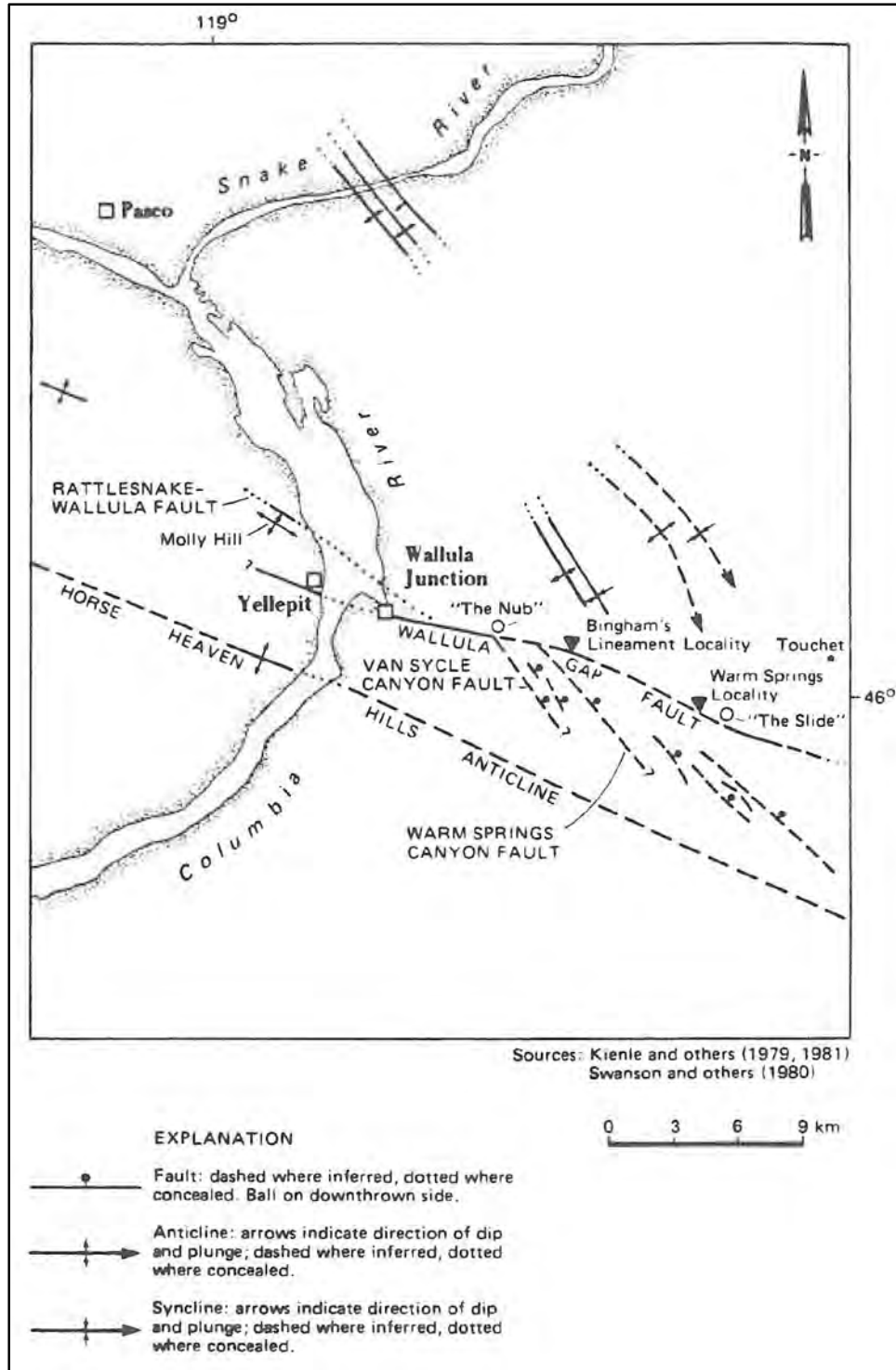


Figure 7.18. Location map showing key localities and structures associated with the Wallula fault zone (from WCC 1982).

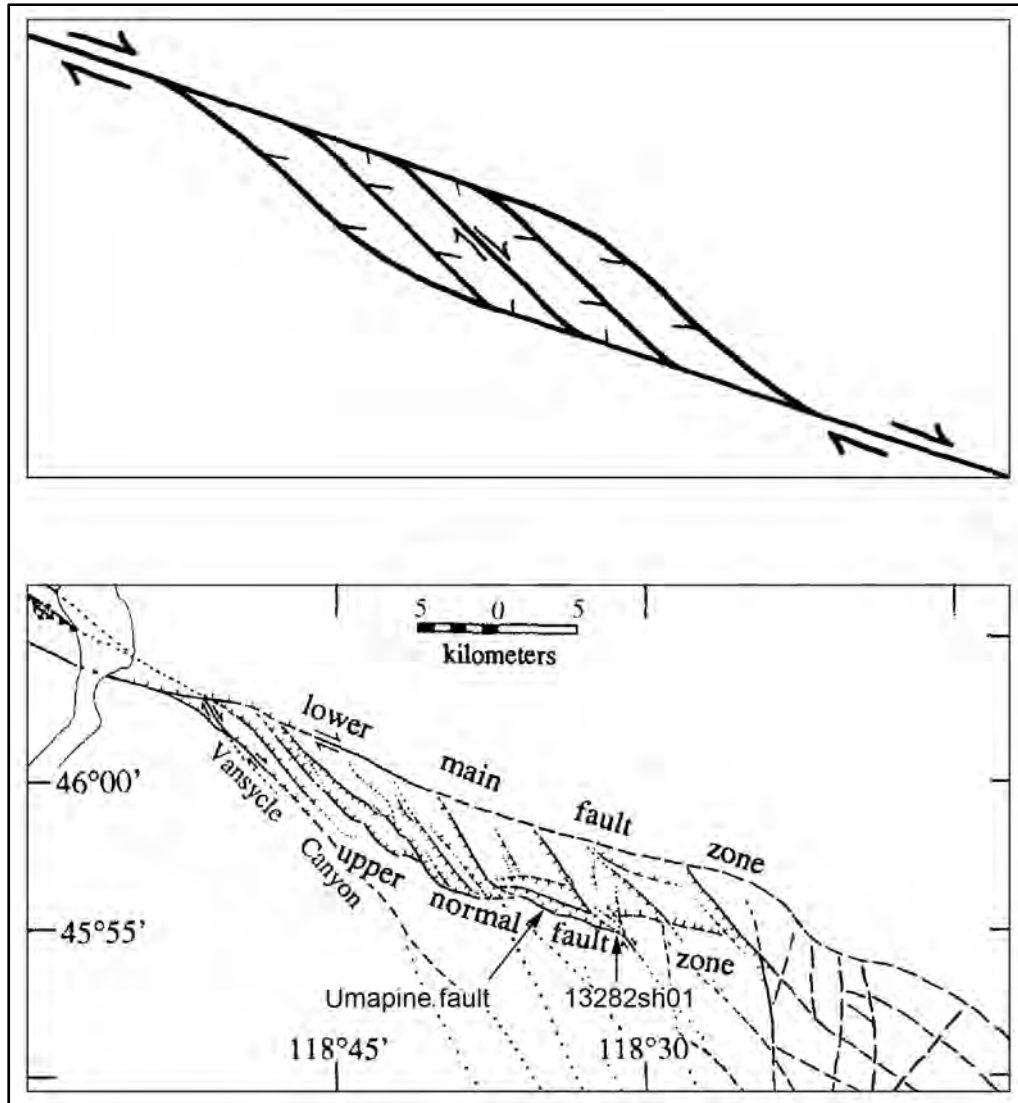


Figure 7.19. Comparison of a right-lateral strike-slip extensional duplex (adapted from Woodcock and Fischer 1986) to the Wallula fault zone (modified from Mann and Meyer 1993).

McQuarrie (1993) notes that kinematic indicators such as horizontal slickenlines on the Wallula fault suggest most recent strike-slip motion, whereas vertical separation of basalt flows and drag folding indicate a past component of dip-slip. Kuehn (1995) suggests that there was predominantly strike-slip motion on the OWL prior to emplacement of the basalts, but provides no specific evidence to support this thesis. He also reports that slickensides in basalts on northwest-trending faults of the OWL zone in northeast Oregon east of Wallula Gap consistently indicate right-lateral displacement. WCC (1982) measured 49 striae, 47 of which were within 300 m of the surface trace of the Wallula Gap fault. Sixty-one percent of all the striae made an angle of 60° or greater with the trend of the Wallula Gap fault, whereas 11 percent of the striae made an angle of 30° or less. From these data, it was concluded that movement was more consistent with a reverse fault/fold model than with a strike-slip model. WCC (1982) also concluded that strike-slip faults within the Wallula Gap structure have an orientation that is more consistent with a conjugate shear system associated with reverse faulting than with a right-lateral Riedel shear system or strike-slip faulting parallel to the Wallula Gap fault.

Gardner et al. (1981) concluded that the maximum normal offset (310 m) and width (300 m) of the fault zone was near Vansycle Canyon and that the amount and width of the fault zone diminished to the west coincident with an apparent change in the fault geometry from normal to reverse. Approximately 2 km west of the Yellepit trench locality the fault is buried by Quaternary sediments, but mapping suggests that the fault merges with the Jump-Off-Joe anticline (Gardner et al. 1981) (Figure 7.11).

Quaternary deformation has been reported at several sites along the Wallula fault system as summarized by Reidel et al. (1994), Bjornstad et al. (2012), and Barnett and Sherrod (In Review). These included features in the vicinity and west of Vansycle Canyon, the Bingham lineament, the Warm Springs Canyon locality, and the Umapine fault gully locality (Figure 7.20). Mann and Meyer (1993) and McQuarrie (1993) report geomorphic features suggestive of Quaternary displacement, such as faceted spurs and offset drainages, along the Wallula Gap and Umapine strands of the Wallula fault zone. Mann and Meyer (1993) also documented evidence of post-10.7 ka movement along the Umapine strand of the fault zone.

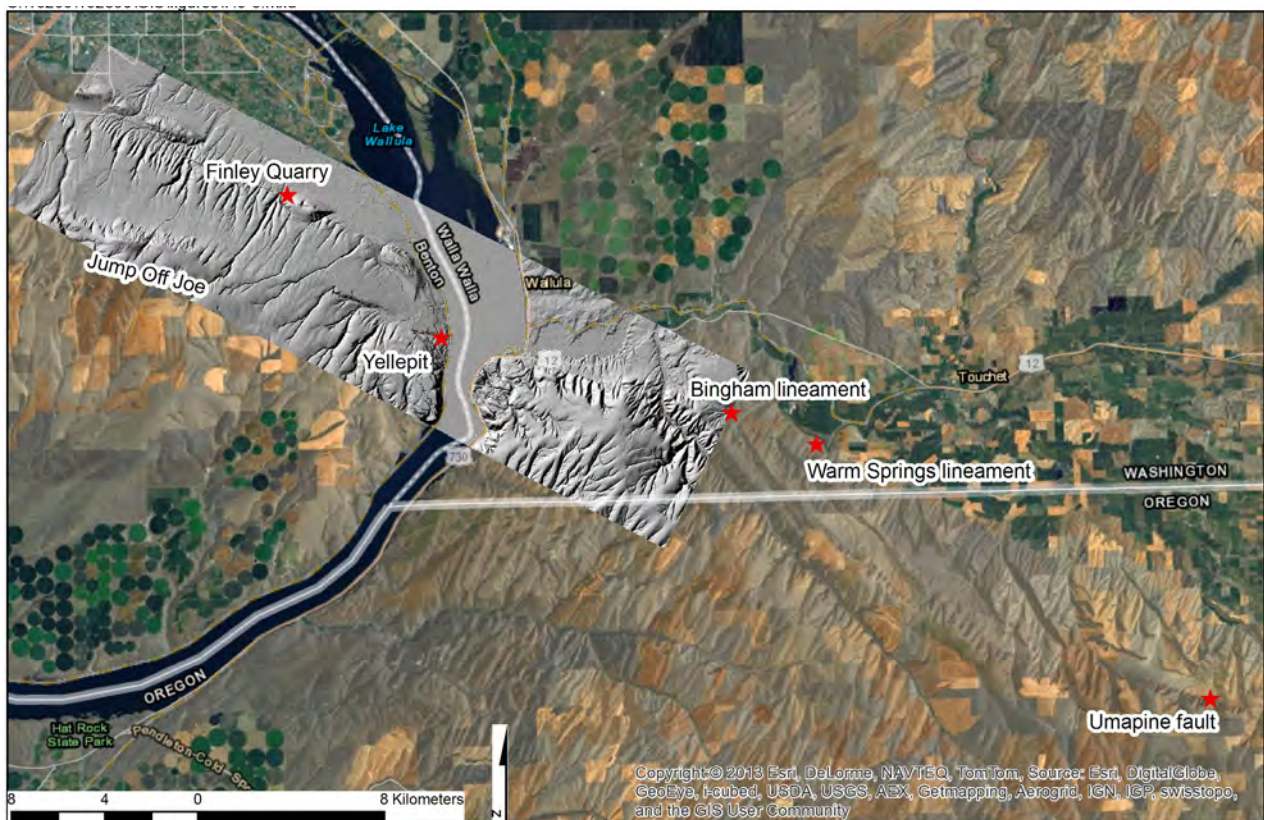


Figure 7.20. Map showing locations of paleoseismic investigations along the Wallula (Wallula Gap) fault.

The USGS is currently conducting studies along the Wallula fault zone, which they define as including the RAW alignment, Yellepit fault, Wallula Gap fault, and Horse Heaven Hills fault (Sherrod et al. [In Review]). Based on analysis of magnetic data, Blakely et al. (2013) conclude that Ice Harbor dikes are right laterally offset as much as 6.9 km across the Wallula fault, suggesting a long-term average dextral slip rate of 0.8 mm/yr since dike emplacement 8.5 Ma.

As part of the QGS, the Quaternary Studies Team reviewed previous licensing documents and reports, examined hillshade and slope maps from high-resolution LiDAR data, and visited selected localities along the Wallula (Wallula Gap) fault zone. Field observations and commentary regarding previously published observations pertaining to both style of faulting and timing and recency of faulting along the Wallula fault zone at key localities are provided below.

7.5.1 Yellepit Station Canyon Trench Locality

Trenching investigations of the Wallula Gap fault west of Wallula Gap in the vicinity of the Yellepit Station Canyon are documented by Gardner et al. (1981). The primary conclusions from this study and subsequent licensing documents are as follows:

- Exploratory trenching at Yellepit Station revealed high-angle reverse faulting and confirmed indications from mapping that the amount of displacement and width of the fault zone diminish to the west.
- Horizontal striae as well as randomly oriented striae were noted. The CGS FSAR (Energy Northwest 1998) states that both vertical and horizontal striations were observed, but the former were more prominent.
- The fault offsets the Ice Harbor flow (~8.5 Ma), but is overlain by apparently undeformed glaciofluvial sediments (13–20 ka). A response to NRC Q 360.015 (Amendment No. 23 to the WNP-2 FSAR) notes the age of the glaciofluvial gravels (referred to as the Kennewick fanglomerate) originally was estimated to be ~50 ka by Shannon and Wilson, Inc. in WPPSS 1977) but was later interpreted to be a minimum of 21 ± 4 ka based on the age of caliche that had been dated using the uranium-thorium method.

7.5.2 Northwest-Striking Faults, U.S. Highway 730 Roadcut

Several small faults are exposed along U.S. Highway 730 where it enters Wallula Gap. Gardner et al. (1981) state that the shears, striking N35°W, are most prominent in the Two Sisters unit, but are present throughout the other basalts, and that the shears are most numerous near the Wallula Gap fault. The shears are filled with basaltic rubble, yellow clays, sand, and silt. Differential weathering has enlarged some shears to as much as 2 m in width, but prominent horizontal slickensides and the presence of protomylonite, as revealed by petrographic examination, document that the shears are not the results of weathering along a joint (Gardner et al. 1981). Reidel et al. (2013) note that basalt dikes exhibit a similar N30°–50° orientation and suggest that dikes were emplaced along faults and that a preexisting fault pattern controlled the dike trends west of the Hite fault.

Farooqui (1979) states that strong slickensided surfaces with horizontal to 10°W dipping grooves and striations are present in the basalt and breccia zone along the Wallula fault as exemplified by the features exposed in the U.S. Highway 730 roadcut near the mouth of Wallula Gap. At this location, Farooqui (1979) also describes a vertical 1/4-inch-thick clastic dike with vertical silt partings and sand fill within the shear zone. Horizontal striations on the clastic dike were interpreted by Farooqui (1979) as being evidence of some post-dike movement in the shear zone. WCC (1981a) concluded that these reported slickensided dikes, unlike the faulted clastic dikes observed in trenches on Gable Mountain, do not show conclusive evidence of displacement and they do not have highly polished surfaces, and that an alternative explanation is that the striations observed on the clastic dike might be casts of the grooved fault plane.

The roadcut exposures were briefly observed during reconnaissance for this project. Due to the limited daylight available during the stop, we did not evaluate the purported striations on the clastic dike. Subhorizontal moulins (13°S) were observed on a N30°W, 64°S fault (Figure 7.21).

The northwest orientation of the faults exposed in the U.S. Highway 730 roadcut and the evidence for predominantly strike-slip movement indicate that these faults are not responsible for the general uplift of the basalt units south of the Wallula Gap fault.

7.5.3 Northwest-Striking Faults, Vansycle Canyon

Gardner et al. (1981) interpret two faults in the northern portion of Vansycle Canyon that intersect the Wallula Gap as graben-bounding faults. Deflected stream courses mark the arcuate trace of the western fault, which is characterized by intense shearing and cataclastic breccias. Gardner et al. (1981) observe that the Grande Ronde Basalt-Frenchman Springs Member contact is vertically offset ~122 m relative to its position on the Horse Heaven Hills. This same contact is down-dropped relative to its true position on the eastern wall of Vansycle Canyon by a concealed fault in the canyon bottom.

Mann and Meyer (1993) cite this locality as evidence for Quaternary activity along the Wallula fault. They suggest that three minor drainages and intervening ridges show right deflections varying from 0.1 to 0.2 km are indicative of probable post-early Pleistocene offset (Figure 7.22). Evidence cited that the offsets are tectonic rather than just deflections are that 1) the shear zone controlling the offsets is well exposed in drainage C, and 2) the clear offset of ridge axes between drainages and the presence of beheaded drainages. Reidel and Tolan (1994) in a comment to the Mann and Meyer (1993) paper, note that the deflected drainages are coincident with a fault, the Vansycle fault as mapped by Gardner et al. (1981), but note that field evidence (e.g. ridge D) show that adjacent ridges and drainages show no evidence of right-lateral offset. Based on examination of the hillshade maps derived from the new high-resolution LiDAR data obtained for this project, we agree with the observation of Reidel and Tolan (1994). Given the limited length of the fault (~ 1.2 km) along which the postulated deflections are present, and the evidence for no offset of ridges and drainages along adjacent parts of the fault both to the northwest and to the southeast, it is likely that the apparent drainage offsets are due to fault-line erosion (i.e., deflections) rather than tectonic offset.

7.5.4 Bingham Lineament

Bingham et al. (1970) interpreted a curved linear geomorphic feature along the inferred trace of the Wallula Gap fault in the vicinity of Warm Springs Canyon as possible evidence of recent (post-Touchet, less than 12 ka, but pre-historic, greater than 100 yr) tectonic movement.

WCC (1982) conducted detailed surface and subsurface investigations along Bingham's lineament to evaluate the origin of the lineament, and to assess the nature and amount of post-Touchet displacement if the lineament was the result of tectonic faulting. Figure 7.23 shows the location of test pits, trenches, and magnetometer traverse at the Bingham's lineament locality. The magnetometer profile showed a uniform gradient that was interpreted to reflect a sloping magnetically susceptible body below the surface (Figure 7.23d). The absence of a magnetic anomaly greater than 20 gammas within a field whose intensity ranges from 56,300 to 56,000 gammas showed that there is no disturbance in the underlying susceptible unit (basalt bedrock) that might be indicative of a fault (WCC 1982). Two trenches were excavated across the



Figure 7.21. Photographs of the fault plane exposed along Highway 730. The fault plane has a strike of N30°W dipping 64°S and prominent moulins along the fault plane dip 13°S.

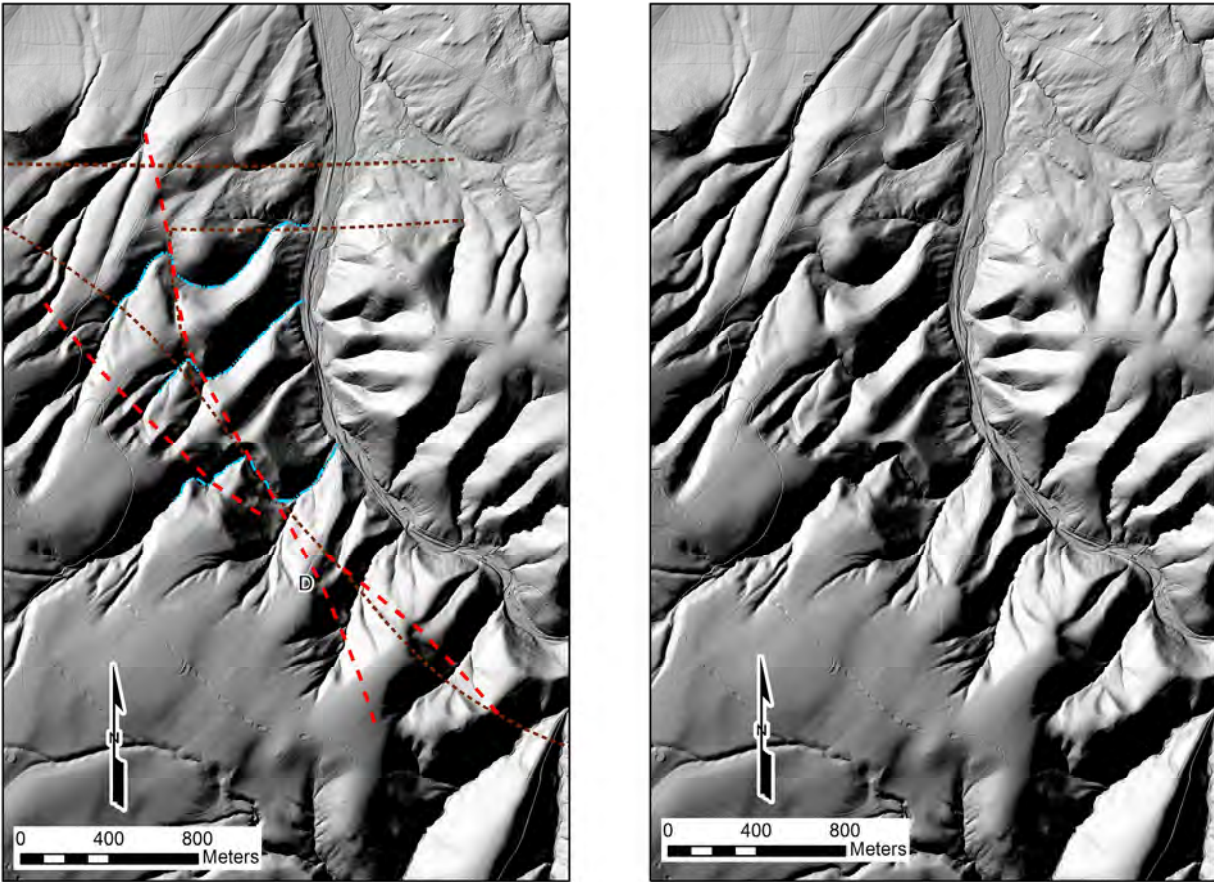


Figure 7.22. LiDAR-generated DEM base map near the mouth of Vansycle Canyon. a) Prominent lineament (red dashed lines) and offset drainages (blue lines) interpreted by Mann and Meyer (1993) relative to bedrock faults mapped by Gardner et al. (1981). b) Uninterpreted LiDAR-generated DEM.

lineament. No through-going faults cutting either the Touchet Beds or the overlying loess were observed in trenches BL-1 or BL-2. A couplet of white volcanic ash was observed imbedded within the rhythmite units in both trenches. Based on its stratigraphic position and similarity to ashes that occur elsewhere in the Pasco and Walla Walla basins (WCC 1981b), the ash was interpreted to be the Mount St. Helens set S tephra, which was then considered to have been ejected approximately 13 ka (more recently assigned an age of ~ 15.5–16 ka, see Table 4.2). The rhythmites underlying the lineament in trench BL-2 showed evidence of deformation due to liquefaction, but no clastic dikes or faults penetrated the upper Touchet Beds in the trench (Figure 7.23d). Based on the results of the trenching, the magnetometer survey, and evidence suggesting the lineament was likely a trail or roadway connecting now abandoned homesteads, WCC (1982) concluded that the lineament was a cultural feature, which coincidentally lies along the postulated eastern extension of the Wallula Gap fault.

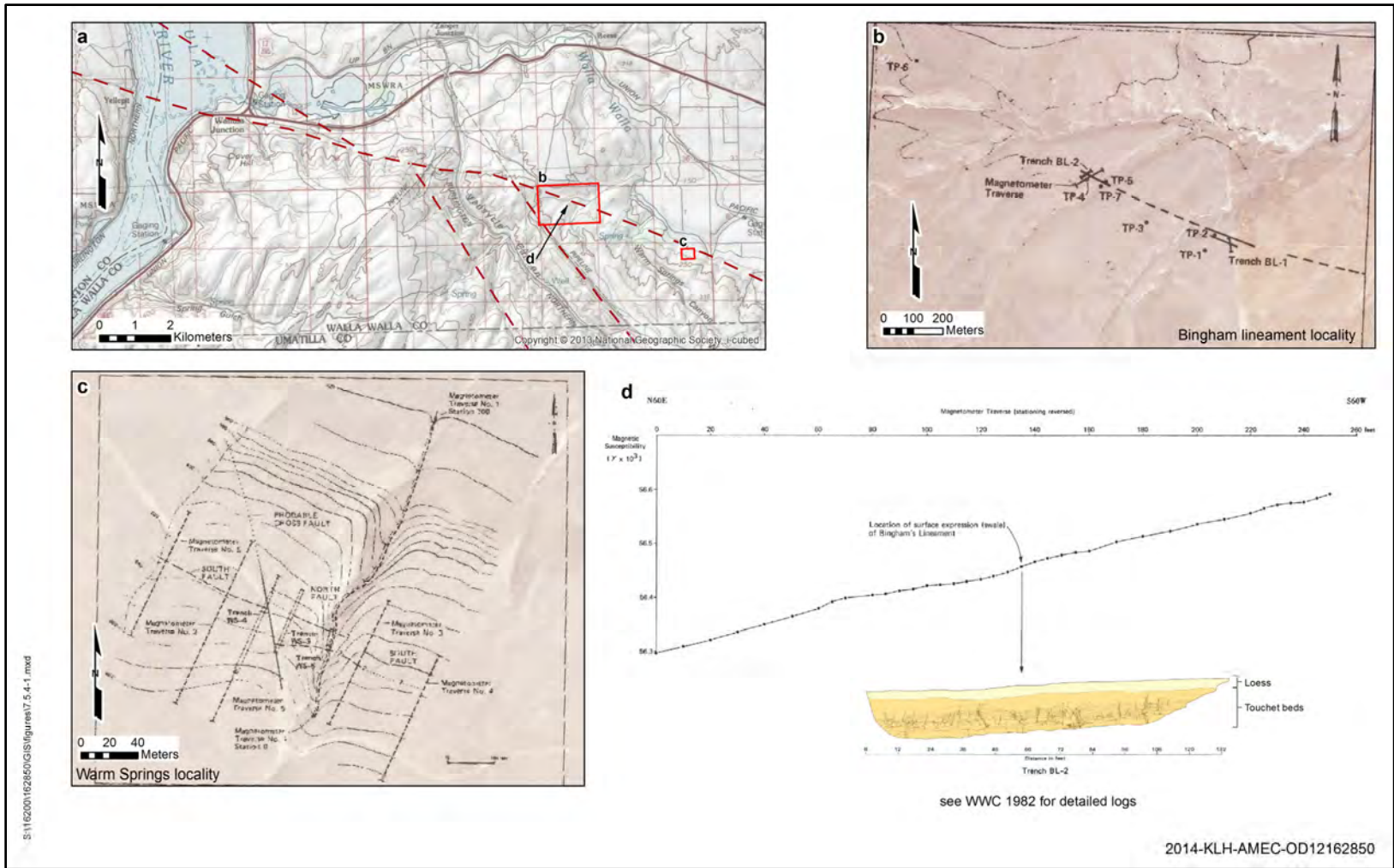


Figure 7.23. a) Location map showing trenching and magnetometer studies from WCC (1982). b) Map showing studies along mapped trace of the Bingham lineament. c) Map showing locations of trenches and 5 of 19 magnetometer survey lines along the mapped Warm Springs lineament. d) Magnetometer survey data and simplified trench log along the Bingham lineament.

7.5.5 Warm Springs Canyon Locality

Farooqui (1979) first described faulted colluvium exposed in a natural stream cut approximately 1.5 km southeast of the mouth of Warm Springs Canyon along the Wallula Gap fault as mapped by Farooqui (1979) and Swanson et al. (1980) (Figure 7.24). Within this exposure the fault zone consisted of two northwest-striking, south-dipping fault traces. The colluvium was between and juxtaposed against basalt by both faults. Farooqui (1979) suggested the faulting was pre-Holocene, but that displacement had probably occurred during the Quaternary.

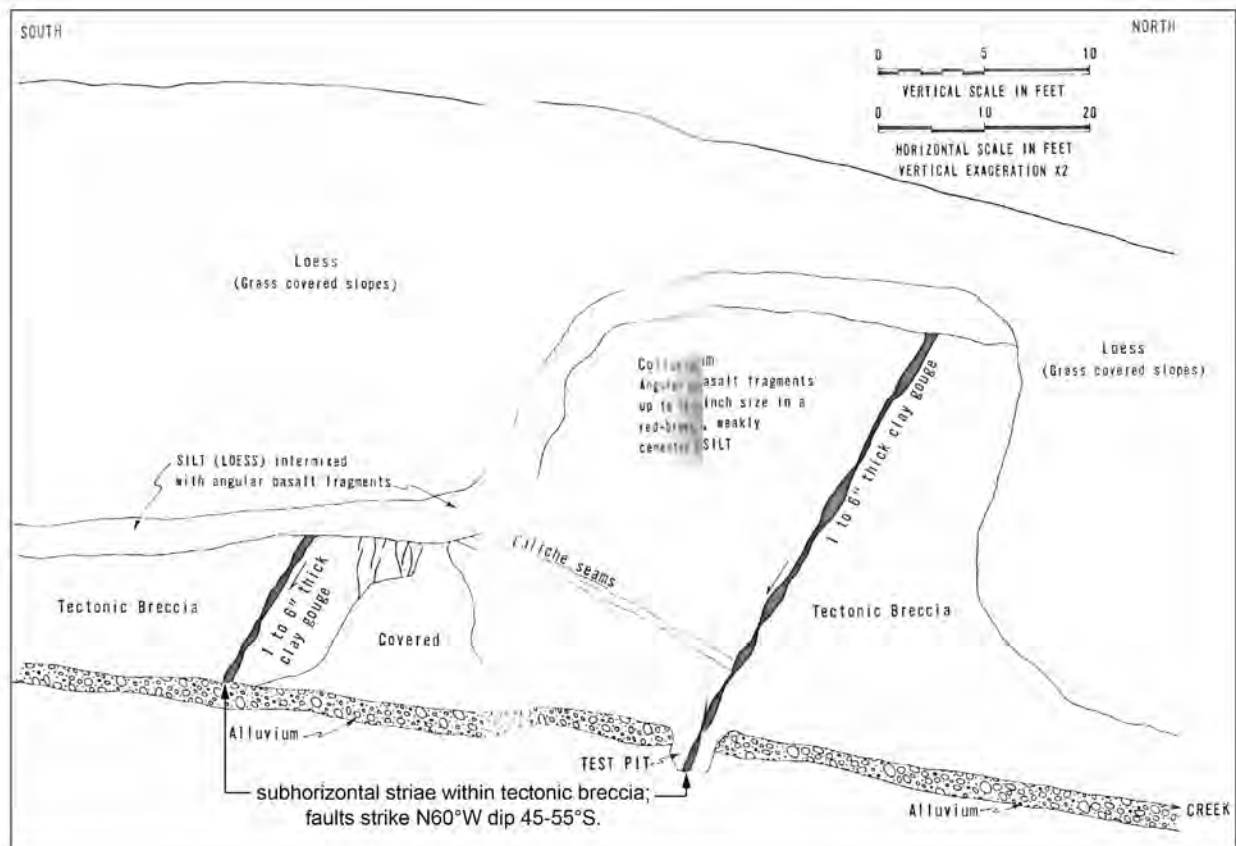


Figure 7.24. Geologic sketch of faulted colluvium of probable Quaternary age at the Warm Springs locality (from Farooqui 1979).

WCC (1982) conducted detailed geologic mapping and trenching at the Warm Springs locality to assess the capability of the fault as well as the amount of displacement (Figure 7.23c). In addition, 19 magnetic profiles were run approximately perpendicular to the fault zone. The conclusions from this study were as follows:

- Two major faults and one minor fault were exposed in the trenches. The South fault, as exposed in trench WS-5, strikes N55°W and dips 50° to the southwest. Striae on a N62°W striking, 82°S dipping polished and striated surface that bifurcates from the main fault exhibited a rake of 6 degrees. For a distance of approximately 12 m south of the South fault, limited exposures in the Frenchman Springs basalt show very closely spaced fracturing and breccia zones. The South fault as exposed in trench WS-3 had a N66°W strike and dip of 55°SW. It places Frenchman Springs basalt above older

colluvial deposits. The North fault, which was exposed in trenches WS-3 (Figure 7.25) and WS-5, strikes N50°W to N70°W and dips approximately 60°S. It juxtaposes Ice Harbor basalt and younger and older colluviums with minimum net apparent vertical displacements of 3.4 and 3.1 m down to the south (trenches WS-5 and WS-3, respectively).

- A cross fault may cut the Wallula Gap fault between trenches WS-3 and WS-4 based on an apparent right-lateral displacement of 20 m of the trough of a magnetic low (that can be correlated with bedrock structures exposed in the trenches) along a line trending approximately N5°W.
- Two colluvial deposits (older and younger colluviums) that post-date the CRB but pre-date late Pleistocene flood deposits are in fault contact with the Frenchman Springs Member.
- The age of the faulted colluvial deposits is uncertain. They could be as old as the Ringold Formation (Miocene-Pliocene), but are more likely Pleistocene in age.
- Based on the degree of weathering and soil formation, the younger faulted colluvium is probably Sangamon or older (older than approximately 100 ka).
- Late Pleistocene Touchet Beds (approximately 13 ka) overlie the fault and are not displaced (Figure 7.25).

7.5.6 Umapine Fault

The Umapine fault, a west-northwest striking fault ~10 km west of Milton-Freewater, was identified as a Quaternary-active fault based on strong aerial lineament (surface scarp) 7 km in length (Mann and Meyer 1993) (Figure 7.21). Mann and Meyer (1993) investigated a natural gully exposure that passed through the tonal lineament exposing a fault. They cleaned and logged the exposure finding a steeply dipping brecciated basalt shear zone. They interpreted the basalt to be in fault contact with a series of loess, ash, and colluvial units. The dip of the fault was ~65°N–55°N (roughly perpendicular to the N68°-trending scarp) with vertical striae implying dip-slip movement. They recorded 5 m of vertical separation of a 10,700-year-old ash, yielding a slip rate of 0.47 mm/yr (Figure 7.26).

Members of the Quaternary Studies Team (R. Coppersmith, K. Hanson, C. Slack, and J. Unruh) accompanied by Steve Reidel visited the natural exposure logged by Mann and Meyer (1993) (locality 13282sh01). We observed relationships similar to those described in that study. We measured a prominent fault plane in the basalt striking N46°W with a subvertical dip at an oblique angle to the lineament (Figure 7.27b). Along the bedrock fault plane we found reasonably preserved subhorizontal moulins. We also observed fractures in the younger loess/colluvial units with a similar strike as the inferred fault scarp, N66°W dipping 68° north (Figure 7.27c). We interpreted the older bedrock units to be internally sheared with strike-slip kinematic indicators. This strike-slip movement appears to be localized on a northwest-trending fault rather than on the Umapine fault as mapped by Mann and Meyer (1993). The younger units appear to have recent vertical offset. The morphology of the lower part of the slope near the fault exposure suggested that the recent faulting is related to gravitational slumping, possibly localized where the older bedrock fault intersected the slope. The stratigraphy in the hanging wall of the recent fault, which consists of interbedded colluviums and loess, is more consistent with repeated slumping and mass wasting during the Holocene rather than multiple Holocene tectonic surface faulting events.

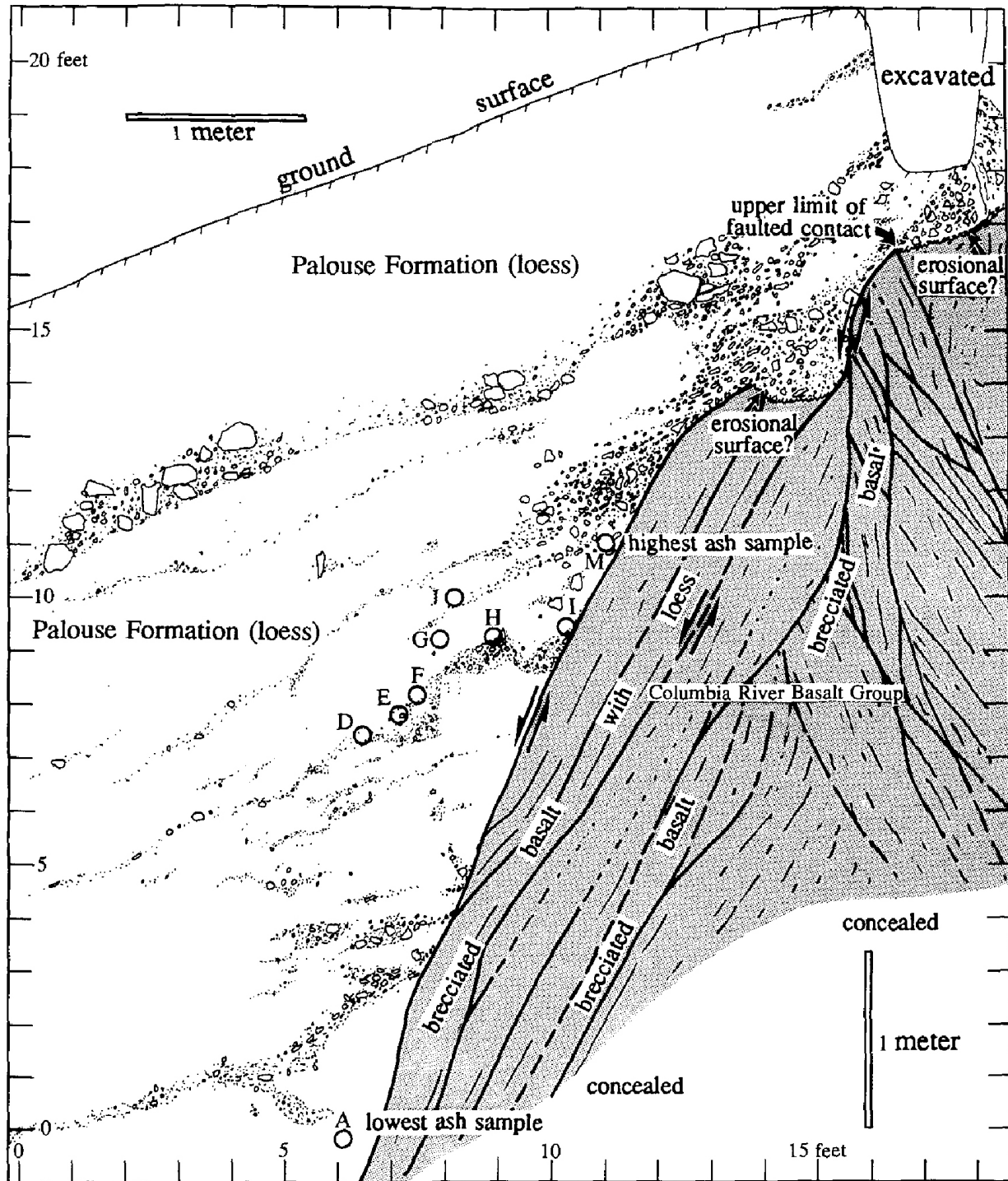


Figure 7.26. Diagram of the east wall of the gully exposure of the Umapiine fault. Samples that yielded ash for microprobe analysis are indicated by letters. The results for a majority of the samples correlated to MSH 'J', which is 10,700 yr BP (Mullineaux 1986). (From Mann and Meyer 1993)



Figure 7.27. Photographs from locality 13282sh01 showing a) the present outcrop, b) bedrock shear zone with $N46^{\circ}W$ subvertical fault exhibiting subhorizontal moulins, and c) fractures ($N66^{\circ}W$ $68^{\circ}N$) within loess/colluvium.

8.0 Fluvial Geomorphic Analyses

Preliminary observations and conclusions from the fluvial geomorphic analyses and preliminary mapping of fluvial terraces in Yakima Canyon conducted by Amos and Sorsby (Appendix E.2) are as follows:

- Differential uplift and tilting of older terraces is centered near Umtanum Ridge.
- Localized channel narrowing across Manastash, Umtanum, and Yakima ridges, as well as Selah Butte is coincident with increasing channel sinuosity, suggesting modest late Quaternary deformation.

9.0 Preliminary Constraints on Quaternary Uplift Rates – Manastash and Umtanum Structures

Preliminary observations regarding differential rates of Quaternary uplift across the Manastash and Umtanum structures that pertain to the characterization of faults associated with these folds are outlined below. These observations synthesize previous work (e.g., Bentley 1977; Waitt 1979; Ladinsky 2012; Ladinsky and Kelsey 2012), the preliminary mapping of fluvial terraces of Amos and Sorsby (Section 8.0, Appendix E.2), preliminary ages of terraces based on cosmogenic nuclide burial ages reported by Bierman (Appendix C), and reconnaissance field observations of the Quaternary Studies Team SSC team members. Table 9.1 summarizes estimated uplift rates based on these observations. Mapping and dating of the Yakima River fluvial terraces is ongoing and due to the preliminary nature of both the dating results and terrace correlations, these results are used primarily as a check on the long-term rates inferred from the structural analysis described in Section 5.0.

9.1 Kittitas Valley

Ladinsky and Kelsey (2012) estimate a long-term incision rate in the southern Kittitas Valley based on stratigraphic and geomorphic features exposed in quarry exposures at Potato Hill, a low ridge at the east end of Fern Road that is about 2 km north of the mouth of Yakima Canyon and CRBG exposures at Manastash Ridge (Figure 9.1). A package of fluvial gravel unconformably overlying Miocene Ellensburg Formation exposed in the quarry cuts is correlated to the Thorp Gravel by Bentley (1977) despite the lack of stratigraphic continuity and indistinct geomorphic relationships to the more extensive Thorp Gravel alluvial deposits further up valley to the north and west that have been dated by fission track methods to be 3.7 Ma (Waitt 1979; Ladinsky and Kelsey 2012). As illustrated in Figure 9.1b, the incision rate on the footwall of the Manastash range-front fault is represented by the lowering of the Kittitas Valley relative to the isolated, elevated remnant of the paleo-valley floor at Potato Hill represented by the Ellensburg/Thorp contact. The relative difference in elevation of the paleo-valley floor and the modern valley floor (26–40 m) and estimated age of the Thorp Gravel of 3.7 Ma imply a lowering rate of the valley floor of 0.01–0.007 m/kyr (Ladinsky and Kelsey 2012).

Stratigraphic relations observed in the Potato Hill quarry exposure in southern Kittitas Valley appear to document progressive uplift and northward tilting of post-CRBG strata deposited along Manastash Ridge piedmont west of the Yakima River. As noted above, two distinct gravel packages are present, separated by an angular unconformity. The lower gravel package, interpreted to be the Ellensburg Formation, consists of interbedded sand, gravel, and boulder conglomerate. Bedding within the lower unit dips approximately 8°–10° north, and appears to project over the crest of Manastash Ridge to the south (Figure 4.20). The upper gravel package, interpreted to be Thorp Gravel, has more extensive iron oxide staining and lacks the large boulder beds in the lower unit. A white zeolitized tuff layer, which is observed in the upper part of the Thorp Gravel unit at the northern end of the exposure, suggests that a shallow lake existed during the deposition of the tuff (Figure 4.20). Uplift of the Manastash Ridge may have led to aggradation and ponding in the Kittitas Valley. The contact between the Ellensburg and Thorp units dips about 5° or less to the north, and is a distinct angular unconformity because it cuts down section through the lower unit from north to south.

Table 9.1. Summary of estimated incision rates –Southern Kittitas and Yakima Canyon that constrain rates of uplift for the Manastash and Umtanum fault sources.

Area or Structure (Source)	Terrace (Elevation)	Sample No. Age	Incision Rate (m/kyr)	Long-term Geologic Vertical Rate (this study)			
				Structural Relief	Amount	6 Ma Start time	10 Ma Start time
Southern Kittitas Valley (Ladinsky and Kelsey 2012)	Potato Hill paleo-valley floor (+ 26–40 m above modern valley floor)	Correlation to Thorp Gravels (3.7 Ma)	0.007–0.01 m/kyr	--	--	--	--
Manastash (MR-C) (this study)	Qg4 (+48 m, strath)	YK05 (Toff Road) 1.08 (\pm 0.29) My (one sigma)	0.044 m/kyr (-0.01/+0.02) (0.03–0.06)	Average	300 m	0.05 m/kyr	0.03 m/kyr
				Site Specific	380 m	0.06 m/kyr	0.04 m/kyr
West of Yakima Canyon mouth (Ladinsky 2012; Ladinsky and Kelsey 2012)	Qf4 (18 m above present channel)	Range for MN10-1, MN10-3, and MN10-4 206–310 ka (minimum age based on IRSL)	0.06–0.09 m/kyr (maximum)	--	--	--	--
Same as above	Qf3 (10 m above present channel)	Correlation of tephra to Carp Lake tephra (~100 ka, or slightly older, less than 190 ka)	0.1 m/kyr (minimum of 0.05 m/kyr using maximum constraint on tephra age)	--	--	--	--
Same as above	Qf2	2–3 m (age estimated based on AM10-1 loess sample 84.2–93.3 ka)	0.02–0.036 m/kyr	--	--	--	--

Table 9.1. (contd)

Area or Structure (Source)	Terrace (Elevation)	Sample No. Age	Incision Rate (m/kyr)	Long-term Geologic Vertical Rate (this study)			
				Structural Relief	Amount	6 Ma Start time	10 Ma Start time
Same as above	Qf2	2–3 m (age estimated based on AM10-1 loess sample 84.2–93.3 ka)	0.02–0.036 m/kyr	--	--	--	--
East of Yakima Canyon Mouth (abandoned Meander) (Ladinsky and Kelsey 2012)	Qg2	Q12 (AM10-1) 84.2–93.3 ka 19–20 m of incision	0.16–0.18 m/kyr (maximum)				
Same as above	Qg4 48 m	AM10-2 237.2–271.3 ka 48 m of incision	0.18–0.20 m/kyr (maximum)	--	--	--	--
Footwall of Umtanum (terrace mapping from Amos and Soresby, Appendix C)	T4 sta.29 km (10 m)	Use YK04 age (below)	0.006 m/kyr (-0.001,+0.001) (0.005–0.007)	--	--	--	--
Meander Roadcut (this study)	T4 ~Sta. 30 km 16 m	YK04 (Meander site) 1.59 (± 0.25) My	0.01 m/kyr (-0.001, +0.002) (0.009–0.012)	--	--	--	--
Umtanum Ridge (UR-W) (this study)				Average (Site Specific)	400 m	0.07 m/kyr	0.04 m/kyr

Table 9.1. (contd)

Area or Structure (Source)	Terrace (Elevation)	Sample No. Age	Incision Rate (m/kyr)	Long-term Geologic Vertical Rate (this study)			
				Structural Relief	Amount	6 Ma Start time	10 Ma Start time
Umtanum Ridge (Hanging wall) (terrace mapping from Amos and Soresby, Appendix C)	T4 Sta 35.5 (38 m)	Use YK04 age	0.024 m/kyr (-0.003,+0.004) (0.021–0.028)				
Hanging wall of Umtanum	T5 ~Sta 40 km (~1.8–3 m)	YK03 (Big Pines site) (indistinguishable from modern) Top of terrace ~7 m above river level; sample 5.2–5.6 bgs; suggests bedrock strath (less than 1.4 m)	Estimated age based on assumed incision rate from hanging wall Sta 35.5 site				
			0.024 m/kyr and 1.4 m = 58 ka 0.021 m/kyr and 1.4 m = 67 ka				
Hanging wall of Umtanum			0.028 m/kyr and 1.4 m = 50 ka Using rates of 0.04–0.07 m/kyr and 1.4 m yields ages of 20–35 ka.				

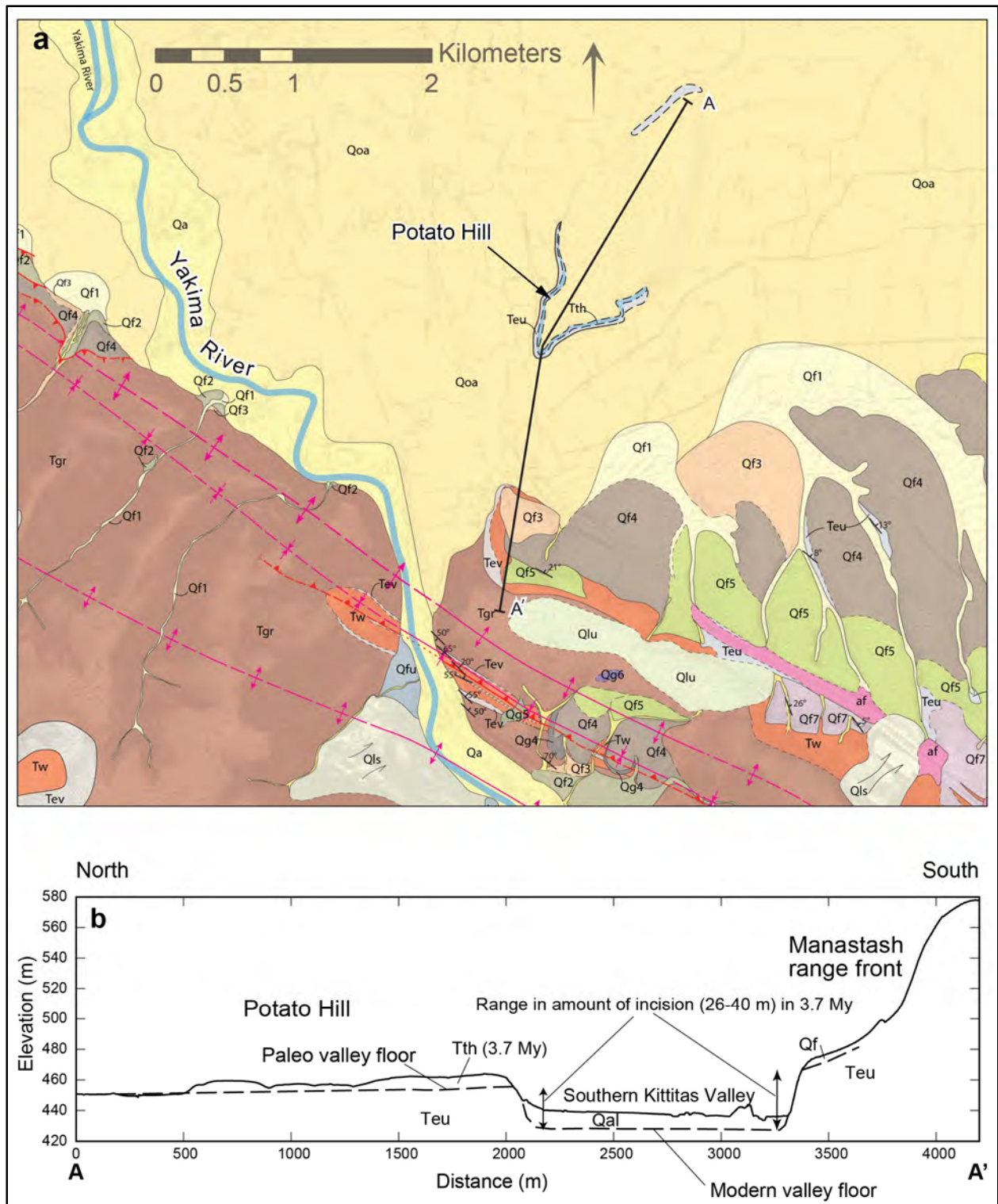


Figure 9.1. Map showing a) the location of Potato Hill and b) the cross section extending from Manastash range front northward to Potato Hill within the southern Kittitas Valley. Teu, Upper Ellensburg Formation; Tth, Thorp Gravel of Waitt (1979); Qf, Quaternary fan deposit (from Ladinsky and Kelsey 2012).

The Potato Hill quarry exposure documents northward tilting of the lower Ellensburg Formation gravels, followed by erosion of these deposits and deposition of the overlying Thorp Gravel package, and further uplift and tilting of both units. The flattish upper surface of Potato Hill extends east of the quarry exposure and may be the original depositional surface of the Thorp Gravel, but more likely is a strath surface beveled across the (tilted) Thorp Gravel. A discontinuous 0.5-m-thick petrocalcic horizon (Stage IV) appears to be associated with this beveled surface. Bentley (1977) suggested that the Thorp Gravel was truncated on the top of Potato Hill by what he referred to as the Thrall pediment surface, which he suggested was equivalent to an early (?) Pleistocene outwash gravel surface observed elsewhere in Kittitas Valley. There are other nearby flattish surfaces inset below the top of Potato Hill that may be a sequence of straths cut into the older deposits as they were progressively uplifted and tilted.

9.2 Manastash Ridge

Ladinsky (2012) and Ladinsky and Kelsey (2012) estimated Quaternary rates of incision (used as a proxy to estimate tectonic uplift) of the Manastash fold/fault based on mapping of Quaternary deposits in both the hanging and footwalls of the structure; geochronology of Quaternary units using IRSL and tephrochronology, geomorphic/neo-tectonic mapping on LiDAR imagery, morphometric analyses of DEMs and incorporation of seismic reflection data across the range front.

A maximum incision rate of approximately 0.18–0.20 m/kyr was estimated for the hanging wall of the Manastash fold/fault based on IRSL age constraints for mainstream Yakima River alluvial deposits (Qg 2, estimated to be slightly older than the fade-corrected age [88,750 ± 4,520 yrs BP] of a capping loess unit; Qg4 [254,250 ± 17,080 yr BP] within the abandoned meander in the Yakima Canyon entrance area). Ladinsky and Kelsey (2012) acknowledge that the ages provide only minimum limiting bounds and thus, the incision rates inferred from these two terraces are maximum limiting incision rates.

The cosmogenic nuclide burial age determined for sample YK05 collected from the same Qg4 terrace yielded a much older age of 1.08 (± 0.29) Ma (Bierman, Appendix C). Using an elevation of 48 m above the present river level and the cosmogenic burial age suggests a lower rate of incision (0.03–0.06m/kyr) (Table 9.1).

The lower rate is more consistent with the estimated incision rate west of the canyon mouth based on the estimated age (100 ka) of a reworked tephra unit in an elevated Qf3 fan remnant and IRSL age constraints for elevated Qaf 4 fans (Ladinsky 2012; Ladinsky and Kelsey 2012) and with long-term uplift rates calculated based on structural analyses conducted for this study (Section 5.0) (Table 9.1).

9.3 Umtanum Ridge

The discontinuous nature of terrace remnants and limited age information inhibit direct correlation of terraces across the Umtanum structure. Preliminary terrace correlations based on tread elevations extracted from LiDAR data as shown by Amos and Sorsby (Appendix E.2) are roughly consistent with broad, low-amplitude warping centered on Umtanum Ridge. The meander terrace (YK04, +16 m above river level), which is located in a synclinal area, yielded a $^{26}\text{Al}/^{10}\text{Be}$ age of 1.6 ± 0.25 Ma (Appendix C). This terrace, which is correlated with terrace 4 a-b, is much higher (+ 35.5 ± 5 m above river level) in the hanging wall of the Umtanum fault/fold (see Appendix E.2, Figure 11). Assuming the preliminary correlation and cosmogenic nuclide ($^{26}\text{Al}/^{10}\text{Be}$) age are correct, these observations suggest a Quaternary

incision rate of 0.024 m/kyr across the Umtanum structure. This is a similar order of magnitude but slightly less than the long-term rate estimated from the structural analyses conducted for this study, which ranges from 0.04–0.08 m/kyr (Section 5.0) (Table 9.1). Correlation of the meander terrace to higher terrace remnants (~+47 m or +90 m) in the hanging wall of the Umtanum fold would yield higher incision (uplift) rates more comparable to the estimated long-term structural analysis rates. Additional dating and mapping are needed to confirm terrace correlations across the Umtanum fault/fold structure.

$^{26}\text{Al}/^{10}\text{Be}$ cosmogenic analysis of a lower terrace in the hanging wall of the Umtanum structure (Big Pine sample YK03) yielded an age that is indistinguishable from modern. Carbonate soil development in the terrace is Stage IC of Forman and Miller (1984) and Stage 1+ of Birkeland (1999). The bedrock strath for this terrace appears to be ≤ 1.4 m above the present level. If it is assumed that the hanging wall block is being uplifted at a rate of ~ 0.24 m/kyr, the terrace would be late Pleistocene in age (50–67 ka, MIS 4). Using the long-term average structural rate of ~ 0.04 – 0.07 m/kyr, the terrace would be ~ 20 – 35 ka (MIS 2).

10.0 References

- Bacon CR. 1983. Eruptive History of Mount Mazama and Crater Lake Caldera, Cascades Range, U.S.A. *Journal of Volcanology and Geothermal Research* 18:57–117.
- Baker VR. 1973. Paleohydrology and sedimentology of the Lake Missoula flooding in eastern Washington. *Geological Society of America Special Paper* 144
- Baker VR. 1978. “Quaternary Geology of the Channeled Scabland and Adjacent Areas.” In Baker VR and D Nummedal (eds.), *The Channeled Scablands*. National Aeronautics and Space Administration, Washington, D.C.
- Baker VR, BN Bjornstad, AJ Busacca, KR Fecht, EP Kiver, UL Moody, JG Rigby, DF Stradling, and AM Tallman. 1991. Quaternary Geology of the Columbia Plateau. In *Quaternary Nonglacial Geology: Conterminous U.S., The Geology of North America*, Volume K-2215–250, RB Morrison (ed.). Geological Society of America, Boulder, Colorado.
- Barnett E and B Sherrod. In Review. Inventory of Paleoseismic studies from the Yakima Fold and Thrust Belt to the Puget Lowland. USGS Scientific Investigations Map (SIM), U.S. Geological Survey, Seattle, Washington.
- Barton BR and GV Last. 2010. The discovery and distribution of mammoth remains in Benton County, Washington State. *Geological Society of America Abstracts with Programs* 42(5):250.
- Barton BR, GV Last, and GC Kleinknecht. 2012. Initial Radiocarbon Dating Of The Coyote Canyon Mammoth, Benton County, Washington State. In *AMQUA 2012, American Quaternary Association, 22nd Biennial Meeting, 2012, Program and Abstracts*. June 21-25, 2012, p. 44. Available at: <http://www.cce.umn.edu/American-Quaternary-Association-Meeting/index.html>.
- Bentley RD. 1977. Stratigraphy of the Yakima basalts and structural evolution of the Yakima ridges in the western Columbia Plateau. In *Geological Excursions in the Pacific Northwest*, EH Brown and RC Ellis (eds.), pp. 339–390. Western Washington State University, Bellingham.
- Berger GW and AJ Busacca. 1995. Thermoluminescence dating of late Pleistocene loess and tephra from eastern Washington and southern Oregon and implications for the eruptive history of Mount St. Helens. *Journal of Geophysical Research* 100:22,361–22,374.
- Bingham JW, CJ Londquist, and EH Baltz. 1970. *Geologic Investigation of Faulting in the Hanford Region, Washington*. Open File Report, U.S. Geologic Survey, Washington, D.C.
- Birkeland PW. 1999. *Soils and Geomorphology*, 3rd edition. Oxford University Press, Oxford, United Kingdom.
- Bjornstad BN. 1980. Sedimentology and Depositional Environment of the Touchet Beds, Walla Walla River Basin, Washington. RHO-BWI-SA-44, Rockwell Hanford Operations, Richland, Washington.

- Bjornstad BN. 1982. Catastrophic flood surging represented in the Touchet Beds of the Walla Walla valley, Washington. In *AMQUA 7th Biennial Meeting, Program and Abstracts*, American Quaternary Association, Maramec, Oklahoma.
- Bjornstad BN and KR Fecht. 1989. Pre-Wisconsin glacial outburst floods: pedogenic and paleomagnetic evidence from the Pasco Basin and adjacent Channeled Scabland. *Geological Society of America Abstracts with Programs* 21:58.
- Bjornstad BN, KR Fecht, and CJ Pluhar. 2001. "Long History of Pre-Wisconsin, Ice Age Cataclysmic Floods: Evidence from Southeastern Washington State." *Journal of Geology* 109:695-713.
- Bjornstad BN, PD Thorne, BA Williams, GV Last, GS Thomas, MD Thompson, JL Ludwig, and DC Lanigan. 2010. *Hydrogeologic Model for the Gable Gap Area, Hanford Site*. PNNL-19702, Pacific Northwest National Laboratory, Richland Washington.
- Bjornstad BN, K Winsor, and SD Unwin. 2012. *A Summary of Fault Recurrence and Strain Rates in the Vicinity of the Hanford Site – Topical Report*. PNNL-17497, Pacific Northwest National Laboratory, Richland, Washington.
- Blair TC and JG McPherson. 2009. Chapter 14, "Processes and Forms of Alluvial Fans" in AJ Parsons and AD Abrahams (eds.), *Geomorphology of Desert Environments*, 2nd edition. DOI 10.1007/978-1-4020-5719-9J4, © Springer Science+Business Media B.V.
- Blakely RJ, BL Sherrod, CS Weaver, RE Wells, and AC Rohay. 2013. The Wallula fault and tectonic framework of south-central Washington, as interpreted from magnetic and gravity anomalies. *Tectonophysics* 608:288-302. DOI: 10.1016/j.tecto.2013.11.006.
- Bond, JG, TD Kauffman, DA Miller, and W Barrash. 1978. Geology of the Southwest Pasco Basin. RHO-BWI-C-25, Rockwell Hanford Operations Richland, Washington.
- Bretz JH, HTU Smith, and GE Neff. 1956. Channeled Scabland of Washington: new data and interpretations. *U.S. Geological Society Bulletin* 67:957–1049.
- Brown RE. 1968. Reported Faulting in the Pasco Basin. BNWL-SA-1704, Battelle Memorial Institute, Pacific Northwest Laboratories, Richland, Washington.
- Bryan K. 1927. The "Palouse soil" problem. *U.S. Geological Society Bulletin* 790:21–45.
- Bunker RC. 1982. Evidence of late Wisconsin floods from glacial Lake Missoula in Badger Coulee, Washington. *Quaternary Research* 18:17–31.
- Burns ER, DS Morgan, RS Peavler, and SC Kahle. 2011. *Three-dimensional Model of the Geologic Framework for the Columbia Plateau Regional Aquifer System, Idaho, Oregon, and Washington*. U.S. Geological Survey (USGS) Scientific Investigations Report 2010-5246, USGS, Tacoma, Washington.
- Clague JJ. 1981. Late Quaternary Geology and Geochronology of British Columbia, Part 2: Summary and Discussion of Radiocarbon-Dated Quaternary History. *Geologic Society of Canada Paper* 80–35.

- Clague JJ, R Barendregt, RJ Enkin, and FF Foit. 2003. Paleomagnetic and tephra evidence for tens of Missoula floods in southern Washington. *Geology* 31:247–250.
- Clynne MA, AT Calvert, EW Wolfe, RC Evarts, RJ Fleck, and MA Lanphere. 2008. The Pleistocene Eruptive History of Mount St. Helens, Washington, from 300,000 to 12,800 Years Before Present. *U.S. Geological Survey Professional Paper 1750:593–627*. Available at: http://pubs.usgs.gov/pp/1750/chapters/pp2008-1750_chapter28.pdf
- Davis JO. 1978. Quaternary tephrochronology of the lake Lahontan Area, Nevada and California. *Nevada Survey, Archeological Research Paper No 7*.
- DOE (U.S. Department of Energy). 1988. *Consultation Draft, Site Characterization Plan, Reference Repository Location, Hanford Site, Washington*. DOE/RW-0164 Volume 1, U.S. Department of Energy Office of Civilian Radioactive Waste Management, Washington, D.C.
- DOE-RL (U.S. Department of Energy- Richland Operations Office). 2002. *Standardized Stratigraphic Nomenclature for the Post-Ringold-Formation Sediments Within the Central Pasco Basin*. DOE/RL-2002-39, Rev. 0, Richland, Washington.
- Energy Northwest 1982 – Finley Quarry, Response to Q. 360.015 (Amendment No. 23, WNP-2 FSAR)
- Energy Northwest. 1998. “Geology, Seismology and Geotechnical Engineering.” Section 2.5 in *Columbia Generating Station Final Safety Analysis Report*. Amendment 53, Richland, Washington.
- Farooqui SM. 1979. *Evaluation of Quaternary Faulting in the Warm Springs Canyon Area Southeast Washington*. Prepared for the Washington Public Power Supply System by Shannon & Wilson Inc., Portland, Oregon.
- Farooqui SM and RE Thoms. 1980. *Geologic Evaluation of Selected Faults and Lineaments Pasco and Walla Walla Basins – Washington*. Shannon & Wilson, Inc., Lake Oswego, Oregon.
- Fecht KR, SP Reidel, and MA Chamness. 1992. Contour Map of the Top of the Basalt of the Hanford Site. Scale 1:62500. Washington State University Open-File Map 2014-1. (Contact Steve Reidel at Washington State University to obtain a copy.)
- Fecht KR, BN Bjornstad, DG Horton, GV Last, SP Reidel, and KA Lindsey. 1999. Clastic Injection Dikes of the Pasco Basin and Vicinity: Geologic Atlas Series. BHI-01103, Rev. 0, Bechtel Hanford, Richland, Washington.
- Fecht KR and TE Marceau. 2006. *Late Pleistocene- and Holocene-Age Columbia River Sediments and Bedforms: Hanford Reach Area, Washington – Part 2*. Geologic Atlas Series, WCH-46, Rev. 0, Washington Closure Hanford, Richland, Washington.
- Fecht KR, SP Reidel, and AM Tallman. 1987. “Paleodrainage of the Columbia River System on the Columbia Plateau of Washington State – A Summary.” Chapter in *Selected Papers on the Geology of Washington*, JE Schuster (ed.), Bulletin 77, pp. 219–248. Washington Department of Natural Resources, Division of Geology and Earth Resources, Olympia, Washington.

Fecht KR, TE Marceau, BN Bjornstad, DG Horton, GV Last, RE Peterson, SP Reidel, and MM Valenta. 2004. *Late Pleistocene- and Holocene-Age Columbia River Sediments and Bedforms: Hanford Reach Area, Washington – Part 1*. Geologic Atlas Series, BHI-01648, Bechtel Hanford, Inc., Richland, Washington.

Flint RF. 1938. Origin of the Cheney-Palouse scabland tract. *Geological Society of America Bulletin* 49:461–524.

Foit FF Jr, PJ Mehringer Jr, and JC Sheppard. 1993. Age, distribution, and stratigraphy of Glacier Peak tephra in eastern Washington and western Montana, United States. *Canadian Journal of Earth Sciences* 30(3):535–552, 10.1139/e93-042.

Forman SL and GH Miller. 1984. Time-dependent soil morphologies and pedogenic processes on raised beaches, Broggerhalvoya, Spitzbergen, Svalbard Archipelago. *Arctic Alpine Research* 16:381–394.

Gardner JN, MG Snow, and KR Fecht. 1981. *Geology of the Wallula Gap Area, Washington*. RHO-BWI-LD-9, Rockwell International, Rockwell Hanford Operations, Richland, Washington.

Gesch DB. 2007. “The National Elevation Dataset.” Pp. 99–118, in Maune D (ed.), *Digital Elevation Model Technologies and Applications: The DEM Users Manual*, 2nd Edition. American Society for Photogrammetry and Remote Sensing, Bethesda, Maryland

Gesch D, M Oimoen, S Greenlee, C Nelson, M Steuck, and D Tyler. 2002. The National Elevation Dataset. *Photogrammetric Engineering and Remote Sensing* 68(1):5–11.

Gile LH, FF Peterson, and RB Grossman. 1966. Morphological and genetic sequences of carbonate accumulation in desert soils. *Soil Science* 101:347–360.

Grolier MJ and JW Bingham. 1978. Geology of parts of Grant, Adams, and Franklin Counties, East-Central, Washington. Bulletin No, 71, Division of Geology and Earth Sources, Washington Department of Natural Resources, Olympia, Washington.

Guenther LD. 2004. Tectonics of the northern California Coast Ranges, past and present, as inferred from analysis of kinematic data. Master’s Thesis, University of California, Davis.

Guettinger MW, GV Last, and BR Barton. 2010. Geology of the Coyote Canyon Mammoth Site, Benton County, Washington State. 2010 Annual Meeting & Exposition, Denver, Colorado, 31 October – 3 November. *Geological Society of America Abstracts with Programs* 42(5):119.

Gufstafson EP. 1978. The vertebrate faunas of the Pliocene Ringold Formation, south-central Washington. *University of Oregon Museum of Natural History Bulletin* 23:1–62, University of Oregon, Eugene, Oregon.

Hammer AA. 1934. The Rattlesnake Hills Gas Field, Benton County Washington. *American Association of Petroleum Geologists Bulletin* 18:847–859.

- Jaffee MA and PK Spencer. 2000. Multiple floods many times over: the record of glacial outburst floods in southeastern Washington. *Geological Society of America Abstracts with Programs* 32:A21.
- Kienle CF. 1980. *Geologic Reconnaissance of Parts of the Walla Walla and Pullman, Washington, and Pendleton, Oregon 10 x 20 AMS Quadrangles*. Report prepared by Foundation Sciences Inc. Portland, Oregon for the U.S. Army Corps of Engineers, Seattle District, Washington.
- Kuehn SC. 1995. *The Olympic-Wallowa Lineament, Hite Fault System, and Columbia River Basalt Group Stratigraphy in Northeast Umatilla County, Oregon*. Master's thesis, Washington State University, Pullman.
- Kuehn SC, DG Froese, PE Carrara, FE Foit Jr., NJG Pearce, and P Rotheisler. 2009. Major- and trace-element characterization, expanded distribution, and a new chronology for the latest Pleistocene Glacier Peak tephras in western North America. *Quaternary Research* 71:201–216. doi:10.1016/j.yqres.2008.11.003. DOI: 10.1016/j.yqres.2008.11.003.
- Ladinsky TC. 2012. *Late Quaternary Evolution of the Manastash Anticline and Manastash Range Front, Yakima Fold Belt, Washington: Influence of Tectonics and Climate*. Master's thesis, Humboldt State University, Arcata, California.
- Ladinsky TC and HM Kelsey. 2012. *Late Quaternary Landscape Evolution and Deformation in the Forelimb Region of the Manastash Anticline, Yakima Fold Belt, Washington*. U.S. Geological Survey, Reston, Virginia. Available from <http://earthquake.usgs.gov/research/external/reports/G10AC00686.pdf> (June 2013).
- Last GV and BN Bjornstad. 2009. Distribution of *Mammuthus* and erratic finds relative to the size of Ice Age floods in southeast Washington. *Geological Society of America Abstracts with Programs* 41(7):16.
- Last GV, BR Barton, and GC Kleinknecht. 2012. Preliminary Stratigraphic Context of the Coyote Canyon Mammoth Site. Oral presentation at the Northwest Scientific Association Annual Meeting, Boise, Idaho, March 28-31, 2012. *Northwest Lichenologists, Northwest Scientific Association, 2012 Program and Abstracts*.
- Lenz BR, HR Gentry, and DL Clingman. 2001. Timing and Characteristics of Early Holocene Aggradation, Columbia River, Washington State. Abstracts with Program, Geological Society of American Annual Meeting, Boulder, Colorado.
- Lewis JC, JR Unruh, and RJ Twiss. 2003. Seismogenic strain and motion of the Oregon coast block. *Geology* 31(2):183–186.
- Lindsey KA. 1995. *Miocene-to Pliocene-Aged Suprabasalt Sediments of the Hanford Site, South-Central Washington*. BHI-00184, Bechtel Hanford Incorporated, Richland, Washington.
- Lindsey KA. 1996. *The Miocene to Pliocene Ringold Formation and Associated Deposits of the Ancestral Columbia River System, South-Central Washington and North-Central Oregon*. Open File Report 96-8, Washington State Department of Natural Resources, Olympia, Washington.

- Lindsey KA and DR Gaylord. 1990. Lithofacies and Sedimentology of the Miocene Pliocene Ringold Formation, Hanford Site, South-Central Washington. *Northwest Science* 4:165–180.
- Lindsey KA, SP Reidel, KR Fecht, JL Slate, AG Law, and AM Tallman. 1994. “Geohydrologic Setting of the Hanford Site, South-Central Washington,” in *Geologic Field Trips in the Pacific Northwest: 1994 Geological Society Annual Meeting*, Chapter C1, pp. 1C-1–1C-16, DA Swanson and RA Haugerun (eds.). Geological Society of America, Boulder, Colorado.
- Machette MN. 1985. Calcic soils of the southwestern United States. *Geological Society of America*. Special paper 203:1–21.
- Mann GM and CE Meyer. 1993. Late Cenozoic structure and correlations to seismicity along the Olympic-Wallowa Lineament, northwest United States. *Geological Society of America Bulletin* 105:853–871.
- Martin BH, HL Petcovic, and SP Reidel. 2005. *Goldschmidt Conference 2005: Field Trip Guide to the Columbia River Basalt Group*. PNNL-15221, Pacific Northwest National Laboratory, Richland, Washington.
- McCaffrey R, RW King, SJ Payne, and M Lancaster. 2013. Active tectonics of northwestern US inferred from GPS-derived surface velocities. *Journal of Geophysical Research*, Solid Earth 118:1–15. DOI: 10.1029/2012JB009473.
- McClay, K., and M Bonora. 2001, Analog models of restraining stepovers in strike-slip fault systems: *American Association of Petroleum Geologists Bulletin*, v. 85, p. 233–26
- McDonald EV and AJ Busacca. 1988. Record of pre-late Wisconsin giant flood in the Channeled Scabland interpreted from loess deposits. *Geology* 16:728–731.
- McDonald EV and AJ Busacca. 1990. Interaction between aggrading geomorphic surfaces and the formation of a late Pleistocene paleosol in the Palouse loess of eastern Washington State. *Geomorphology* 3:449–470.
- McDonald EV and AJ Busacca. 1992. Late Quaternary stratigraphy of loess in the channeled scabland and Palouse of Washington State. *Quaternary Research* 38:141-156.
- McDonald EV, MR Sweeney, and AJ Busacca. 2012. Glacial outburst flood and loess sedimentation documented during Oxygen Isotope Stage 4 on the Columbia Plateau, Washington State. *Quaternary Science Reviews* 45:18–30. DOI: 10.1016/j.quascirev.2012.03.016.
- McKee EH, DA Swanson, and TL Wright. 1977. Duration and Volume of Columbia River Basalt Volcanism: Washington, Oregon, and Idaho. *Geological Society of America Abstracts with Programs* 9(4):463–464.
- McQuarrie N. 1993. Structural analysis of the Wallula Gap Fault, southeastern Washington. *Geological Society of America Abstracts with Programs* 25(5).
- Moody UL. 1978. *Microstratigraphy, Paleoecology, and Tephrochronology of the Lind Coulee Site, Central Washington*. PhD Dissertation, Washington State University, Department of Anthropology, Pullman, Washington.

- Moody UL. 1987. *Late Quaternary Stratigraphy of the Channeled Scabland and Adjacent Areas*. PhD Dissertation, University of Idaho, Moscow, Idaho.
- Mullineaux DR. 1986. Summary of pre-1980 tephra-fall deposits from Mount St Helens, Washington State, USA. *Bulletin of Volcanology* 48:17–26.
- Myers CW, SM Price, JA Caggiano, et al. 1979. *Geologic Studies of the Columbia Plateau – A Status Report*. RHO-BWI-ST-4, Rockwell Hanford Operations, Richland, Washington.
- Newcomb RC. 1958. Ringold Formation of Pleistocene age in type locality, the White Bluffs, Washington. *American Journal of Science* 256:328–340.
- Newcomb RC, JR Strand, and FJ Frank. 1972. Geology and groundwater characteristics of the Hanford Reservation of the U.S. Atomic Energy Commission, Washington. *U.S. Geological Survey Professional Paper* 717:1–78.
- NRC (U.S. Nuclear Regulatory Commission). 1982 *Safety Evaluation Report Related to the Construction of Skagit/Hanford Nuclear Project, Units 1 and 2 - Docket Nos. STN 50-522 and 50-523*. NUREG-0309, Supplement No. 3, Office of Nuclear Reactor Regulation, U.S. Nuclear Regulatory Commission, Washington, D.C.
- Nummedal D. 1978. “Field trip stop descriptions.” In Baker VR and Nummedal D (eds.), *The Channeled Scabland*. National Aeronautics and Space Administration, Washington, D.C.
- O'Connor JE and VR Baker. 1992. Magnitudes and implications of peak discharges from Glacial Lake Missoula. *Geological Society of America Bulletin* 104:267–279.
- Packer DR and JM Johnston. 1979. *A Preliminary Investigation of the Magnetostratigraphy of the Ringold Formation*. WCC Report, RHO-BWI-C-42, Woodward-Clyde Consultants, San Francisco, California.
- Patton PC and VR Baker. 1978. New evidence for Pre-Wisconsin flooding in the Channeled Scabland and eastern Washington. *Geology* 6:567–571.
- Personius SF and DJ Lidke (compilers). 2003. Fault Number 565, Rattlesnake Hills Structures. In *Quaternary Fault and Fold Database of the United States*. U.S. Geological Survey, <http://earthquakes.usgs.gov/regional/qfaults>, accessed March 20, 2013.
- Pluhar CJ, BN Bjornstad, SP Reidel, RS Coe, and PB Nelson. 2006. Magnetostratigraphic evidence from the Cold Creek bar for onset of ice-age cataclysmic floods in eastern Washington during the Early Pleistocene. *Quaternary Research* 65:123–125.
- Porter SC. 1978. Glacier Peak Tephra in the North Cascade Range, Washington: Stratigraphy, Distribution, and Relationship to Late-Glacial Events. *Quaternary Research* 10:30–41.
- Reidel SP. 1984. The Saddle Mountains: The evolution of an anticline in the Yakima Fold Belt. *American Journal of Science* 284(8):942–978.

Reidel SP. In Press. Geologic Map of the Iowa Flats 1:24,000 Quadrangle, Washington. U.S. Geological Survey, Olympia, Washington.

Reidel SP, VE Camp, TL Tolan, JD Kauffman, and DL Garwood. 2013a. Tectonic evolution of the Columbia River flood basalt province. In *The Columbia River Flood Basalt Province*, SP Reidel, VE Camp, ME Ross, JA Wolff, BS Martin, TL Tolan, and RE Wells (eds.), GSA Special Paper 497, pp. 293–324. Geological Society of America, Boulder, Colorado.

Reidel SP, VE Camp, TL Tolan, and BS Martin. 2013b. “The Columbia River Flood Basalt Province: Stratigraphy, Areal Extent, Volume, and Physical Volcanology.” Pp. 1–44 in *The Columbia River Flood Basalt Province*, SP Reidel, VE Camp, ME Ross, JA Wolff, BS Martin, TL Tolan, and RE Wells (eds.). GSA Special Paper 497, Geological Society of America, Boulder, Colorado.

Reidel SP, NP Campbell, KR Fecht, and KA Lindsey. 1994. Late Cenozoic structure and stratigraphy of south-central Washington. *Washington Division of Geology and Earth Resources Bulletin* 80:159–180.

Reidel SP and MA Chamness. In Press. Geologic Map of the Snively Basin 1:24,000 Quadrangle, Washington. U.S. Geological Survey, Olympia, Washington.

Reidel SP, RW Cross, and KR Fecht. 1983. “Constraints on Tectonic Models.” Chapter 5 in DOE 1983. *Preliminary Interpretation of the Tectonic Stability of the Reference Repository Location, Cold Creek Syncline, Hanford Site*. U.S. Department of Energy-Richland Operations Office, Richland, Washington.

Reidel SP and KR Fecht. 1994. *Geologic Map of the Richland 1:100,000 Quadrangle, Washington*. Open File Report 94 8, 21p., Plate 1, Washington Division of Geology and Earth Resources, Washington State Department of Natural Resources, Olympia, Washington.

Reidel SP and TL Tolan. 1994. Late Cenozoic structure and correlations to seismicity along the Olympic-Wallowa lineament, northwestern United States: discussion and reply. *Geological Society of America Bulletin* 106:1634–1638.

Reidel SP and TL Tolan. 2013. The late Cenozoic evolution of the Columbia River system in the Columbia River flood basalt province. *Geological Society of America Special Papers* 497:201–230. DOI: 10.1130/2013.2497(08).

Reidel SP, NP Campbell, KR Fecht, and KA Lindsey. 1994. Late Cenozoic structure and stratigraphy of south-central Washington. *Washington Division of Geology and Earth Resources Bulletin* 80:159–180.

Reidel SP, TL Tolan, PR Hooper, KR Fecht, MH Beeson, RD Bentley, and JL Anderson. 1989. The Grande Ronde Basalt, Columbia River Basalt Group: Stratigraphic descriptions and correlations in Washington, Oregon, and Idaho, Volcanism and Tectonism in the Columbia River Flood-Basalt Province. *Special Paper – Geological Society of America* 238:21–53.

Reidel SP, KD Reynolds, and DG Horton. 1998. *Immobilized Low-Activity Waste Site Borehole 299-E17-21*. PNNL-11957, Pacific Northwest National Laboratory, Richland, Washington.

- RHO (Rockwell Hanford Operations). 1982a. *Site Characterization Report for the Basalt Waste Isolation Project*. DOE/RL 82-3, Volume 1, U.S. Department of Energy, Richland Operations Office, Richland, Washington
- Richardson, CA, EV McDonald, and AJ Busacca. 1997. Luminescence dating of loess from the Northwest United States. In *Quaternary Science Reviews (Quaternary Geochronology)* 16(3–5):403–415.
- Rigby JG and K Othberg. 1979. *Reconnaissance Surficial Geologic Mapping of the Late Cenozoic Sediments of the Columbia Basin, Washington*. Open-File Report 79-3, Division of Geology and Earth Resources, State of Washington Department of Natural Resources, Olympia.
- Schaetzl RJ and S Anderson. 2005. *Soil Genesis and Geomorphology*. Cambridge University Press, Cambridge, UK.
- Schuster JE. 2000. Geologic map of Washington State. Washington Division of Geology and Earth Resources, Washington State Department of Natural Resources, Olympia, Washington.
- Schuster JE, CW Gulick, SP Reidel, KR Fecht, and S Zurenko. 1997. *Geologic map of Washington – southeast quadrant*. Geologic Map GM-45, Division of Geology and Earth Resources, Washington State Department of Natural Resources, Olympia.
- Sherrod BL, RB Blakely, JP Lasher, A Lamb, S Mahan, FF Foit Jr. and EA Barnett. In Review. Active Faulting on the Wallula Fault within the Olympic-Wallowa Lineament, Washington State, USA. *Journal of Geology*.
- Smith GR, N Morgan, and E Gustafson. 2000. Fishes of the Mio-Pliocene Ringold Formation, Washington: Pliocene Capture of the Snake River by the Columbia River. University of Michigan, *Papers on Paleontology* No. 32.
- Spencer PK and AN Knapp. 2010. New stratigraphic markers in the late Pleistocene Palouse loess: novel fossil gastropods, absolute age constraints and non-aeolian facies. *Sedimentology* 57:41–52.
- Swanson DA, TL Wright, VE Camp, JN Gardner, RT Hely, SM Price, SP Reidel, and ME Ross. 1980. Reconnaissance Geologic map of the Columbia River Basalt Group, Pullman and Walla Walla Quadrangles, southeast Washington and adjacent Idaho. U.S. Geological Survey Miscellaneous Investigations Series I-1139, 2 sheets, scale 1:250,000, Denver, Colorado.
- Sweeney MR, AJ Busacca, and DR Gaylord. 2005. Topographic and climatic influences on accelerated loess accumulation since the last glacial maximum in the Palouse, Pacific Northwest, USA. *Quaternary Research* 63:261–273.
- Tallman AM, KL Fecht, MC Marratt, and GV Last. 1979. *Geology of the Separation Areas, Hanford Site, South-Central Washington*. Report RHO-ST-23, Rockwell Hanford Operations, Richland, Washington.
- Thorne PD, AC Rohay, and SP Reidel. 2014. *Development of a Basin Geologic and Seismic Property Model Used to Support Basin-Effects Modeling for the Hanford Probabilistic Seismic Hazards Analysis*. PNNL-23305, Pacific Northwest National Laboratory, Richland, Washington.

Twiss RJ, BJ Souter, and JR Unruh. 1993. The effect of block rotations on the global seismic moment tensor and patterns of seismic P and T axes. *Journal of Geophysical Research* 98:645–674.

Twiss RJ and JR Unruh. 1998. Analysis of fault-slip inversions: do they constrain stress or strain rate? *Journal of Geophysical Research* 103:2,205–12,222.

Unruh J and E Hauksson. 2009. Seismotectonics of an evolving intracontinental plate boundary, southeastern California. In JS Oldow and PH Cashman (eds.), *Late Cenozoic Structure and Evolution of the Great Basin-Sierra Nevada Transition*. *Geological Society of America Special Paper* 447:351-372. DOI: 10.1130/2009.2447(16).

Unruh JR, E Hauksson, FC Monastero, RJ Twiss, and JC Lewis. 2002. Seismotectonics of the Coso Range-Indian Wells Valley region, California: “Transtensional deformation along the southeastern margin of the Sierran microplate.” In AF Glazner, JD Walker, and JM Bartley (eds.), *Geologic Evolution of the Mojave Desert and Southwestern Basin and Range*. Geological Society of America (GSA) Memoir 195, p. 277–294, GSA, Boulder, Colorado,

Waite RB. 1979. Late Cenozoic deposits, landforms, stratigraphy and tectonism in Kittitas Valley, Washington. *U.S. Geological Survey Professional Paper* 1127:18. U.S. Government Printing Office, Washington, D.C. Available at: <http://pubs.er.usgs.gov/publication/pp1127>.

WCC (Woodward-Clyde Consultants). 1981a. Logs of Trenches at Finley Quarry. Prepared for Washington Public Power Supply System under the direction of United Engineers & Constructors, Inc. by WCC, San Francisco, California.

WCC (Woodward-Clyde Consultants). 1981b. *Task D3 Quaternary Sediments Study of the Pasco Basin and Adjacent Areas*. Prepared for the Washington Public Power Supply System, by WCC, San Francisco, California.

WCC (Woodward-Clyde Consultants). 1982. *Draft Wallula Gap Fault Trenching and Mapping*. Report prepared for the Washington Public Power Supply System, by WCC, San Francisco, California.

West MW. 1997. *A Continuation of a “Pilot” Study of Quaternary Surface Deformation, Saddle Mountains Anticline, Northern Pasco Basin, Washington – Program Element I – Evaluating National and Regional Hazard and Risk*. Michael W. West & Associates, Inc., Castle Rock, Colorado.

Westgate JA and ME Evans. 1978. Compositional variability of Glacier Peak tephra and its stratigraphic significance. *Canadian Journal of Earth Science* 15:1554–1567.

Wicks C, W Thelen, C Weaver, J Gomberg, A Rohay, and P Bodin. 2011. InSAR observations of a seismic slip associated with an earthquake swarm in the Columbia River flood basalts. *Journal of Geophysical Research* 116, B12304. DOI: 10.1029/2011JB008433.

Woodcock N and M Fischer. 1986. Strike-slip duplexes. *Journal of Structural Geology* 8(7):725–735.

WPPSS (Washington Public Power Supply System). 1977. Preliminary Safety Analysis Report, Volumes 1 and 2, Amendment 23, Washington Public Power Supply System, Inc. Richland, Washington.

Zdanowica C and G Zielinski. 1999. Mount Mazama eruption: calendrical age verified and atmospheric impact assessed. *Geology* 27:621–624. DOI: 10.1130/0091-613(1999)027<0621:MMECAV>2.3.CO;2.

Appendix E.1

Geochronology – Th/U Dating of Carbonate Rinds

**U-Series Dating Results
USGS Denver Radiogenic Isotope Lab**

**²³⁰Th/U Ages Supporting Hanford Site-Wide
Probabilistic Seismic Hazard Analysis – [Report](#)**

**²³⁰Th/U Ages Supporting Hanford Site-Wide
Probabilistic Seismic Hazard Analysis – [Appendix](#)**

**James B. Paces
U.S. Geological Survey**

Appendix E.2

Fluvial Analysis of Active Deformation in the Yakima Fold and Thrust Belt, WA

**Colin B. Amos and Skyler J. Sorsby,
Geology Department
Western Washington University**

Appendix E.3

Geochronology–Cosmogenic Nuclide ($^{10}\text{Be}/^{26}\text{Al}$) Dating of Fluvial Gravels-Yakima River Canyon

Yakima Canyon fluvial terrace cosmogenic isotope analysis

Paul R. Bierman

Appendix E.4

Inventory of Paleoseismic Studies from the Yakima Fold and Thrust Belt to the Puget Lowland

Appendix E.4

Inventory of Paleoseismic Studies from the Yakima Fold and Thrust Belt to the Puget Lowland

Paleoseismic Summary

Available paleoseismic data for Yakima Fold Belt structures were compiled by the U.S. Geological Survey (USGS) and will be published as a USGS Scientific Investigations Map (Barnett and Sherrod, In Review). A preliminary draft of this information is provided in this appendix. The information is summarized in a text file, in an excel spreadsheet, and on a regional map.

Barnett E and B Sherrod. In Review. *Inventory of Paleoseismic studies from the Yakima Fold and Thrust Belt to the Puget Lowland*. USGS Scientific Investigations Map (SIM), U.S. Geological Survey, Seattle, Washington.

- **Paleosites_text_2.0**
- **Inv-paleosites_6.1 (Excel file)**
- **Paleosites_Map.5.exp**